

STATUS OF THESIS

Title of thesis DEVELOPMENT OF SUBAERIAL KARST IN THE KINTA VALLEY, PENINSULAR MALAYSIA

I, SOLOMON KASSA

hereby allow my thesis to be placed at the Information Resource Center (IRC) of Universiti Teknologi PETRONAS (UTP) with the following conditions:

1. The thesis becomes the property of UTP
2. The IRC of UTP may make copies of the thesis for academic purposes only.
3. This thesis is classified as

Confidential

Non-confidential

If this thesis is confidential, please state the reason:

The contents of the thesis will remain confidential for _____ years.

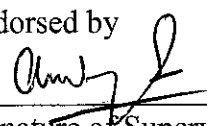
Remarks on disclosure:



Signature of Author

Permanent address: 09 Kebele,
Debere Birhan, North Shoa,
Ethiopia

Date : 31/5/2013

Endorsed by


Signature of Supervisor

Name of Supervisor
Assoc. Prof. Dr. Chow Weng
Sum

Date: 31/5/2013

Dr Chow Weng Sum
Associate Professor
Geoscience & Petroleum Engineering Department
Universiti Teknologi PETRONAS
Bandar Seri Iskandar, 31750 Tronoh,
Perak Darul Ridzuan, MALAYSIA.

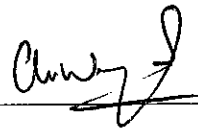
UNIVERSITI TEKNOLOGI PETRONAS
DEVELOPMENT OF SUBAERIAL KARST IN THE KINTA VALLEY,
PENINSULAR MALAYSIA

by

SOLOMON KASSA

The undersigned certify that they have read, and recommend to the Postgraduate Studies Programme for acceptance this thesis for the fulfillment of the requirements for the degree stated.

Signature:

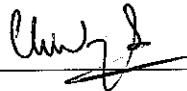


Dr Chow Weng Sum
Associate Professor
Geoscience & Petroleum Engineering Department
Universiti Teknologi PETRONAS
Bandar Seri Iskandar, 31750 Tronoh,
Perak Darul Ridzuan, MALAYSIA.

Main Supervisor:

Assoc. Prof. Dr. Chow. Weng Sum

Signature:



Co-Supervisor:

for Prof. Dr. Bernard J. Pierson

Signature:



Head of Department:

Assoc. Prof. Dr. Abdul Hadi Bin Abdul

Rahman
AP Dr Abdul Hadi B. Abd Rahman
Head, Geosciences Department
Universiti Teknologi PETRONAS

Date:

31/5/2013

DEVELOPMENT OF SUBAERIAL KARST IN THE KINTA VALLEY,
PENINSULAR MALAYSIA

by

SOLOMON KASSA

A Thesis

Submitted to the Postgraduate Studies Programme

as a Requirement for the Degree of

DOCTOR OF PHILOSOPHY

PETROLEUM GEOSCIENCES

UNIVERSITI TEKNOLOGI PETRONAS

BANDAR SERI ISKANDAR,

PERAK

MAY 2013

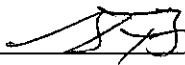
DECLARATION OF THESIS

Title of thesis DEVELOPMENT OF SUBAERIAL KARST IN THE KINTA VALLEY, PENINSULAR MALAYSIA

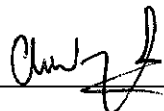
I, SOLOMON KASSA

hereby declare that the thesis is based on my original work except for quotations and citations which have been duly acknowledged. I also declare that it has not been previously or concurrently submitted for any other degree at UTP or other institutions.

Witnessed by



Signature of Author



Signature of Supervisor

Permanent address: 09 Kebele,
Debere Birhan, North Shoa,
Ethiopia

Name of Supervisor
Assoc. Prof. Dr. Chow Weng
Sum

Date: 31/5/2013

Date: 31/5/2013

Dr Chow Weng Sum
Associate Professor
Geoscience & Petroleum Engineering Department
Universiti Teknikal PETRONAS
Bandar Seri Iskandar, 31750 Tronoh,
Perak Darul Ridzuan, MALAYSIA.

DEDICATION

To all who helped me reach this stage.

ACKNOWLEDGEMENTS

First and foremost, may almighty God be praised for all His Blessings. There are a number of people to whom I am immensely indebted. First, I would like to express my heartfelt thanks to my supervisors, Prof. Dr. Bernard J. Pierson and Assoc. Prof. Dr. Chow Weng Sum, for their constructive advice, guidance, comments and suggestions during the course of this research. Particularly I am indebted to Prof. Pierson whose follow-ups continued even when he was not nearby. I am also indebted to Prof. Manuel Pubellier whose continuous comments and suggestions enabled me to polish my work.

I would like to extend my gratitude to Universiti Teknologi PETRONAS for providing me the opportunity to pursue my study, and granting me a fund to undertake my research. My appreciation also goes to Southeast Asia Carbonate Research Lab (SEACARL), where I could undertake my research and to the Shell Chair Endowment Fund that provided financial support which covered part of this study.

I am deeply indebted to all members of my family, whose love, relentless support and encouragement made me strong to overcome all ups and downs, particularly during desperate moments which left the scar of a lifelong lesson.

I would like to extend my deepest gratitude to all my friends in SEACARL, especially my dear friends MD. Habibur Rahman and Haylay Tsegab, for the knowledge we shared and, at times, fun we have had for the past three years. My heartfelt appreciation also goes to all Ethiopians in UTP, and our community in Malaysia.

Last but not least, I am sincerely indebted to the Malaysian Karst Society (MKS) members: Robert Percival, Cheang Kum Seng and Bernard Lee, for their help during reconnaissance surveying and cave mapping.

ABSTRACT

The study area, the Kinta Valley, is located in the western part of Peninsular Malaysia. It is characterized by remnant limestone hills and associated karst features, such as caves, dolines, sinkholes, and tower karsts. Karst development in the Kinta Valley is attributed to various factors, including fracture, lithology, and rock uplift. In order to identify the possible factors that controlled the gradual development of this karst system, and its implications to the understanding of the nature of subsurface karsts, different approaches were used. To ascertain the link between lineament and cave passage orientations, and to identify the main fractures controlling the karst features, standard cave surveying and lineament extraction techniques from Spot image, were employed. Similarly, in order to unravel the influence of uplift in the development of the Kinta Valley karst system, apatite and zircon fission-tracks analysis was conducted.

Mapping of the various karstic caves revealed that there is a general NNW-SSE trend of caves passage orientation. The orientation of the lineaments extracted from the isolated limestone hills also appears to be prominently in the NNW-SSE trend. Thus, the similarity of the general orientation of the lineaments and caves passage trend attests that the development of karst in the Kinta Valley is controlled by fractures. The karst development phenomenon further enhanced by the varied uplifting episodes which were taking place since the early Upper Cretaceous period, with a maximum and minimum rate of 78m/Ma and 6m/Ma, respectively. The average rate of uplift is estimated to be 50.6m/Ma, and as cave streams downcutting rate is equivalent to base level lowering or uplift rate, a similar rate of long-term carbonate rock loss has been inferred.

As the origin of subsurface karsts is primarily attributed to subaerial karstification processes, understanding the development of subaerial karsts is the key to better interpret the subsurface karsts. Thus, the study of the Kinta Valley karst development

and associated formation of the different types of karst features clearly throws light on how this karst system can serve as a good analogue to validate the true nature of subsurface karsts to be interpreted from indirect evidence.

ABSTRAK

Kawasan kajian, Lembah Kinta, terletak di bahagian barat Semenanjung Malaysia. Ia dicirikan oleh sisa bukit batu kapur dan ciri-ciri kars yang berkaitan dengannya, seperti gua, dolina, lubang benam, dan kars penara. Pembentukan kars di Lembah Kinta disebabkan oleh pelbagai faktor termasuk retakan, litologi, dan proses pengangkatan batuan. Pendekatan kajian yang berbeza telah digunakan untuk mengenal pasti faktor-faktor yang berkemungkinan mengawal pembentukan secara beransur-ansur sistem kars ini, serta implikasinya kepada kefahaman berkaitan sifat semulajadi kars subpermukaan. Bagi menentukan hubungan antara orientasi laluan gua dengan lineamen, selain mengenal pasti retakan utama yang mengawal ciri-ciri kars, pengukuran standard gua dan teknik pengestrakan lineamen Spot yang beresolusi 2.5m- telah digunakan. Begitu juga untuk mengenalpasti pengaruh peningkatan dalam pembangunan sistem kars Lembah Kinta, analisis pembelahan-trek (fission-tracks) apatit dan zirkon telah dijalankan.

Pemetaan di beberapa gua kars telah mendapati bahawa arah laluan gua adalah pada orientasi NNW-SSE. Arah lineamen yang diekstrak dari bukit batu kapur yang terpencil juga menunjukkan arah yang sama. Oleh yang demikian, persamaan orientasi lineamen dan laluan gua membuktikan bahawa pembangunan kars di Lembah Kinta dikawal oleh struktur geologi. Proses pembentukan kars dicirikan oleh beberap episod peningkatan yang telah berlaku sejak Awal Kapur Atas, dengan kadar maksimum 78m/Ma dan minimum 6m/Ma. Purata kadar peningkatan dianggarkan 50.6m/Ma, dan kadar memotong (downcutting) saluran dalam gua adalah sama dengan penurunan aras asas atau kadar peningkatan, maka dapat disimpulkan bahawa proses kehilangan (pelarutan) batu kapur pada kadar yang sama mengambil jangka masa yang panjang untuk berlaku.

Memandangkan asalan kars subpermukaan secara utamanya dipengaruhi oleh proses karstifikasi permukaan, pemahaman mengenai pembangunan kars permukaan

adalah kunci kepada penafsiran kars baural permukaan. Oleh itu, pembangunan dan pembentukan perbukitan kars Lembah Kinta dengan ciri-ciri kars formasi berkaitan yang berlainan menunjukkan dengan jelas bagaimana sistem kars ini boleh berfungsi sebagai analog yang baik untuk mengesahkan sifat sebenar kars subpermukaan yang diterjemahkan daripada bukti secara tidak langsung, contohnya kajian data seismik.

In compliance with the terms of the Copyright Act 1987 and the IP Policy of the university, the copyright of this thesis has been reassigned by the author to the legal entity of the university,

Institute of Technology PETRONAS Sdn Bhd.

Due acknowledgement shall always be made of the use of any material contained in, or derived from, this thesis.

© SOLOMON KASSA, 2013

Institute of Technology PETRONAS Sdn Bhd

All rights reserved.

TABLE OF CONTENT

ABSTRACT.....	vii
ABSTRAK.....	ix
LIST OF FIGURES	xv
LIST OF TABLES.....	xxii
CHAPTER 1 INTRODUCTION	1
1.1 Background.....	1
1.2 Problem statement	3
1.3 Objectives	4
1.4 Study area	5
1.5 Thesis Outline.....	12
CHAPTER 2 LITERATURE REVIEW	15
2.1 Karst.....	15
2.1.1 Karst development.....	17
2.1.1.1 Influence of discontinuities in karst genesis and evolution	18
2.1.1.2 Climate.....	21
2.1.2 Paleokarst	24
2.1.3 Karst denudation	25
2.1.4 Collapse of karst cave.....	27
2.1.5 Karst related reservoirs.....	31
2.2 Kinta Valley karst.....	37
2.3 Tectonic and Geologic Setting.....	40
2.4 Fission Tracks	44
CHAPTER 3 MATERIALS AND METHODS	49
3.1 Cave survey and Mapping	49
3.2 Lineament analysis	52
3.2.1 Image processing and enhancement.....	53
3.2.1.1 Color composite	53
3.2.1.2 Contrast manipulation.....	54
3.2.1.3 Spatial enhancement (filtering).....	55
3.2.2 Digitizing or extraction of the lineaments.....	57

3.3 Measuring paleoflow indicators	58
3.3.1 Scallops	58
3.3.2 Notch Measurement	61
3.4 Rock cooling and associated uplifting rate estimation	61
3.4.1 Sample preparation and analysis process	62
3.4.2 Thermal Modelling.....	65
3.4.3 Approach to estimate the rate of uplift.....	67
CHAPTER 4 RESULTS AND DISCUSSION.....	69
4.1 Results	69
4.1.1 Morphological description of karstic caves	69
4.1.1.1 Gua Kanthan	69
4.1.1.2 Gua Layang Layang.....	72
4.1.1.3 Gua Anak Tempurung.....	74
4.1.1.4 Gua Datok	76
4.1.1.5 Gua Kandu	78
4.1.1.6 Gua Kepayang.....	80
4.1.1.7 Gua Masoora.....	82
4.1.1.8 Gua Tempurung	87
4.1.1.9 Gua Paradise Valley.....	89
4.1.1.10 Gua Naga Mas.....	91
4.1.2 Notch Measurement	92
4.1.3 Scallops	97
4.1.3.1 Gua Sam Poh Tong	97
4.1.3.2 Gua Kepayang.....	99
4.1.3.3 Wat Tat Fook	101
4.1.3.4 Gua Angin.....	102
4.1.3.5 Gua Masoora.....	104
4.1.3.6 Gua Layang Layang	105
4.1.4 Lineament.....	107
4.1.4.1 Gunung Rapat and Gunung Lanno	107
4.1.4.2 Gunung Tempurung and Gunung Panjang	108
4.1.4.3 Gunung Datok.....	110

4.1.5 Apatite and Zircon Fission Track.....	112
4.1.5.1 Cooling history.....	116
4.1.5.2 Uplift Rate.....	119
4.2 Discussion.....	121
4.2.1 Karst development in the Kinta Valley.....	121
4.2.1.1 Factors influencing the development of karst in the Kinta Valley.....	122
4.2.2 Estimation of long term denudation rate and onset of karstification	140
4.2.2.1 Estimated original thickness of the limestone	140
4.2.2.2 Measured denudation rates	141
4.2.2.3 The relation between the granite and the limestone.....	142
4.2.2.4 Fission-track age	142
4.2.3 Nature of subsurface karsts	150
4.2.3.1 Analogue from the Kinta Valley karst.....	150
4.2.3.2 Analogue from tropical karst	153
CHAPTER 5 CONCLUSIONS AND RECOMMENDATIONS.....	159
5.1 Conclusion.....	159
5.2 Recommendations.....	163
5.3 Contributions	163
APPENDIX A CAVE SURVEY MEASUREMENTS	178
APPENDIX B FRACTURES TREND MEASUREMENT	197
APPENDIX C URANIUM-LEAD AND FISSION-TRACK AGE	201
APPENDIX D APATITE FISSION TRACK LENGTH DATA	208

LIST OF FIGURES

Figure 1.1: Location map of the study area indicating (a) the distribution of the major remnant hills mainly in the eastern part of the valley, (b) The Kinta Valley bounded by granite ranges, i.e. Main Range (MR) and Kledang Range (KR), and (c) Peninsular Malaysia..... 7

Figure 1.2: (a) The major Kinta River and its tributaries flowing from the Main Range granite and draining SW via the Kinta Valley karst region, and (b) the distribution of karstic caves formed in the isolated limestone hills..... 8

Figure 1.3: (a) Stalactites at the face of the precipitous hill attest to the pre-existence of a cave before it collapsed, and (b) Horizontally layered fine sediment (red arrow) located before the entrance of Kek Lok Tong Cave indicating the collapse of part of this cave. 10

Figure 1.4: Various relict caves passage morphology depicting their formation in phreatic condition. They are part of the cave (a) Gunung Masoora, (b) Angin in gunung Lanno, (c) Gunung Kapayang, (d) Gunung Lyang Lyang, (e) Wat Tat Fook in gunung Lanno, and (f) Sam Poh Tong in gunung Rapat. 11

Figure 1.5: (a) Image of Gunung Rapat depicting intense pitting with dolines and sinkholes, and (b) One of the remnant hills with a small doline in Gunung Datok..... 13

Figure 2.1: A sketch illustrating the major phenomenon encountered in active karst terrain (Ford and Williams, 2007). 16

Figure 2.2: Stratigraphic column for Western Belt (Metcalf, 2000)..... 23

Figure 2.3: Depicting (a) distribution of stress line around water-filled void, and (b) air filled void after lowering of water table. Note incipient collapses at areas of concentrated stress (Gillieson, 1996)..... 29

Figure 2.4: (a) Sketch showing the parameters of the fixed-beam model (White, 2005). 30

Figure 2.5: Schematic diagram for the development of coalesced, collapsed-paleocave system (Loucks, 1999). 34

Figure 2.6: Seismic section depicting one of the typical circular to subcircular sag structures (McDonnell et al., 2007). 36

Figure 2.7: (a) Horizon semblance map showing a large NNE-SSW trending karst system (Varhrenkamp, 2004), and (b) Cores collected from a well in central Luconia, attest to the occurrence of subsurface karst.	37
Figure 2.8: (a) A cartoon indicating two fission fragments produced by each fission decay event move very rapidly away from each other (courtesy Andrew Gleadow, University of Melbourne), and (b) Illustrates etched FTs in apatite (Galbraith, 2005).	46
Figure 3.1: Instruments used during cave surveying – (a) both clinometer and compass, (b) laser distance meter, (c) measuring tape.....	50
Figure 3.2: A cartoon illustrating how the cave mapping was conducted. ‘Up’ indicates the height from the eye of the surveyor (person 1) to the ceiling, whereas ‘Down’ indicates the height from the eye of the surveyor to the floor of the cave passage. ‘Left’ measurement indicates the width of the passage from the left side of the surveyor, and ‘Right’ indicates the width of the passage from the right side of the surveyor.....	51
Figure 3.3: Displaying the Electromagnetic Spectrum (Lillesand et al., 2004).....	54
Figure 3.4: (a) band 1 (red), band 2 (green) and band 3 (blue), (b) band 3 (red), band 2 (green) and band 1 (blue), (c) band 4 (red), band 3 (green) and band 2 (blue), and (d) band 1 (red), band 3 (green) and band 2 (blue).....	55
Figure 3.5: Examples of Sobel filter (top) and Prewitt filter (bottom) to produce a directionally enhanced image, (a) designed to detect vertically oriented edges; (b) designed to detect horizontally oriented edges, and (c) and (d) designed to detect diagonally oriented edges (Gao, 2008).	57
Figure 3.6: Indicates (a) original image of Gunung Lanno, and (b) NW- SE and (c) NE-SW filtered image of Gunung Lanno.	58
Figure 3.7: Scallops in the cave passage wall of Sam Poh Tong.....	59
Figure 3.8: Mechanism of fluid motion and formation of a scallop (Curl, 1974).	60
Figure 3.9: Displays the profile view of Paradise Valley cave.....	60
Figure 3.10: Map of the Kinta Valley indicating sampling locations marked by yellow circles. The remnant limestone hills are marked by surrounding red line.	64
Figure 3.11: A forward model (a) Before measured AFT data is superimposed, and (b) After AFT data is fitted, but without further varying the t-T path to get the best fit...	66

Figure 3.12: A cartoon illustrating the nature of apatite fission-tracks during cooling and associated uplifting through time	68
Figure 4.1: (a) Map of Gua Kanthan, (b) Graph illustrating the variation of cave passages length at different height from the initial survey point (0 m).	71
Figure 4.2: River flowing inside Gua Kanthan; its gradual lowering left its imprint or notch, which indicates a paleo-waterline.	72
Figure 4.3: (a) Map of Gua Layang Layang with an inset rose diagram indicating the prominent passage trend, and (b) Illustrates the variation of cave passage lengths at different heights from the initial survey point (0 m).....	73
Figure 4.4: (A) Map of Gua Anak Tempurung, and (b) Illustrates the variation of cave passages length at different height from the initial survey point (0 m).	75
Figure 4.5: (a) Map of Gua Datok, (b) Variation of cave passage length at different height from the initial survey point (0 m).	77
Figure 4.6: Openings along a fracture line, possibly indicating continuity of Gua Datok passage along a fault or fracture trend.	78
Figure 4.7: Map of Gua Kandu and associated inset rose diagram indicating the multi-layered passages orientations, (b) Variation of cave passages length at different height.....	79
Figure 4.8: 3D view of Gua Kandu.....	80
Figure 4.9: (a) Map of Gua Kepayang, and (b) Variation of cave passages length at different height from the initial survey point (0 m).	81
Figure 4.10: (a) Map of Gua Masoora 1, and (b) Indicates variation of cave passages length at different height from the initial survey point (0 m).	83
Figure 4.11: Pictures illustrating (a) Thick sediment deposit inside Gua Masoora1, (b) Stalactites and columns formed along the direction of fracture trace, (c) Expansive void separated by columns, which were possibly formed along a fracture, and filled with sediment.	84
Figure 4.12: Dissolution features that may provide clues for the origin and gradual development of Gua Masoora1.....	85
Figure 4.13: Map of Gua Masoora2.....	86
Figure 4.14: (a) The Kinta Valley bounded by granite, and the yellow circle marks Gunung Tempurung, close to the Main Range granite, (b) The lower level of Gua	

Tempurung formed by the sinuous extant river flow, (c) Variation of cave passage lengths at different heights from the initial survey point (0 m). 88

Figure 4.15: River entering into the big chamber before disappearing via a narrow conduit, and (e) A chamber that characterize the upper part of Gua Tempurung. 89

Figure 4.16: (a) Map of Gua Paradise Valley and inset rose diagram indicating the prominent cave passage trend, (b) Variation of cave passage lengths at different heights from the initial survey point (0 m). 90

Figure 4.17: Showing map of Gua Nega Mas..... 91

Figure 4.18: (a) Weathered granite viewed from the entrance of gua Nega Mas, and (b) Mud covered ceiling of a small chamber with noticeable fossil bones embedded on it. 92

Figure 4.19: (a) Variation of notches height from southern part of the study area all the way to the north, and (b) Illustrates notches distribution with respect to base of hills increasing elevations a.s.l..... 94

Figure 4.20: Types of multi-layered notches that can be observed in different parts of the Kinta Valley on vertical cliffs. Pictures from (a) to (c) were taken in different parts of Gunung Datok..... 95

Figure 4.21: Pictures indicating types of multi-layered notches taken (a) at Gunung Datok, and (b) to (d) at Gunung Rapat. 96

Figure 4.22: Pictures showing scallops pattern at Sam Poh Tong Cave, (a) The lower level being zoomed, (b) Zoomed scallops on the ceiling..... 98

Figure 4.23: Map of paleoflow trend (red arrow) and flow orientation in river caves (black arrow), and the general SW flowing river trend. 99

Figure 4.24: Scallops pattern (a) on the wall and (b) on the ceiling of Gua Kapayang 100

Figure 4.25: (a) Shows a conduit with thick sediment deposit and linear stalactite formation oriented in the same direction as the conduits in Gua Wat Tat Fook, and (b) Lower and upper level of scallops' pattern, in a small chamber facing the highest level of the cave entrance. 102

Figure 4.26: Picture showing sediment deposits in the conduit of Gua Angin..... 103

Figure 4.27: Pictures indicating (a) large and (b) small width scallops in Gua Masoora 105

Figure 4.28: Pictures indicating large width scallops (a) at the chamber wall, and (b) at the narrow conduits of Layang Layang.....	106
Figure 4.29: lineaments extracted from (a) Gunung Rapat, and (b) Gunung Lanno. The rose diagrams indicate the lineaments trend.....	108
Figure 4.30: Lineaments extracted from Gunung Tempurung. The rose diagram indicates the lineaments trend.....	109
Figure 4.31: Lineaments extracted from Gunung Panjang.....	110
Figure 4.32: Lineaments extracted from Gunung Datok.....	111
Figure 4.33: (a) Showing conjugate sets of fractures in an outcrop in Gunung Datok, and (b) Indicating the distribution of the major hills in the Kinta Valley with the associated inset rose diagram depicting the overall fracture distribution.....	112
Figure 4.34: Illustrating similar variation of fission-track ages and elevation.....	114
Figure 4.35: Graphs illustrating UPb age vs. FT age in zircon for the respective Samples. The UPb age indicates the time of granite emplacement around 215 Ma..	115
Figure 4.36: Inversion model of time-temperature history for Sample CH-6. It is based on 20, 000 time-temperature paths generated by a Montecarlo Method.....	116
Figure 4.37: Inversion model of time-temperature paths depicting the cooling history of Sample CH-7. It is based on 20, 000 t-T paths generated by a Montecarlo Method.....	117
Figure 4.38: Inversion model of time-temperature history for Sample CH-8. It is based on 20, 000 time-temperature paths generated by a Montecarlo Method.....	118
Figure 4.39: Inversion model of time-temperature history for Sample CH-9. It is based on 20, 000 time-temperature paths generated by a Montecarlo Method.....	118
Figure 4.40: Graph displaying variation of uplift rate from the Upper Cretaceous to the Lower Miocene.....	120
Figure 4.41: Formation of karst via an almost vertically dipping bed (a), and along a fracture (b).....	123
Figure 4.42: Rose diagrams showing (a) all fractures trends extracted from the remnant hills, and (b) the prominent caves passages trend obtained from different karstic caves formed in the vestige limestone hills.....	124

Figure 4.43: (a) Showing visible fractures (red line) on the surface of a doline, (b) Showing intersecting fractures further inside the doline, and (c) Illustrates after the intersection in (b) is zoomed out..... 126

Figure 4.44: Schematic diagram showing (a) Extension and conjugate fractures, and (b) Ideal relationship between major joint sets in a folded bed (modified from Singhal and Gupta, 2010)..... 127

Figure 4.45: Displays a slope map of Gunung Tempurung after the Spot image is overlain on it. The inset cross-section, for the yellow line at the base of the hill, indicates stepping which marks gradual uplifting. Gua Tempurung, whose development through time is influenced by uplift is located within the box..... 130

Figure 4.46: Picture of a doline and multiple notch patterns on the precipitous wall of the doline..... 133

Figure 4.47: Schematic diagram showing the mechanism of rock breakdown and associated tension dome formation. As collapse of ceiling rock persists, individual chambers in a single cave passage coalesce to form a big chamber (red dot line) (modified from White, 2005)..... 134

Figure 4.48: Picture (a) and (b) indicating deep corrosion grooves formed at the base of the hill in Gua Masoora; the undercut in picture ‘b’ is situated further deep inside this cave, and (c) indicates deep undercut in Gunung Kanthan..... 136

Figure 4.49: Global sea-level model for Cenozoic (after Haq et al., 1987)..... 138

Figure 4.50: Displaying present day sea-level with respect to the Kinta Valley karst region, assuming an increase of the water level & its possible extent towards the valley after (a) sea-level (0 m), (b) 20m, (c) 40m, and (d) 60m. The inset box indicates 3D view display and water level..... 139

Figure 4.51: A cartoon illustrating the t-T relationship as the four samples (CH-6 to 10) are undergoing gradual cooling while they are uplifted from 97.5Ma onward, marked by zircon fission-track age..... 145

Figure 4.52: Simple sketch depicting the possible thickness of unroofed rock since 97.5 Ma, taking into account the estimated uplift rate is equivalent to the downcutting rate for the corresponding time range. 146

Figure 4.53: Simple sketch depicting the emplacement of Sample CH-6 and CH-8 at different time with corresponding closure temperatures. 147

Figure 4.54: Graphs displaying uplift rate variation and estimated thickness of rock unroofed from the surface, for the corresponding time range, (a) since 97.5Ma, and (b) since 75.5Ma. 148

Figure 4.55: Profile of the largest sections of cave passage in the world (a) Caves of southern Mulu, Sarawak, (b) Hang Son Doong, Vietnam (both caves drawn at the same scale) (<http://www.mulucaves.org>), and (c) Combined caves system profile along the axis of the Ortobalagan valley (Klimchouk et al., 2009). 156

Figure 4.56: Shows (a) Paleocave facies classification (Loucks et al., 2004), and ... 158

LIST OF TABLES

Table 4.1: Measurements collected during the survey of Gua Kanthan	70
Table 4.2: Location of notches and elevation (a.s.l.) of the area, where the maximum level (height) of the notches above the base of the hills were measured.	93
Table 4.3: Summary of Apatite and Zircon fission track data.....	113
Table 4.4: Apatite fission track length data	114
Table 4.5: Measured and modeled FT age and length in the inverse models.....	114
Table 4.6: Approximate thickness of the carbonate rock for the respective time range and associated uplift rate.....	144
Table 4.7: Concise summary of the contemporaneous processes which have been taking place both under and on the surface, since the Triassic period.....	149

CHAPTER 1

INTRODUCTION

1.1 Background

Karst is a special type of landform that occurs in soluble rocks and is characterized by numerous dissolutional features. The study area, the Kinta Valley, is bounded by granites, and is characterized by relict limestone hills which stand out above the alluvium deposit that covers the valley. The extensive dissolution of the carbonate rock in the Kinta Valley is typified by various karstic features, such as tower karst, limestone hills pitted with dolines and honeycombed with caves, collapsed caves, caverns, and pinnacles, in some places. The vestige hills host karst caves of various dimensions that extend up to 1.5 km in length, and chamber width and height that reach up to 60 m and 80m. In general, the vestige limestone hills in the Kinta Valley seem to be aligned in the same orientation as the peninsula, and this karst landform occupies about 25 km², whereas the Valley, which once was covered by the expansive limestone bedrock, covers approximately 996 km². The 2.5% areal coverage of the remnant hills may attest to the fact that this karst region is at an extremely mature stage of karstification.

In many places around the world, karst systems appear to form complex landforms, as the prominent factors responsible for their origin vary (Ford and Williams, 2007). The Kinta Valley karst system is one-of-a-kind and is characterized by very typical dissolutional features that can exemplify a matured karst system. Such karst features are important to comprehend the development of a karst system through time, and to enhance the knowledge of how a contact karst system responds differently to denudational processes, unlike other karst systems of different origin. The unique morphology of the Kinta Valley karst features has led some workers to

suggest a number of explanations about their possible origin. Among the various hypotheses put forward by previous workers (Ingham and Bradford, 1960; Paton, 1964; Gillieson, 2005), factors including the influence of sea-level rise, block faulting, subaerial erosion, folding, and **local ponding behind mudflow deposits** are presumed to be responsible for the occurrence of the limestone hills and associated karst features.

Karstification occurs in different types of carbonate rocks. Limestone karst is the most extensively developed, with the broadest regional extent, the most elaborate and highly integrated underground drainage and cave systems (White and Deike, 1989). Nowadays, the various karst features and their dimensions, in all climatic zones, are well documented. And this knowledge might have led many workers to infer the presence of subsurface karst features to be a direct replica of surface karst. Although it will not be appropriate to completely rule out the possibility of having the same dimensions of karst features in the subsurface, general inference of their similarity merely from the well known karst morphology and scale may lead to erroneous conclusions. If large scale modern karst features are well scrutinized, one can possibly get differences among them in terms of conduits pattern, dimensions and mode of genesis, although their features appear similar. Subsurface karst features, interpreted from indirect measurements, may therefore not necessarily be a carbon copy of surface karst features.

Subsurface karst or paleokarst can be seen or interpreted on seismic (Castillo and Mann, 2006; Evans et al., 1994). Pervasive network of karst channels and collapsed cave features were interpreted from 3D seismic in Vahrenkamp et al. (2004), and subcircular features, 600m wide, were interpreted as sinkholes in Castillo and Mann (2006). Similarly, they interpreted discontinuous and truncated surfaces as the expression of regional paleokarst horizons. Many workers, including Kerans (1988), Loucks (1999), Wang and Al-Aasm (2002), to mention a few, indicated subsurface karsts as good reservoirs. The works of Loucks (1999; 2007) and Loucks et al. (2004) elaborated on reservoirs of paleocave origin which are the product of coalesced collapsed-paleocave systems. Similarly, Luo et al. (2012) indicated a paleocave origin for reservoirs in the Tarim basin (China) with further emphasis on the existence of a

multi-level cave system. Therefore, since it is very likely that paleocave systems had a subaerial origin, detail mapping of a surface cave system will provide a good analogue to the subsurface ones.

The working hypothesis in this study is that studying a subaerial karst system, including its mode of formation, the factors controlling its development, its dimensions, mapping its overall pattern, and how its morphology changed if it was subjected to burial, will be key to unravel the possible nature of subsurface karsts and will provide tools to gauge the validity of interpretations to be made from other evidence.

1.2 Problem statement

Karst landform is complex by nature, and its study has been going on for decades in different parts of the world. Despite the continuous study, there are many karst systems, from different climatic regions and topographic settings, whose origin and evolution needs to be further understood. The Kinta Valley contact karst system can be considered as one of the peculiar tropical karst systems. The study of this unique karst region has received little attention, mostly limited to simple outcrop observation and hypothesis on its formation, fracture analysis and short-term dissolution rate measurements. However, the prominent factors responsible for the development of karst in the area have been overlooked by previous workers, and those considered factors were not studied in detail. Thus, further study of such unique karst enables to comprehend the history of its developments and to unravel the factors which mainly control its gradual evolution. Furthermore, the study will address the following research questions that highlight the importance of studying the Kinta Valley karst system. These include, (1) as the Kinta Valley is characterized by isolated limestone hills, is there any karst feature or other evidence that may lead to infer the continuity of the original carbonate terrain? (2) does the Kinta Valley karst system prominently manifests itself as the consequence of local or regional processes? (3) what is the role of the adjoining granite at the onset and gradual development of karst in the area?

(4) among the various factors that control the origin of karst, which factor(s) dominate(s) in the Kinta Valley, and what are the clues to infer that?

Karst features, which once formed in subaerial conditions, may happen to be subjected to burial, as a consequence of geologic and/or tectonic processes, to form paleokarst. The existence of such subsurface karsts is usually inferred from indirect evidence, such as drilling operations and seismic data. Although features consistent with the scale and dimensions of subaerial karsts can be observed and interpreted from seismic data, a direct correlation or comparison is not always possible. And the erroneous interpretation of subsurface karsts cannot be alleviated unless their history of subaerial origin and development is well scrutinized. Thus, mapping the subaerial karst system in the Kinta Valley and analyzing its development would provide a useful analogue to determine uncertainties about the true nature of subsurface karst features, and to show how subaerial karst features would appear if they were subjected to burial.

1.3 Objectives

The major objectives of the study are:

- To determine how various factors controlled the development of karst in the Kinta Valley.
- To illustrate how the morphology and dimensions of subaerial karsts can be used to understand the nature of subsurface karsts, and to generate maps of different karstic caves.

The specific objectives include:

- To extract evidence from the remnant limestone hills and associated karst features to indicate the principal factor that controls the origin of karst in the area.
- To comprehend the prime factors responsible for the gradual change of the karst system.
- To depict the possible change in dimensions of subaerial karst features after burial.

- To find out the most likely period for the commencement of karstification in the Kinta Valley.
- To illustrate the paleoflow trend and pinpoint the relation between the paleoflow direction in the relict karstic caves and the current hydrologic system.
- To show how the geologic structures relate to the karst features.
- To show the influence of the adjoining granite in the formation of various types of karst features.

1.4 Study area

Peninsular Malaysia is located between 1°20'N to 6°40'N latitude and 99°35'E to 104°20'E longitude. The study area, the Kinta Valley, is situated in the western part of Peninsular Malaysia (Fig.1.1). It is bordered by two granitic ranges; the Kledang Range (KR) and the Main Range (MR) in the west and east, respectively, and is characterized by remnant hills which steeply stand out of the alluvium deposit that covers the valley. According to Geyer et al. (2005), some 47 steep isolated limestone hills that can rise up to 600 m are present in the area. These hills (Fig.1.1), which are the vestiges of an expansive limestone bedrock that has been dissolved and eroded away, are located mainly in the eastern part of the valley.

The Kinta Valley has an elongated shape which is about 50 km long and 8-21 km wide; the valley widens towards the south. The limestone hills which dot the valley are presumed to be of Carboniferous-Permian age (Ingham and Bradford, 1960 and reference therein) or Silurian to Permian (Suntharalingam, 1968; Woon, 1991 and reference therein), and are at an extreme stage of karstification as typified by the vestige hills and associated karst features.

The extensive dissolution of the carbonate rock in the Kinta Valley has led to the development of the extant karst features of the area. This is the result of both allogenic waters, derived from the adjoining granite hills, and autogenic waters, originated from percolating rainwater. Many rivers flow from the bounding Main Range granite and drain southwest via the Kinta Valley karst region, including the

Raya River, the Pari River, the Penjih River, the Dipang River and the Kampar River (Fig.1.2a), which might have played a crucial role in the development of the extant karst morphology of the area. Because of the tremendous dissection caused by these rivers, the western part of the area is typified by very isolated tower karsts with caves formed at the foot of these towers, compared to the eastern part which is characterized by relict caves occurring, in most places, 10-15 m, above their base. At the base of the steep-sided hills, horizontal grooves or notches which might have been formed by ground water or river action or stagnant swamps are noticeable.

The caves located in the vestige hills are very small, about 60 m to 1.5 km long, and are characterized by relatively big chambers, 30-60 m wide and up to 80 m high. Most of the cave chambers appear to be part of a previously long cave network before collapse, as the massive stalactites hanging on the faces of the precipitous hills (for example, Fig.1.3a) suggest. These stalactites are very stiff and grew vertically, unlike those which form on the surface, i.e. after collapse. Cave infilling sediments (Fig.1.3b), which are the same as those observed inside the adjoining uncollapsed caves, are conspicuous. This attests to the pre-existence of long cave networks, which could be kilometers long, in the area.

There are two typical end members of isolated caves: chamber and maze caves. Caves which are considered as chamber caves possess low passage density and their length to width ratio (L/W) is $1 < L/W < 20$, whereas maze caves have characteristic elongated passages, with $20 < L/W < 100$ for short passages and $L/W > 100$ for longer ones (Frumkin and Fischhendler, 2005). The morphology of most of the relict caves in the Kinta Valley indicates that the average length to width ratio lies within $1 < L/W < 20$; hence, they can be considered as chamber caves. Similarly, the isolated caves in the Kinta Valley also possess characteristic features that make them belong to chamber caves, such as phreatic morphology of the cave wall and roof (Fig.1.4), profusion of speleothems, and dome shape rising upward from the cave ceiling. These features are different from what maze caves indicate (Frumkin and Fischhendler, 2005).

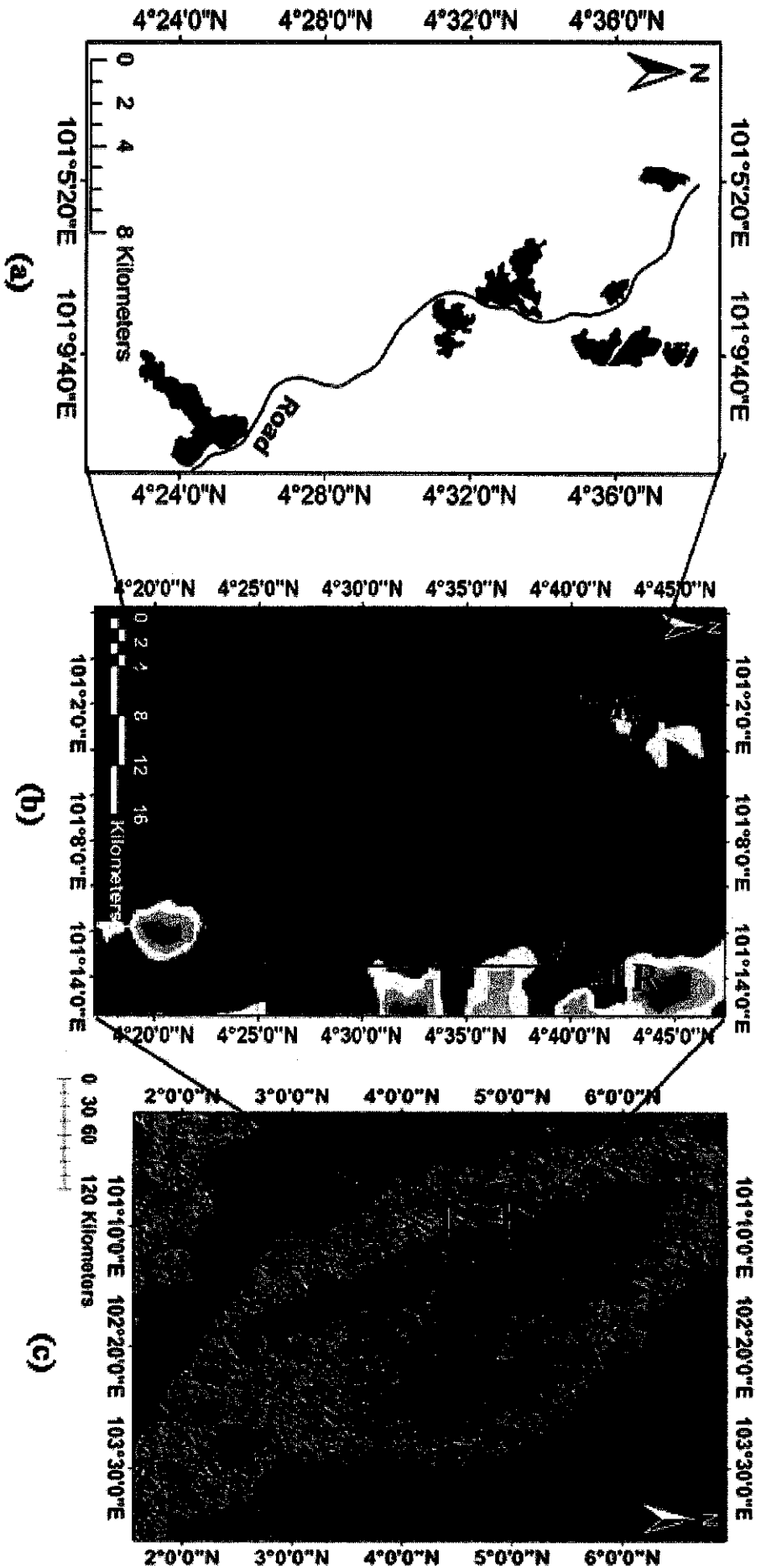
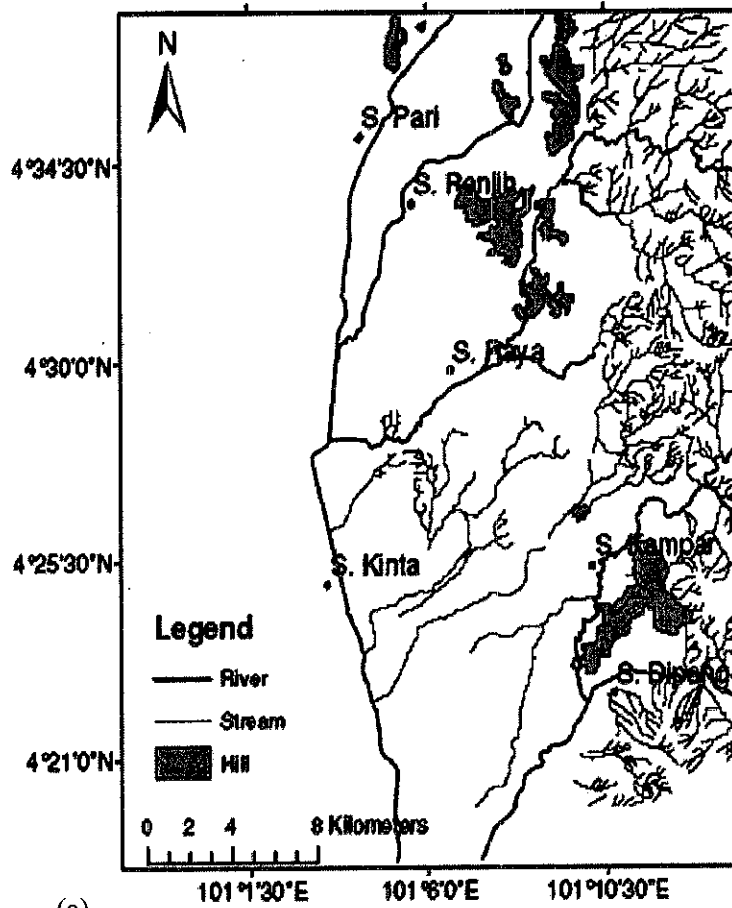
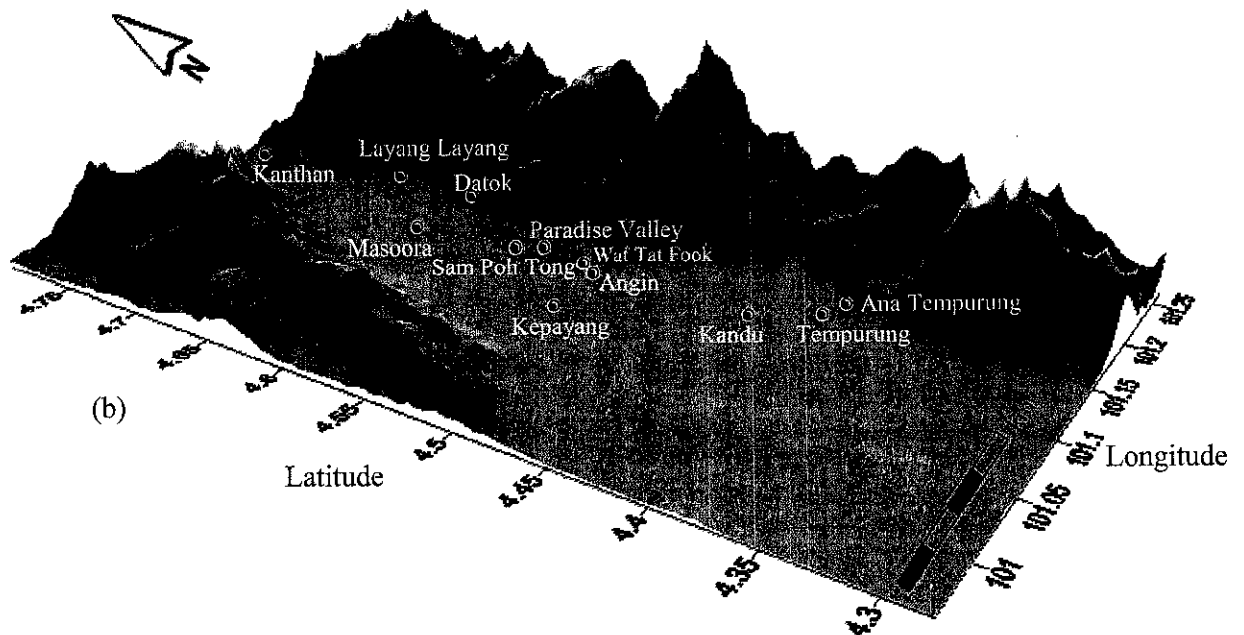


Figure 1.1: Location map of the study area indicating (a) the distribution of the major remnant hills mainly in the eastern part of the valley, (b) The Kinta Valley bounded by granite ranges, i.e. Main Range (MR) and Kledang Range (KR), and (c) Peninsular Malaysia.



(a)



(b)

Figure 1.2: (a) The major Kinta River and its tributaries flowing from the Main Range granite and draining SW via the Kinta Valley karst region, and (b) the distribution of karstic caves formed in the isolated limestone hills.

In the study area, the karstic caves are of two types: (i) Relict Caves, which are related to an earlier hydrologic system, and are relatively very small compared to (ii) Modern (River) Caves. The morphology of most of the surveyed relict caves suggests a formation in phreatic conditions (Fig.1.4), as the smooth wall and ceiling, and the circular to oval shape of the passages suggest. Their linear trend seems to be a result of primary conduit development via fractures. The morphology of the cave passages, besides illustrating their formation in phreatic conditions, clearly indicates their dimensions change by running waters, as sediments deposited along the passages are conspicuous.

Ceiling pockets or cupolas of various dimensions, which might have been formed by mixing corrosion (Ford and Williams, 2007), are common in many caves of the area, and the existence of these features may indicate the occurrence of dissolution near the water table of the phreatic zone. The occurrence of the ceiling pockets, in most caves, on average 20-25m above the floor of the caves, may show a gradual lowering of the base level through time.

Collapsed caves, caves with different passage levels, hills pitted with dolines (Fig. 1.5a), isolated hills with small dolines (Fig. 1.5b), and hills honeycombed with caves (for example in one hill 'Gunung Lanno', 32 caves were surveyed by (Geyer et al., 2005), are characteristic karstic features of the study area. Small caves characterized by collapsed passages are common, and relatively narrow and linear caves are also evident in the area.

In general, the distribution of the small and isolated limestone hills, which host all disolutional features, in the Kinta Valley appears to have almost the same orientation as the overall direction of the peninsula, when they are observed from topographic map or satellite imageries.

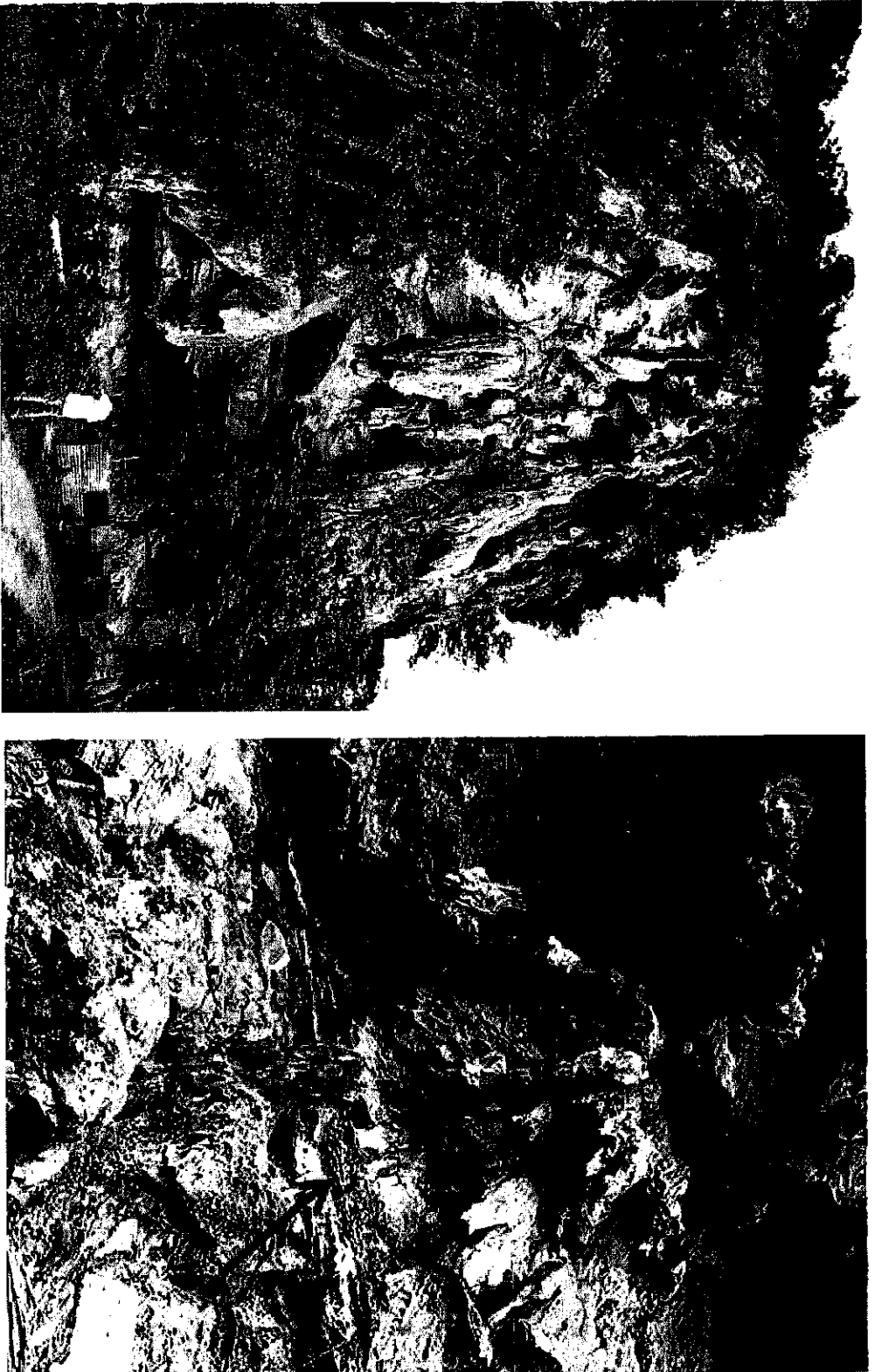


Figure 1.3: (a) Stalactites at the face of the precipitous hill attest to the pre-existence of a cave before it collapsed, and (b) Horizontally layered fine sediment (red arrow) located before the entrance of Kek Lok Tong Cave indicating the collapse of part of this cave.

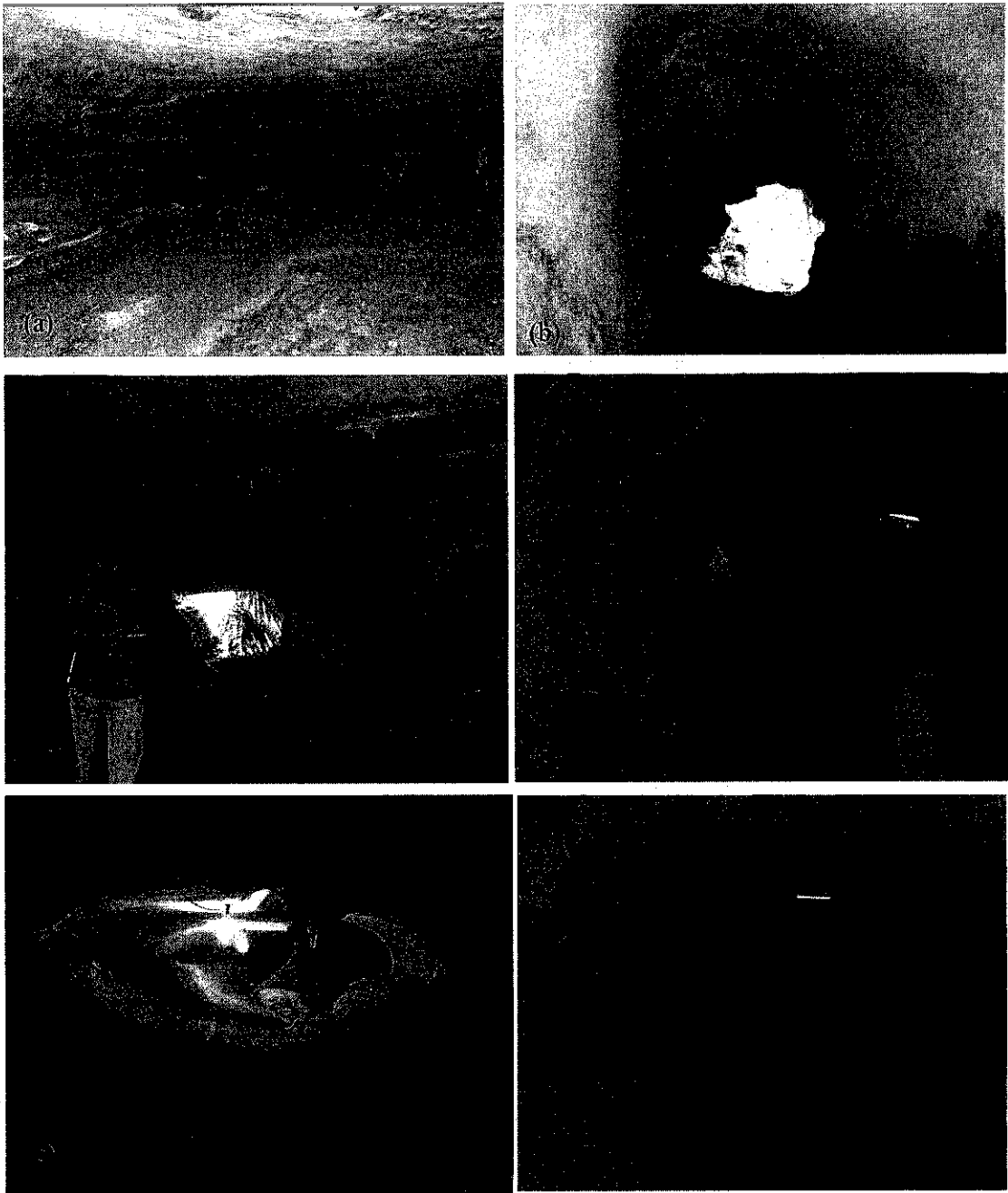


Figure 1.4: Various relict caves passage morphology depicting their formation in phreatic condition. They are part of the cave (a) Gunung Masoora, (b) Angin in gunung Lanno, (c) Gunung Kapayang, (d) Gunung Lyang Lyang, (e) Wat Tat Fook in gunung Lanno, and (f) Sam Poh Tong in gunung Rapat.

1.5 Thesis Outline

This thesis contains five chapters. The first chapter, “introduction”, includes background of the study, problem statement of the research, objectives and description of the study area. The second chapter, “literature survey”, includes related works that have been done in relation to the research problem to be dealt with, and summarizes on the state of the art of the subject. Chapter three deals with the method employed to achieve those objectives described in Chapter One. Chapter Four is dedicated to the description of the results and associated discussion. Finally, the summary of the work or conclusion and recommendations for further studies are described under Chapter Five.

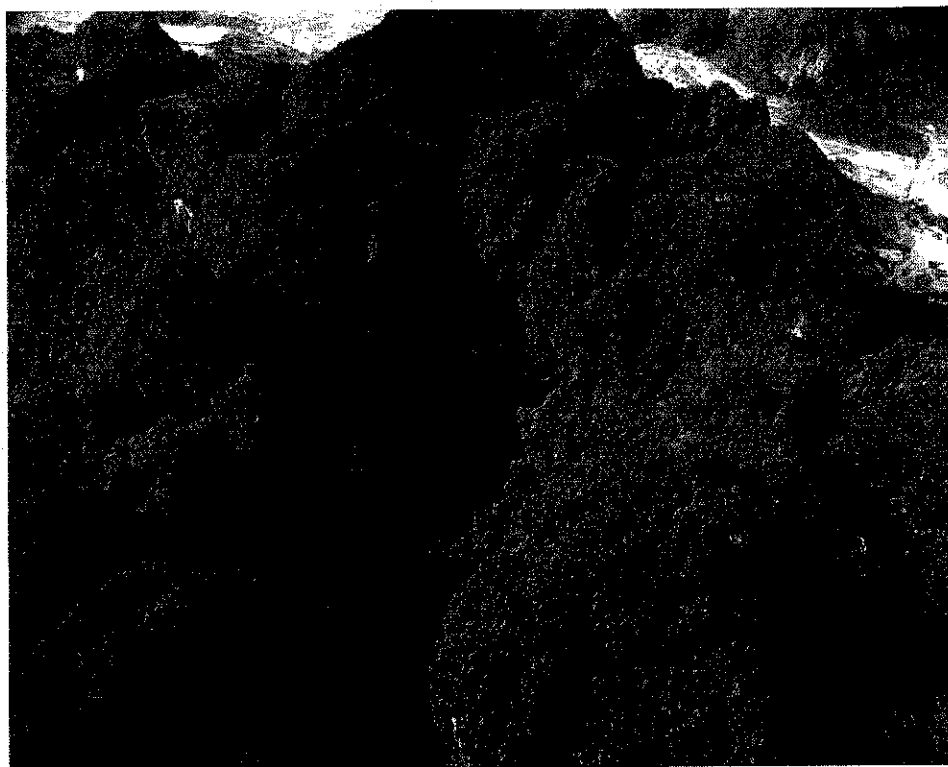
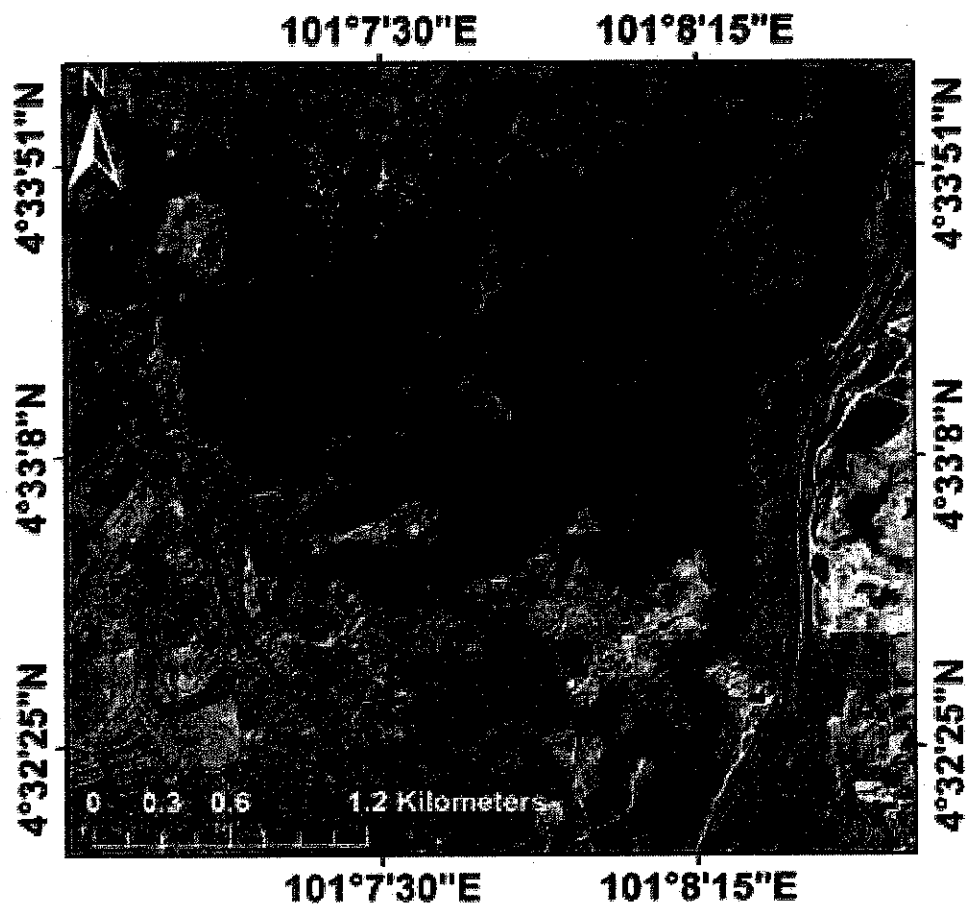


Figure 1.5: (a) Image of Gunung Rapat depicting intense pitting with dolines and sinkholes, and (b) One of the remnant hills with a small doline in Gunung Datok.

CHAPTER 2

LITERATURE REVIEW

2.1 Karst

Karst landform is a distinct environment characterized by dissolution features occurring in soluble rocks such as limestone, marble and gypsum, and contains caves and extensive, complex underground water systems (Ford and Williams, 2007). Karst is a variant of the fluvial geomorphic system; when fully developed, the karst system has three morphological components: input landforms that direct water underground, subterranean conduit systems, and discharge areas (Ford et al., 1988). Limestone karst is the most extensively developed, with the broadest regional extent, and the most elaborate and highly integrated underground drainage and cave systems (White and White, 1989). The scale of karst features ranges from minute cracks and fissures to large conduits and channels, and extensive cave systems that drain hundreds of square kilometers (Ford and Williams, 2007). Karst landscapes are the result of a complex interplay of geology, climate, topography, hydrology, and biological factors. The level of karst landscape evolution depends particularly on (1) the intensity of dissolution and (2) the period of time that the bedrock remained emergent (Bosák, 2008).

There are two major types of karst systems: Hypogenic Karst, originating from depth and not related to recharge from the overlying surface, and Epigenic Karst, formed by water infiltrating or in-flowing from overlying or immediately adjacent recharge surfaces and developed in genetic relation to landscape (Hill, 2000; Klimchouk, 2009), and they are associated with different types, patterns and segments of flow systems.

Karst can be viewed as an open system composed of two closely integrated hydrological and geochemical subsystems operating upon the karstic rocks (Ford and Williams, 2007), and caves are considered as a measure of the intensity and persistence of the karst process (Gillieson, 1996).

In general, the term 'karst' is applied to all carbonate dissolutional features which are the consequence of mainly chemical processes. Solution of carbonate rocks can occur under two contrasting situations: (i) an open system, where carbon dioxide gas, percolation water and calcite-rich rock are continuously in contact (Ford et al., 1988; Gillieson, 1996), (ii) closed system, where the aqueous solution has an initial concentration of CO₂ that reacts with the solid phase and the depleted carbonic acid cannot be replaced, and the amount of solution achieved at equilibrium is much reduced (Ford et al., 1988). Thus, any percolating water in contact with the limestone will gradually reach saturation, beyond which no more dissociation of the rock will occur unless conditions change. However, one way in which this may occur is if two bodies of saturated water mix, as they may do at tributary junctions in a cave or below the water table in the phreatic zone (Gillieson, 1996). It is indicated in Ford et al. (1988) and Ford and Williams (2007) that initiation and early expansion of dissolutional conduits in the rock will almost always occur when ideal open-system conditions prevail.

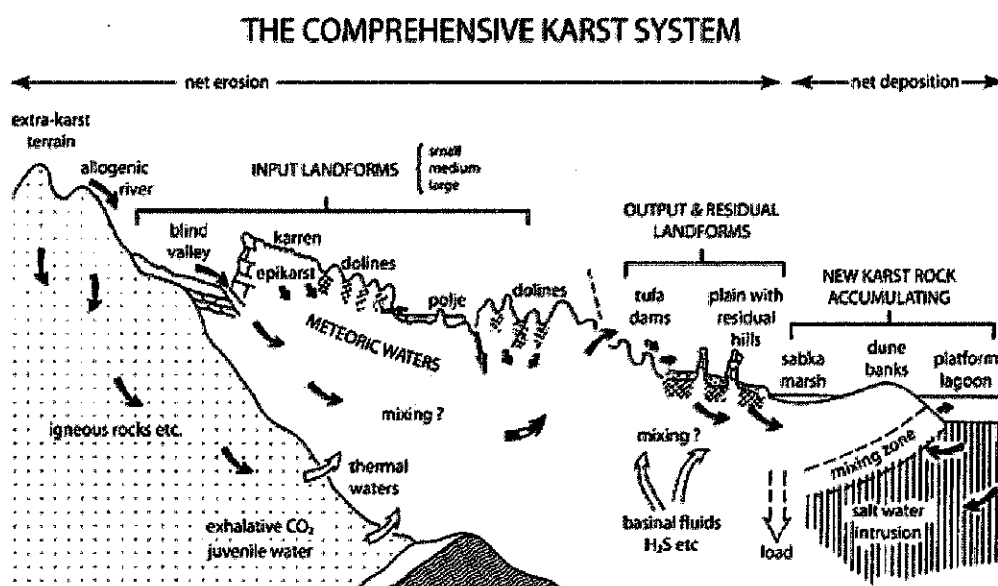


Figure 2.1: A sketch illustrating the major phenomenon encountered in active karst terrain (Ford and Williams, 2007).

Whenever a rock–water system is out of equilibrium, dissolution will take place, as the water will be undersaturated with respect to CaCO_3 . A continuous supply of undersaturated water will make the dissolution process continuous until the water becomes saturated, a point where dissolution stops. Thus, such dissolutional process creates karst features, such as caverns and sinkholes, and similarly may enlarge pores to form molds and vugs (Ford and Williams, 2007).

2.1.1 Karst development

Whenever carbonate platforms are subaerially exposed, karst development occurs. The exposure can be the result of eustatic or local (tectonic) sea-level change (Myloie and Carew, 2003). Karstification is a complex process, as it is difficult to establish clear and quantifiable relations between its various components: calcite dissolution, surface runoff and groundwater flow (Fleurant et al., 2008). Karstification of the host rocks may start during their formation phases – diagenesis – converting the soft sediment into consolidated material shortly after deposition itself (Bosák, 2008). Further, this work indicated that karstification is a result of the emergence of part of a depocenter (sedimentary basin) and the introduction of meteoric water into the diagenetic system.

There are various factors that contribute to the diversity of forms and development of karst, namely geological structure and tectonic history, climate, relief, geomorphic history and lithology (Ford et al., 1988). A single or a combination, usually the case, of these factors may dominate in a certain area. The two important processes that are responsible for karst development are mechanical and chemical denudational processes (Ford and Williams, 2007). These processes may have equal impact on the karstification processes or one may dominate depending on the aforementioned controlling factors. Development of karst differs when the area is subjected to allogenic and autogenic recharge (Reeder et al., 1996). On exposed carbonate platforms that have only autogenic recharge, the dominant karst landforms are closed depressions and caves (Myloie and Carew, 2003).

Karst areas with large inputs of allogenic water experience more chemical erosion than areas entirely recharged by autogenic water, with the size of the catchment area contributing allogenic recharge greatly influencing the rate of solution (Reeder et al., 1996). Further, the influence of allogenic waters, in the development of mainly positive karst landforms, arises when the carbonate terrains are subjected to uplifting, as it enhances the denudational power of the running waters. Such kind of karst system, where water flowing from adjoining uplifted insoluble terrains creates exceptionally high densities or large sizes of landforms along the geological contact with the soluble strata, and known as contact karst (Ford and Williams, 2007).

Before the development of main karst conduits, flow may take place along several fissures, and the first route enlarge the conduit dimension and capture most of the flow (Ford, 2003); hence, the developed karst system is typified by well organized conduit flow and the diminishing of the importance of diffuse flow in the karst water circulation (Glazek, 1989).

2.1.1.1 Influence of discontinuities in karst genesis and evolution

Previously various hypotheses about the genesis of karstic caves have been advocated by a certain group of workers or others, including vadose, phreatic and water-table hypothesis. It is indicated in Ford (2003) that these differing hypotheses can be reconciled by a fourth state model, which illustrates the frequency of penetrable fissuration controlling the system geometry.

According to Bosák (2008) and reference therein, there are three generally accepted phases of speleogenesis: (1) initiation: a fracture initially enlarged to a critical size; (2) breakthrough: a sudden transition to rapid dissolution, which results in the growth of an incipient cave into a true cave, and (3) enlargement: the growth of an incipient cave to full conduit size. In the case of metamorphosed carbonate, only open fracture routes provide the opportunity for dissolution and enlargement into cave passages (Faulkner, 2006) as the metamorphic process leads to the destruction of primary sedimentary structures which are important targets for speleogenesis (Ford and Williams, 2007). However, void development is considered pre-tectonic, as it is

avored along inception horizons and commences during diagenesis (Lowe, 1999). Faulkner (2006) indicated that the solutional karst caves of the Caledonide marbles were initiated by tectonic inception, in contrast to inception horizons (Lowe, 1999), as the metamorphosed carbonate is typified by the lack of (1) primary porosity, (2) stratigraphic horizons, and (3) regional-scale systems.

The role of fractures, joints and faults has been taken into consideration for karst genesis. However, further emphasis has also been given for the hydrogeological importance of bedding planes as a key opening for groundwater flow and conduit development in the karst terrains (Bakalowicz, 2006 and references therein; Marco and Pierre-Yves, 2008). The difference between these discontinuities is that major bedding planes are considered to be continuous entities when solution caves are propagating through them, whereas penetrable joints and most faults are discrete, which enhances the significance of bedding planes in cave genesis (Ford and Williams, 2007).

According to Bakalowicz (2006) and references therein, conceptual approaches considered that surface and underground karst features develop following an original fracture network, i.e. the main faults bear principal conduits and large karst landscape features, whereas second order fractures bear the secondary conduits and small surface terrains. Flow paths in karst are developed preferentially along fault zones, joints and bedding planes, as they host and guide almost all parts of the underground solution conduit networks that distinguish the karst system from all others (Ford and Williams, 2007), and tectonic structures, in general, are considered invaluable for the development of karst (Glazek, 1989).

The relation between structures and caves development has previously been indicated by Deike (1969), Palmer (1975), Reeder et al. (1996), and Florea (2002). The distribution and geometry of structures control the original solutional shapes of the natural drainpipes that make up the conduit system (White and Deike, 1989). Similarly, evidences that may attest to the influence of fracture traces in controlling the orientation and location of karst features such as dolines are documented in Deike (1989). Ford (2003) indicated that the locus of main karst cave depends upon the

distribution and orientation of whichever fissures happen to be the most penetrable by groundwaters, which also efficiently directs towards potential discharge points.

It is indicated in Bakalowicz (2006) and references therein that the trend of fracture opening is the potential flow path direction that karst processes use for developing conduits, and joints and faults are considered as the main openings, making all hardened rocks permeable to water, and are responsible for the potential vertical and horizontal hydraulic continuity. Gabrovšek and Dreybrodt (2010) presented a model which couples flow in the fractures with dissolution rates. The model describes the evolution of karstification by dissolutional widening of the fractures downgradient from the local input of surface water. They indicated that mixed corrosion, which proceeds on time scales of 100 ka, a sufficient time to create a conduit of 100 m length and a width of about 1 cm, is an important control on karstification of karst plains.

According to Jameson (2006), in order to study conduit evolution, structural segments should be identified and analyzed. He stated some primary conditions that should be fulfilled to identify early fracture conduits: (1) main fractures should be retained as fracture traces within the perimeters of bed rock passage, (2) fracture traces must be accessible within the cave and there has to be minimal covering, and (3) fracturing occurring with later cave enlargement has to be minimal and distinguishable from those pre-existing fractures. Although various works clearly indicated the significant influence of tectonic structures in the development of karst, tectonic interpretations of paleokarst features, according to Glazek (1989), it is extremely difficult to correlate many ancient karst phenomena with particular tectonic stages. A number of works cited in Glazek (1989) indicated the various scales of karstification and their differing relationships to the tectonic processes and cycles. Nonetheless, in a different perspective, it is hypothesized in this study that knowing the principal factors that control the karst features is quite invaluable to relate karstification phenomenon with most likely periods of tectonic episodes.

2.1.1.2 Climate

As karstification process depends on the availability of water, climate plays a crucial role in controlling the development of karst. That is, whenever dry conditions prevail it is inevitable that the dissolution process diminishes or comes to a latent stage. This is not only influenced by the absence of water, but also the lowering of soil thickness during the dry period; because as soil thickness lowers, its capacity to hold water decreases, and as such, it cannot sustain plants which enhance the karstification process via the release of CO₂. Hence, during the prevalence of dry periods karst development ceases or becomes insignificant. The development of karst in the Kinta Valley, like any other karst system in different geographic settings, may have been influenced by climate. The following review indicates the possible periods in which karst development in the area might have come to a latent stage ensuing climatic variations. This may further suggest that karst development cannot necessarily be a continuous process.

The Mesozoic Era as a whole has been interpreted as a warm and arid interval (Frakes et al., 1992; Royer, 2006 and references therein). Paleoclimate proxies show that during the Middle to Late Jurassic period the equatorial regions were drier than today, as the Asian climate indicates warmer and drier condition through this period (Rees et al., 2000). According to Rees et al. (2000), large areas of the equatorial zone are devoid of Jurassic deposits, and Frakes et al. (1992) indicated that the late Jurassic appears to have been arid, at least in low and mid-latitudes, as attested by the extensive development of evaporites, which diminished during the Early Cretaceous as coal deposits became more prominent.

Similarly, until the Upper Jurassic period, according to Metcalfe (2000), the Kinta Valley is characterized by the absence of any sedimentation (Fig. 2.2), and even the whole Peninsula is typified by the absence of any sedimentation from the lower Jurassic to the Early Upper Jurassic (Abdullah, 2009 p.130). This may possibly correspond with the dry period suggested from other proxy studies. Despite the occurrence of fractures which are conducive for karst formation, the possible prevalence of dry condition until the Late Jurassic does not enable to deduce the onset of intense karstification process in the Jurassic period.

During the Early Cretaceous, a humid climate prevailed as lithological climate indicators (precipitation > evaporation) (Rees et al., 2000) attests to the wet condition of this period (Frakes et al., 1992). By the Early Cretaceous, the Kinta Valley was characterized by emerged carbonate rock, as marked by the Indosinian orogeny (Tjia, 1999), affected by faulting mainly trending NNW-SSE and NE-SW, and significant wet condition. Thus, the right conditions for dissolution process had been established and continued until the Middle Cretaceous period, and slowed down from Early Mid-Cretaceous to Early Tertiary period, as dry conditions intensified. Similarly, the amelioration of the climatic condition during the Cretaceous period may have also occurred in the Kinta Valley as this period is typified by sediments deposited in fluvial environments (Saiong Beds) (Fig. 2.2) (Metcalf, 2000) which indicate a wetter condition. Therefore, due to the coexistence of favorable conditions, the Cretaceous period can be marked by the onset of intense karstification process; however, this has to be further substantiated by other evidence which may or may not prove otherwise.

Significant karst development in the Kinta Valley most likely occurred in the Cenozoic Era, especially in the Mid-Cenozoic, as various factors responsible for karst formation and gradual evolution reached their maximum influence because of: (i) the increment in hydraulic gradient which is associated with the lowering of base level as the denudation process continued, and (ii) possible increment in dissolution rate through time, as indicated in Ford and Williams (2007) and reference therein that whenever the basin loses the soluble rock from 100% to 50% the dissolution increases by 60%.

The Paleocene to Eocene period is typified by higher temperature than the preceding periods, and the highest global temperatures of the Cenozoic occurred during the Paleocene-Eocene thermal maximum (PETM) (Rafferty, 2011; Zachos et al., 2005). In spite of this, the Paleocene to Eocene Epoch, in general, is characterized by wet climate conditions (Harrington et al., 2004; McInerney and Wing, 2011 and references therein). Global climate cooling starts in the middle Eocene with a rapid temperature decrease at the end of the Eocene (Zachos et al., 2001), and with this the low-latitude climates also changed substantially, becoming tremendously cooler and

drier, especially in Southeast Asia where palynological and lithological evidence suggests that the ever wet climates became of very limited extent (Morley, 2007). The karstification processes which were possibly very intensive during the Cretaceous might have diminished gradually until the warmer and wetter climate commences in the Early Tertiary possibly continuing to the Middle Eocene period. The intensity of the denudation process became slower towards the Late Eocene as cooler and drier condition prevailed.

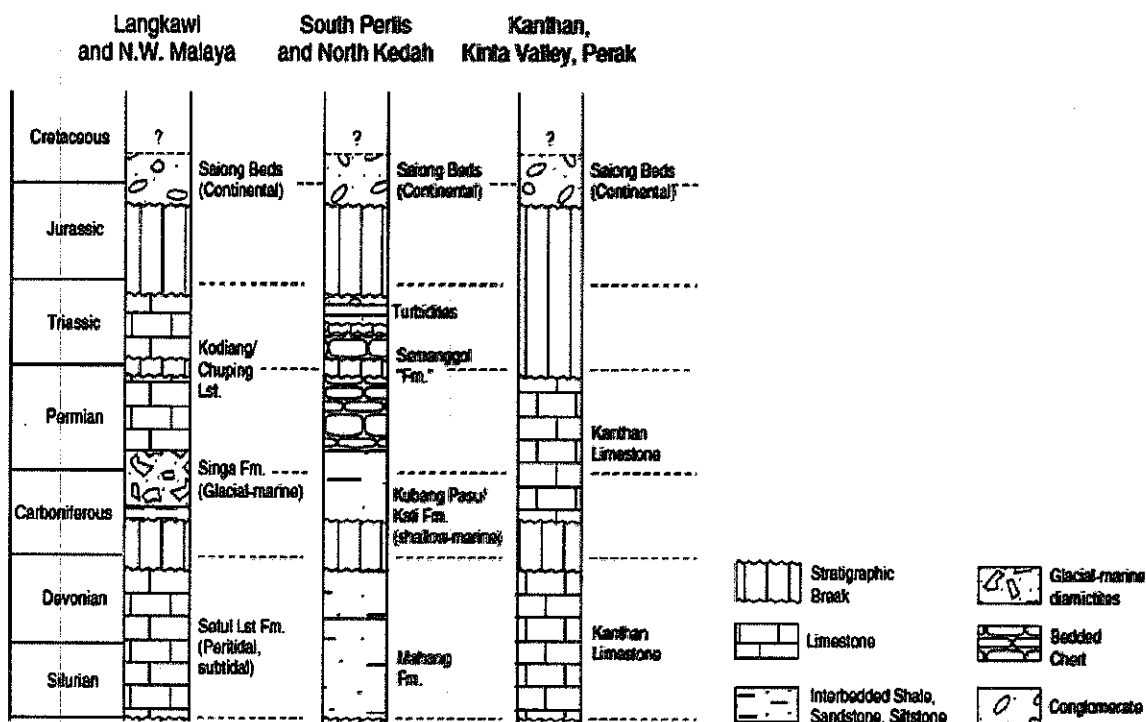


Figure 2.2: Stratigraphic column for Western Belt (Metcalf, 2000).

The karstification process, which was slowing down towards the Late Eocene, came to a latent stage in the Early Oligocene, as the paucity of elements (taxa) which are characteristics of wet climates indicates (Morley, 2007). Karst development is inextricably linked to climatic variation. During glacial intervals climates were cooler and much drier than now at low latitudes (Coventry et al., 1980), so those transition periods such as Late Eocene to Early Oligocene were dry. The review on Cenozoic Pollen records by Morley (1998), indicated that the Early Oligocene and Earliest Miocene were periods of much drier and cooler climates than the Mid-Miocene in which warm and moist climate conditions over a large part of Southeast Asia

prevailed. The latent stage of karst development may have again occurred during the Late Oligocene period. Although the Early Miocene is also characterized by a dry spell, the karstification process was not passive during the Oligo-Miocene boundary, as this period is marked by a drastic climate change, which is from seasonally dry to ever wet, in the Southeast Asia region (Morley, 2007). After the Mid-Miocene period, the active phase of karstification process may have resumed, and probably continued for the rest of this period.

2.1.2 Paleokarst

Paleokarst refers to karstic (dissolution-related) features formed in the past, related to an earlier hydrological system or land surface (Wright and Smart, 1994). The terms paleokarst and fossil karst are widely used, although sometimes being used as synonyms, and at times treated as opposites (Bosák et al., 1989 and references therein). Both terms are defined similarly- as features formed by agents active in the karst environment in the past, and under morphogenetic conditions differing from the present (Bosák et al., 1989). Two simple subdivisions of paleokarst can be made (Wright and Smart, 1994), between surface paleokarst (formed at an ancient landsurface) and subsurface paleokarst (formed beneath the ancient landsurface).

Broadly speaking, three types of paleokarst can be recognized: buried, exhumed, and relict. However, it is indicated in Bosák et al. (1989) and references therein that paleokarst is divided into (1) buried karst and (2) intrastratal karsts, and the former is considered to have formed at the surface of the earth and then covered by later rocks, which is the most widely agreed category of paleokarst. In contrast, the latter is formed within rocks already buried by younger strata, the karstification is younger than the cover. The buried karsts are those which often experienced tectonic subsidence and lie unconformably beneath clastic cover rocks (Ford and Williams, 2007). According to this work, the buried karsts occasionally exhumed and reintegrated into the active system to resume the interrupted development; however, contrary to these karsts the relict karsts are those karst forms which are remnants from previous morphogenetic conditions that are no longer operative (Sweeting, 1972).

When karst is hydrologically decoupled from the contemporary hydrological system, it becomes paleokarst, independent of whether the karstification is halted definitely or only temporarily (Ford and Williams, 2007). The most common reasons for such interruptions or cessations are metamorphism, marine transgressions, burial by continental deposits or volcanic products, tectonic movements (uplift, subsidence), climatic change (desertification, glaciation) (Bosák, 2008), and the interruption of the karstification process can be reflected in cave morphology (Gillieson, 1996).

2.1.3 Karst denudation

Solutionally transported mass loss from karst basins, expressed as if it was removed uniformly from the land surface, is commonly known as karst denudation (Ford et al., 1988). Gabrovšek (2007) defined denudation rate as the rate of lowering of a karst surface due to the dissolution of bedrock. Karst denudation rate is considered to be the sum of both chemical and mechanical erosion processes, although solutional denudation rates are usually used, since in practice it is much easier to estimate chemical than mechanical erosion (Ford and Williams, 2007). The greatest rate of solutional denudation of limestone in the world occurs where it is wettest; hence precipitation rather than temperature is the principal control (Ford and Williams, 2007). Further Ford and Williams (2007) indicated that although climate is important it is not necessarily an overriding factor since geological and morphological conditions also play a crucial role.

Plan (2005) illustrated the influence of factors, such as altitude, subsoil vs. sub-aerial exposure, vegetation, karst morphology, soil humidity, lithology, and surface morphology, in the rate of karst denudation. His result, obtained by measuring the mass difference of carbonate tablets, indicates that the dissolution rate varies between 13 and 40 $\mu\text{m}/\text{a}$ for subcutaneous samples and about 11 $\mu\text{m}/\text{a}$ for sub-aerial exposure, and a rate of 48 $\mu\text{m}/\text{a}$ in a doline, further attesting the influence of karst morphology on the dissolution rate. He also documented the lowering of subcutaneous denudation rate with altitude, from 40 $\mu\text{m}/\text{a}$ at 660 m to 14 $\mu\text{m}/\text{a}$ at 2130 m, whereas dissolution

of bare rock surfaces, with a rate of only 11 $\mu\text{m/a}$, does not show any significant change within this height interval.

Although there are different denudation rate measurement methods, carbonate tablet and micrometers, were used by Plan (2005) and Häuselmann (2008), respectively, and they got almost similar results. The dissolution rate for subaerial exposure, obtained by the former is 11 $\mu\text{m/a}$ but it appears to be $14 \pm 7 \mu\text{m/a}$ for the latter. These results are comparable to the denudation rate measured by other workers using the same or different methods. However, at times much higher rates have been indicated by the other workers and are a consequence of rapid corrosion during rainfall, not averaged for a whole year like Häuselmann (2008).

Although the method employed by Zambo and Ford (1997) is different, i.e. understanding the variation of limestone dissolution in a doline typified by clastic fills, they documented comparable lowering rate as Plan (2005) and Häuselmann (2008). According to the result they obtained, the lowering rate of the inter-doline crests and the steep side slopes appears to be 0.4 cm/ka, while at the base of the doline filling it is increased to 0.7–1.0cm/ka. Thus, they inferred that the differential deepening rate for the doline is in the range of 0.3-0.6 cm/ka. Karst features are the result of denudation by both allogenic and authogenic waters (Ford and Williams, 2007) and their development is not a linear process but **instead takes place at irregular rates that typically include episodes of stagnation and even retrograde processes** (Palmer, 2007). Because of this, quantifying the long term denudation rate is difficult. Short-term denudation rates can be achieved via hydrochemical data (Crowther, 1989; Gunn, 1981), carbonate tablets (Plan, 2005), micro-erosion meter measurement (Spate et al., 2006).

A common formula for calculating solutional denudation is based on the presumed equilibrium concentration and the amount of water which infiltrates into the subsurface, which is summarized in the famous Corbel's equation ($X = 4ET/1000$, where 'X' is the value of limestone solution, 'E' is runoff, 'T' is the average CaCO_3 content of the water) (Ford and Williams, 2007; Gabrovšek, 2007). Albeit this formula has drawbacks, it is considered as an appropriate method to obtaining a first-order estimate of solutional denudation particularly when data are limited (Ford and

Williams, 2007). In addition to the commonly used methods of short-term denudation rate estimation, mathematical models were also used by Gabrovšek (2007) who calculated denudation rate from the time needed to remove a certain thickness of rock and indicated that the denudation rate increases with the thickness of removed layer. A different approach, on the basis of a differential equation system that describes the lowering speed of the limestone surface, was used by Szunyogh (2005) to establish the duration of denudation rate. He indicated that the denudation rate does not increase in proportion to the intensity of precipitation, rather, long and soft rain results in higher annual denudation as compared to a short and abundant downpour.

Although karst denudation is a combined effect of allogenic and autogenic waters, the influence of the former generally outweighs the latter. Works cited in Ford and Williams (2007) clearly indicated that comparisons of solution denudation rates from different areas can be made only when the relative proportions of carbonate rock are taken into account. Further this work showed that if the proportion of limestone in a basin is reduced from 100% to 50% then the specific dissolution can increase by about 60%, assuming that the non-karst rock is on the upstream side of the basin and a source of allogenic runoff.

2.1.4 Collapse of karst cave

Cave breakdown is a mechanical process which may occur following the widening of channels. The breakdown rocks or breccias form piles on the floor, and if the development of the cave is influenced by running waters, the piles of breccias will be transported further whereby the passages are enlarged and leaving the ceiling of the host rock less supported. When such a process persists, the ceiling rocks fail, which leads to the formation of cave chambers. If neighboring chambers happen to intersect as a result of the upward stopping, the ultimate formation of a big cave chamber will take place.

Mostly breakdown results from simple mechanical processes of bed failure under gravitational load (White and White, 2003). There are two types of breakdown block features: terminal breakdown, which occurs at the end of collapsed major cave

passages, and breakout domes, which are huge rooms that form as a result of major ceiling collapse (White, 2005). Factors that lead to breakdown events include (a) passage enlargement below the water table, until it becomes mechanically unstable, (b) draining of phreatic conduits, which removes buoyant support. For limestone with a typical density of 2.65 g/cm^3 , 35% of the buoyant support of the ceiling is considered to be lost when the cave is drained, (c) vadose streams, which widen a passage beyond its beam or cantilever width limits, (d) aggressive vadose seepage waters that weaken the roofs (Ford and Williams, 2007; White, 2005).

Since those factors that cause breakdown or collapse are primarily related to removal of support, one may expect that breakdown would be very common in large passages and very rare in passages of relatively small dimensions (Osborne, 2002). Despite the established views of karst breakdown development, which is related to karstic cavities and dissolutionally enlarged fissures, Klimchouk and Andrejchuk (2005) show that breakdown initiation in large gypsum caves is not guided directly by the size of cavities, or that there is no direct correlation between large passage diameter and the occurrence of breakdown.

The load on a point in a rock mass can be expressed simply as $p = \rho gh$ (where, ' ρ ' is rock density, ' g ' is gravity, and ' h ' is thickness of the rock mass), and the distribution of this force creates a stress field and tension dome in the rock above the cave passage (Ford and Williams, 2007). It is indicated that the stress field tremendously increases on the adjoining cave wall as the overlying weight is transferred to them when the rock in the dome is subjected to sagging. Further it is elaborated in Gillieson (1996) that stress lines in the rock are evenly distributed around the cavity while the passage is water filled, once the water is removed local concentration of stress leads to failure of the arched section (Fig. 2.3), usually along bedding planes. This process propagates upwards, leading to the development of breakdown domes. Breakdown processes are most active during the enlargement and decay phase of cave development (White, 2005). This author further elaborated that the role of breakdown in the enlargement phase may cause upward stopping which can create large chambers, if actively circulating water removes the breakdown blocks at floor level. And during the stagnation and decay phases of cave development, the

breakdown processes can stop upward to interconnect previously isolated cave levels into an integrated system of passages.

For a ceiling to be stable, the bending strength of the beams must be greater than the gravitational force acting on the weight of the unsupported span (White, 2005). Thicker beds are stronger than thin beds, for example, a thick-bedded carbonates of medium strength can support roofs up to 20m wide before failure, and may extend to

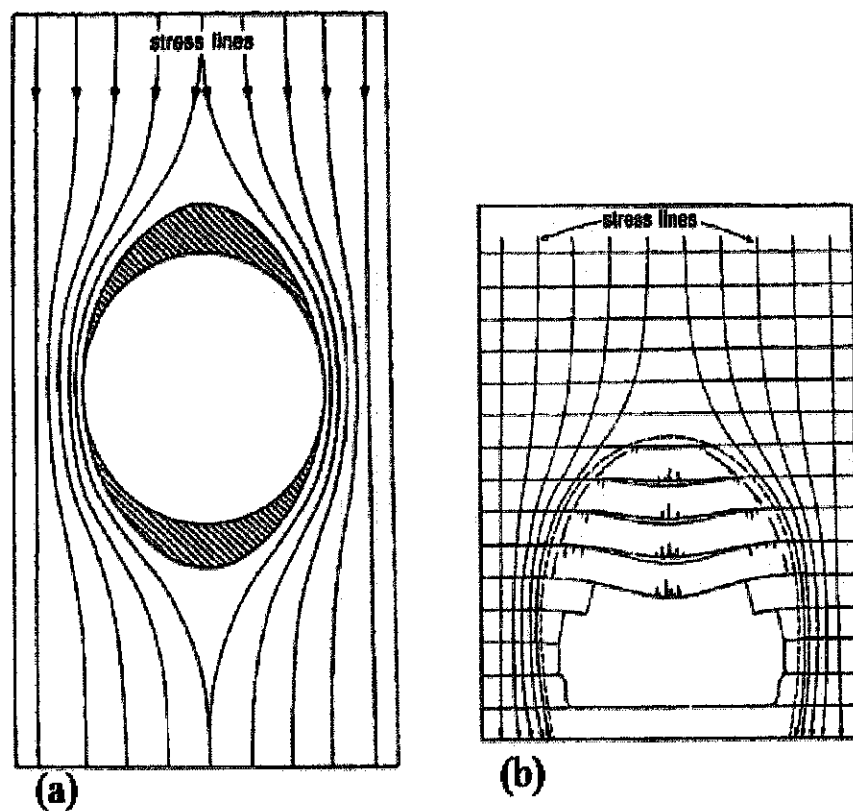


Figure 2.3: Depicting (a) distribution of stress line around water-filled void, and (b) air filled void after lowering of water table. Note incipient collapses at areas of concentrated stress (Gillieson, 1996).

35m or more where there are unbroken beams, and massive beds (>1.0m thick) (Ford and Williams, 2007). There will be a critical thickness (t_{CRIT}) for any given passage width at which the strength of the bed is just sufficient to support its weight (White, 2005).

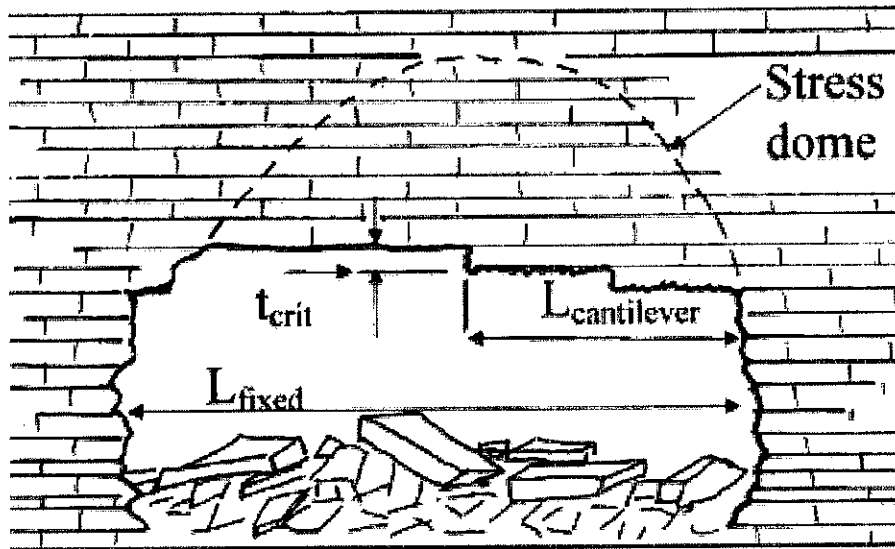


Figure 2.4: (a) Sketch showing the parameters of the fixed-beam model (White, 2005).

Ford and Williams (2007) illustrated that, each bed can be considered to function as a separate beam if it extends the full width of the passage, or as a cantilever where it is fractured through or does not extend the full width (Fig. 2.4). Further, they indicated that mechanical rupture and fall of the bed will occur where a critical span is exceeded for a given thickness and strength, and vice versa. A simple equation for a beam is given by -

$$t_{crit} = \frac{\rho \lambda^2}{2S(\cos \theta)}$$

, where t_{crit} = is critical thickness,
 λ = the span of the beam (passage width),
 ρ = is rock density,
 S = the bending stress, and
 θ = is the bedding dip (in degrees).

For a cantilever:

$$t_{crit} = \frac{3\rho \lambda^2}{2S(\cos \theta)}$$

As the collapse of cave passages take place, it is inevitable that the cross sectional area of the collapsed zone will be greater than that of the original conduit dimension. In order to estimate the hypothetical maximum extent of this zone resulting from cave-passage collapse, mass-balance relationship is used by Loucks (1999). This relationship (given by the following equation) relates the porosity and area of an open

cave passage to the porosity and area of a collapsed cave passage and the associated brecciated host rock.

$$\phi_{op} * \pi r_{op}^2 = \phi_{bz} * \pi r_{bz}^2$$

where, ϕ_{op} = porosity of original cave passage, r_{op} = radius of original cave passage, ϕ_{bz} = porosity of brecciated zone following collapse, and r_{bz} = radius of brecciated zone following collapse.

It is certain that after breakdown takes place the volume of the collapsed blocks will be higher than that of the previously unbroken rock. As Klimchouk and Andrejchuk (2005) and Ford and Williams (2007) indicated, breakdown ultimately stabilizes and clogging will occur unless there is concomitant removal of the collapsed rocks by dissolution or stream action. According to these works and a reference they cited, the stabilizing height or height of closure, where there is no concurrent removal, is given by:

$$h = h_0 \frac{k}{k-1}, \text{ where } h_0 - \text{initial height of the cave (before there is any collapse into it)}$$

k - the volume increase created by piling the breakdown

2.1.5 Karst related reservoirs

Although karstic carbonate reservoirs are typically heterogeneous in character, they are considered to have constituted one of the most economically significant categories of reservoir types (Chilingarian et al., 1996). Further, Chilingarian et al. (1996) indicated that many hydrocarbon reservoirs in karstic carbonate rocks have values of porosity and permeability that far exceed those for typical, average-porosity (i.e., 15% or less) carbonate reservoirs, and are considered to have some of the highest flow rates and recovery efficiencies of all reservoirs.

It is elaborated in many works including Kerans (1988), Loucks (1999), Wang and Al-Aasm (2002) and reference therein that the development of karst by meteoric water during subaerial exposure is an important geologic phenomenon that can lead to the formation of petroleum reservoirs. Mazzullo and Chilingarian (1996) also indicated that the formation of most karst reservoirs commonly is ascribed to extensive dissolution of carbonate rocks exposed to meteoric fluids beneath and along

unconformities that represent periods of subaerial exposure. According to Kerans (1988), potential hydrocarbon reservoirs within the upper Ellenburger Group, Texas, were produced by prolonged subaerial exposure and karstification of the carbonate platform. Thus, near-surface histories and later burial modifications must be understood so as to define reservoir geometry, scale, pore networks and spatial complexities of these reservoirs (Loucks, 1999).

To understand the change and distribution patterns of petroleum reservoirs, it is necessary to recognize the processes of dissolution, breakdown, and infilling (Wang and Al-Aasm, 2002). In this case, Kerans (1988) observation of reservoir compartmentalization, which is generated by regionally extensive karst modification, is exemplary. He illustrated that vertical reservoir compartmentalization is produced by a relatively impermeable shale-rich cave-filled interval that acts as a vertical flow barrier between the upper cave-roof fracture-mosaic breccia facies and lower collapse zones.

It is emphasised in Loucks (1999) that petroleum reservoirs are notable in karst-related paleocave systems and have significant spatial complexity, and an understanding of their origin and burial evolution helps in exploring and developing these reservoirs. It is also indicated in McMechan et al. (2002) and references therein that paleocave systems form an important class of carbonate reservoirs that are products of near-surface karst processes and later burial compaction and diagenesis. After subaerial karst caves are subjected to burial, they may end up being coalesced, collapsed paleocave systems (Fig. 2.5), which is clearly illustrated and discussed in Loucks (1999; 2007) and Loucks et al. (2004).

Hydrocarbon reservoirs of paleocave origin are commonly considered to be the product of coalesced collapsed-paleocave systems (Loucks, 1999). Coalesced collapsed-paleocave systems and associated suprastratal deformation appear to be prominent diagenetic/structural features in carbonate sections at/near composite unconformities (Loucks, 2007). According to Loucks (1999), regional distribution of coalesced, collapsed cave systems commonly appears as large scales (hundreds to thousands of meters across, thousands of meters long, and tens of meters thick) and as rectilinear patterns with areas of concentrated, coalesced breccias separated by

relatively undisturbed host rock. Such interconnection or coalescing of a cave system into large, connected porosity zones results in a heterogeneous reservoir hundreds to several thousand meters across, forming a much larger exploration target than would result from collapse of a single cave passage (Loucks et al., 2004; McMechan et al., 2002).

As paleocaves happen to collapse, after burial, the dimension of the original cave passage may increase by 4 times the surface diameter of the original caves passage, after considering the porosity decreases from 100% to 5% (Loucks, 1999). As a consequence of cave collapse, interconnected fracture networks and cave-fill breccias that may expand to several times the diameter of the original cave passages can be created (Feazel, 2009). Thus, as to Feazel (2009), productive wells need not penetrate the initial cave, so long as they intersect the connected volume of the coalesced collapsed cave system.

If the aerial density of passages is low, the collapsed cave system will feature isolated, collapsed passages (non-coalescing paleocave system) (Loucks, 2007). As a matter of fact, if the cave formation is influenced by fractures, the chance of numerous passages formation, which lead to large scale coalesced paleocave system, could be lower despite the high fracturing. This is because water flow may take in a different direction but the diffuse flow will ultimately follow a single prominent passage. Hence, numerous passages formation is minimal and no amalgamation of the passages to form large scale coalesced, collapsed-paleocave systems. Nonetheless, this coalescence may take place, as to the model of (Loucks, 1999), when collapse of wall and roof strata, as a cave system is buried into deeper subsurface, intersect with fractures and breccias from other collapsed passages within the system.

The works of McMechan et al. (2002) and Loucks et al. (2004), which integrated Ground Penetrating Radar (GPR) with well core data, supported the model of paleocave reservoirs of coalesced collapsed cave systems, with dimensions of hundreds or thousands of meters, to form after burial of subaerial paleocave system. Furthermore, the work of McDonnell et al. (2007), which depicted the origin and geometry of circular sag structures, for example Fig. 2.6, strengthened the coalesced,

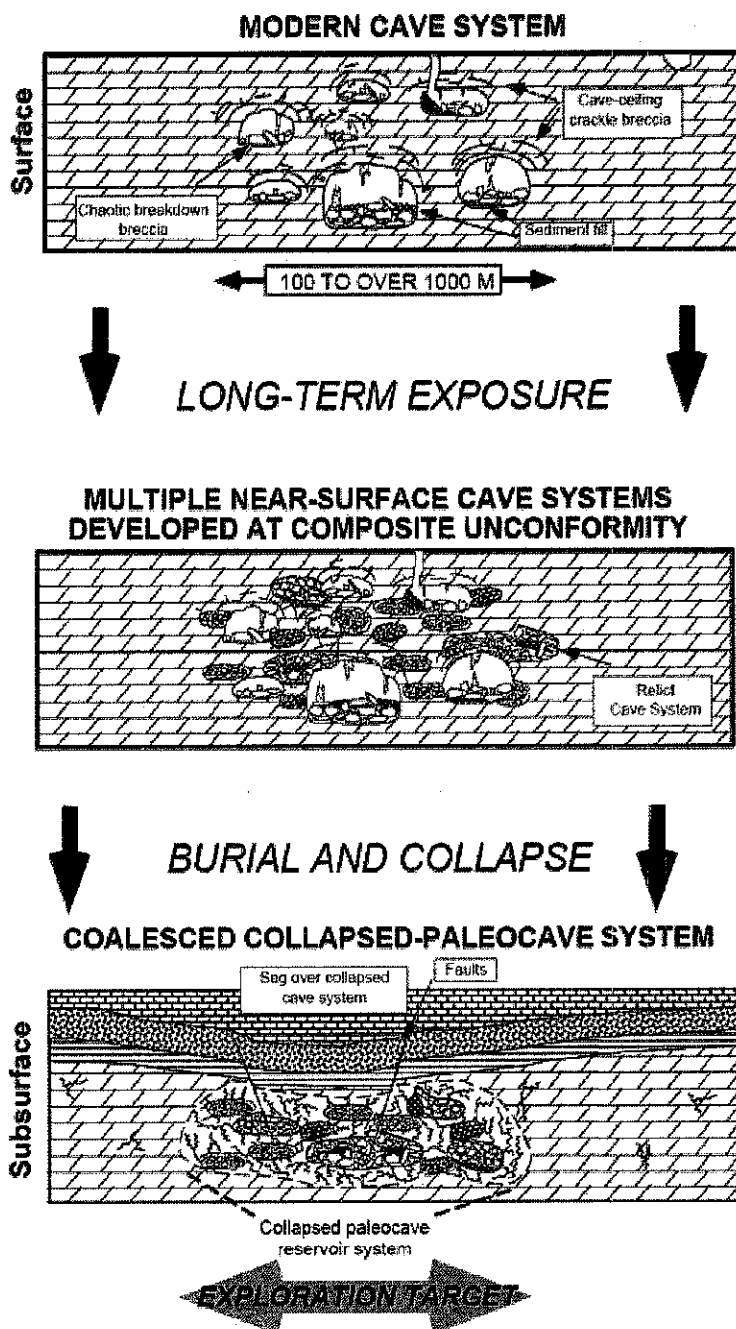


Figure 2.5: Schematic diagram for the development of coalesced, collapsed-paleocave system (Loucks, 1999).

collapsed paleocave model. They clearly indicated that most of the circular sag features, observed in the Lower Ordovician Ellenburger Group, range from 500 to 1200m in diameter. The most plausible explanation they gave for the formation of these features was by incremental collapse and suprastratal deformation above a linked system of subsiding, coalesced collapsed paleocaves. Similarly, the three-dimensional architecture of the coalesced, collapsed paleocave system based on core

and GPR data (Loucks et al., 2004) indicates that there are trends of brecciated bodies that are as much as 350 m wide, greater than 1000 m long, and tens of meters high. Such observation further ascribed to the fact that these brecciated zones cannot be individual collapsed cave passages, since they are too wide and almost all modern cave passages are less than 12 m wide (Loucks, 1999 and reference therein).

In addition to the aforementioned works of coalesced collapsed paleocave systems and their importance as reservoirs, a number of other studies, for instance Vahrenkamp et al. (2004), Shen et al. (2007), Zheng et al. (2011), also indicated the existence of paleokarst channels, collapsed caves and sinkholes, by analysing the seismic reflection characteristics of these features and from well logs.

Although Shen et al. (2007) described the difficulty of clearly explaining features of karst networks on 3D seismic, because of the complexity in geometry and lateral variability in thickness, Vahrenkamp et al. (2004) indicated the existence of karst networks and collapsed cave (Fig. 2.7a), which could be ascribed to the repeated exposure, syndepositional faulting or periods of renewed faulting, in Jinta and adjacent carbonate platforms. From the same province (central Luconia), the existence of subsurface karst was documented from core data (Fig. 2.7b). Barbed type paleocave channels and collapsed paleocaves, which have been observed in seismic discontinuity and dip attributes, were illustrated in Zheng et al. (2011).

Paleocave systems have complex histories of formation, and they are products of near-surface cave development, including dissolutional excavation of passages, breakdown of passages, and sedimentation in cave passages, which are followed by later-burial cave collapse, compaction, and coalescence (Loucks, 1999). Surveys of modern cave systems provide useful analogs for understanding paleokarst reservoirs (Feazel, 2009). According to Feazel (2009), the geometry and scale of modern caves can be keys to interpreting subsurface paleocave systems known only from their log signatures, drilling histories, or seismic character.

van Golf-Racht (1982a) indicated that a carbonate reservoir is defined as being "fractured" only if a continuous network of various degrees of fracturing is distributed

throughout the reservoir. In general, the most intense karst occurs along linear fault and fracture-controlled karst channels, and such faults and fractures have an important

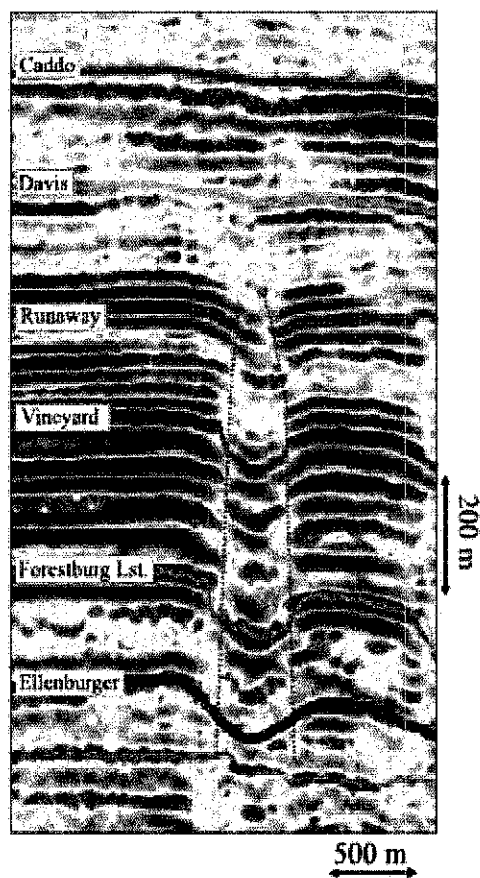


Figure 2.6: Seismic section depicting one of the typical circular to subcircular sag structures (McDonnell et al., 2007).

van Golf-Racht (1982a) impact on reservoir connectivity (Shen et al., 2007). In spite of that, it may be difficult to interpret continuity of fracturing in matured subsurface karst system, but comprehending subaerial karst features can be a way forward to unearthing the most likely trend of the subsurface structures. And may help to fill gaps in the knowledge base that still exists, concerning particularly connectivity (how individual fractures link to form coherent networks) and scaling (how small features are related to large ones) (Odling et al., 1999).

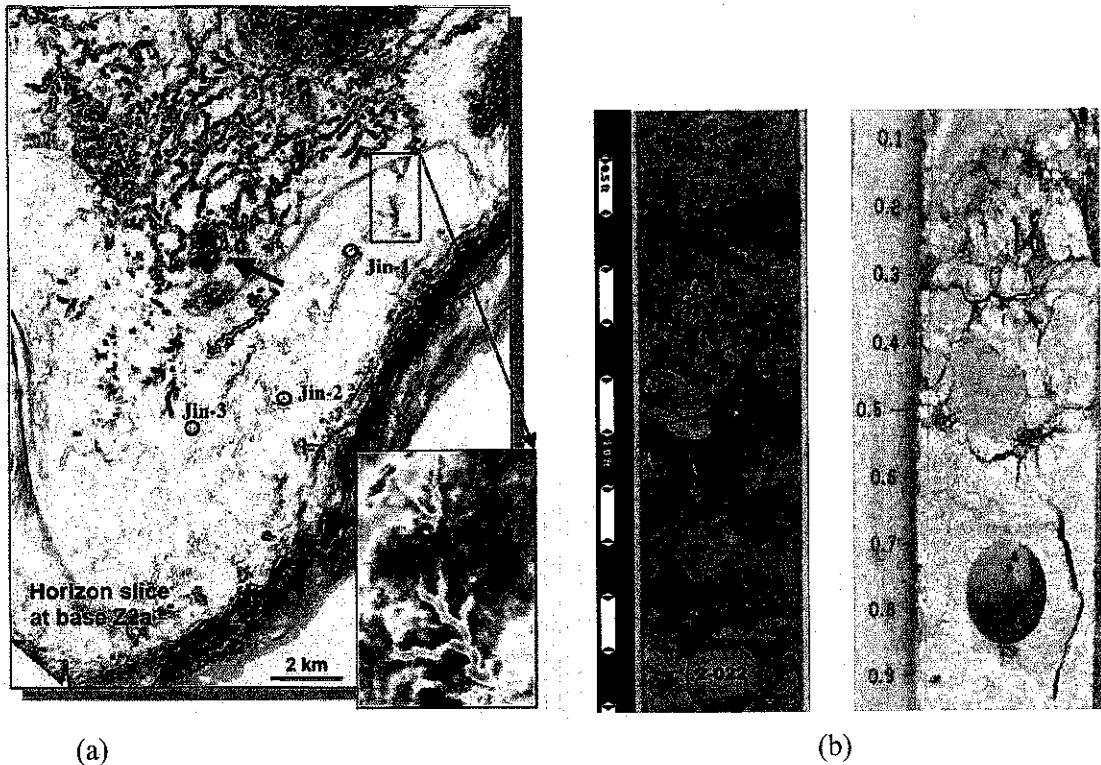


Figure 2.7: (a) Horizon semblance map showing a large NNE-SSW trending karst system (Varhrenkamp, 2004), and (b) Cores collected from a well in central Luconia, attest to the occurrence of subsurface karst.

2.2 Kinta Valley karst

The study of karst in the Kinta Valley may date back to the early twentieth century following the exploration of tin in the area, as the works done in 1913, 1917, and 1923 (cited in Ingham and Bradford, 1960; Paton, 1964) indicate. Besides the picturesque karst features that stand above the alluvium, karsts are being located below the alluvium as stripping of the sediments uncover them. Paton (1964) believed that the limestone, which is hidden beneath the sediment, was part of the original limestone platform and he stressed that the original level of the platform at any particular place can be deduced from the peaks of the highest pinnacles.

Previously many theories, including block faulting, sub-aerial erosion and folding, have been put forward as possible factors that are responsible for the development of the limestone hills in the area. Paton (1964) reviewed a number of works and argued that, because of the exposure of many sections in the Kinta Valley there is no longer

any doubt that the limestone of the valley floor is continuous with that of the hills. Thus, he inferred that there is no horizontal breaks or major vertical faults, unconformity or thrust plane, which are suggested in the early theories. The recent theories, according to him, include aeolian erosion, marine erosion and sub-aerial erosion. Richardson (1950) (cited in Raj, 2009) was among the earlier workers who believed that the limestone hills were formed by denudation, and the influence of joint and bedding plane patterns.

The limestones of the Kinta Valley have been steeply folded and partially metamorphosed. This has resulted, according to Gillieson (2005), a diversity of tropical karst landforms found in a smaller area. He further indicated that the Kinta Valley karst shares similarities with the fenglin (tower karst) and fengcong (cone karst) styles of tropical karst, with the towers on the eastern side of the valley resembling fenglin and the western side fengcong. These hills, which are of variable heights and situated mainly in the eastern part of the valley, are part of the same limestone which underlies the alluvium in the valley and the overall topography is strongly the reminiscent of an old, matured, karst system (Ingham and Bradford, 1960 and reference therein).

Paton (1964) believed that steep-sided and isolated hills can be formed by constant corrosion of underground channels which are derived from erosion along joints. As the floors of the channels are corroded, the walls and roofs are actively built up by stalactite and carbonate deposits, and in the latter stage of the cycle, the limestone gorges expand laterally with the collapse of overhangs, leaving behind steep-sided hills.

Although there are a number of karst caves in the remnant hills of the Kinta Valley, only Gua Tempurung appeared to have been subjected to the study of its origin and the influence of allogenic and autogenic waters. According to Gillieson (2005), the eastern side of the tower karst with juxtaposed granite has resulted in a massive limestone-marble lithology weathering to rugged tower karst relief. Further Gillieson indicated that Gua Tempurung is a classic example of a through-cave which breaches a strike ridge of limestone, and its passages is divided into two types, namely, those initiated by dissolution of autogenic water percolating down from the

upper tower surface and those related to allogenic water draining from the marginal granite into the stream sink. Although earlier works, such as Ingham and Bradford (1960) and Paton (1964) and references therein, advocate the idea of karst formation as a result of higher sea level which was asserted to be common from Miocene epoch onwards, no unequivocal evidence has yet been obtained (Gillieson, 2005), and in the absence of such evidence, the high-level passages and notches observed in the precipitous hills can be related to local ponding behind mudflow deposits and valley incision by Kampar river (Gillieson, 2005). As a matter of fact, Paton (1964) also described the objections to the hypothesis that marine erosion was entirely responsible for the hills, since, firstly, marine erosion cannot be used to explain all the hills as a number of them are too high to have been affected by it; thus the resulting topography could have remained unmodified. Secondly, marine erosion does not explain why such features as caves, cliffs, and grooves are not found on other rocks in the areas subjected to marine erosion in recent times.

At the face of the precipitous hills in the Kinta Valley, notches are quite conspicuous and these features, because of their possible origin by the effect of marine, freshwater, and stagnant water, they lead some workers to suggest various explanations for the origin of karst in the area. According to Paton (1964), if the formation of the grooves or notches is caused by the erosive action of streams and swamps, then one would expect grooves of these types to be low, deep, and smooth, with a relatively flat floor and roof with limited vertical extent. On the contrary, Paton indicated that marine notches or grooves would tend to be higher from floor to roof, reflecting wave and tidal ranges and should be traceable over considerable distances and should occur at consistent levels. However, Ingham and Bradford (1960) and reference therein described such grooves as cavities which may have been variously modified since their formation. Most of such modifications take the form of minor cavities, cut into the back wall of the main cave, often leaving horizontal ledges of rock between them. Therefore, grooves cut found in most limestone hills in the Kinta Valley with freshwater cut, since the grooves are horizontal and only continuous for short distances. It is also indicated in Raj (2009) that the notches might have arisen through mechanical action of streams and waves, although he believed that many

notches are a result of solution by ground water in the surrounding alluvial plains of the area.

2.3 Tectonic and Geologic Setting

Southeast Asia is a geologically complex region which has evolved through various phases of continental accretion, and is composed of different blocks or microcontinents that have rifted and drifted from the Gondwanaland (Gatinsky and Hutchison, 1987; Metcalfe, 1996, 1998, 2002). And Malaysia occupies a central position in Southeast Asia so that its geological history is inextricably linked to that of the whole region (Madon, 1999). The Peninsula has traditionally been subdivided in to three belts; Western, Central and Eastern belt (Metcalfe, 2000; Peng, 2009). The N-S to NNW-SSE structural grain is used for this division (Shuib, 2009). Tectonically, Peninsular Malaysia is part of the Sundaland that includes Thailand, Sumatra, Java, Indochina (Cambodia, Laos, Vietnam), Borneo, and the shallow seas located in between (Sunda shelf), which were assembled during the Triassic Indosinian Orogeny (Hall and Morley, 2004; Simons et al., 2007).

The Indosinian Orogeny, which was a profound mountain building phenomenon caused by the collision of Sibumasu and Qiangtang to Cathaysia land during the Late Triassic (Metcalfe, 2000; Hutchison, 2009), created the main geographic features of the region (Hutchison, 2005). The Triassic collision between Sinoburmalaya and the Indochina Block (the Indosinian Orogeny) eliminated the intervening Palaeotethys Ocean and caused crustal thickening, resulting in the emplacement of large composite S-type granite batholiths, such as the Main Range of Peninsular Malaysia (Cobbing, 1992).

Following the Late Triassic-Early Jurassic Indosinian orogeny, which is responsible for the Main Range granite formation (Metcalfe, 2000; Hutchison, 2009), the region underwent erosional processes as voluminous sediments were transported and infilled existing basins (Abdullah, 2009). Until the Cretaceous period, the region has also been subjected to further post-orogenic uplift, crustal extension, strike-slip faulting (Madon, 1999; Abdullah, 2009), which resulted in the formation of new

basins where redbeds, which marked the end of marine sedimentation throughout the Peninsula during Jurassic to Cretaceous times, were infilled (Abdullah, 2009). The Upper Triassic-Lower Jurassic deformation is also considered as a period to have brought marine deposition to an end, in the Central domain and in the entire Peninsula (Tjia, 1999).

The collision of Sibumasu and Indochina-East Malay blocks is represented by the Bentong-Raub suture, which is a narrow zone with deep-marine sediments associated with oceanic basalts, melange and accretionary complexes including Permian rocks, marks the elimination of the paleoethethy (Metcalf, 2000; Metcalf, 2002; Hutchison, 2009), and the elimination resulted in a major mountain building event, which gave rise to the major Main Range, 220-200 Ma old, S-type collision related granite belt (Hutchison, 2005 and reference therein). The collision must have allowed Sibumasu to underthrust the Bentong-Raub accretionary prism, so that the Main Range granite batholiths intrude into the subduction complex as well as into the platform sequence on the margin of Sibumasu (Hutchison, 2005). It is indicated that the oceanic materials preserved in the Bentong-Raub suture zone range in age from Middle Devonian to Middle Permian, for ribbon-bedded cherts, and from Lower Carboniferous to Lower Permian, for melange which includes chert and limestone (Metcalf, 2000).

Before the Late Triassic Indosinian Orogeny, the elongated Cimmerian continent, consisting of Qiang-Tang and Sibumasu, had rifted from Gondwanaland and began its northwards drift by Late Permian (Hutchison, 2005). According to Hutchison (2009) and reference therein, during the Lower Permian, the Sibumasu was attached to eastern Gondwanaland as indicated by cold temperate brachiopods. He went on to say that, the Late Lower Permian limestone contains warm water fauna such as fusulinids, ammonoids and abundant gastropods, and this abrupt change in provinciality made them infer a rapid northward migration of Sibumasu, causing a reorganisation of warm currents that brought in the warm water fauna or indicates northward drifting of Sibumasu into the warmer parts of the Paleo-Tethys, from the periglacial Gondwanaland (Tjia, 1999 and references therein). Similarly, in Kedah the platform limestone facies locally continues across the Permian-Triassic boundary, and the

Chuping Formation is believed to have extended from Permian to Late Triassic (Hutchison, 2005). Hence, until Sibumasu gets sutured onto the Indochina/East Malay block in Late Triassic, the Kinta Valley, which contains exceptional Carboniferous limestone that is not present in the Gondwana-affinity Sibumasu terrane, may have been under water and may have not gone through karstification process.

According to Peng (2009), the site of the Kinta Valley was a stable shelf during the Late Palaeozoic, with ongoing calcareous sedimentation interrupted by argillaceous invasions from the deeper more rapidly subsiding flanks from time to time. Triassic sediments are absent in the Kinta Valley (Peng, 2009), and Tjia (1999) indicated that the regional deformational period at the Triassic-Jurassic transition is apparent by a difference in structural style and absence of sedimentary rocks of that time. Following the end of this deformation period, a new sedimentation pattern resulted in the deposition of redbeds (red, ferric-rich siliclastics) which marked the end of marine sedimentation during Jurassic to Cretaceous times (Abdullah, 2009).

During the Early to Middle Triassic, subduction and crustal thickening generated the syn- to post-orogenic Main Range granites, which were emplaced in the Late Triassic–Early Jurassic (Metcalf, 2000). Almost immediately after the collisional orogeny, pre-rift structures formed in many localities away from the collision zone, and major strike-slip faulting cut obliquely across the collisional fold belt in a predominantly NNW-SSE direction and also possibly sub-parallel to the suture zone (Hutchison, 2005).

Malaysian granites post-date the Triassic (Twidale, 2005), as strata of Triassic age are affected by mineralization associated with granites. The distribution of the Main Range granite is believed to have influenced the NNW-SSE main structural trend of the Peninsula (Shuib, 2009). He went on to say that, the NNW-SSE structural trend is believed to be the result of three main deformational phases: (1) the Upper Triassic–Lower Jurassic transpression – this period of orogenic event is popularly believed to be due to the collision between Sibumasu and East Malay (Tjia, 1999), (2) Upper Cretaceous – during this period it was a major faulting event that affected the whole Peninsula and the great extent of this event obliterated the surface expressions of

earlier deformations, (3) Lower Tertiary extensional and strike-slip events reactivated most of the earlier structures.

Shuib (2009) and references therein indicated that the earliest faults which are formed as a result of the amalgamation of the two tectonic blocks of the Peninsula during Permian to Triassic times are terrane-bounding faults, such as Bentong-Raub Suture Zone and Lebir Fault Zone, and terrane-crossing faults. Further, it was indicated that, the NNW-SSE and N-S dextral strike-slip movement along major dextral faults followed, after or at the late stage of the emplacement of the Main Range Granite in Late Triassic to Jurassic.

In the Kinta Valley, the environment of deposition during the Palaeozoic time was predominantly clear, warm, shallow marine with occasional influxes of carbonaceous terrigenous sediments which gave rise to the consolidation of argillaceous lenses intercalated with the limestone (Ingham & Bradford, 1960). However, a sequence of thinly bedded to laminated micritic limestone with abundant slumps and thin interbedded chert laminations is documented and interpreted to be deep marine slope deposits (Pierson et al., 2009). Later metamorphism resulted in the formation of schists, marbles and phyllites (Ingham & Bradford, 1960).

An accurate estimation of the thickness of the carbonate rock cannot be made, since some portion have been eroded from above the present surface and others may have been assimilated in depth by the granite magma (Ingham and Bradford, 1960). However, they estimated that the thickness may be as much as 3048 m or more considering the extant limestone which rises 579 m above the limestone plain and the width that reaches approximately 16 miles. They also indicated that the approximated thickness could be much less since the beds are repeatedly folded.

The Main Range Granite, which adjoins the Kinta Valley carbonate and forms the backbone watershed mountain range of the Peninsula, is believed to be a result of several large granitic batholiths (Hutchison, 2007; Ghani, 2009). In the study area, the carbonate rocks are laterally bounded by Late Mesozoic granite plutonic rocks emplaced by activity related to the Late Triassic uplift from plate boundary stresses along the western edge of the Malay Peninsula (Gillieson, 2005). The limestone,

compressed by the granites (Fig.1.2b), has been altered by contact metamorphism to marbles and skarn (Gillieson, 2005; Hutchison, 2007). Nonetheless, the effect of metamorphism diminishes away from the contact zone, as the eastern side, where the limestone-granite contact situated, is characterised by crystalline carbonate rocks whereas the western side is affected by slight metamorphism as it is typified by feebly crystalline rocks having clear sedimentary structures. Where the metamorphism effect is insignificant, sedimentary structures marked by thicker beds which occasionally interrupt the monotonous thinly bedded sequence containing breccia beds and shallow marine fragments or fossils (Pierson et al., 2009), are conspicuous.

Ingham & Bradford (1960) believed that most of the rock structures in the Kinta Valley were developed during the emplacement of the granite ranges during the late Mesozoic times. Similarly, Shuib (2009) indicated that the prominent regional structures are formed **after or at the late stage of the emplacement of the Main Range Granite in the Late Triassic to Jurassic**. The structure of the area is quite complex; it is probable that more than one phase of tectonics has affected the area in the past to bring about the present structural settings. Ingham & Bradford (1960) recognized two types of faults: (a) shear faults, running parallel to the strike of the beds, and (b) tension faults that run obliquely across the valley. The complex structure of the area is believed to have invariably exerted its influence on the drainage pattern of the area.

2.4 Fission Tracks

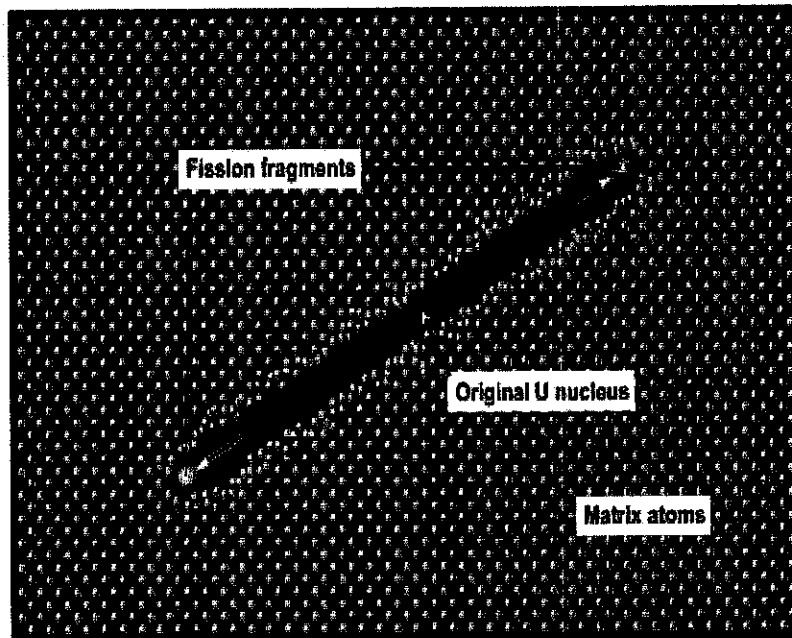
Fission tracks are trails of intense radiation damage through the surrounding crystal structure of a mineral. Such trails are formed by spontaneous fissioning of ^{238}U atoms, which split into two parts and move rapidly in opposite directions, creating a single linear trail of ionization damage referred to as fission track (Fig. 2.8) (Galbraith, 2005; Braun et al., 2006). Thus, fission tracks develop in a crystal through time as uranium spontaneously decays, and the longer the time elapses the higher the number of tracks to be formed. Hence, fission track age is a function of the number of tracks that have been formed. Fission tracks are submicroscopic features with an initial width of approximately 10nm and a length of 20 μm (Lisker et al., 2009 and

references therein) or with an initial length of about 17 microns (Galbraith, 2005). Fission tracks are originally 10-20 μm long and only 25-50Å wide, and their length depends on the density of the crystal lattice (i.e. $\sim 11 \mu\text{m}$ in zircon; $\sim 16 \mu\text{m}$ in apatite) (Braun et al., 2006).

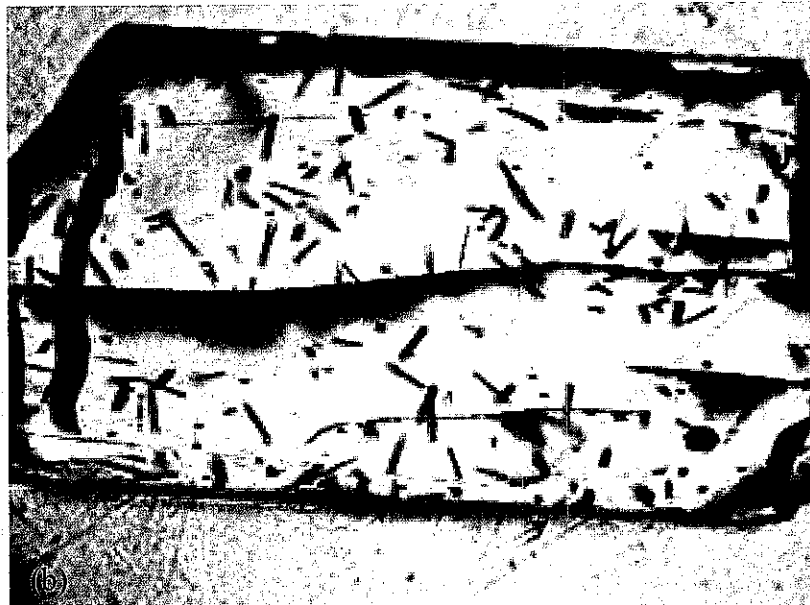
Fission track dating (FTD) uses principles similar to radiometric dating, as both approaches use radioactive isotopes. Nonetheless, what makes fission tracks dating different from other radiometric dating which record **the time passed since the mineral first crystallised**, is that FT age records cooling through a temperature interval between total resetting of fission tracks and relative stability, known as the partial annealing zone (Lisker et al., 2009 and reference therein) or it dates **the time at which the fission tracks began to accumulate**. Simply, the major difference between fission track dating and other conventional isotopic dating, according to Gallagher et al. (1998) is that the daughter product is physical damage to the crystal lattice, rather than another isotope. Or, FT dating is a radiometric dating technique based on analyses of tracks or damage trails caused by fissioning of uranium.

Fission track analysis provides detailed information on the low-temperature thermal histories of rocks, below $\sim 120^\circ\text{C}$ for tracks in apatite and below $\sim 350^\circ\text{C}$ for zircon (Gallagher et al., 1998). However, it is indicated in Lisker et al., 2009 and references therein that typical temperature ranges for the PAZ for heating durations of 10^7 are $60\text{--}110^\circ\text{C}$ for apatite and $170\text{--}330^\circ\text{C}$ is for zircon. The zircon FT partial annealing zone, $\sim 200\text{--}350^\circ\text{C}$, is derived by the extrapolation of laboratory annealing results based on confined track length measurements, as indicated in (Tagami et al., 1996). Although such a wide range of annealing temperatures for zircon are suggested, commonly $240 \pm 50^\circ\text{C}$ (Hurford, 1986) is adopted as effective closure temperature, since it is in reasonable agreement with estimates of later workers (Gallagher et al., 1998). Similarly, $240 \pm 30^\circ\text{C}$ is indicated in (Yan et al., 2010) and references therein as the effective annealing temperature for zircon.

Since fission tracks can be used as temperature-sensitive radiometric dating, the quantitative study of thermal histories of rocks can be achieved using these radiation trails (Braun et al., 2006; Galbraith, 2005; Ketcham et al., 2009; Lisker et al., 2009). Such understanding of thermal histories in the upper crustal rocks is considered to



(a)



(b)

Figure 2.8: (a) A cartoon indicating two fission fragments produced by each fission decay event move very rapidly away from each other (courtesy Andrew Gleadow, University of Melbourne), and (b) Illustrates etched FTs in apatite (Galbraith, 2005).

be so useful for the study of uplifting of mountains (Benjamin et al., 1987; Lisker et al., 2009). The approach for such understanding is based on the increase of temperature with depth in the Earth, where a body of rock, which is uplifted and cools

through the various mineral closure temperatures, recording the times at which each temperature was reached.

Fission tracks are not stable features and will tend to be repaired (shorten and eventually disappear) by a diffusive process known as annealing, during which atoms and electrons move through the crystal lattice towards the ionised track (Braun et al., 2006). This process takes place at a rate which is a function of both time and temperature. According to Braun et al., 2006 and references therein, below $\sim 60^{\circ}\text{C}$ the annealing rates are very slow, but they increase very rapidly at depths corresponding to the temperature range of $60\text{-}120^{\circ}\text{C}$, an interval that has been termed as partial annealing zone (PAZ). Since heating of a sample above the annealing temperature causes the fission tracks to heal or anneal, the technique of FTD is useful to understanding of cooling event in the history of the sample.

The importance of apatite fission tracks lies in its application for reconstruction of low-temperature thermal histories, which is out of detection of most other radiometric dating systems, in the upper crustal rocks (Galbraith, 2005). Thermochronology provides information only on the thermal history of rocks, which, among other processes, depends on the rate at which rocks are brought towards the surface by exhumation (Braun et al., 2006). Further, this work indicated that, since tracks are formed continuously, each track experiences a different portion of the integrated thermal history. Thus, the track-length distribution, which is obtained by measuring the lengths of a sufficient number of confined tracks (tracks parallel to the polished face of the grain that do not cut the surface), contain information on the thermal history experienced by the sample. Actually, the thermal history can be influenced by the chemical composition of a mineral, as it controls the annealing rate, particularly because of the relative proportions of Cl, F, and OH (Gallagher et al., 1998).

According to Braun et al. (2006) p.13, there are two principal assumptions that underlie the elementary approach of interpreting cooling ages in terms of rates of tectonic process, (1) Samples must be exhumed from below the depth at which the crustal temperature is equal to the closure temperature of the chronometer in question, (2) The isotopic ages observed should be at steady-state values, such that they reflect the time taken for a sample to be exhumed from its closure depth.

CHAPTER 3

MATERIALS AND METHODS

3.1 Cave survey and Mapping

Cave surveying is the common technical activity undertaken to measure a cave and produce an accurate map of it, which enables to determine the relationship between the cave and the surface landform. In order to produce maps of the Kinta Valley karstic caves, and collect data that can be used to study the morphology of the karst system, the following approaches were used:

a) Reconnaissance study

Preliminary examination or observation of the various karst caves morphological variations and similarities, dimensions, shape, distributions, was made to facilitate later surveying and detail karst features study.

b) Surveying

The survey method may differ based on the interest of the surveyor; however, for this study foresight or forward measurements, which take a series of consecutive line-of-sight measurements between stations, were used. The survey was accomplished by only a team of two and for some caves three people.

The instruments used during cave surveying (Fig. 3.1), and the measurements taken between the stations were:

- Clinometer –inclination (slope)
- Laser distance meter and measuring tape – distance between stations, and to the wall and ceiling away from the observer

- Compass – azimuths
- Notebook – for data and sketch

The clinometers scale ($0\pm 90^\circ$, $0\pm 150^\circ$), and compass scale (0 to 360°). The laser distance meter and measuring tape were used interchangeably; particularly the laser meter was employed to measure the ceiling to floor height. At times, the accuracy of the dimensional measurements was counterchecked by the two instruments.

In order to assess the precision and accuracy of cave maps and related data, a cave survey grading system has been given by Häuselmann (2011), which is officially recognized by the International Union of Speleology (UIS). The survey grade is based on what instruments one used during surveying. The survey method used in this study can be considered as Grade 4, as grade 4 is achieved by using compass, clinometers, tape survey, and using deliberately chosen fixed stations. And the simple sketch in Figure 3.2 illustrates the way the survey was conducted and the different measurements which have been taken. The expected error of this survey approach is presumed to be up to 5%.

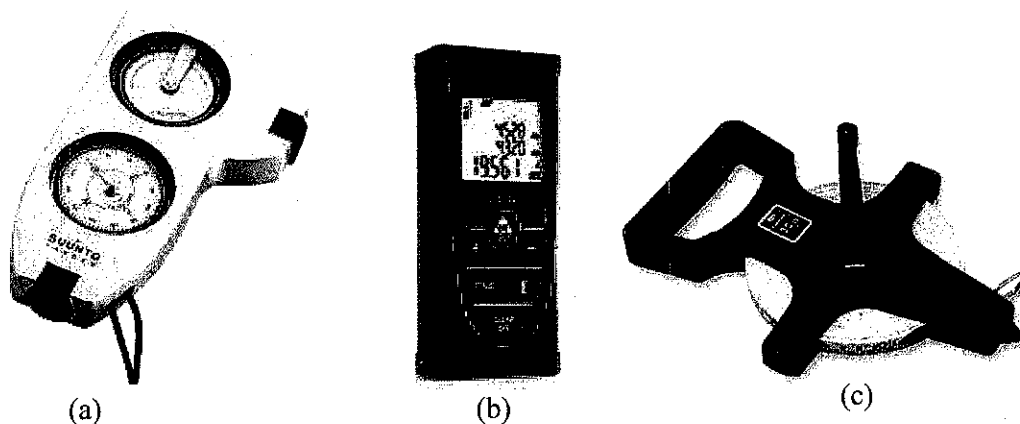


Figure 3.1: Instruments used during cave surveying – (a) both clinometer and compass, (b) laser distance meter, (c) measuring tape.

(c) Post survey data processing

To generate the cave maps, the survey data were keyed into COMPASS (cave mapping software) to produce a plot file (*.plt) and the plot file was brought to SVG exporter where various adjustments were made prior to exporting the map to a

drawing program. The ultimate cave maps were produced in Inkscape (drawing software). In addition, the data were also used to see the prominent trend of the cave passages, using rose diagrams which were produced in a graph tool (COMPASS). However, before indicating the orientations of the caves passages using the graph tool, the following considerations were made: (i) the minimum length of the survey line should be 8m, since a shorter length is considered to be non representative of the prominent trend, and (ii) the passages should be straight, and have not undergone collapse.

In order to check the similarity between the overall trends of the cave passages with that of the general trend of the remnant hills and lineament orientations, all survey data points were merged, and a rose diagram that indicates this general trend was made by employing GEOrient software.

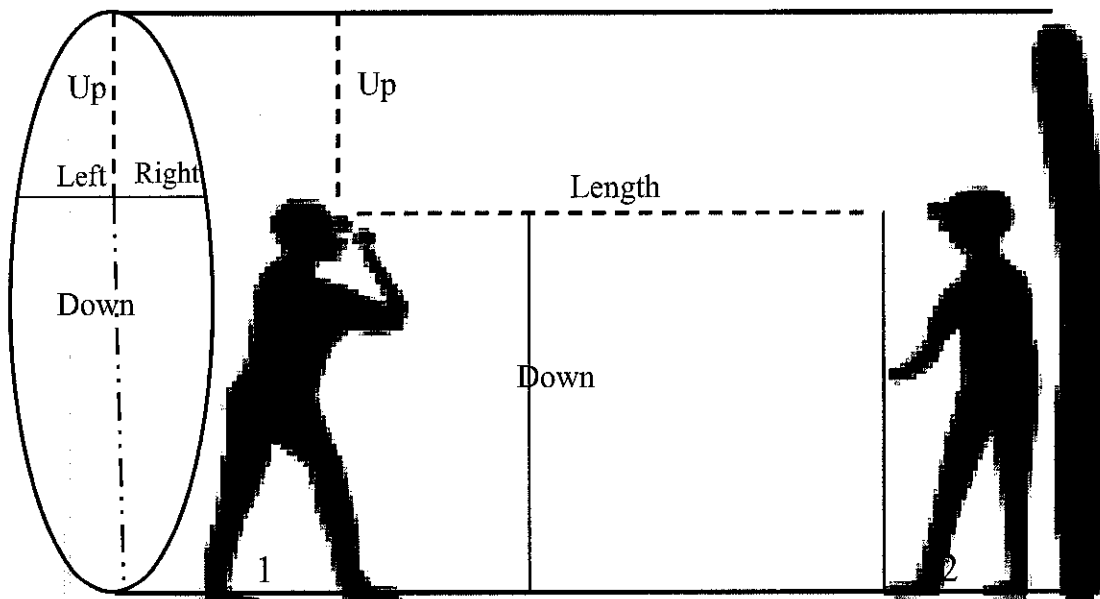


Figure 3.2: A cartoon illustrating how the cave mapping was conducted. ‘Up’ indicates the height from the eye of the surveyor (person 1) to the ceiling, whereas ‘Down’ indicates the height from the eye of the surveyor to the floor of the cave passage. ‘Left’ measurement indicates the width of the passage from the left side of the surveyor, and ‘Right’ indicates the width of the passage from the right side of the surveyor.

3.2 Lineament analysis

The general term “lineament” applies to all linear features seen on aerial photographs and images (Spencer, 1969). Aerial photography has been the most widely used form of remote sensing, and lineament interpretations from them were common. However, as the resolution of satellite images continued to improve, they replaced aerial photographs for a variety of remote sensing applications (Lillesand et al., 2004). Thus, to analyze the relation between geological structures and karst features, extraction of lineaments was made from a Spot image, which provided large areal coverage and good resolution.

Image processing techniques have previously been used to extract lineaments from satellite images as a means of identifying linear surface traces of geologic structures such as faults and joints (Henderson et al., 1996; Leech et al., 2003; Nama, 2004). Hence, similar image processing methods were adapted to extract lineaments from the remnant hills of the study area.

A Spot image, with a resolution of 2.5 m, acquired in 2010 (path 268/row 341), provided by the Malaysian Remote Sensing Agency (MRSA), was employed as a data source. The extraction of the lineaments was performed after the identification of linear features in the image. The main clues to identifying lineaments in an image include: systematic offset of rivers, continuous scarps, straight valley and stream segments, and tonal anomaly, which are the consequence of geological structures (Koike et al., 1998). Therefore, the lineaments, in our data, were traced based on distinct tonal differences, shape and pattern.

There are two methods of extracting lineaments from satellite imagery: manual (visual interpretation) and automatic. For this study the former is used, as it is easier to manually identify geological elements from non-geological ones. However, before extracting the lineaments, the following image enhancement techniques were undertaken to facilitate the visual interpretability of the image.

3.2.1 Image processing and enhancement

Image enhancement refers to data processing that aims to increase the overall visual quality of an image or to enhance the visibility and interpretability of certain features of interest in it. Although this process improves the visual interpretability of an image, and of course there are different approaches for that, it is difficult to infer the effectiveness of a certain enhancement procedure, as it may vary with the type of image. In this study, the following methods of enhancement were used to better identify the lineaments and improve the interpretability of the image.

3.2.1.1 *Color composite*

Most satellite images are acquired in the Visible and Near-IR region of the electromagnetic spectrum (Fig. 3.3), and they are known as multispectral images. Multispectral image consists of several bands of data. For visual display, each band of the image may be displayed one band at a time as a grey scale image, or in combination of three bands at a time as a color composite image (Lillesand et al., 2004). Further this work indicated that if a multispectral image consists of the three visual primary color bands (red, green, blue), the three bands may be combined to produce a "true color" image, in which the appearance of the displayed image resembles a visible color photograph. When images acquired in different bands are displayed with colors other than their own, the resulting product is known as False Color Composite (FCC) (ERDAS, 1999). There are many possible schemes of producing false color composite images. However, some scheme may be more favorable for identifying certain objects in the image. Thus, FCC was undertaken, using the multispectral Spot image data, to achieve a maximum contrast by combining different bands (RGB), for the ease of manually identifying linear patterns of geological elements.

For instance Figure 3.4 depicts how the best FCC was selected. In this case, one of the hills, Gunung Tempurung, is considered to illustrate the color composite, and the combination of band 1 (NIR), 2 (red band) and 3 (green band), or band 4 (SWIR), band 2 (NIR) and band 3 (red), to mention just a few, are assigned respectively to the

R, G, and B colors to get an image with better visual quality and interpretability of the data.

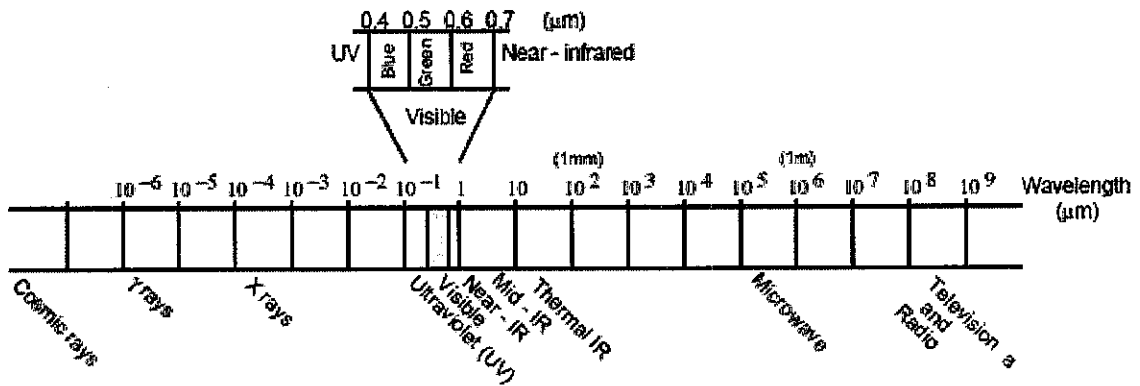


Figure 3.3: Displaying the Electromagnetic Spectrum (Lillesand et al., 2004).

3.2.1.2 Contrast manipulation

As the limestone hills are distributed all over the Kinta Valley, the image of each hill cropped out from the Spot image which covers the whole valley. Contrast manipulation was applied subsequently to each of them. This approach increased the visibility of the image, as it improves the contrast between features. Out of the different types of contrast stretching, histogram-equalization is applied to the best band combination. Similarly, in a certain portion of the image, where there is poor contrast, enhancement was applied not in the entire image as by default, but in the small area of interest (AOI) by locating the AOI box in the area of low contrast.

These enhancement processes were made using ERDAS IMAGINE 8.4 software. In this software, the entire image was enhanced following the sequence: Interpreter → Radiometric Enhancement → Histogram Equalization. However, for the enhancement technique used in small areas of contrast, the procedure is: Raster → Tools → AOI box → mark AOI. Although further steps were employed, these procedures highlight how the enhancement processes were undertaken.

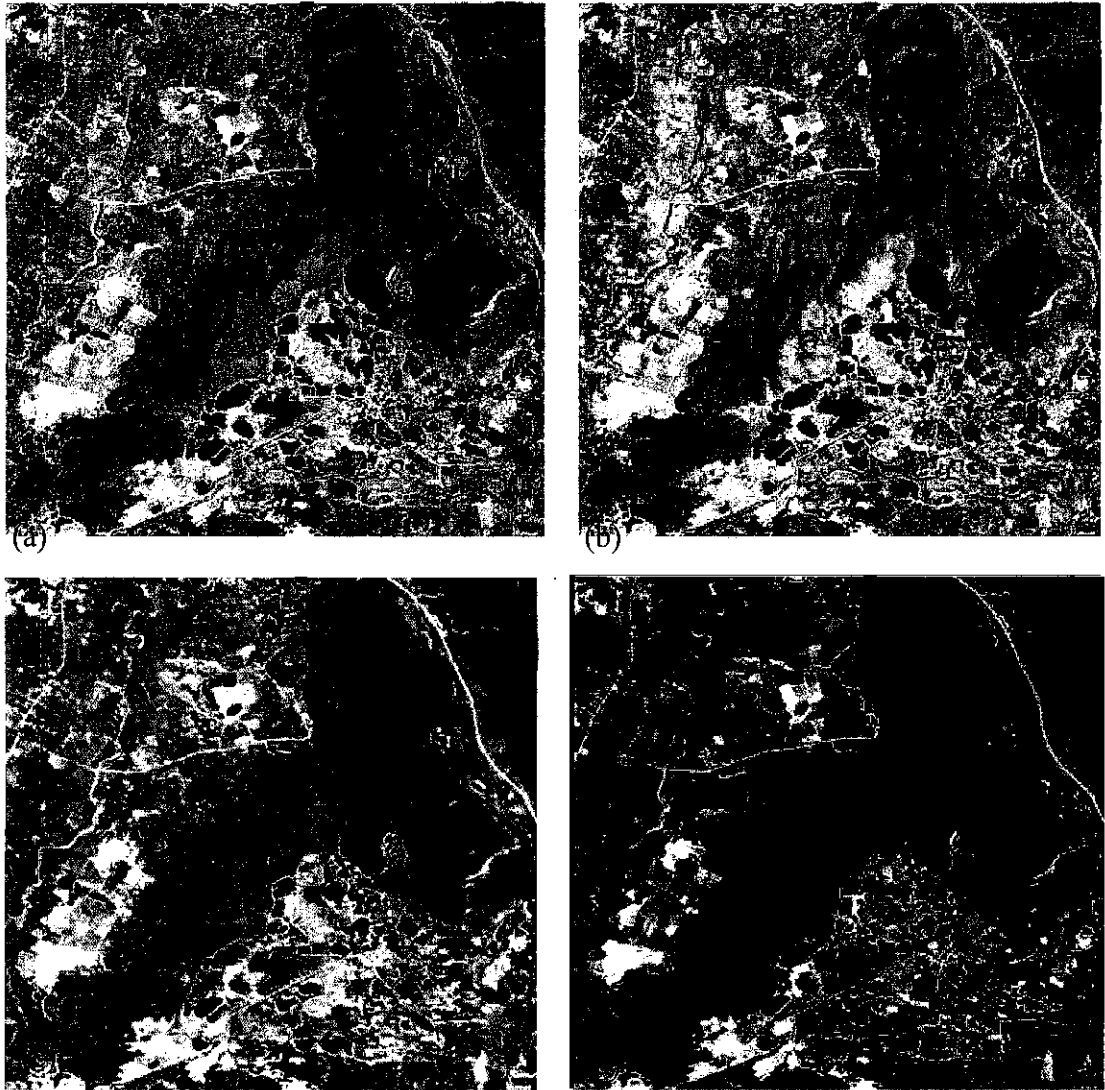


Figure 3.4: (a) band 1 (red), band 2 (green) and band 3 (blue), (b) band 3 (red), band 2 (green) and band 1 (blue), (c) band 4 (red), band 3 (green) and band 2 (blue), and (d) band 1 (red), band 3 (green) and band 2 (blue).

3.2.1.3 Spatial enhancement (filtering)

Since our primary objective was lineament extraction, directional filtering was conducted to enhance linear features in specified direction. Directional filter was applied to the selected band combination in N-S, E-W, NE-SW and NW-SE directions to increase frequency and contrast in the image. ERDAS IMAGINE 8.4 software was employed in the directional filtering technique. However, before using this method to enhance the lineaments, the following theoretical background (adapted from ERDAS, 1999; Lillesand et al., 2004; Gao, 2008) was used.

Spatial enhancement (filters) is designed to emphasize or deemphasize features in an image based on their spatial frequency, which is the difference between the highest and lowest values of a contiguous set of pixels. The spatial frequency is related to the textural characteristics of an image. Rapid variations in brightness levels (roughness) reflect a high spatial frequency, smooth areas with little variation in brightness level or tone are characterized by a low spatial frequency, where gray levels vary abruptly and only gradually.

Directional filter is a first derivative edge enhancement filter that is designed to highlight features which are oriented in specific directions, such as linear geologic structures. An edge or linear feature is manifested as an abrupt change in DN (digital number) along a certain direction in an image. The Sobel and Prewitt methods are the two kinds of special edge-detection operants (Fig. 3.5). All edge detection templates have one characteristic in common: the sum of all elements in a kernel is zero. These zero-sum kernels smooth out areas of low spatial frequency (e.g., absence of any edge), and cause a lower output in areas of low spatial frequency. In areas of high spatial frequency, a sharp contrast results (Gao, 2008).

A zero-sum kernel is an edge detector, which usually smoothes out or zeroes out areas of low spatial frequency and creates a sharp contrast where spatial frequency is high, which is at the edges between homogeneous (homogeneity is low spatial frequency) groups of pixels (ERDAS, 1999). In a nutshell, it implies that areas with uniform pixel values are zeroed out in the output image, and areas with variable pixel values are indicated as bright edges.

Spatial filtering requires a convolution kernel or template. A kernel is a matrix of numbers that is used to average the value of each pixel with the values of surrounding pixels in a particular way. The numbers in the matrix serve to weight this average toward particular pixels. Thus, convolution filtering is the process of averaging small sets of pixels across an image. Sobel kernel emphasizes high frequency changes in the image function by reducing the intensity of pixels of low frequencies as it increases the intensity of pixels with a higher frequency. The nine elements can be arranged horizontally, vertically, or diagonally to detect edges oriented in a direction perpendicular to them. For this study, Sobel directional filtering technique was

adapted, although the Prewitt filter also appears to be similarly effective. An example of an original image and its filtered equivalent or product which passed through Sobel filter can be seen in Figure 3.6.

$$\begin{array}{cccc}
 \begin{pmatrix} -1 & 0 & 1 \\ -2 & 0 & 2 \\ -1 & 0 & 1 \end{pmatrix} & \begin{pmatrix} -1 & -2 & -1 \\ 0 & 0 & 0 \\ 1 & 2 & 1 \end{pmatrix} & \begin{pmatrix} -2 & -1 & 0 \\ -1 & 0 & 1 \\ 0 & 1 & 2 \end{pmatrix} & \begin{pmatrix} 0 & 1 & 2 \\ -1 & 0 & 1 \\ -2 & -1 & 0 \end{pmatrix} \\
 \begin{pmatrix} -1 & 0 & 1 \\ -1 & 0 & 1 \\ -1 & 0 & 1 \end{pmatrix} & \begin{pmatrix} -1 & -1 & -1 \\ 0 & 0 & 0 \\ 1 & 1 & 1 \end{pmatrix} & \begin{pmatrix} -1 & -1 & 0 \\ -1 & 0 & 1 \\ 0 & 1 & 1 \end{pmatrix} & \begin{pmatrix} 0 & 1 & 1 \\ -1 & 0 & 1 \\ -1 & -1 & 0 \end{pmatrix} \\
 \text{(a) Vertical (N-S)} & \text{(b) Horizontal (E-W)} & \text{(c) Diagonal (NE-SW)} & \text{(d) Diagonal (NW-SE)}
 \end{array}$$

Figure 3.5: Examples of Sobel filter (top) and Prewitt filter (bottom) to produce a directionally enhanced image, (a) designed to detect vertically oriented edges; (b) designed to detect horizontally oriented edges, and (c) and (d) designed to detect diagonally oriented edges (Gao, 2008).

3.2.2 Digitizing or extraction of the lineaments

After using all the above methods of enhancing the interpretability of the image data, the next step was extracting the linear features. The lineament extraction and merging of the outputs were undertaken by employing ArcGIS 9.3 software. The lineaments were traced based on tonal variation, shape and pattern from each input analyzed in the above methods. Then, the extracted lineaments were merged (in ArcToolbox → Data Management Tools → General → Merge) to produce a single map, but wherever there was overlap of the extracted lineaments, editing was made to avoid the redundant ones.

The lineaments were extracted and merged into a single map in ArcGIS 9.3 software. The shape files were exported into Geomatica 10.1 software to measure the lineaments orientation; in order to see their distribution in each hill, rose diagrams were constructed using GEOrient software.

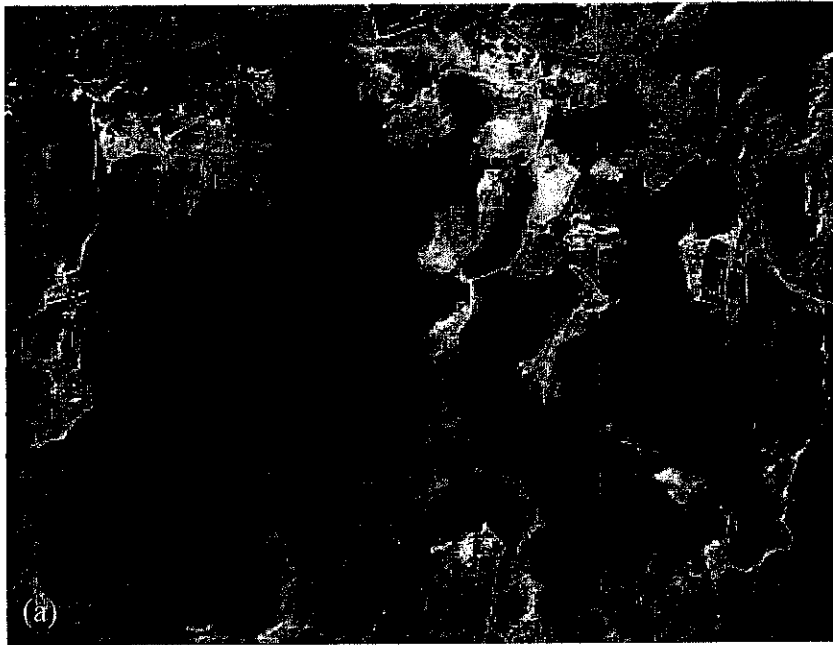


Figure 3.6: Indicates (a) original image of Gunung Lanno, and (b) NW- SE and (c) NE-SW filtered image of Gunung Lanno.

3.3 Measuring paleoflow indicators

In order to understand the paleoflow trend and paleowater level, the following measurements on scallops and notch patterns were undertaken.

3.3.1 Scallops

As water flows through caverns, it forms ripple-like dissolutional features, known as scallops, for example Figure 3.7, which appear on the wall or ceiling. Such features

were measured to study the paleoflow trend in the relict karst caves of the area. However, the fundamental concept was adapted from the empirical study of the following works. Goodchild and Ford (1971) and Curl (1974) considered scallops as good flow markers. And their empirical work showed the relationship between scallop morphology and hydrodynamic parameters. According to Goodchild and Ford (1971), the paleoflow direction can be inferred from the scallops pattern since their orientation is always steeper at the upstream side and the smooth slope is on the downstream side.

Curl (1974) showed that the basic setting for the formation of scallops is the turbulent flow of a solvent over a soluble surface. Figure 3.8 clearly shows the basic mechanism of fluid motion and formation of a scallop, where the main flow (point1) separates to form a jet flow which becomes irregular and turbulent (point 2), above a slow and re-circulating flow (point3), and turns toward the surface to reattach at point 4 (Curl, 1974). This mechanism makes the scallops pattern move downstream as it dissolves further into the cave wall. After the pioneering empirical studies on scallops, many later works reflected the importance of these features in determining paleoflow routes, including Auler (1998) and Ford and Williams (2007).



Figure 3.7: Scallops in the cave passage wall of Sam Poh Tong

In the study area, some of the caves do not show the scallops conspicuously; however, when these features appear quite visibly (for example, Fig. 3.7), the dimensions of the scallops and the conduits were measured. In order to indicate the paleowater flow trends, the pattern of the scallops and their dimensions were measured, and the prominent flow orientations were indicated by adapting the basic concept, from the aforementioned works, on scallops formation and their mode of propagation. In order to show the paleoflow trend in the relict karstic caves, where the scallop features were not conspicuous, passage inclination measurements obtained during cave surveying were taken in to consideration. For example Figure 3.9 illustrates how the passage inclination measurements were used to show the possible overall flow trend. The analyses of these measurements were also compared with that of scallop measurements to indicate if there was any similarity between the flow orientations that could be inferred from them. To show the flow trends from the passage inclination measurements, rose diagrams were made using graph tool.

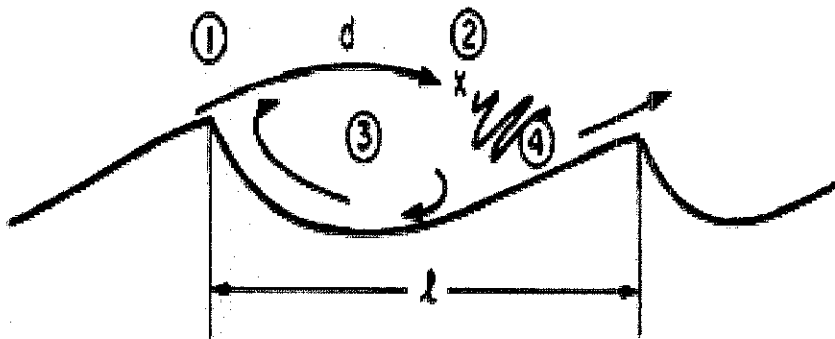


Figure 3.8: Mechanism of fluid motion and formation of a scallop (Curl, 1974).

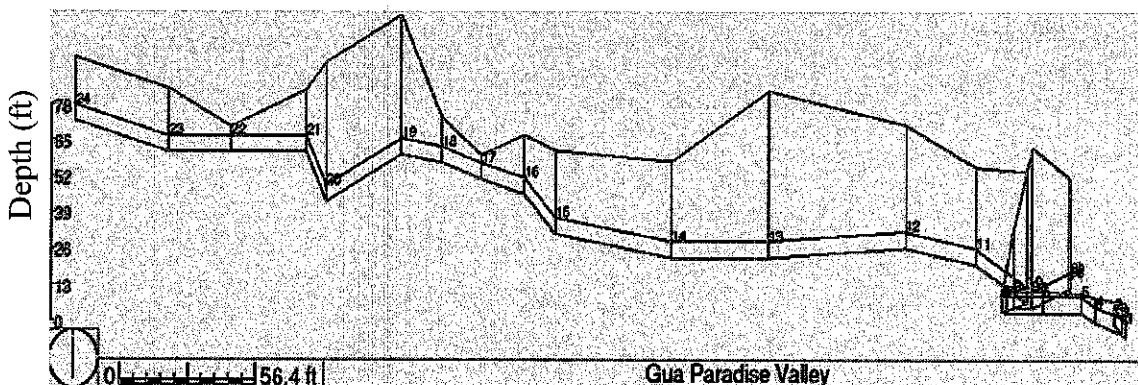


Figure 3.9: Displays the profile view of Paradise Valley cave

3.3.2 Notch Measurement

Like scallops, notches are also dissolution features. However, paleoflow trend cannot be measured from them, rather they can be used as indicators of the existence of paleowater level at a certain height. As a matter of fact, notches are formed by marine or stagnant (pond) or fresh waters, and their appearance at the wall and base of the precipitous hills in the Kinta Valley may mark their formation by one or an alternate effect of these mechanisms.

In order to identify which mechanism/s dominated and the consequent effect on the development of karst in the area, all those notches conspicuously appearing on the face of the precipitous hills, located all over the valley, were measured. The measurement was undertaken using clinometer and measuring tape, and also the elevation of each level of the notch was recorded.

The clinometer was employed to estimate the slope angle from the eye of the observer to the top of the notch, and the measuring tape was utilized to get the horizontal distance from the observer to the wall of the precipitous hill. Thus, the vertical distance (height) was calculated by using simple trigonometric formula. This vertical distance adds up to the height of the observer to get the height of the notches from the base of the hills.

3.4 Rock cooling and associated uplifting rate estimation

Apatite and zircon fission-track analyses are widely used in various geological settings, and they were employed in the estimation of uplift rates (Benjamin et al., 1987; Roden, 1991; Pérez-Arlucea et al., 2005; Lisker et al., 2009). Fission-tracks serve as a thermometer by recording the temperatures at which a sample reached during its uplifting history. That is, by using the distribution of fission-tracks, it is possible to infer the time-temperature relationship or rate of cooling, which in turn enables to calculate the rate of uplift. The detailed description about fission-tracks is given in the literature review part, and the basic notion and application of these linear tracks were adapted to estimate the uplift rate in the study area.

Before determining the uplift rate, the samples passed through the sample preparation and analysis processes. After such processes, the data were employed for modelling the cooling and uplifting history.

3.4.1 Sample preparation and analysis process

From the granite, which adjoins the limestone at the foot of the Cameroon Highlands, five Samples (CH-6 to CH-10) were collected; the locations of the sampling points are as indicated in Figure 3.10. The elevation difference between Sample CH-6 to Sample CH-10 is 766 m; the first sample was collected at an altitude of 944 m a.s.l., and subsequently the other samples were collected from elevations (a.s.l.) of 717 m, 577 m, 340 m, and 178 m. Since the samples were collected almost along the same vertical profile, they are considered to have passed through similar thermal conditions.

The granite samples used in this study were prepared and analyzed by A to Z, Inc., Idaho, USA, according to the following sequence. Firstly, the presence of apatite and zircon must be determined and then separated from the rock sample. Thus, the samples were crushed, and density and magnetic mineral separation techniques were used, which resulted in finding up to 40 apatite and zircon grains in each sample. After separation of the mineral grains they were mounted in epoxy resin and polished, to create a grain mount containing a sufficient number of apatite grains that are individually distinguishable. They are then properly polished to reveal clear and flat internal grain surfaces across which spontaneous fission tracks have accumulated. After polishing, the exposed grains on each apatite mount are easily etched by immersing the grain mount in dilute 5.5 Molar HNO_3 for 20 seconds at 21°C to reveal any spontaneous fission track that intersects the polished surface. Once etched, the feasibility of measurement of the AFT parameters (i.e., grain ages and confined track lengths) is then assessed by quickly scanning the polished and etched grain mount to determine the amount and quality of any apatite present.

A detailed process was used by A to Z Inc. in determining the fission track length and age, and the following steps (Ketchman, 2005) briefly explain the methods undertaken to measure AFT grain ages:

Step 1 Selection of an apatite grain for fission-track age analysis

Step 2 Confined track-lengths were measured together with the angle between the confined track and the C-crystallographic axis

Step 3 The kinetic parameter, D_{par} , for the selected apatite grain, was measured.

Step 4 Spontaneous fission tracks over some area of the selected apatite grain were counted

Step 5 Uranium concentration (or relative concentration) for the selected apatite grain were measured using LA-ICP-MS.

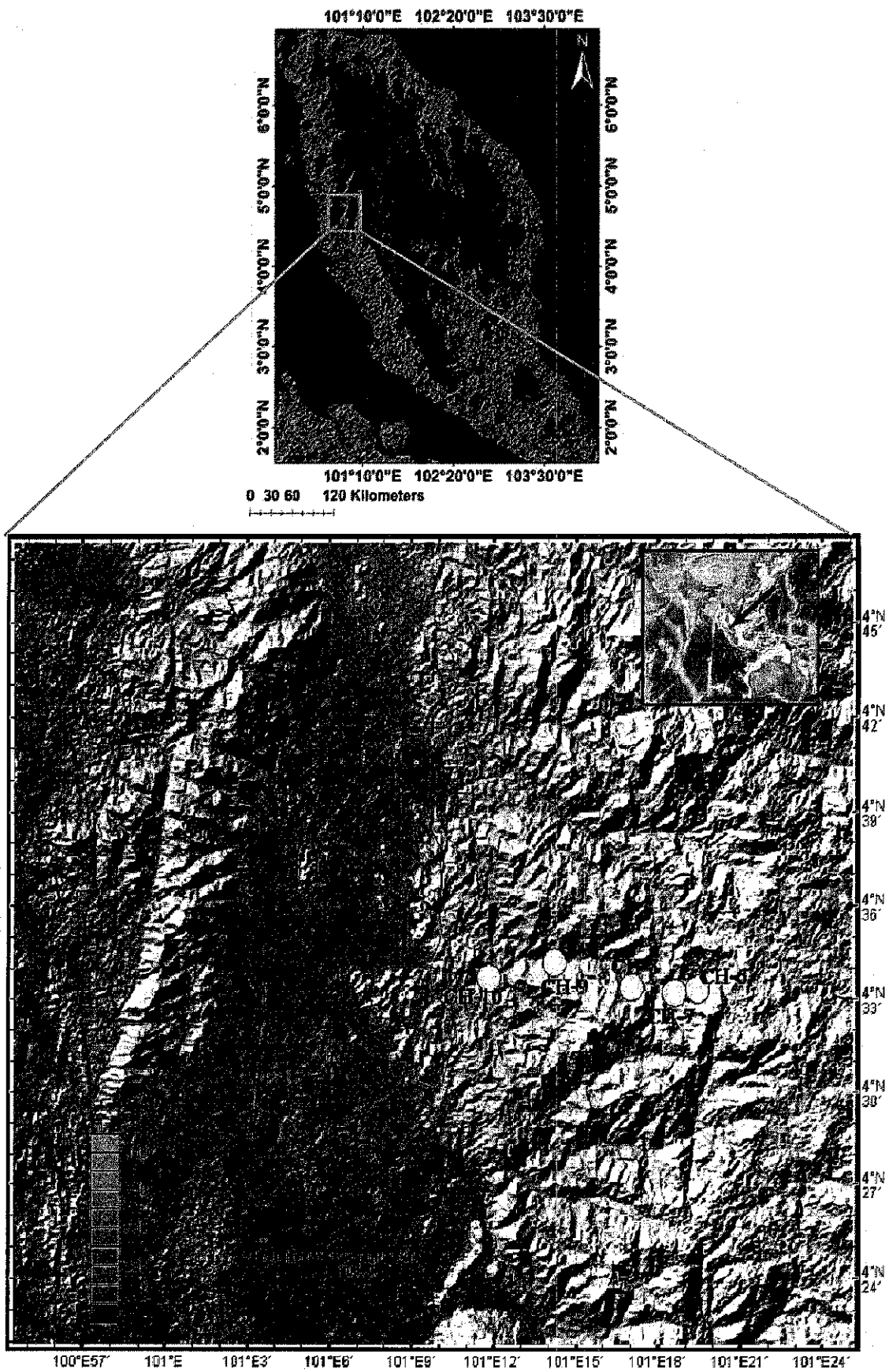


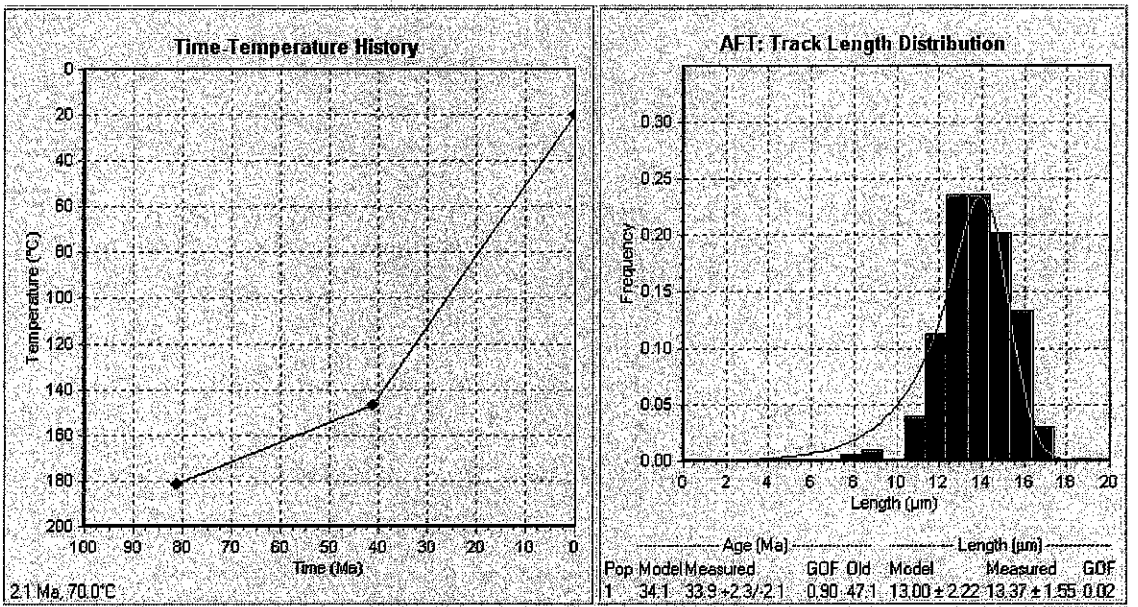
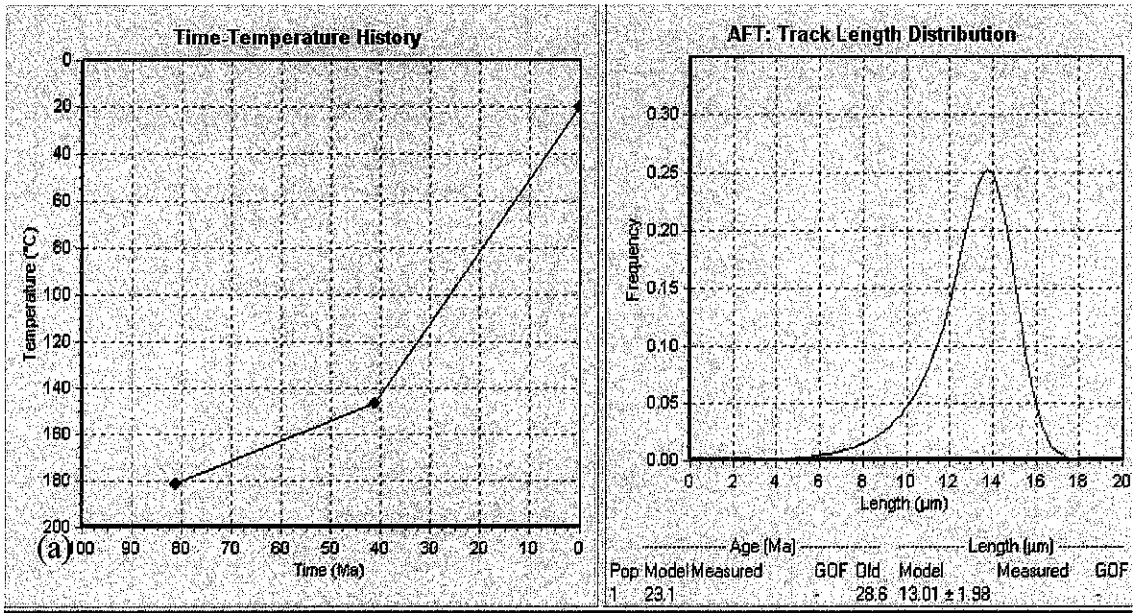
Figure 3.10: Map of the Kinta Valley indicating sampling locations marked by yellow circles. The remnant limestone hills are marked by surrounding red line.

3.4.2 Thermal Modelling

To interpret the cooling histories of the samples and their exhumation through the upper crust, forward and inverse models were constructed. Forward modeling was performed to predict what fission-track age and track length distribution we get for a particular time-temperature history; the model takes into account the possible information on the geological evolution of the area.

In order to compare the predicted fission track parameter with the measured values in the forward model, the measured fission track data was superposed. This model is done in the HeFTy program, a software that enables the changing of the time-temperature paths, and observation of the associated variations in FT age and track length values. For instance, the way how the forward model is constructed is illustrated in Figure 3.11a, which shows the time temperature path and associated modelled FT age and length. When this forward model is superimposed by a measured FT data, it appears as in Figure 3.11b. The time-temperature path is consistently varied so that the program updates the predicted FT parameters by undertaking experimentally calibrated calculations of fission-track annealing. This is done until the program finds a good agreement or fit, as indicated by the GOF (goodness-of-fit), between the time-temperature path and the kinetic model. This observation, in turn, is used to interpret the real data.

Secondly, inverse modeling is performed. In this model the thermal histories are constrained to reproduce the observed data. And this is undertaken after generating a number of forward models, where in each of these models the predicted apatite fission-track parameters are compared to the measured values, and then the good and acceptable forward models are used to provide quantitative constraints on the time-temperature histories. In this inverse model, the default Monte Carlo modeling scheme (search method), which generates a large number of independent time-temperature paths, is used. In order to get a good fit or solution, many time-temperature paths can be tested, and for this study, 20,000 time-temperature paths were tested for each model.



(b)

Figure 3.11: A forward model (a) Before measured AFT data is superimposed, and (b) After AFT data is fitted, but without further varying the t-T path to get the best fit.

Since the samples used in this study were collected from a vertical section of massive granite, various geological constraints were not considered in the inverse model, except for the timing of earliest intrusion, arbitrary time before the maximum annealing temperature and fission-track age, and surface temperature. And with this, it is supposed that the HeFTy program (i) will have the liberty to determine the possible time range in which the sample entered to a certain temperature range where the tracks are retained, and (ii) will search many possible paths (out of the 20,000 paths),

and will find any likely cooling phenomenon and associated timing. This enables to determine which of the possible paths pass certain statistical criteria, so as to exhibit the acceptable or good fit to the data.

This study uses the acceptable and good fit to the data based on the definition given in Ketcham (2005), which indicates that a model is considered to be 'good' if all statistics for all populations being modelled are above 0.50, and the model is considered to be 'acceptable' if all statistics for all populations are above 0.05. Although it is common to get thousands of acceptable time-temperature paths through a number of inverse model run, it is possible to obtain an interpretation which is reasonable and well constrained. Thus, for the GOF with 0.5 and above, the time-temperature path is considered to be perfectly matched with the data.

3.4.3 Approach to estimate the rate of uplift

Since fission-tracks are partially annealed at different temperature zones (PAZ), the fission-track age indicates the time at which the mineral passed the PAZ. The basic idea here is that, it is possible to understand at what age and depth a sample of rock possibly reached the zone of effective closure temperature when it is uplifted from the depth of crystallization. For instance, the cartoon in Figure 3.12 illustrates the time at which the fission-tracks in apatite partially annealed as the cooling and uplifting episode continued.

Commonly estimation of the uplifting rate is performed via the mineral pair method, i.e. using data from apatite and zircon of a single sample. However at times, it is also performed by considering two samples at different elevations. In this case, only one mineral, apatite or zircon, can be taken into consideration. Although the former method is usually used, this study takes into account the estimation of uplift rates from both methods.

In the case of mineral pair method, the following data are used, (a) the difference in cooling ages of two different minerals (e.g. apatite and zircon), (b) the difference in their annealing temperatures, and (c) the regional geothermal gradient (Benjamin et

al., 1987; Copeland et al., 1987). The second approach considers only the difference in cooling ages for a single mineral.

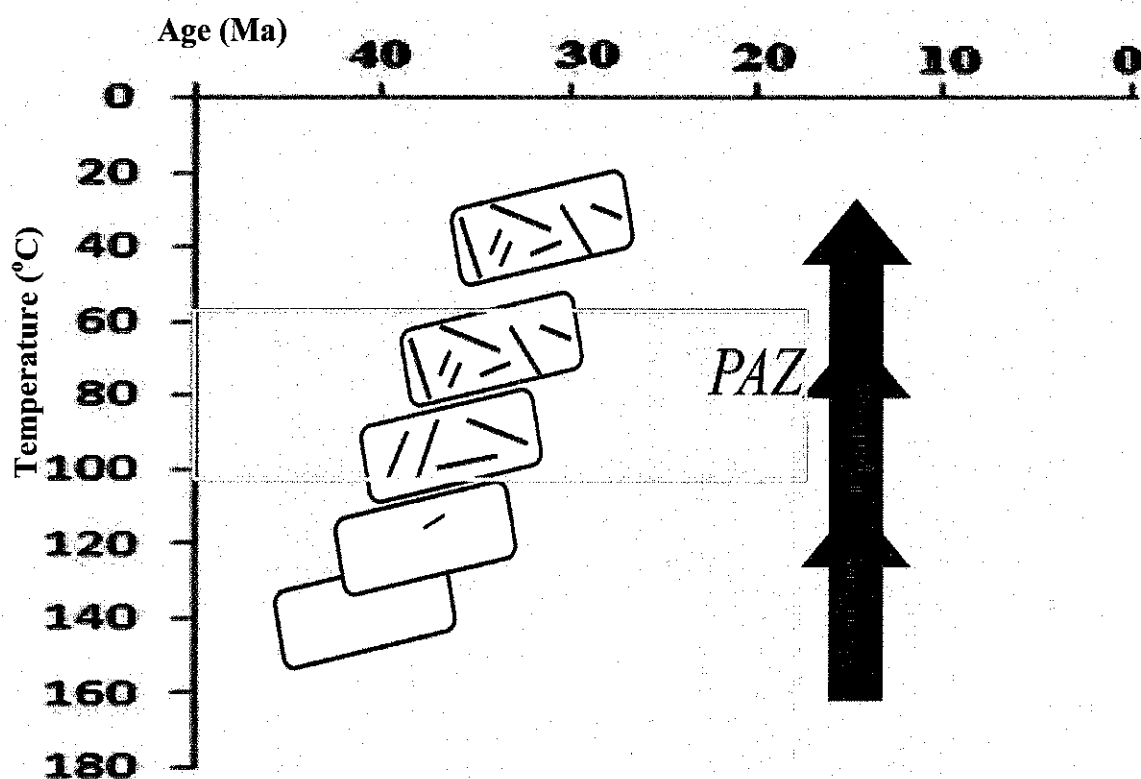


Figure 3.12: A cartoon illustrating the nature of apatite fission-tracks during cooling and associated uplifting through time

CHAPTER 4

RESULTS AND DISCUSSION

4.1 Results

4.1.1 Morphological description of karstic caves

The Kinta Valley is typified by a number of small hills, but the major ones that characterize the valley are Tempurung, Lanno, Rapat, Datok, Lang (Fig. 1.1). The diameters of these hills are 6.5 km, 2.6 km, 3.4 km, and 1.6 km respectively. These hills, including the smaller ones, occupy about 2.5% (~25km²) of the valley area. The hills are honeycombed with karst caves whose lengths range from 60m to 1500m. The surveyed karstic caves located in the isolated limestone hills of the area are described below. Henceforth, some common local terms such as Gunung (Hill), Gua (Cave) will be used in the text. Furthermore, since the elevation inside a cave cannot be measured, the frequently mentioned term 'height', in all graphs, is synonymous to elevation differences between two points along the passage. All tables indicating each cave survey measurements, except for Gua Kanthan (Table 4.1), are placed in Appendix A. The following cave maps are constructed based on the survey data indicated in each table.

4.1.1.1 *Gua Kanthan*

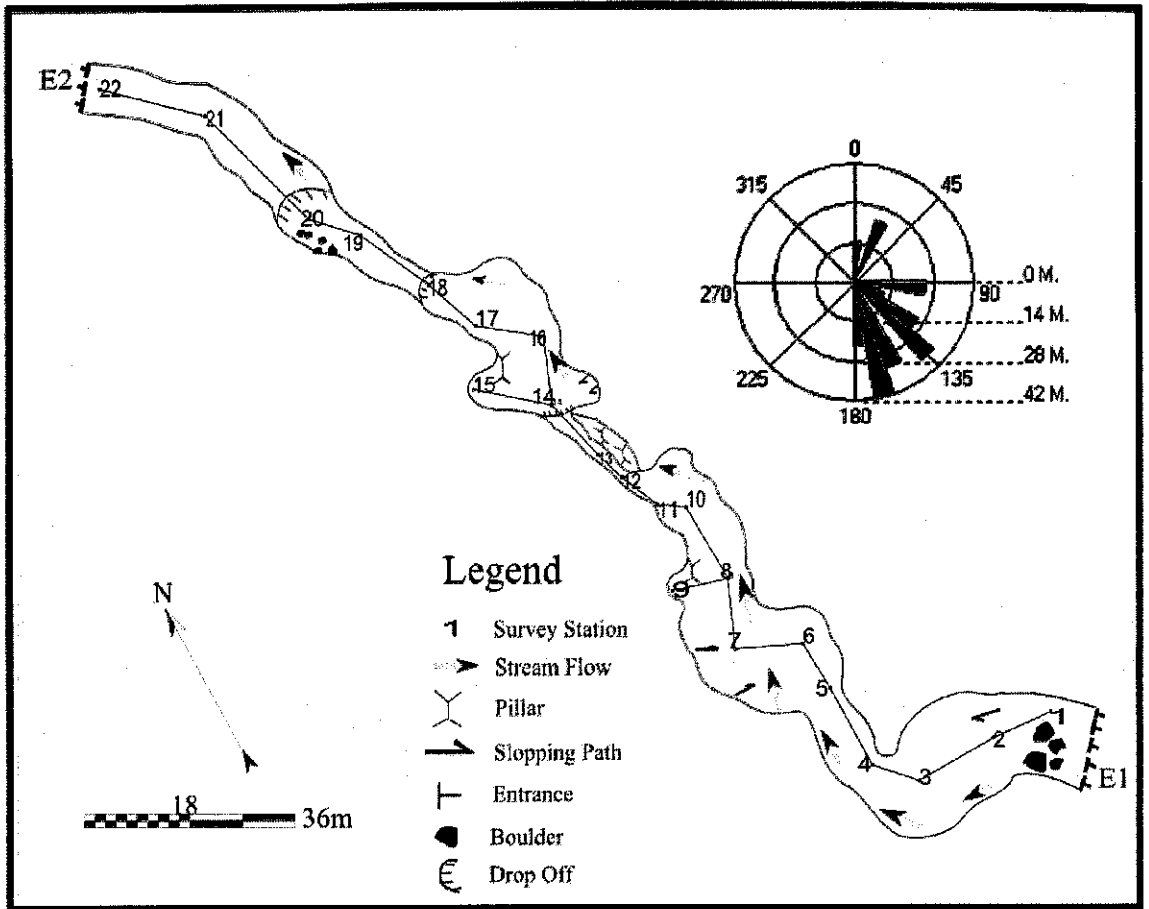
This cave is situated at 101°7.3' Easting and 4°45. 6' Northing, at an elevation of 72m a.s.l. The entrance of this cave is located about 25m above the base of the hill. A stream flowing inside this cave (Fig. 4.1a) appears and disappears under the cave floor, along the course of its flow to the other opening (entrance). Above the surface

of this stream, notches that are 1.4 m high and 1.2 m deep are conspicuous (Fig. 4.2). The undulating notches appear gently dipping and making a smooth plane. At the base of Gunung Kanthan, outside Gua Kanthan, shallow depth corrosion notches, located about 13.4 m above the base, are noticeable.

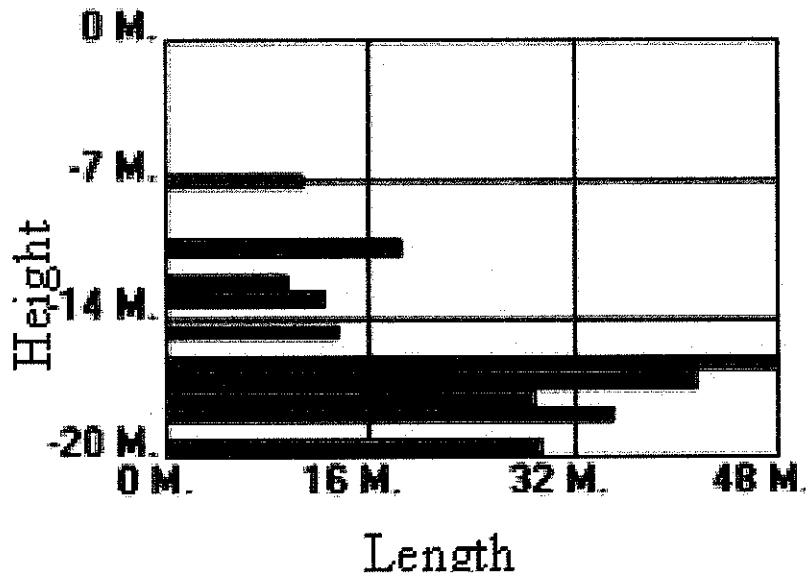
The inset rose diagram in Figure 4.1a indicates the general orientation of the passage, which prominently follows a NNW-SSE trend. The total survey length of Gua Kanthan is 260m. Its maximum width is about 24m, where its height is 19m (Table 4.1). The cave passage is generally steep, with collapsed breccias forming undulations. Between the upper and lower entrances of the cave there is a 20m height difference, where 0 m is a benchmark for the first entrance at which the survey begins. In this cave, the longest passage is found at 15-18m below the top entrance (Fig. 4.1b).

Table 4.1: Measurements collected during the survey of Gua Kanthan

From	To	Length	Azimuth	Inclination (deg.)	Left	Right	Up	Down
1	2	13.0m.	275	-33	14.0m.	1.7m.	3.8m.	1.8m.
2	3	18.0m.	270	-35	7.2m.	7.5m.	27.0m.	1.8m.
3	4	8.8m.	317	-16	10.0m.	14.0m.	19.0m.	1.8m.
4	5	15.0m.	0	6	3.2m.	0.8m.	1.6m.	1.8m.
5	6	8.8m.	357	-1	3.5m.	1.3m.	29.0m.	1.8m.
6	7	12.0m.	295	11	12.0m.	5.7m.	32.0m.	1.8m.
7	8	11.8m.	23	0	8.5m.	12.0m.	28.0m.	1.8m.
8	9	10.6m.	287	23	15.3m.	3.7m.	28.0m.	1.8m.
8	10	14.0m.	358	8	8.3m.	3.5m.	28.0m.	1.8m.
10	11	5.4m.	305	20	5.0m.	6.4m.	13.0m.	1.8m.
11	12	7.6m.	335	-5	0.7m.	9.8m.	7.8m.	1.8m.
12	13	7.0m.	342	-35	0.5m.	0.8m.	8.0m.	1.8m.
13	14	11.5m.	345	0	0.6m.	0.5m.	13.0m.	1.8m.
14	15	14.0m.	310	6	3.0m.	8.1m.	12.8m.	1.8m.
14	16	12.0m.	22	-13	3.0m.	8.1m.	12.8m.	1.8m.
16	17	12.0m.	307	7	6.5m.	5.3m.	17.0m.	1.8m.
17	18	11.0m.	339	12	1.6m.	12.0m.	20.0m.	1.8m.
18	19	14.5m.	334	-5	2.5m.	0.8m.	15.6m.	1.8m.
19	20	10.0m.	316	-18	4.5m.	1.2m.	26.0m.	1.8m.
20	21	25.0m.	343	8	4.3m.	5.0m.	20.0m.	1.8m.
21	22	20.0m.	313	20	3.0m.	3.0m.	15.0m.	1.8m.



(a)



(b)

Figure 4.1: (a) Map of Gua Kanthan, (b) Graph illustrating the variation of cave passages length at different height from the initial survey point (0 m).

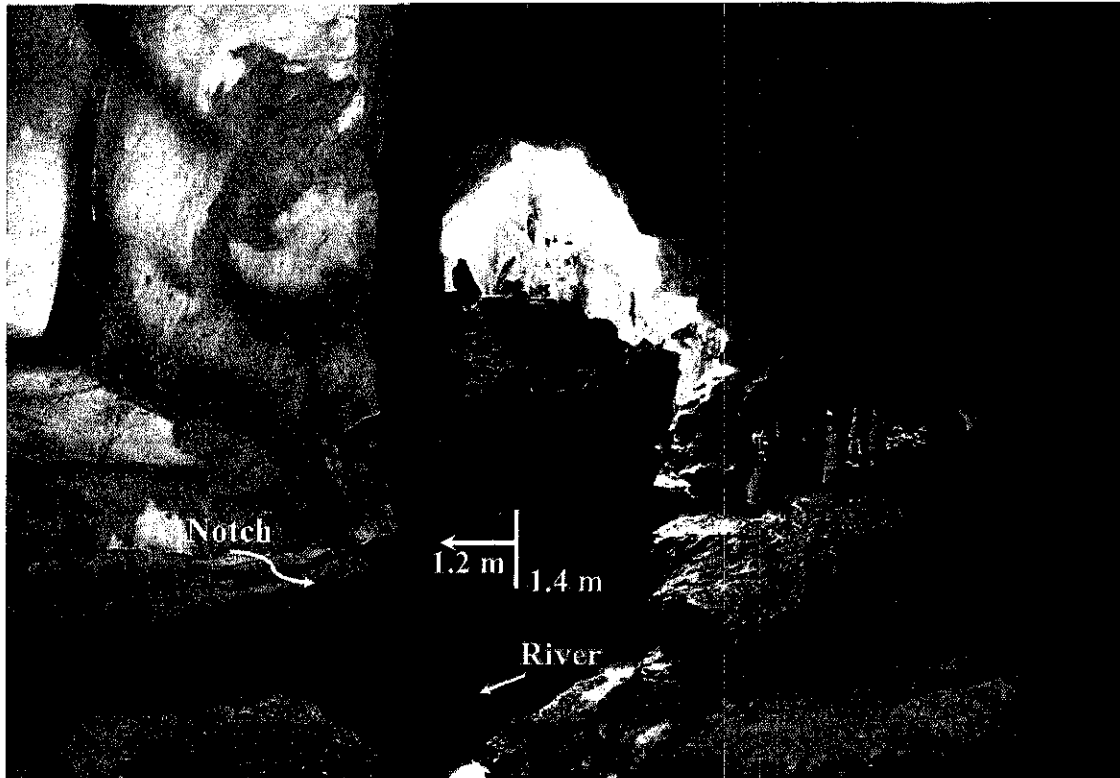


Figure 4.2: River flowing inside Gua Kanthan; its gradual lowering left its imprint or notch, which indicates a paleo-waterline.

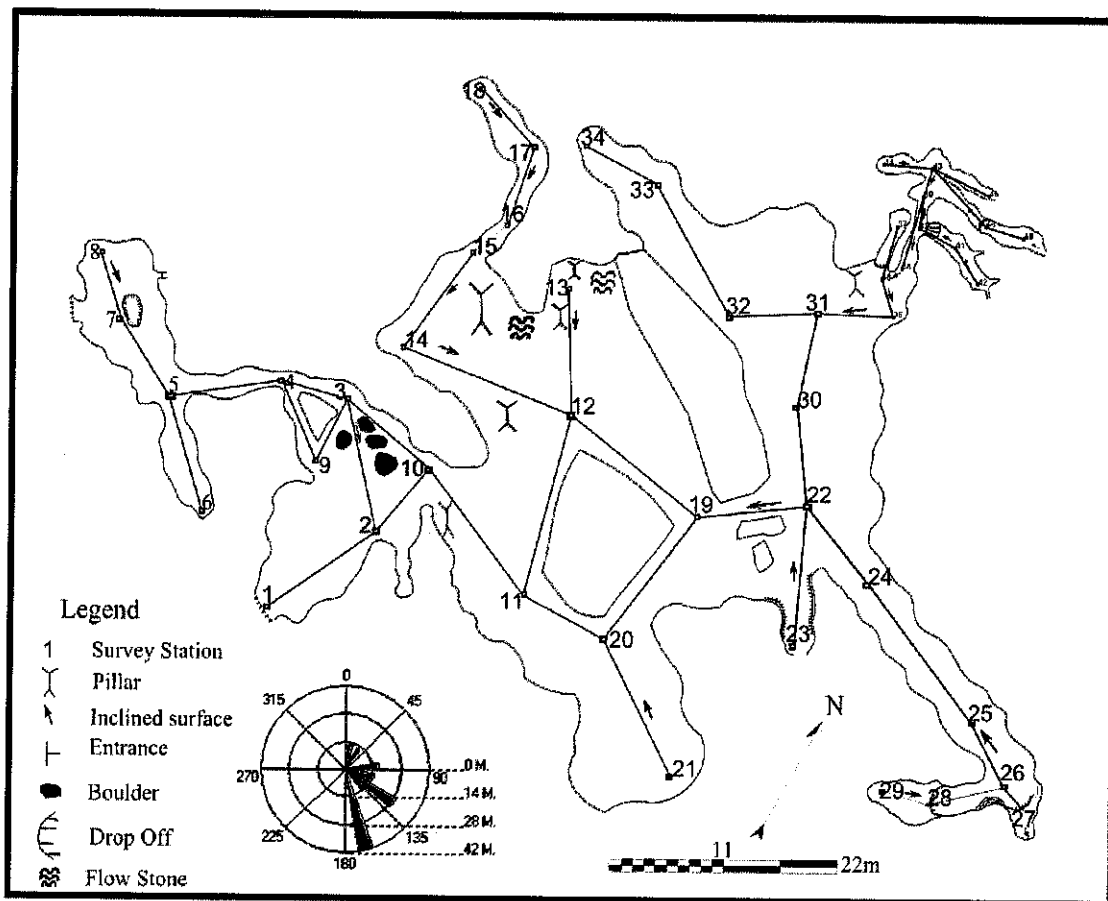
4.1.1.2 *Gua Layang Layang*

This cave is located at 101°9.2' Easting and 4°39.2' Northing, at an elevation of 80m a.s.l. It is characterized by various dead ends and narrow conduits, up to 1.5m wide. In general, *Gua Layang Layang* is typified by collapsed passages which form relatively big chambers, compared to the overall dimension of the cave.

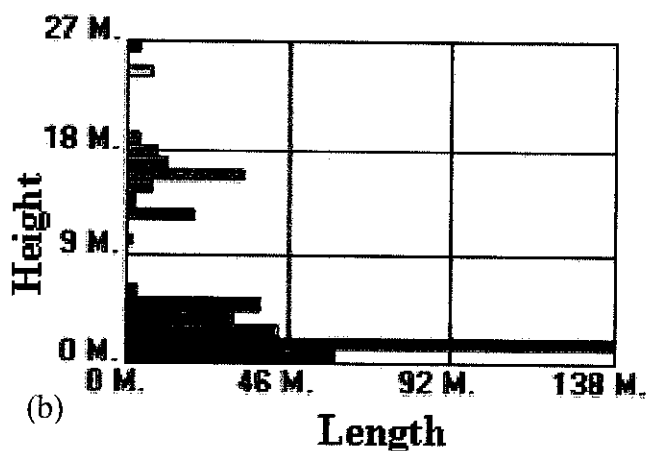
Below the floor of this cave, ground water is visible, and the cave chamber wall appears to be smooth and scalloped. The bedrock appears to dip 32° to the west and its strike direction is N40°E. The azimuth of the scalloped passage is 290° and the inclination is towards this trend. Considering only the short and linear passages, the prominent trend of this cave is NNW-SSE, as the inset rose diagram (Fig. 4.3a) indicates.

The longest passage of *Gua Layang Layang* is situated at the base of the hill, as

Figure 4.3b attests, and it is also characterized by a short and narrow upper level passage which is 1m wide. The presence of relatively fast drip water, which is seeping through the ceiling, scalloped passage walls and speleothems that are deposited in a linear pattern are characteristic features of the big chamber which is about 32m wide.



(a)



(b)

Figure 4.3: (a) Map of Gua Layang Layang with an inset rose diagram indicating the prominent passage trend, and (b) Illustrates the variation of cave passage lengths at different heights from the initial survey point (0 m).

4.1.1.3 *Gua Anak Tempurung*

The entrance of this cave is situated at 4°24'20'' N and 101°12'10'' E, at an elevation of 65m. The cave is located about 50m away from the bounding granite. It is formed in beds that are dipping almost vertically, where the precipitous hill is marked by a fault scarp orientated N70°E. The dipping angle of the bedding, in which the cave is located, is almost vertical, about 85° and has a N7°E strike trend.

Although the morphology of the cave passage appears to be convoluted, the prominent trend, as the inset rose diagram in Figure 4.4a indicates, is NNW-SSE. The total survey length of Gua Anak Tempurung is 397m. The height difference between the two ends of the cave entrance is 9 m, and the longest passage is located at 6-9 m (Fig. 4.4b) below the first entrance. This cave is characterized by narrow passages, varying from 2m to 10m in width, but with a big height difference, i.e. 0.5m to 20.8m (Apendix A, No. 3).

A river which comes from the adjoining granite crosses this cave. Sediments embedded in the shallow grooves of the cave wall, at about 6 m from the floor, are conspicuous, and may mark the pre-existing level of the river. The upper and lower entrances of this cave are generally oriented in the N-S direction.

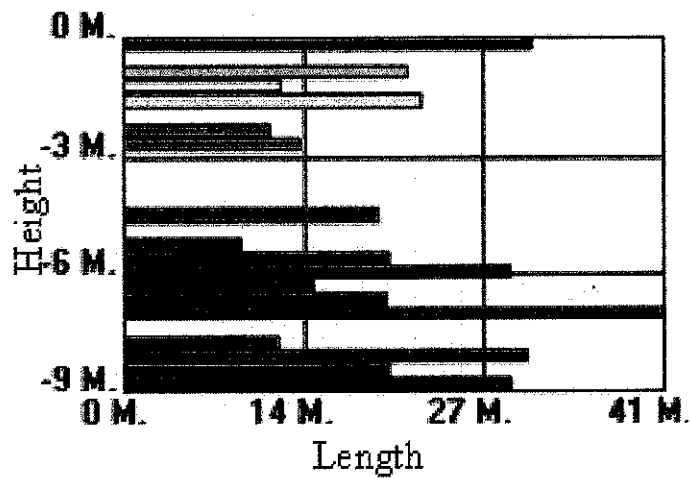
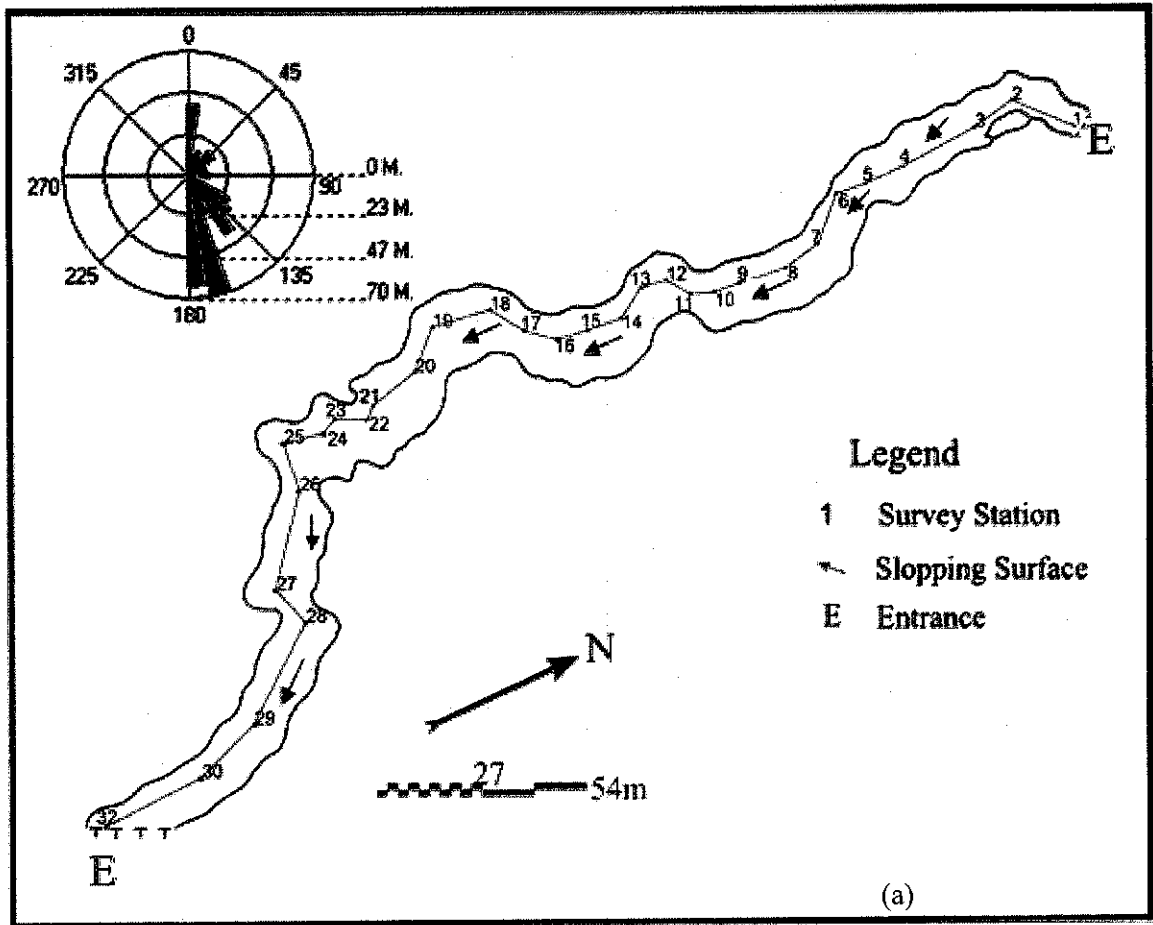
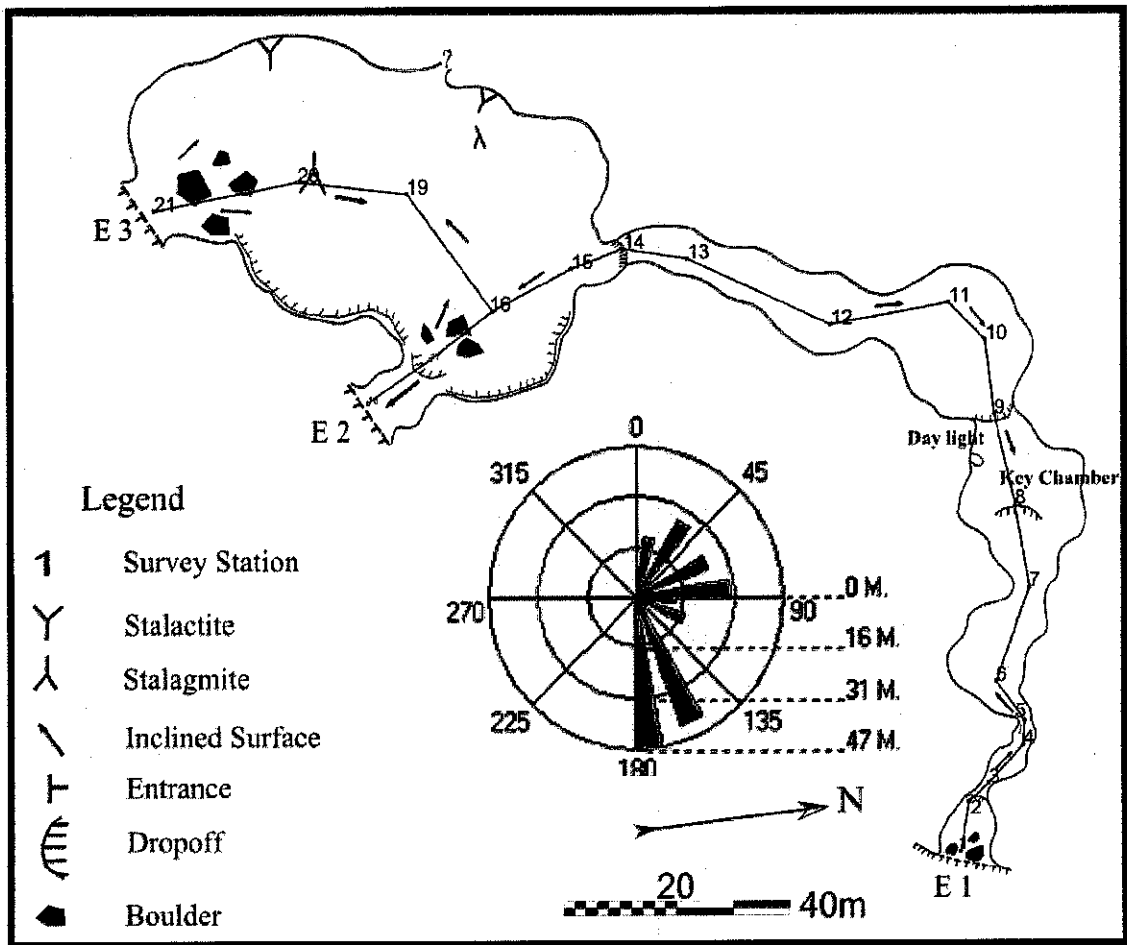


Figure 4.4: (A) Map of Gua Anak Tempurung, and (b) Illustrates the variation of cave passages length at different height from the initial survey point (0 m).

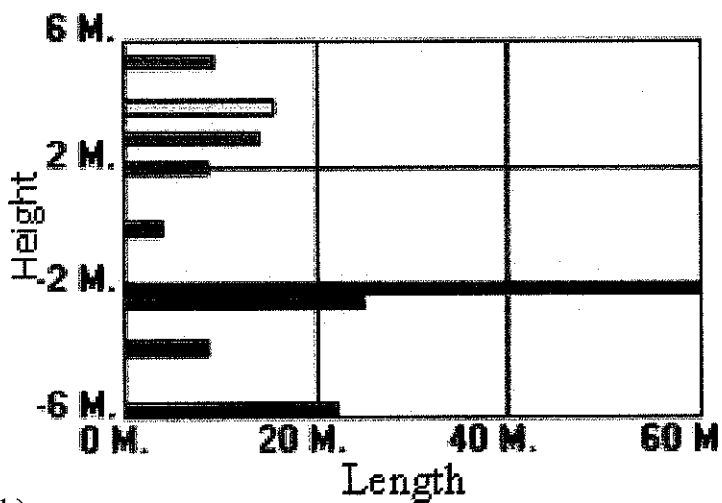
4.1.1.4 *Gua Datok*

It is located at 4°37.3' Northing and 101°9.7' Easting, at an elevation of 70 m a.s.l. The bedding in Gunung Datok stands almost vertically with a strike direction almost N-S and dips about 85° to the east. The main entrance of Gua Datok is situated very close to the granite-limestone contact, and about 100 m above the base of the hill. The entrances of this cave are opened in a general southern direction facing the adjoining granite. Between the two extreme sides of the cave openings, E1 and E2 (Fig. 4.5a), there is a height difference of about 12 m (Fig. 4.5b), excluding the chambers' length. Because of the collapse of the cave passages and the associated formation of the chambers, the passage shows extreme inclination values (Appendix A, No. 4). Similarly, as a result of the influence of the collapse, the general orientation of the cave appears to be E-W, NE-SW and N-S (Fig. 4.5a).

Gua Datok is characterized by a big chamber, which is about 60 m wide and 70 m high. The presence of relatively smaller chambers, collapsed breccias, and cave fill sediments, all the way through this cave, are quite conspicuous. Outside this cave, about 50 m above the base of the hill, small openings along a fracture are clearly visible as indicated by the small blue circles (Fig. 4.6). These openings can be further extensions of Gua Datok, as the last opening of this cave is indicated as E3 in Figure 4.5a, and from the outside it is marked by the yellow circle (Fig. 4.6).



(a)



(b)

Figure 4.5: (a) Map of Gua Datok, (b) Variation of cave passage length at different height from the initial survey point (0 m).

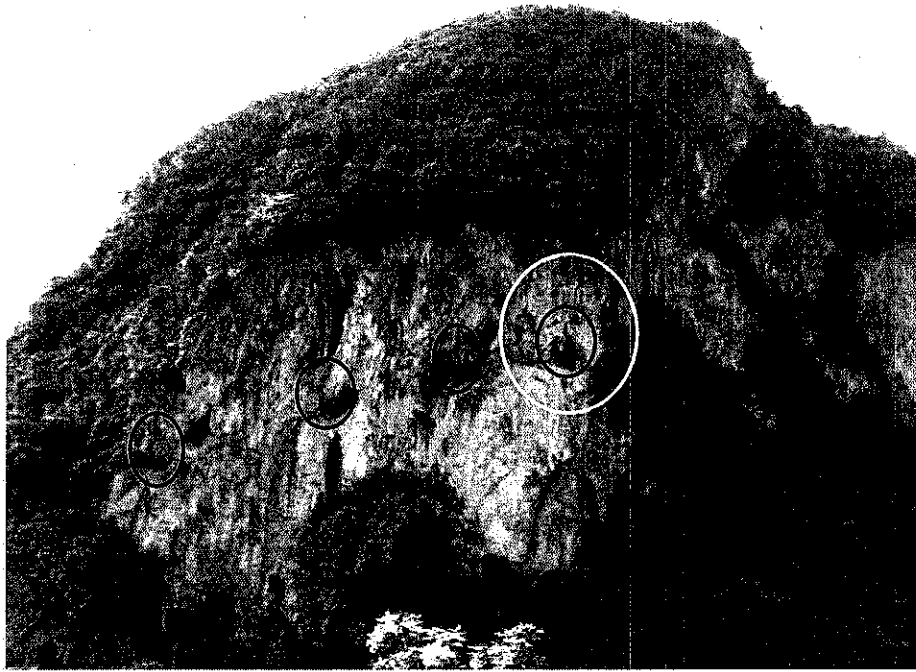


Figure 4.6: Openings along a fracture line, possibly indicating continuity of Gua Datok passage along a fault or fracture trend.

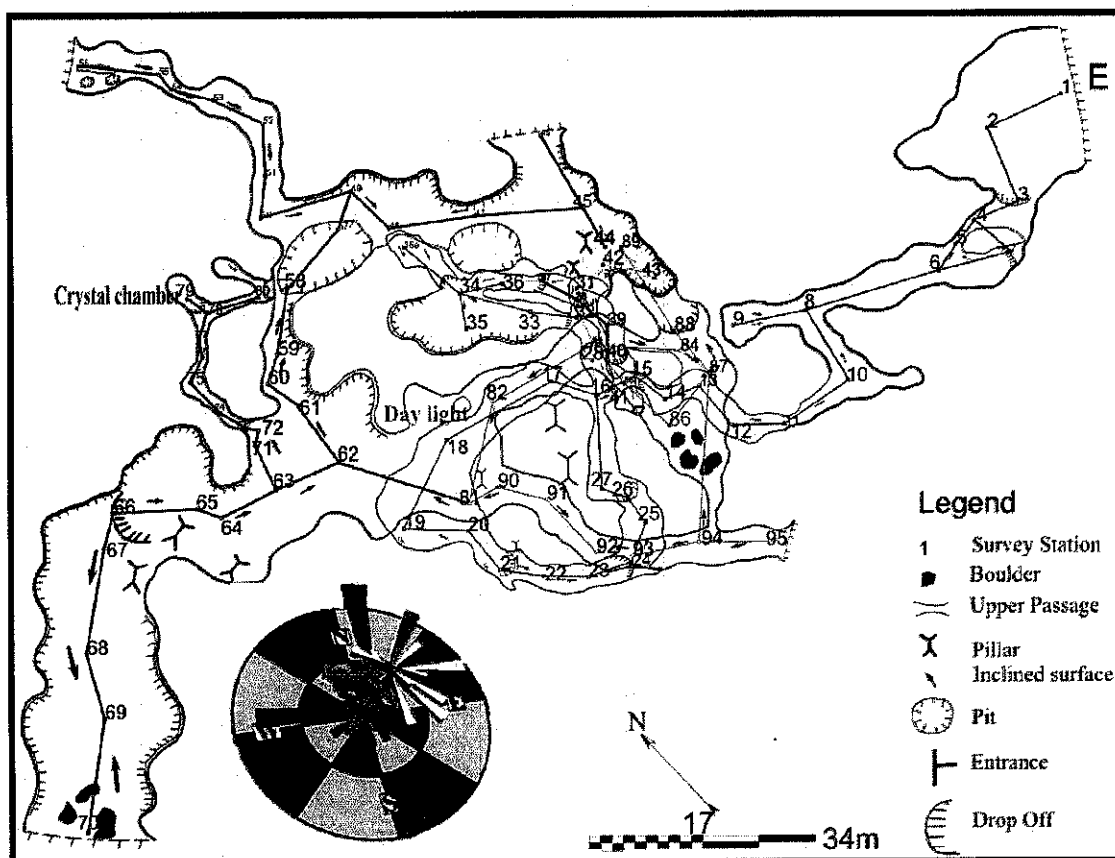
4.1.1.5 *Gua Kandu*

It is located at 4°26'52'' Northing and 101°10'27'' Easting, and at an elevation of 73m a.s.l. The bedding, within which this cave is formed, appears to dip 60° to the NW. Kandu Cave has different entrances located at the base of the hill, at 6 m, 15 m, and 35m above the ground surface. The main entrance at the base is a chamber with a diameter of 25 m and a height of 18 m.

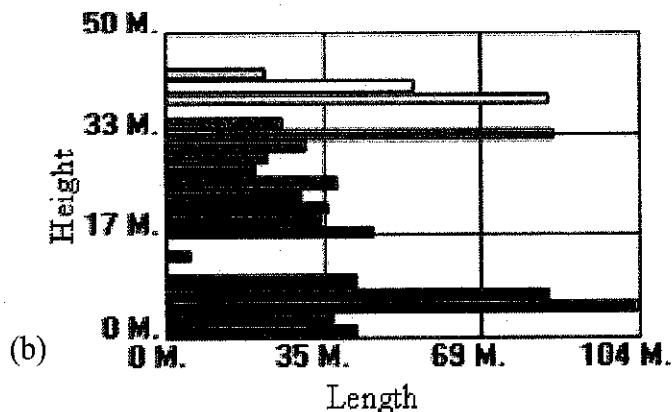
Gua Kandu is typified by multi-layered passages, as indicated in Figure 4.7a and its 3D view in Figure 4.8. Merging of these passages, in some places, formed chambers as wide as 20 m. Collapsed passages, which are 5 m wide and 12 m high, appear to be connected by narrow passages which have widths within the range of 0.5 to 1m.

Linear and circular passages are characteristic patterns of this cave, and these passages have very smooth walls and ceilings. The narrow passages in the upper level of this cave have a prominent NNW-SSE orientation, and the general trend for the multi-levelled passages is N-S, as indicated by the inset rose diagram in Figure 4.7a.

Fine sediments deposited at various levels of the cave passages are conspicuous, and in some places, a mixture of collapsed breccias and sediments which resulted from the merging of multi-layered passages are evident. The longest surveyed cave passages occur mainly in the lower level of the cave (Fig. 4.7b), as the majority of the middle layer is typified by collapse. The lower part of Gunung Kandu, which hosts Gua Kandu, shows deep undercuts, and ground water which possibly lies underneath the cave floor, is evident at the base of this hill.



(a)



(b)

Figure 4.7: Map of Gua Kandu and associated inset rose diagram indicating the multi-layered passages orientations, (b) Variation of cave passages length at different height.



Figure 4.8: 3D view of Gua Kandu.

4.1.1.6 *Gua Kepayang*

It is situated at $4^{\circ}30'43''$ northing and $101^{\circ}7'42''$ Easting, at an elevation of 63m a.s.l. The cave is hosted in an isolated small hill located in the western part of the valley. Gua Kepayang is characterized by two levels, at the base of the hill and at 13m above the base, respectively. The base of the hill is typified by deep undercuts and narrow conduits, but the upper level is characterized by collapsed passages which form a big chamber, with a diameter of about 30m.

The entrance and the major breached part of this cave, at the upper level, face towards the southeast, and appear to have generally an arc shape. Typical characteristic features of this cave include, (1) sediment deposited in both the upper and lower levels of the cave, (2) expansive void below the upper level of the cave floor, (3) smooth and ripple-like pattern on the ceiling and wall of the cave, and (4) dome-shaped ceiling pockets.

Because of the unevenness of the cave floor, which appears to be caused by the collapse of small chambers and passages, the height difference between the two extreme entrances, i.e. E1 and E2 (Fig. 4.9a) is 4m. The morphology of this relict

cave may attest to the pre-existence of a multiple karstification process. Thus, it is difficult to draw a prominent trend of the cave passages, as the inset rose diagram in Figure 4.9a indicates. Despite that, the ENE-WSW and NW-SE trends appear as principal orientations of the cave passage, excluding the chamber.

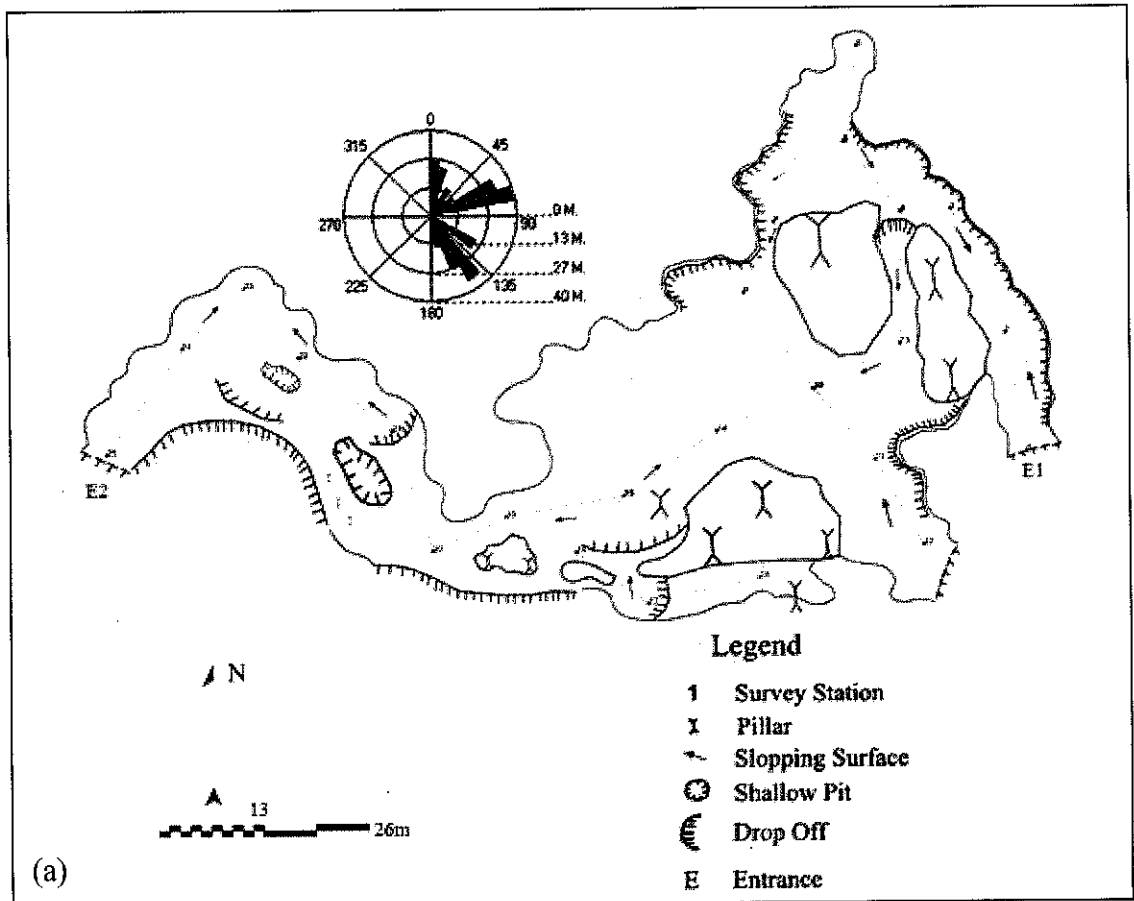


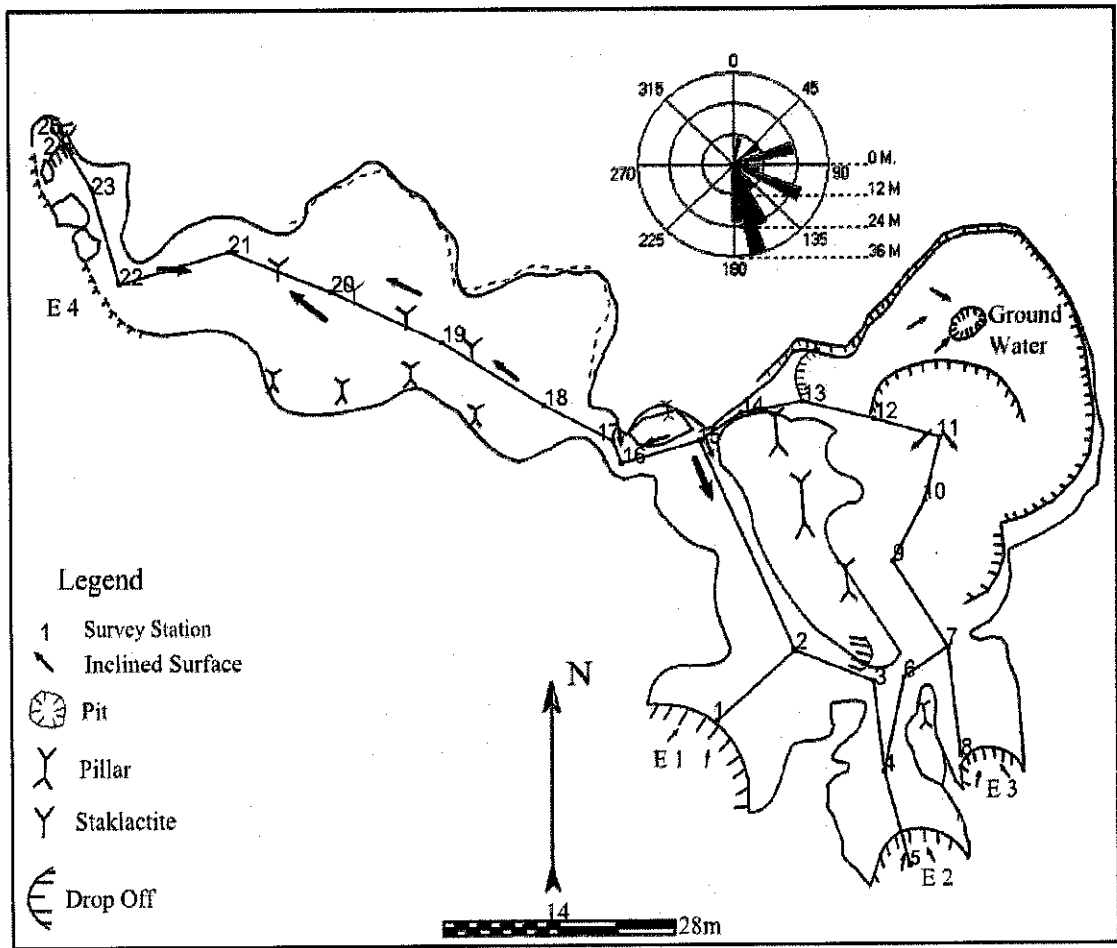
Figure 4.9: (a) Map of Gua Kepayang, and (b) Variation of cave passages length at different height from the initial survey point (0 m).

4.1.1.7 *Gua Masoora*

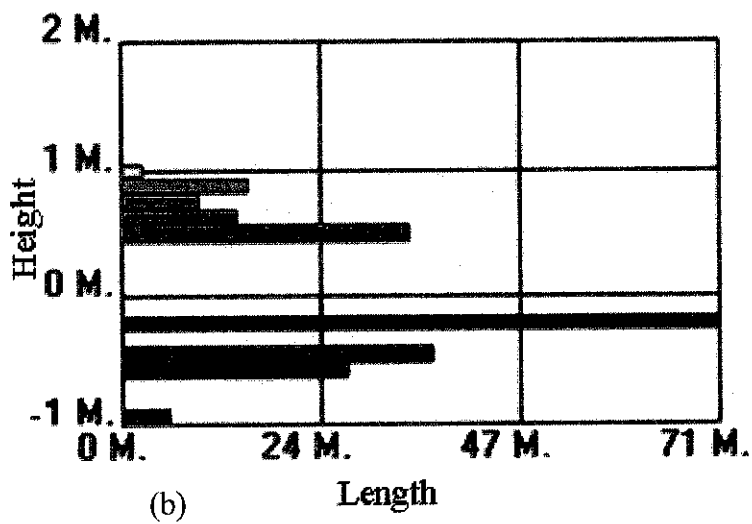
a) *Gua Masooral*

It is situated at 4°37'35'' Northing and 101°5' 5'' Easting, at an elevation of 66m a.s.l. This cave is hosted in a small hill which is located in the western part of the valley. In this hill, the bedding dips 35° to the northwest and its strike direction is N-S. *Gua Masooral* (Fig. 4.10a) is located at the base of the hill, and is characterized by breached openings in the southern and western sides of the cave. Though *Gua Masooral* seems to have been influenced by multiple karstification processes, its general trend, as indicated in the inset rose diagram (Fig. 4.10a), is NW to NNW. It is the trend of the longest path that aligns with the direction of the NW-SE oriented fracture trace and associated stalactites which are formed along the trace. Since this cave is filled with sediment, the height of the passage (Fig. 4.10b), unlike other caves, does not as such vary at different locations. It has almost 1.5m height difference between the higher and lower levels.

Some of the typical features that are evident inside this cave include, (1) thick sediment deposit, about 3.5m thick (Fig. 4.11a). The sediment which is observed sticking to the cave wall is of clay size, but the sediment which covers the cave floor, as indicated in the inset picture on Figure 4.11a, is grey in color and has a mixed texture, i.e. fine sand mixed with silt-size sediment, (2) linear trends of stalactites along a NW-SE direction, which matches or is aligned with the big passage having a width of 11m and 8m height (Fig. 4.11b) (3) cave ceiling which has ripple-like pattern, particularly in the upper level of the cave (Fig. 4.11b) and smooth ceiling at the lower level of the cave (Fig. 4.11c), (3) subsurface water, which appears stagnant, underneath the cave floor, and a big chamber, as wide as 20m and 15m high, and (4) expansive void, which is about 1m high, and has a smooth and flat ceiling, are characteristic features of this cave.



(a)



(b)

Figure 4.10: (a) Map of Gua Masoora 1, and (b) Indicates variation of cave passages length at different height from the initial survey point (0 m).

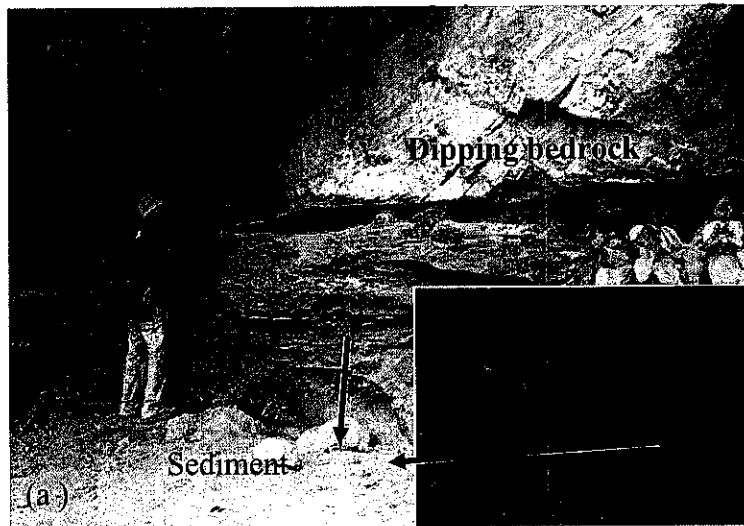


Figure 4.11: Pictures illustrating (a) Thick sediment deposit inside Gua Masooral, (b) Stalactites and columns formed along the direction of fracture trace, (c) Expansive void separated by columns, which were possibly formed along a fracture, and filled with sediment.

There are various evidences in Gua Masoora 1 that indicate the origin of extant relict karst features. Such evidences also provide clues for the origin and gradual evolution of this karstic cave. Figure 4.12 illustrates the different dissolution features that may be the result of a sequence of events or concomitant origin.

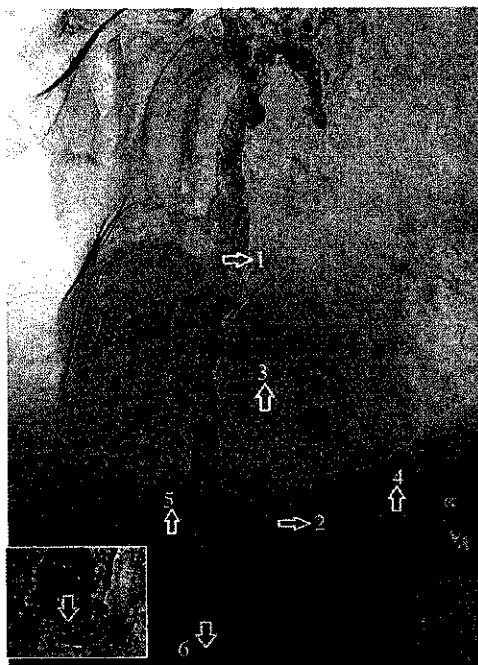


Figure 4.12: Dissolution features that may provide clues for the origin and gradual development of Gua Masoora 1.

In this figure, the mark labelled as number one (1) indicates stalactites which are formed along a fracture trace orientated 60° - 240° , different from the orientation of similar features, for example Figure 4.11c; however, the fracture trace, labelled as 2, has almost the same trend as Figure 4.11c. The small dome-shaped ceiling, labelled as 3, appears to be different from the underlying flat ceiling, labelled as 4. A stalactite formed via a vertical opening, possibly a shaft, labeled as 5, is observed vertically above the hole, where the blue arrow is located, labeled as 6, through which the subsurface water is clearly evident. This water, below the cave floor, is indicated in the inset picture in Figure 4.12.

b) Gua Masoora 2

About 80m far away from Gua Masoora 1, a small cave, Gua Masoora 2 (Fig. 4.13), is situated in the same hill, i.e. Gunung Masoora. Generally, Gua Masoora 2

appears elongated along a N-S prominent trend, as the inset rose diagram in Figure 4.13 indicates. It can be considered as a small chamber cave, with a maximum width of 13.2m and a height of 4.9m, but a wide passage, 2.9m wide and 5.7m high, seems to separate it into two small chambers. This cave does not show any distinct dissolutional features, including smooth ceiling and wall, and scallops, that may indicate flow trend, unlike the nearby Gua Masoora1.

Gua Masoora 2 is mainly typified by the existence of pools of water underneath the cave floor. Although there is no seepage or surface water flow in between the two caves that may suggest a link between the two, the presence of subsurface water underneath their floor attests to the possible connection or flow of water from the same source. Furthermore, the presence of a quite narrow conduit that goes away from this chamber cave, for example the conduit with the '?' symbol in Figure 4.13, indicates the continuity of the passage, and its possible connection with Gua Masoora1.

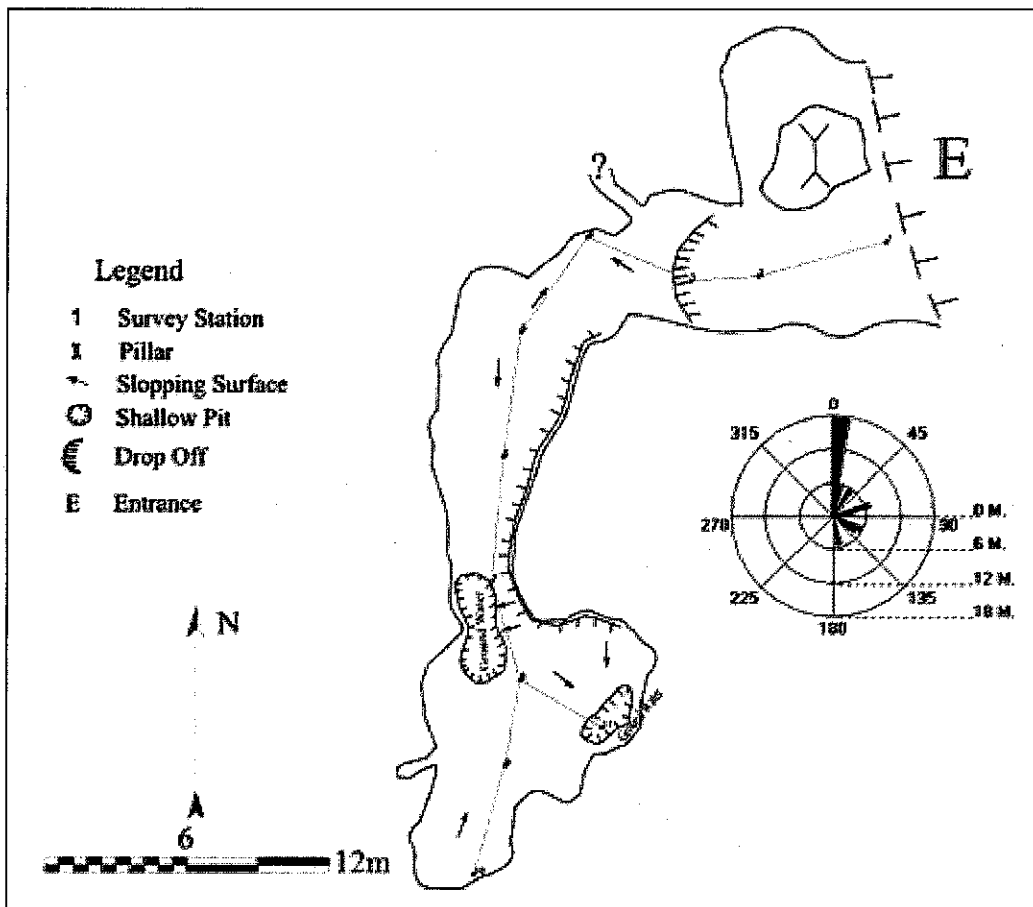


Figure 4.13: Map of Gua Masoora2

4.1.1.8 *Gua Tempurung*

The lower part of the Gua Tempurung entrance is located at 4°24.96' Northing and 101°11.26' Easting, and at an elevation of 61m. It is situated along an almost vertically dipping bed of Gunung Tempurung, which is found close to the adjoining Main Range granite (Fig. 4.14a). Gua Tempurung is characterized by a multi-layered cave system, where big chambers in the upper layer are underlain by narrow channels or conduits. Figure 4.14b shows the narrow and undulating channel formed by the extant river, which is still eroding the channel, and the inset rose diagram (Fig. 4.14b) exhibits the prominent and longest flow trend towards the NNW. As Figure 4.14c indicates, between the upper and lower entrances, i.e. E1 and E2, there is a 26m height difference, and the longest passage of it is found at the lower level of the cave.

The measurement (Appendix A, No. 9) is taken only for the lower level of the cave passage marked by the convoluted river flow, as the upper layer is characterized by collapsed cave passages and associated formation of big chambers. The presence of relatively big chambers (Fig. 4.15a) in the upper layer and the lower part of the cave appears to be the result of merging of small chambers. These chambers, particularly in the lower part of the cave, appear in between the narrow passages, and Figure 4.15b indicates the flow of a river entering the chamber before it disappears again through the other narrow conduit. The total surveyed length of Gua Tempurung is 1.51 km.

There is evidence of sediments deposited at various levels of the cave. At the higher level of the collapsed passages, which formed big chambers, about 90m above the extant river flowing underneath this chamber, vestiges of sand deposits embedded on the wall of the chamber are conspicuous. At the bottom of the chamber and above the extant flowing river sand deposits with similar textures are also evident. The dimensions of the chambers in Gua Tempurung vary in different locations, from entrance one (E1) to entrance two (E2). The widest chamber has a diameter of about 80m and is 90m high, whereas the smallest one is 16m wide and 18m high. The convoluted passage underneath the big chambers also has different dimensions. The dimensions range from a very narrow conduit, i.e. 2.2m in width and 0.6m in height to

6m in width and 22m in height. In some places, very wide but low-height channels, i.e. 28m in width and 0.7m in height exist.

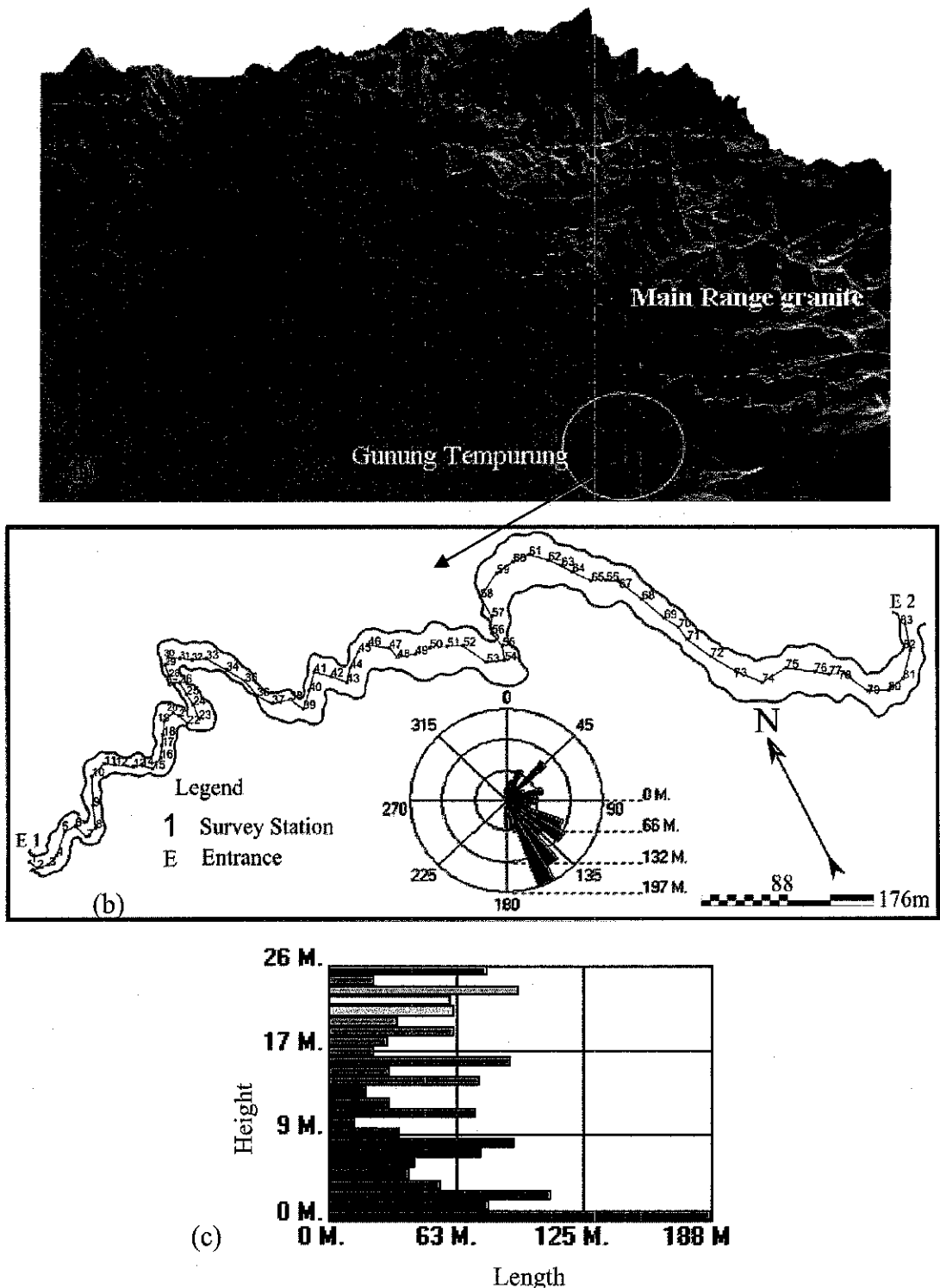
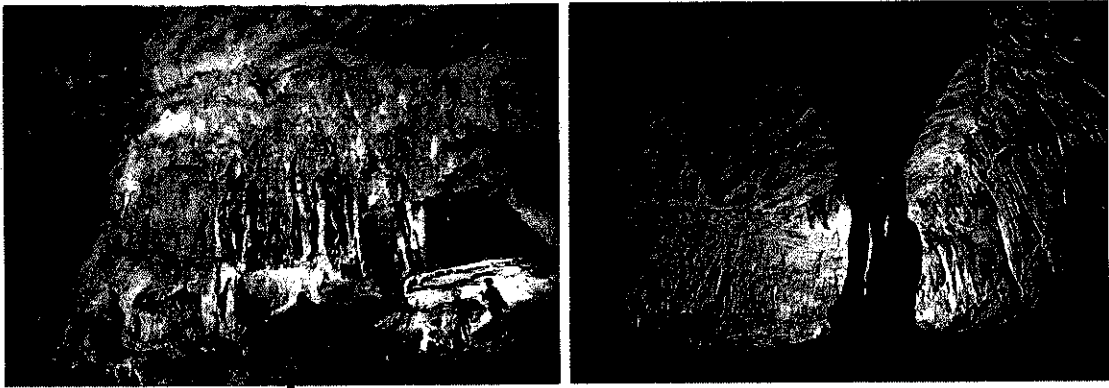


Figure 4.14: (a) The Kinta Valley bounded by granite, and the yellow circle marks Gunung Tempurung, close to the Main Range granite, (b) The lower level of Gua Tempurung formed by the sinuous extant river flow, (c) Variation of cave passage lengths at different heights from the initial survey point (0 m).



(a) River flowing through the narrow conduit to the chamber (b)

Figure 4.15: River entering into the big chamber before disappearing via a narrow conduit, and (e) A chamber that characterize the upper part of Gua Tempurung.

4.1.1.9 *Gua Paradise Valley*

It is situated at 4°33' Northing and 101°8' Easting, and at 67m a.s.l. In general, the cave appears as a linear passage cave (Fig. 4.16a), with its upper entrance located about 25m from the base of the hill. The upper part of the linear passage morphology covers about 210m, and the lower narrow and convoluted passage covers about 47m. In between the two entrances, the dimension of this cave passage varies at different locations. In the upper level, where the passage has collapsed, the dimension reaches up to 16m wide and about 12m high, and forms a small chamber. On the contrary, in the lower level of the cave, where there is a narrow and uncollapsed passage, the passage becomes 1.8m wide and 0.5m high (Appendix A, No. 10). The inset rose diagram in Figure 4.16a illustrates the prominent trend of the cave passage towards the NNW-SSE. Since the cave has a gently dipping passage, the overall height difference between the two entrances is only 24m, and is relatively the longest passage that can be seen in the upper and lower levels (Fig. 4.16b). The profile of this cave (Fig. 3.9) further indicates the variation of passage depth at different survey points, and the locations where collapsed passages took place.

Because of the thick fine sediment deposit inside the cave and its dry condition, due to hydrologic loss which is responsible for its development, this cave can be considered as a relict. However, drips of water coming via a column and disappearing

underneath the upper part of the cave floor have been observed. A very narrow and linear conduit, about 0.5m wide and 0.5m high, which diverts away from the main passage morphology, near to the collapsed passage, at Station 20 (Fig. 3.9), is also conspicuous in this linear cave.

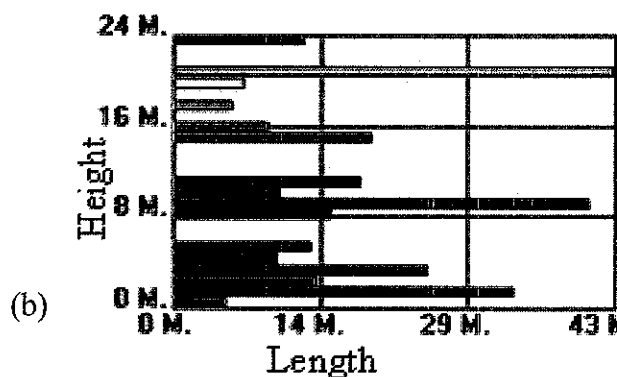
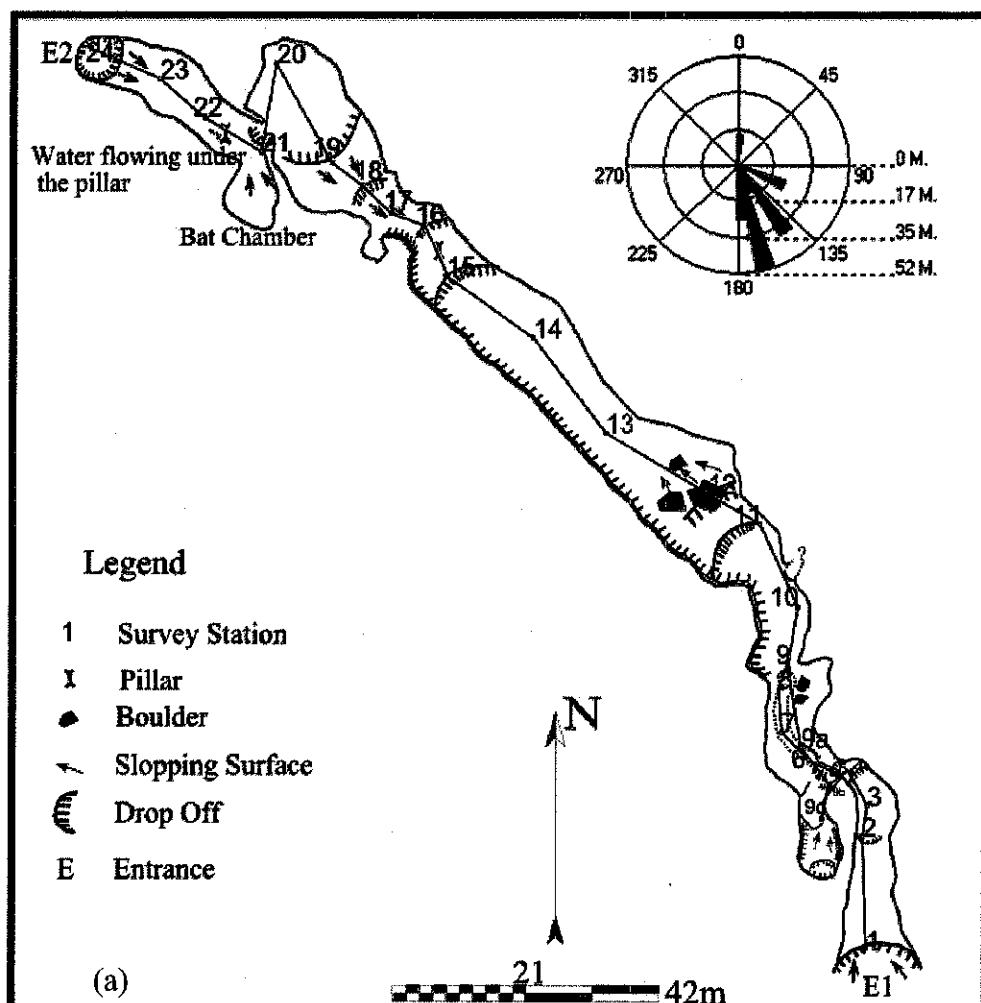


Figure 4.16: (a) Map of Gua Paradise Valley and inset rose diagram indicating the prominent cave passage trend, (b) Variation of cave passage lengths at different heights from the initial survey point (0 m).

4.1.1.10 Gua Naga Mas

It is situated at $4^{\circ}30.5'$ Northing and $101^{\circ}8.9'$ Easting, and at 86 m a.s.l. Gua Naga Mas can be considered as a chamber cave, and the entrance of the cave is located about 35m above the base of the hill. The entrance of this chamber cave (E) (Fig. 4.17) faces the weathered granite which is located 200m away (Fig. 4.18b). This cave is characterized by the presence of fine sediment (mud) deposit on its floor and is even evident on the ceiling of the chamber; and this may indicate that the chamber cave might have been flooded before. The presence of an underlying chamber, though with smaller dimensions, is conspicuous further inside this cave (Fig. 4.17). In a small chamber, which is located at the breached entrance of the cave, about 40m above the base of the hill, fossil bones embedded in the ceiling is quite noticeable (Fig. 4.18b). Small domes inside this mud-covered ceiling are also evident.

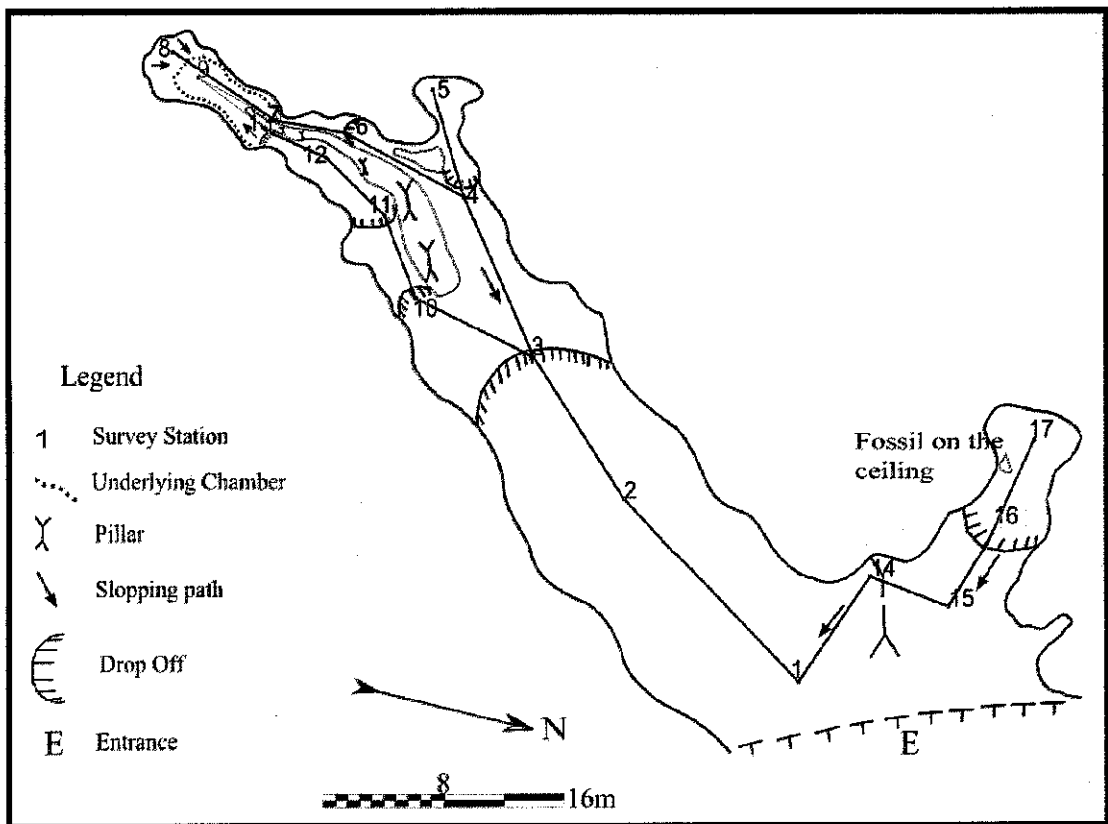


Figure 4.17: Showing map of Gua Nega Mas



(a)

(b)

Figure 4.18: (a) Weathered granite viewed from the entrance of gua Nega Mas, and (b) Mud covered ceiling of a small chamber with noticeable fossil bones embedded on it.

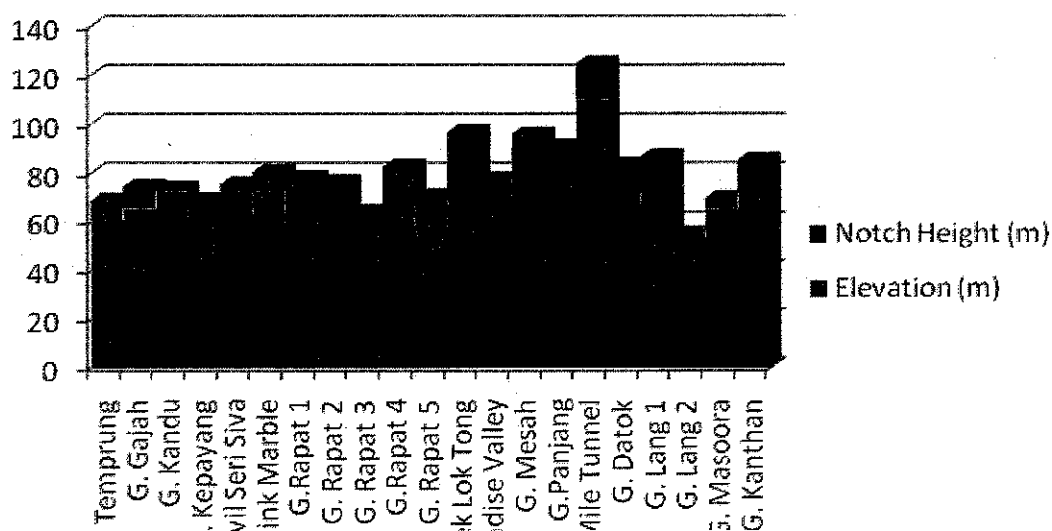
4.1.2 Notch Measurement

Notches are grooves formed on carbonate rock walls as a consequence of gradual lowering of flowing water, wave action, or stagnant water. Commonly, notches appear horizontal, with shallow or deep indentation, possibly marking paleowater level. On the face of the precipitous hills, whether they host karst caves or not, different types of notches at various levels (Fig. 4.20 and 4.21) are quite evident in different places of the Kinta Valley. Although multi-leveled notches are observed and measured in all places, only the highest level of the notches is considered to see the spatial relation among them.

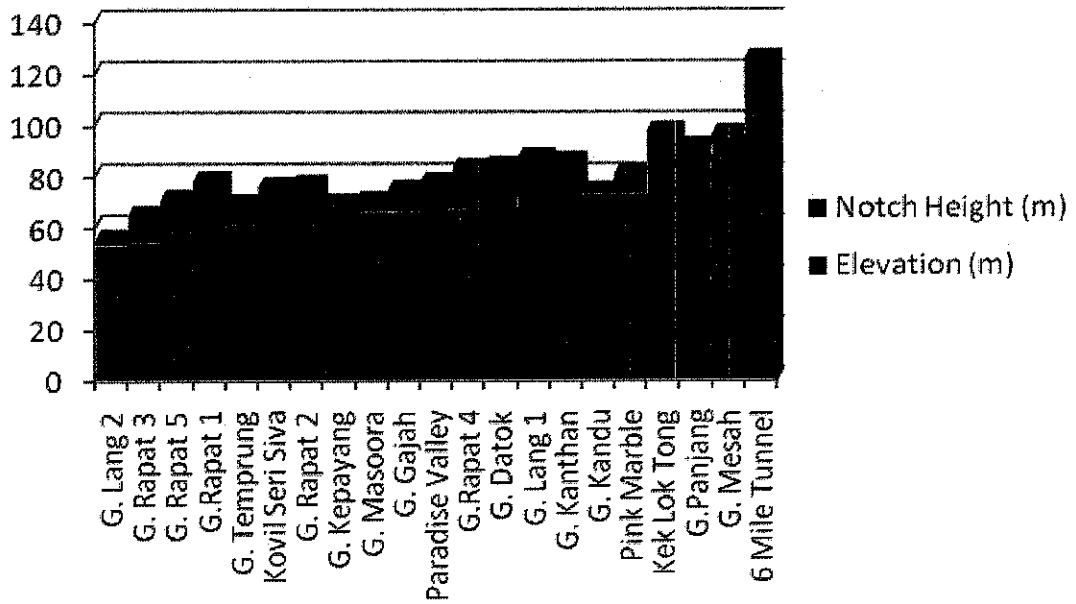
Various types of notch morphology are conspicuous in different hills. There is no uniformity in their type even within the same hill, and in many places it is possible to see mixed types of notches in one exposure. The following table summarizes the distribution of these notches in the area.

Table 4.2: Location of notches and elevation (a.s.l.) of the area, where the maximum level (height) of the notches above the base of the hills were measured.

No.	Name	Coordinate		Elevation (m) at the base of hill	Max. Notch Height (m) above base of hill
		Northing	Easting		
1	G. Temprung	4°25'5''	101°11'12''	61	8
2	G. Gajah	4°22'58''	101°10'12''	66	8.6
3	G. Mesah	4°26'42''	101°12'51''	95	1
4	G. Kandu	4°26'56''	101°10'23''	73	1
5	G. Kepayang	4°30'47''	101°7'42''	62	7.1
6	Kovil Seri siva	4°31'3''	101°8'22''	61	14.6
7	Pink Marble	4°31'53''	101°6'50''	73	7.6
8	G.Rapat 1	4°33'29''	101°6'54''	59	19
9	G. Rapat 2	4°33'8''	101°7'12''	61	15.5
10	G. Rapat 3	4°33'4''	101°7'21''	54	10.6
11	G.Rapat 4	4°33'50''	101°7'15.4''	67	15.9
12	G. Rapat 5	4°33'43''	101°7'32''	58	12.8
13	Kek Lok Tong	4°33'14''	101°7'50''	88	9
14	Paradise valley	4°33'35''	101°8'17''	67	10.5
15	G.Panjang	4°36'16''	101°7'47''	88	3
16	6 Mile Tunnel	4°36.6'	101°9.5'	110	15
17	G. Datok	4°34'59''	101°9'40''	68	15.5
18	G. Lang 1	4°36'31''	101°5'3''	72	14.8
19	G. Lang 2	4°37'21''	101°5'29''	53	2.2
20	G. Masoora	4°37'32''	101°5'56''	66	4
21	G. Kanthan	4°45'36''	101°7'11''	72	13.4



(a)



(b)

Figure 4.19: (a) Variation of notches height from southern part of the study area all the way to the north, and (b) Illustrates notches distribution with respect to base of hills increasing elevations a.s.l.

The notch measurements were taken from the precipitous hills where the caves are situated, and in some places far from the surveyed caves. The height of the notches is consistent inside and outside the caves, particularly where the rivers are still flowing through them.

Considering all the observed notches in the area, and putting them according to their place of occurrence (Fig. 4.19a), which is in this case from the south (Gunung Tempurung) to the north (Gunung Kanthan), there is an irregular distribution or variation in maximum height of the notches above the base of the hills. Similarly, putting sites of measurements having the same elevation together (Fig. 4.19b) shows variations in notches height. However, when the elevation at the base of the hills and the maximum level (height) of the notches above the base of the hills are added, it is evident that in some places the notches appear at similar elevation.

Besides the occurrence of the notches at different elevations, the shapes and repetition of these features in a vertical section varies from place to place. In general, single and composite types of notches are evident in the study area.

Some of these notches appear as arc shape with a deeply incised wall at the base, but with shallow grooves with high frequency, i.e. sharp change in the subsequently occurring ones, appearing on top (Fig. 4.20a & b). Such conspicuous cascade pattern is particularly observed on the wall of a big doline which has a diameter of about 150m and is 200m high. Stagnant water lies at the base of this doline, and a river comes through the higher level of the bounding precipitous wall and ultimately leaves the doline via a narrow conduit.

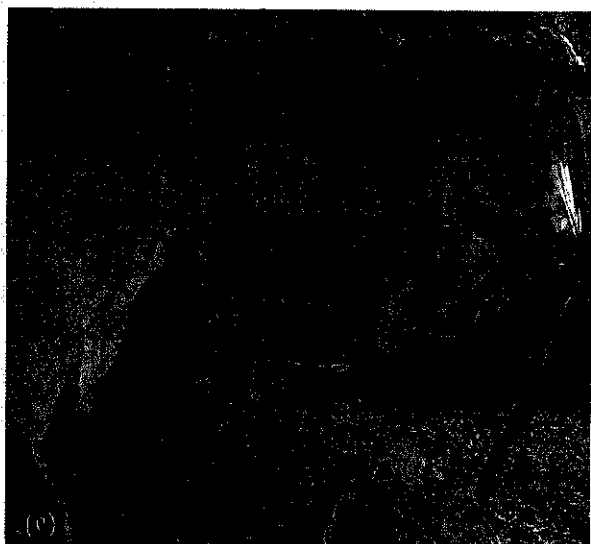


Figure 4.20: Types of multi-layered notches that can be observed in different parts of the Kinta Valley on vertical cliffs. Pictures from (a) to (c) were taken in different parts of Gunung Datok



Figure 4.21: Pictures indicating types of multi-layered notches taken (a) at Gunung Datok, and (b) to (d) at Gunung Rapat.

Notches appearing with a lower frequency but which are relatively wider and filled with cave sediments (Fig. 4.15e) are apparent in the area. Such notches appear much deeper where the cave deposits exist. These notches are very similar to the ones observed in river caves.

In many places within the Kinta Valley, stagnant waters at the base of the hills are common. And where these ponds exist, the occurrence of the notches is not uncommon. Such notches, for example Figure 4.21b, appear as protruding overhangs with deep grooves and flat ceiling. They are different from those in areas where the water is dynamic. Figure 4.20 and 4.21 summarizes the various types of notches that exist in the vestige limestone hills of the Kinta Valley. There is one common

characteristic on the composite notches in almost all hills, i.e. wherever these features were observed, the upper part is typified by more frequent and narrow ones (approximately 25-30 cm), but the opposite is true for the lower part notches, which are very wide and relatively deeply incised.

4.1.3 Scallops

Scallops are undulating ripple-like dissolutional features prominently seen on cave walls, formed by flowing water via caverns. Scallops are not typical features that have been observed in all caves of the study area, rather they were conspicuous only in some caves where the passages did not collapse. Scallop features of different sizes were measured from the various karstic caves of the area. Their width varies from 0.3m to more than 2.2m. Similarly, the length of the scallops also varies, especially in the upper and lower levels of the cave passages. Some of the caves where measurements of the scallops were taken include :-

4.1.3.1 Gua Sam Poh Tong

This cave is situated in Gunung Rapat at 4°33'49.7'' Northing and 101°6'56'' Easting, and it is found at the base of the hill. The scallops which appear to be quite conspicuous (Fig. 4.22) vary in size. The variation of the length of the scallops, from one crest to the other, shows a gradual increment from top to bottom. At the bottom (Fig. 4.22a), the length, on average, appears to be 1.2m; in the middle, the average length is 0.56m, and on top of this level, scallops as large as 0.3m (Fig. 4.22b) exist.

The conduit is on average 3m wide and 2.2m high. The orientation of the passage is along a NW-SE axis. The morphology of the scallops pattern and measurements of their length clearly indicate a paleoflow trend towards the SE; this flow trend is oriented towards a doline, where the cave passage ends. Figure 4.23 illustrates the paleoflow trend in some of the karstic caves, and the paleoflow trend in the Sam Poh Tong relict cave is oriented towards the extant river, which flows in between the remnant limestone hills.

Determination of the shallower downstream end of the very small scallops on the ceiling is a bit difficult; however, considering the fact that the length of the scallops is inversely proportional to the velocity of the fluid that formed them (Curl, 1974), it is possible to infer that the smaller scallops on the ceiling of the conduit clearly indicate fast flow of water. Thus, this in turn implies that the gradual increasing length of the scallops illustrates the sluggish or laminar flow of the water, further away from the ceiling.

The conduit, in Figure 4.22a, ultimately ends up in a small doline, which is about 40m wide and 100m high. The more frequent shorter scallops occurred particularly near the end of the conduit, where it joins the doline (Fig. 4.22b). Sediment encrusted inside the relict conduit is evident, and this may indicate later flooding of the cave, after the formation of the scallops.

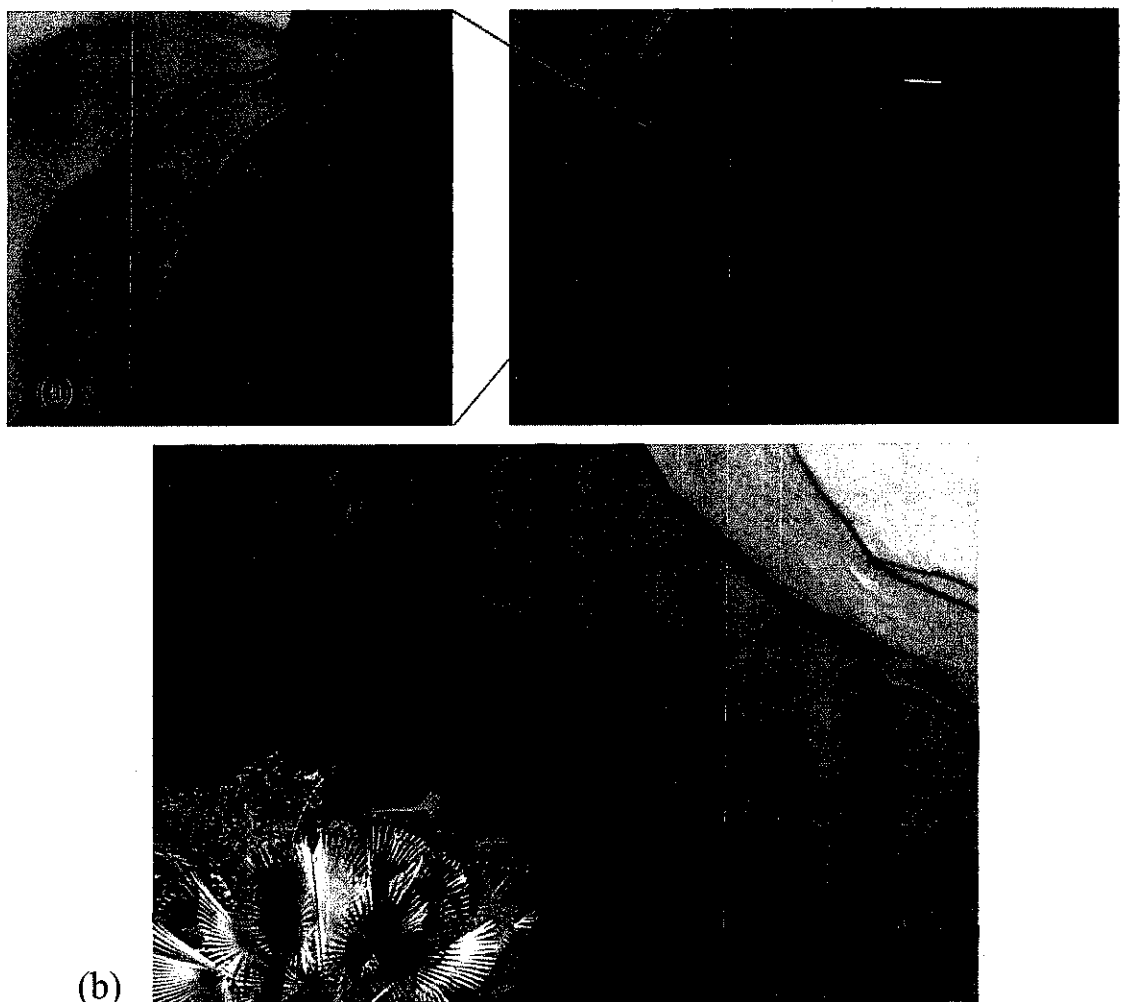


Figure 4.22: Pictures showing scallops pattern at Sam Poh Tong Cave, (a) The lower level being zoomed, (b) Zoomed scallops on the ceiling.

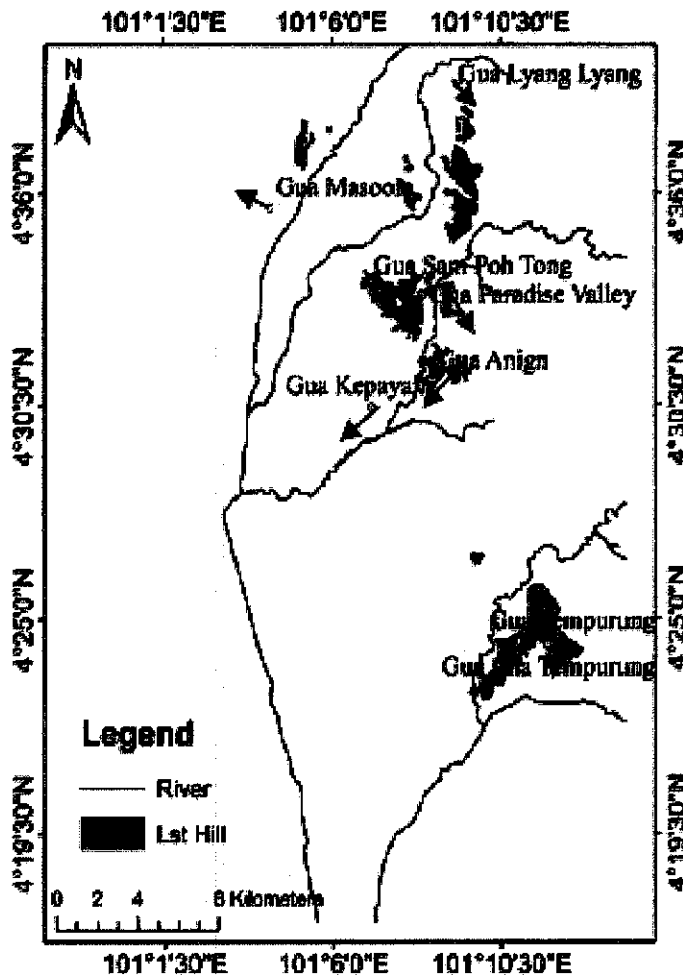


Figure 4.23: Map of paleoflow trend (red arrow) and flow orientation in river caves (black arrow), and the general SW flowing river trend.

4.1.3.2 *Gua Kepayang*

Although the entrances of this cave appear to be breached and collapsed, scallop features on their wall are quite apparent, and their lengths vary from 2m at E1 to 1.2m E2 (Fig. 4.9a). Analysis of the scallops pattern clearly indicates that the paleoflow trend in this relict cave was in the direction of 210° (SW). And Figure 4.23 shows that the paleoflow orientation is along the direction of the extant river which is flowing in between the remnant hills.

In this cave, the scallops are formed on a deeply incised wall (Fig. 4.24a); similarly they are also quite evident on the ceiling, with shallow corrosion (Fig. 4.24b). The length of the scallops on the ceiling is about 0.3m. Although inferring the

flow trend from such pattern is a bit ambiguous, there are places which indicate that the flow trend on the ceiling is towards the SW, which is the same as the flow trend inferred from the analysis of scallops pattern on the wall of a partially collapsed cave passage.

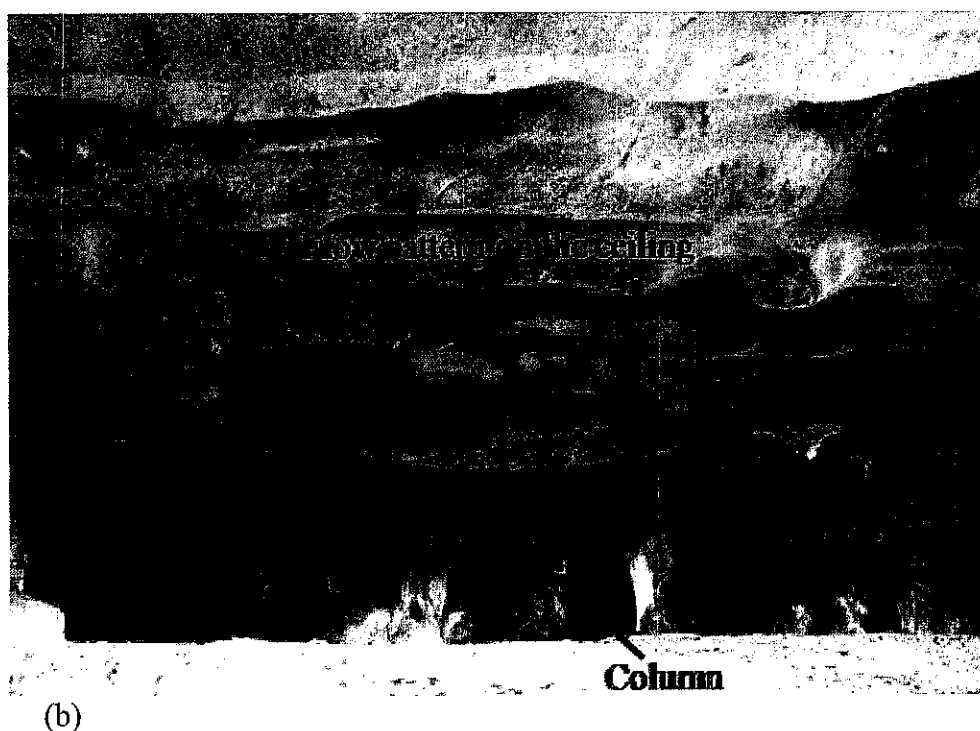
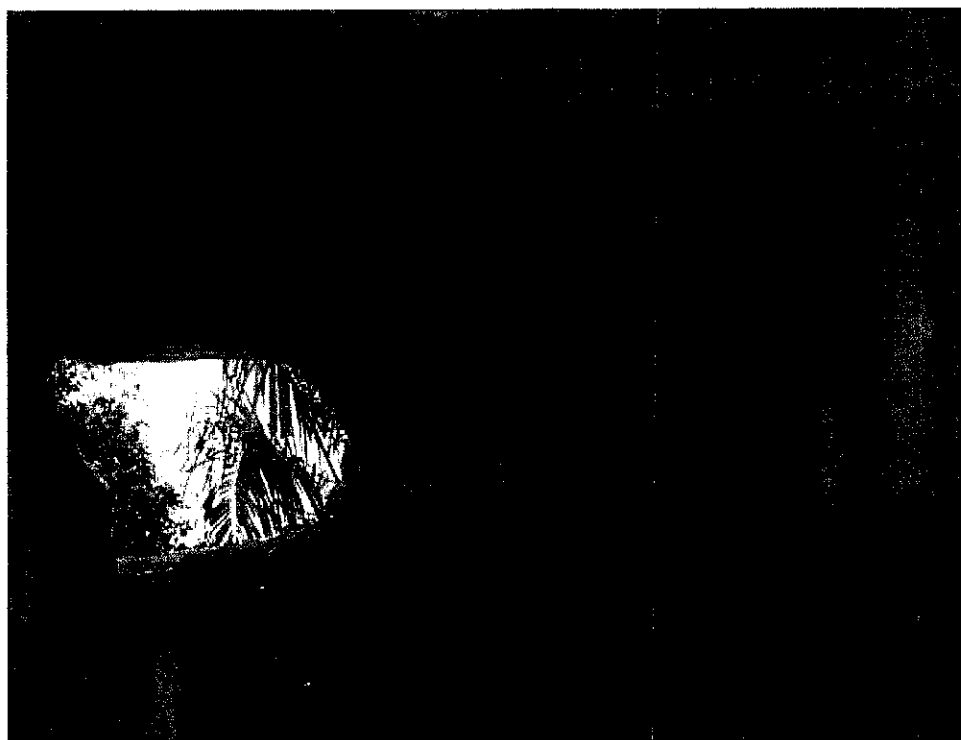


Figure 4.24: Scallops pattern (a) on the wall and (b) on the ceiling of Gua Kapayang

4.1.3.3 *Wat Tat Fook*

This is one of the caves that exist in Gunung Lanno, and it is located at 4°31' Northing and 101°8.31' Easting. The entrance to this cave is situated about 20m from the base of the hill. This cave is typified by some short and dead-end passages which are not more than 0.6m wide and 2.2m high. Thick sediment deposit, about 1.2m depth and linear stalactites oriented along the conduit direction (Fig. 4.25a) also typify the cave.

Different dimensions of conduits characterize this cave. A more persistent passage, where the scallops size and flow orientation were measured, is 3m wide and 0.5m high, and it is oriented along a 050°-230° direction. This long conduit has average scallops length of 1.3m, and it ends in another passage oriented along 160°-340°. The latter passage, which has a width of 1.6m, has scallops of variable size before and after the junction of the two passages. Before the junction, the scallops length, on average, appears to be 0.8m, and after the junction the scallops get wider, on average, 1.2m.

Although the conduit in the long passage (Fig. 4.25a) is almost filled with sediment and the scallops do not appear quite distinct, it is possible to draw an inference that the flow trend was possibly towards the southwest (230°). However, in the other passage, which is oriented NNW-SSE, the scallops pattern indicates the paleoflow trend towards the SSE.

In addition to the presence of linear conduits in this relict cave, there is a small chamber 12m wide and 15m high. This chamber contains scallops which have a similar width at different levels (Fig. 4.25b), and this may indicate that the scallops might not have a concomitant origin.

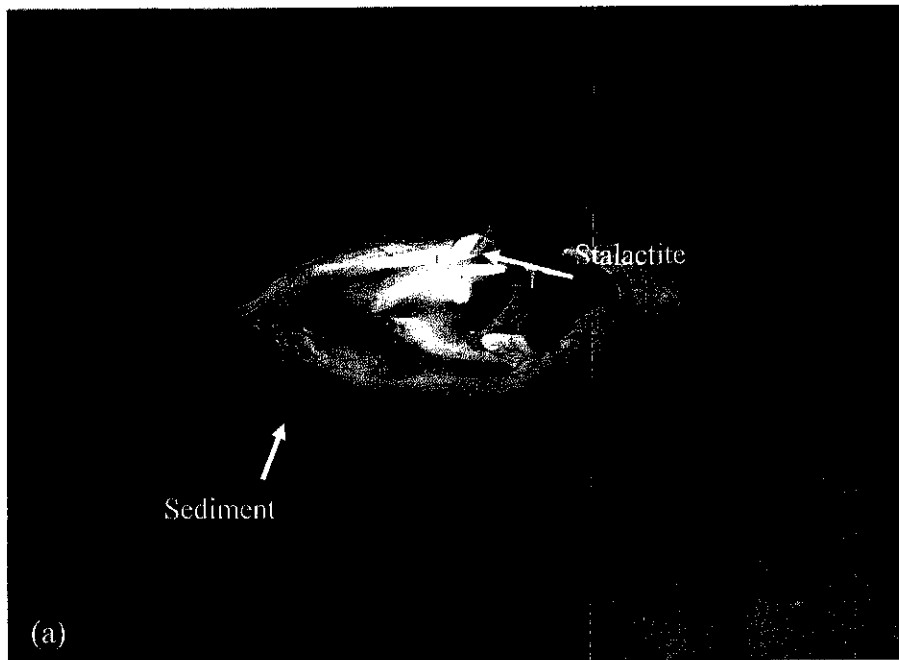


Figure 4.25: (a) Shows a conduit with thick sediment deposit and linear stalactite formation oriented in the same direction as the conduits in Gua Wat Tat Fook, and (b) Lower and upper level of scallops' pattern, in a small chamber facing the highest level of the cave entrance.

4.1.3.4 *Gua Angin*

It is located at 4°31' Northing and 101°8'25'' Easting. The entrance of the cave is situated about 8m above the base. Linear conduits, collapsed passages and dead ends

characterise this cave, and this relict cave is also typified by, like other caves, thick sediment deposit (Fig. 4.26).

Scallop features have been observed in two different passages which have an average width of 2.5m. The narrow conduits appear to have an average scallop length of 0.7m. Where the conduit orientation is 070°-240°, the paleoflow direction is interpreted to be 240° (SW), since the shallower end of the scallops which marks the downstream part is oriented along this trend. Whereas, in the other main passage which is oriented 040°-200°, analysis of the scallops pattern indicates the paleoflow orientation towards 200° (SSW). This paleoflow trend is almost aligned with the general SW flow orientation of the extant river (Fig. 4.23).

This cave conduit indicates almost consistent scallops length. The large average size of the scallops illustrates the slow water flow at the time of their formation, since scallops length is inversely proportional to the velocity of the water. Furthermore, the fine sediment deposited in this cave may illustrate the absence of variable fluid transport energy, and the sediment could possibly be deposited by laminar flow. This is likely to be concordant to the velocity of flow inferred from the scallops morphology.

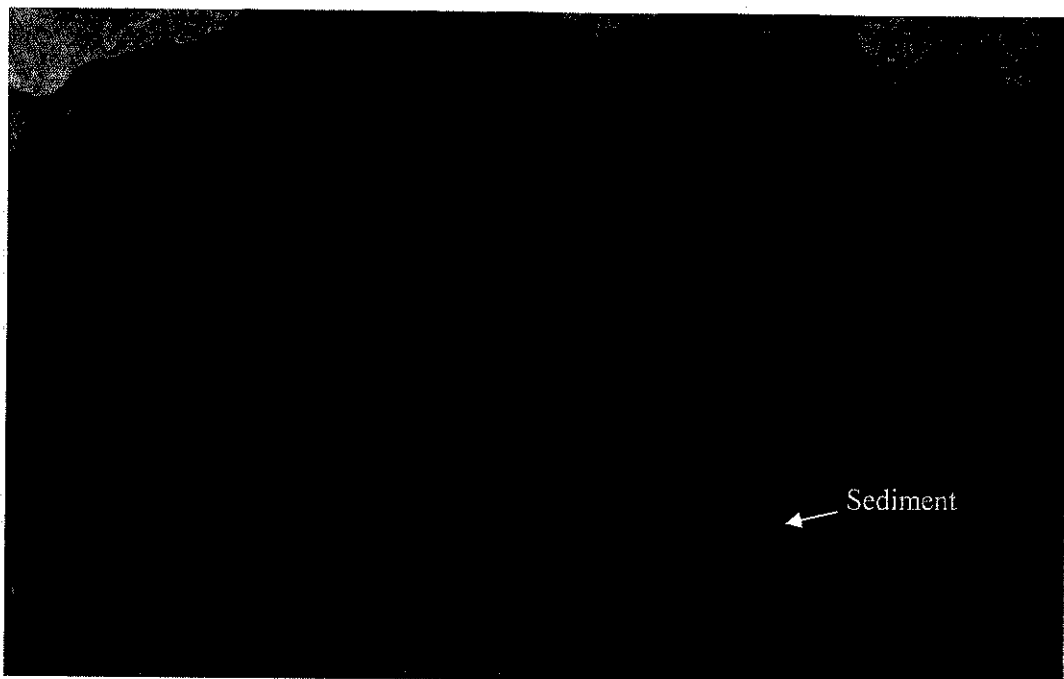


Figure 4.26: Picture showing sediment deposits in the conduit of Gua Angin.

4.1.3.5 *Gua Masoora*

Although most of the scallop features in Gua Masoora are not evident, particularly at the lower part of the cave, possibly due to the expansive void formation, large scallops (Fig. 4.27a) are conspicuous in the upper part of the cave. The length of the large scallops is on average 1m, and based on the morphology of the scallops' pattern, the paleoflow trend is towards 320°. This paleoflow trend, unlike that of other caves, is not oriented towards or along the extant river, as indicated in Figure 4.23.

Under such large width scallops (Fig. 4.27a), the presence of relatively small width scallops (Fig. 4.27b) is quite evident. These scallops are 0.5 m long, and their upper level is bounded by the expansive smooth and flat ceiling, unlike the larger scallops which are located below the dome shaped ceiling. From the size of such kind of scallops pattern, it is possible to infer that their formation took place under laminar flow.

The shallow downstream end of the scallops pattern in both the upper and lower level scallops indicate a similar NW trend. The expansive passage, in which the lower level scallops were formed, might have been breached by a later coming fluid flow which is different from the one responsible for the formation of the scallops.

From the inverse relationship of flow velocity and scallops length, and similarly based on the size and morphology of the scallops pattern in Gua Masoora, it is possible to draw an inference that the scallops were formed by laminar flow water. Although the fine sediment, which is evident in Figure 4.27b substantiates the possible laminar flow, this cave is also characterized by deposits of relatively coarser sediments particularly at the breached entrance of the cave. The presence of such sediments of different size may suggest the possibility of having different fluid flow mechanisms. However, such mechanism is not evident in the general morphology of the scallops.

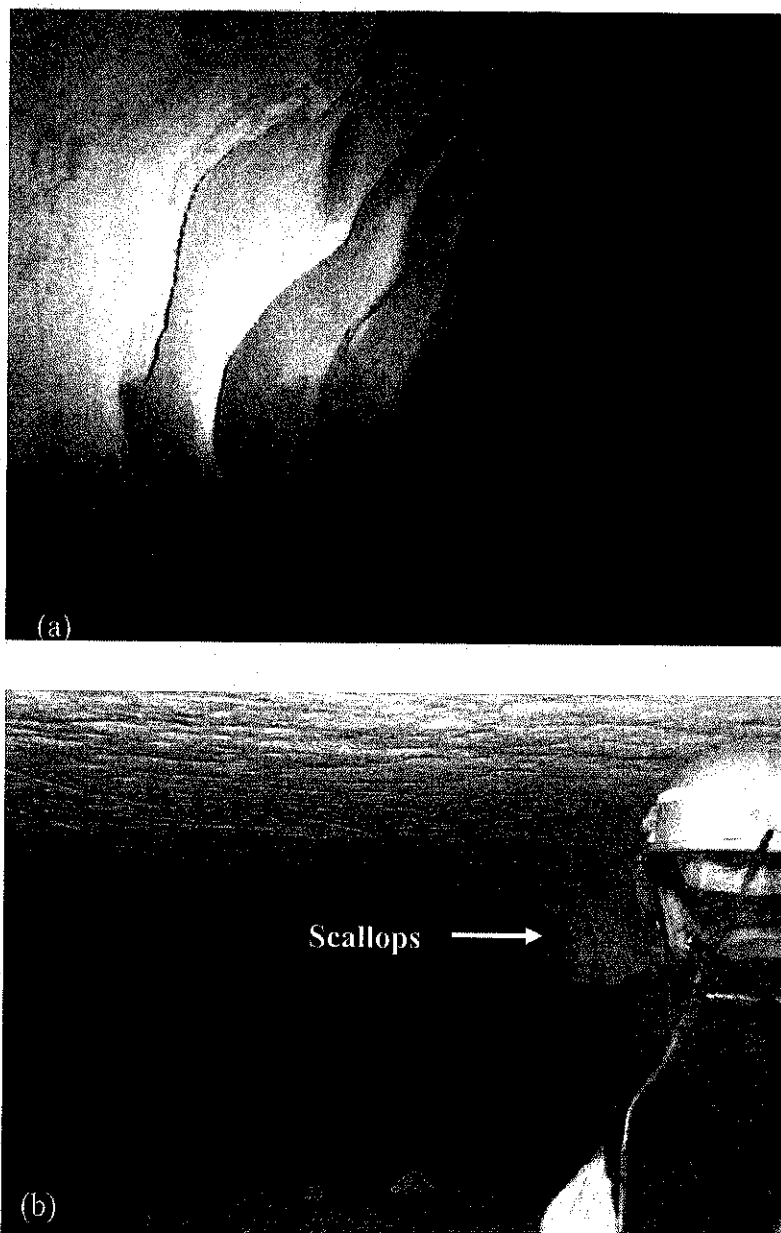


Figure 4.27: Pictures indicating (a) large and (b) small width scallops in Gua Masoora

4.1.3.6 *Gua Layang Layang*

This cave is typified by collapsed passages and the formation of a big chamber. However, the presence of scallops on the wall of the chamber and on the wall of narrow conduits is evident. The very large scallops, which have an average length of 2m (Fig. 4.28a), mark the wall of the chamber, and the relatively small length scallops, on average 1m (Fig. 4.28b), are prominent in the narrow conduit, which has

an average width of 2m. The average length of the scallops shows a big variation and there is no consistency of the pattern, albeit they are aligned along the same trend.

Despite the heterogeneous appearance of the scallops, marked by a variation in their deep grooves, particularly on the chamber wall, the shallower downstream end of the scallops which is oriented in the direction of 300° indicates the possible paleoflow trend towards this trend. Considering the inverse relation of scallops' length and velocity of the water that formed them, it is possible to infer that the laminar flow of water was responsible for the ultimate formation of the conduits and chamber.

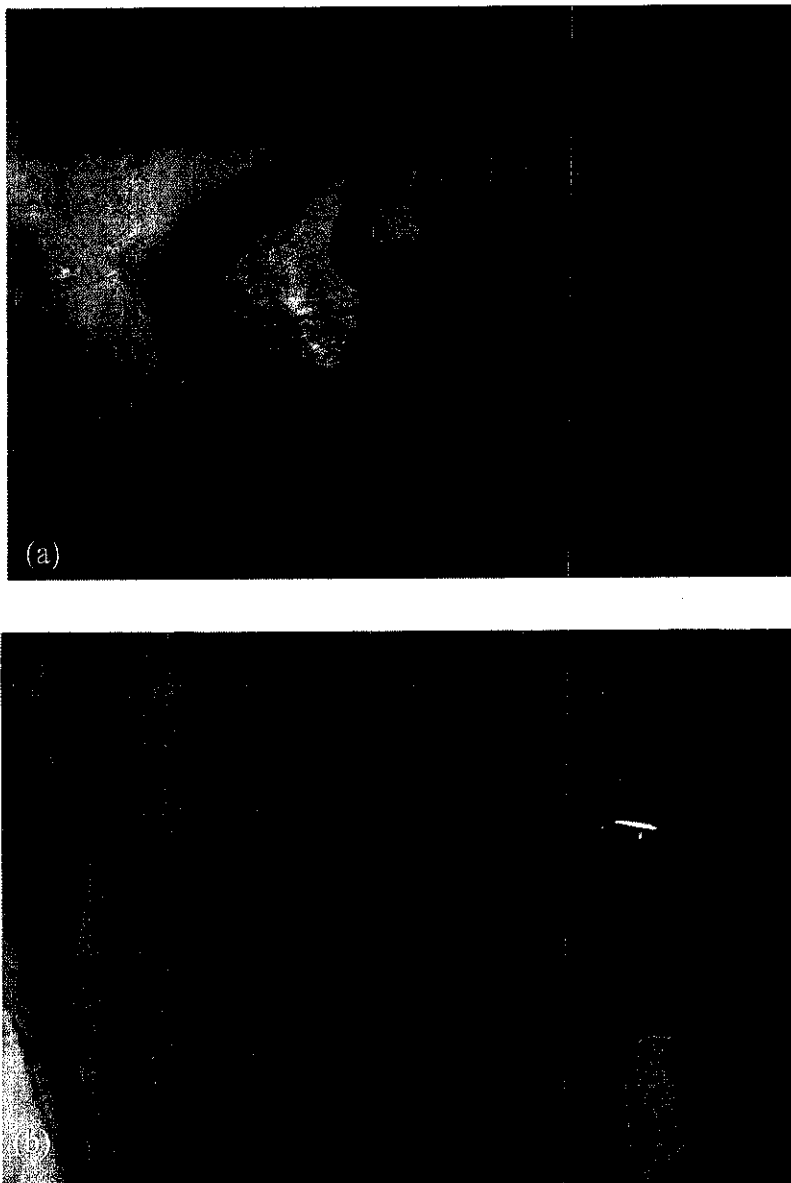


Figure 4.28: Pictures indicating large width scallops (a) at the chamber wall, and (b) at the narrow conduits of Layang Layang.

4.1.4 Lineament

Although there are a number of small limestone hills which are scattered all over the Kinta Valley, lineaments were extracted only from the major five hills, since the rest of the hills are too small for the extraction of lineaments. However, because of the wide spatial distribution of the major limestone hills, it is presumed that the result would be representative for the rock mass covering the whole valley. As the following fracture distribution maps and associated rose diagrams illustrate, the lineaments in each hill appear oriented almost in all directions, but their prominent trend is towards NNW-SSE. The rose diagram indicates that the lineaments distribution is based on the frequency of occurrence; the sector angle is 10° with a tick interval of 2% and with the respective number of data indicated in the bracket.

4.1.4.1 *Gunung Rapat and Gunung Lanno*

Despite Gunung Rapat being highly pitted with dolines, which makes the extraction of persistent fracture traces difficult, the extracted lineaments show a relatively higher frequency of fractures occurring along the NNW-SSE, but fractures oriented along the NNE-SSW to ENE-WSW are evident as well (Fig. 4.29a). Based on the rose diagram result, the prominent NNW-SSE trend constitutes 31%, i.e. 23 data (measured lineaments) out of the overall 74 number of data.

Fractures extracted from Gunung Lanno are few in number, but the relatively higher number of fracturing appears to be in the NNW-SSE trend and ENE-WSW (Fig. 4.29b). And the maximum proportion, i.e. 41.6% (10 data out of the 24 overall number of data), is covered by the NNW-SSE and ENE-WSW trends.

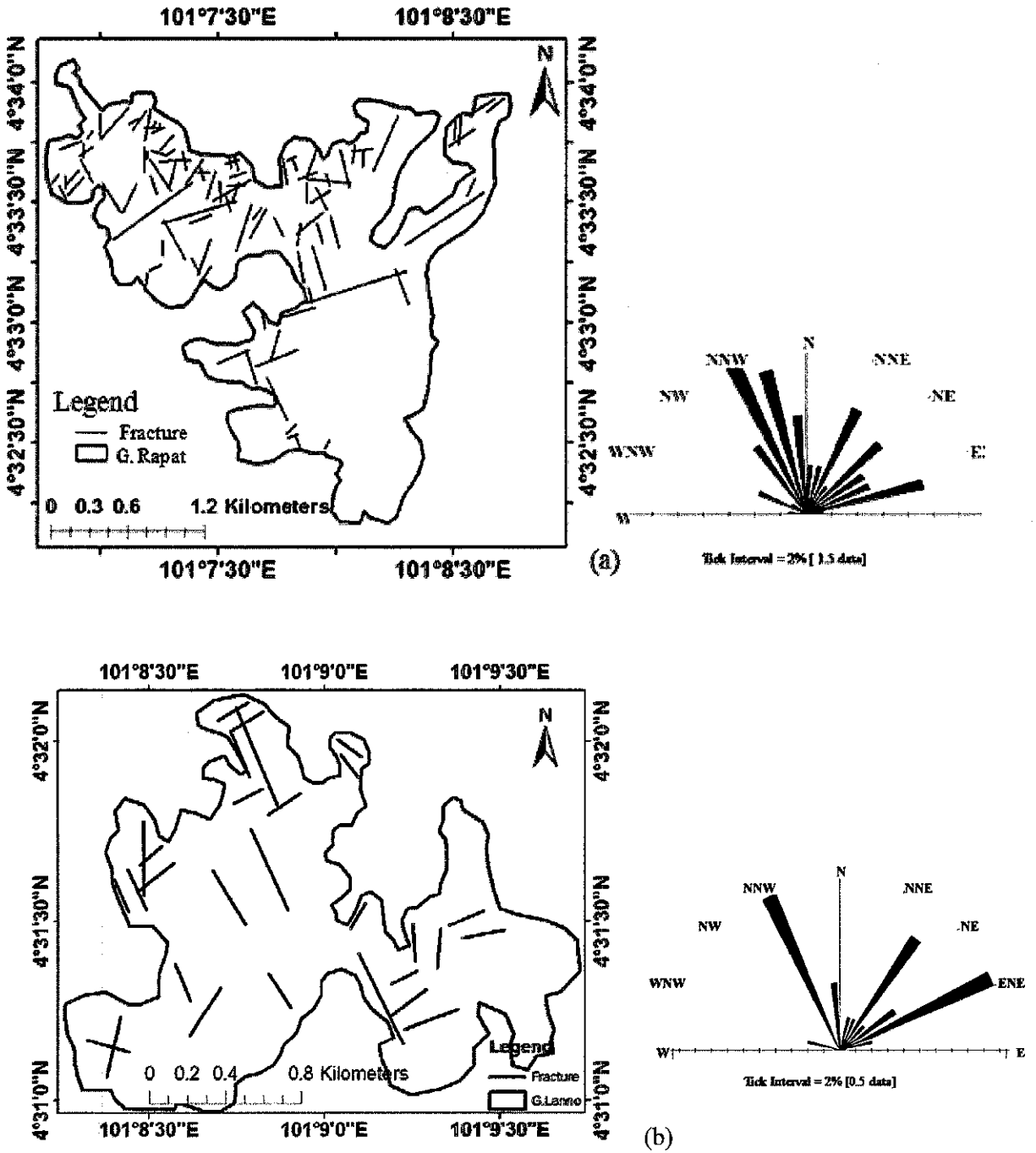


Figure 4.29: lineaments extracted from (a) Gunung Rapat, and (b) Gunung Lanno.

The rose diagrams indicate the lineaments trend.

4.1.4.2 Gunung Tempurung and Gunung Panjang

Gunung Tempurung is one of the major hills which indicate intense fracturing, and the relatively highest frequency of occurrence clearly appears in the NNW-SSE

trend (Fig. 4.30). Those fractures oriented in the NNE-SSW, NE-SW and ENE-WSW trends are also the dominant ones. Out of a total 72 data points, the maximum number, which is 26.4% (19 data points), is covered by the main lineament trend, i.e. NNW-SSE.

Persistent fracture traces, mainly oriented in the NNW-SSE, typify Gunung Panjang (Fig. 4.31). Although those fractures oriented in the ENE-WSW appear relatively short, they have also the same frequency of occurrence. The result obtained from the rose diagram indicates that the maximum number of data covered by the main trends, i.e. NNW-SSE and ENE-WSW, is 81% which has 13 data points out of the total 16 data points.

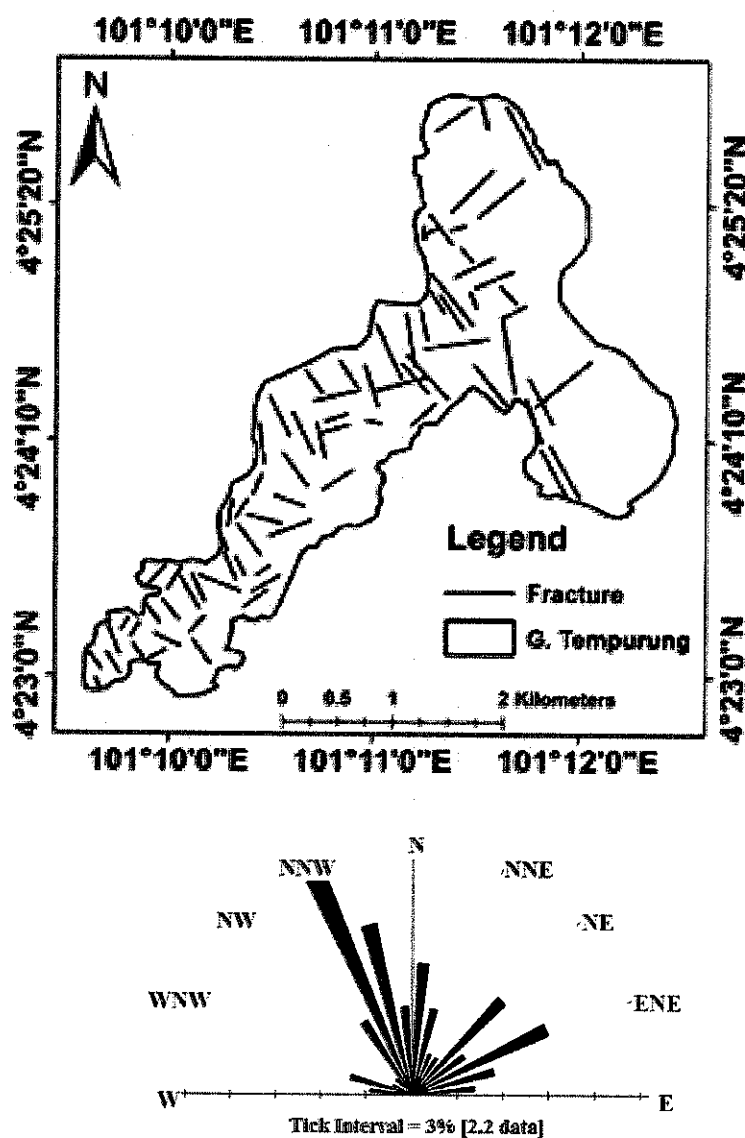


Figure 4.30: Lineaments extracted from Gunung Tempurung. The rose diagram indicates the lineaments trend.

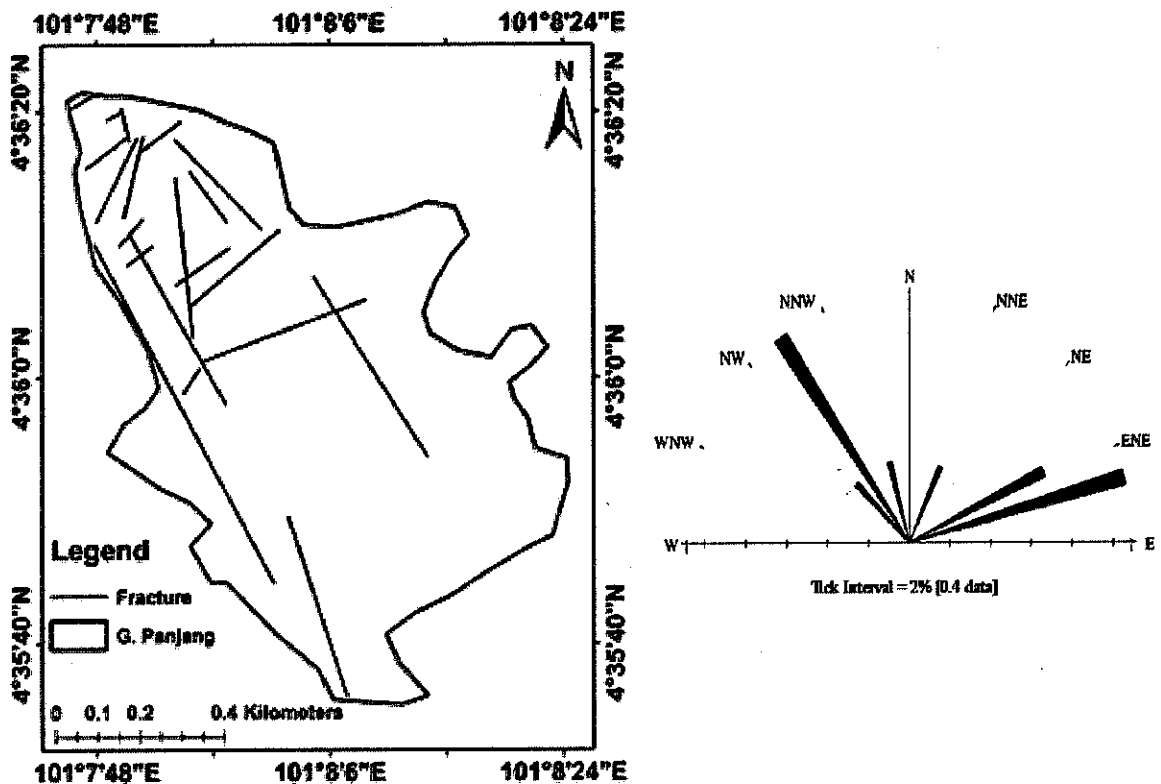


Figure 4.31: Lineaments extracted from Gunung Panjang.

4.1.4.3 Gunung Datok

Fractures oriented in all directions are extracted from Gunung Datok. And the rose diagram in Figure 4.32 shows the relatively higher number of fractures, like the other major hills, oriented along a NNW-SSE axis. Similarly, fractures oriented in the WNW-ESE, NNE-SSW, N-S and ENE-WSW occur at higher frequency. The prominent NNW-SSE trend appears to cover 17.4% which is 12 data points out of the total number of 69 data points. Similarly, the N-S oriented fractures appear to be prominent, covering 16% or 11 data points.

The complex trends of fractures extracted from the hill are almost the same as the orientation of fractures measured in an outcrop of the same hill (Fig. 4.33a) located at 4°37'26''Northing and 101°9'24''Easting. However, in this outcrop, the conjugate sets of fractures and the highly frequent vertical set of fractures are quite remarkable.

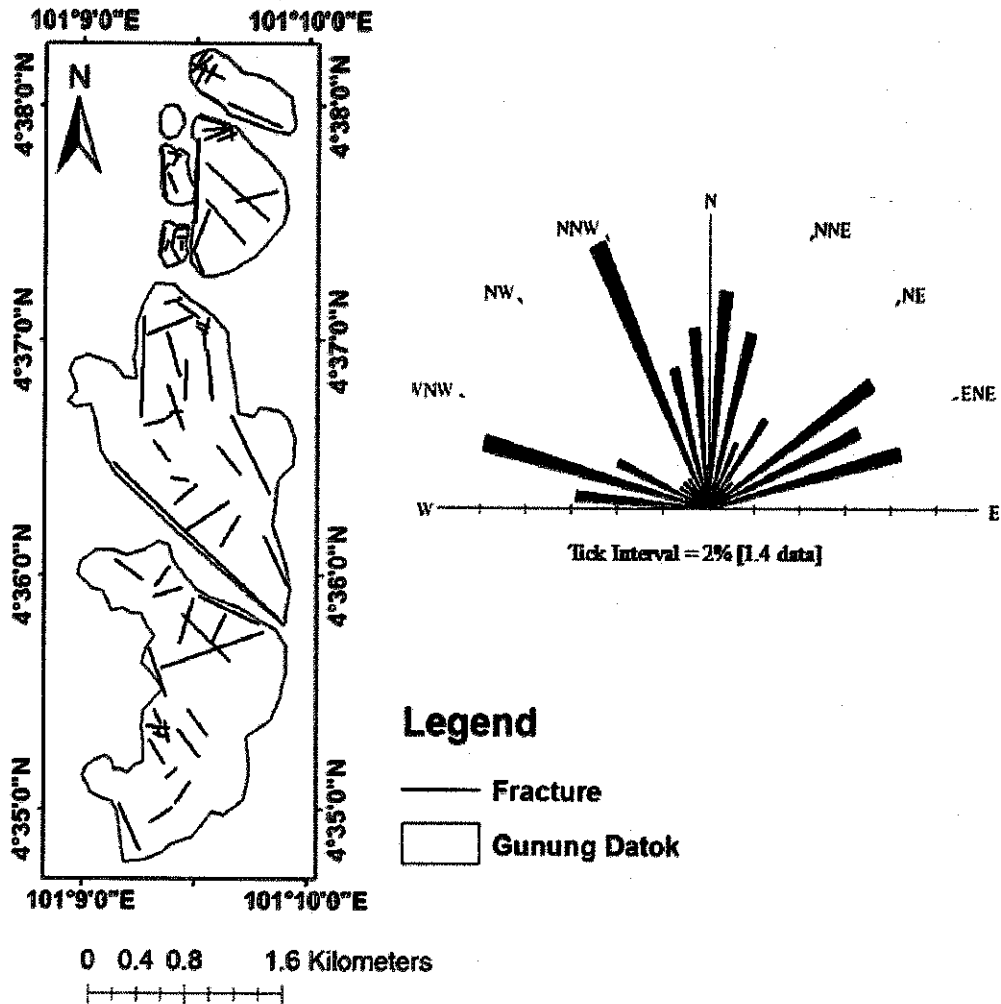


Figure 4.32: Lineaments extracted from Gunung Datok

The lineaments extracted from the various isolated remnant hills appear to have different orientations; however, merging all data points together to see the overall distribution reveals that their dominant orientation is towards the NNW-SSE (Fig. 4.33b). Compared to other fracture sets, those fracture traces oriented along the ENE-WSW appear relatively more frequent. The fractures are extracted from the isolated hills, but the dominance of such fractures may illustrate their continuity and influence on the pre-existing expansive limestone bedrock.

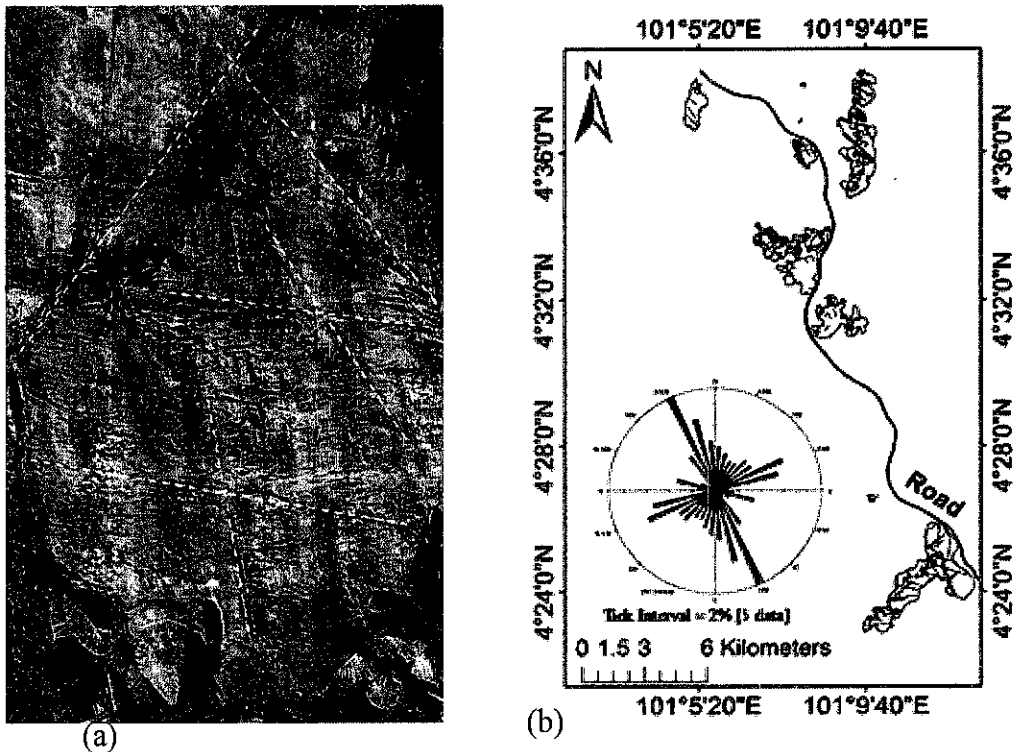


Figure 4.33: (a) Showing conjugate sets of fractures in an outcrop in Gunung Datok, and (b) Indicating the distribution of the major hills in the Kinta Valley with the associated inset rose diagram depicting the overall fracture distribution.

For some of the remnant limestone hills, the lineaments trend inferred in this study appear to be similar to the result obtained by Muhammad and Djin (2003), who used a different approach, i.e. aerial photograph. Similarly, the prominent orientation of the lineaments extracted from the granites (Gobbett, 1971) is the same as the main trend of the lineaments indicated in the inset rose diagram under Figure 4.33b.

4.1.5 Apatite and Zircon Fission Track

Fission tracks are linear trails of intense radiation damage caused by spontaneous fissioning of uranium-238. Fission track analysis provides detailed information on the low-temperature thermal histories of rocks. Thus, fission tracks can be used as temperature-sensitive radiometric dating, since the tracks' length distribution is a reflection of time-Temperature history, and the fission-track age records cooling through a temperature interval between total resetting of fission tracks and relative stability. In order to see the time-Temperature relationship, which in turn provides

information about the timing of cooling episodes and uplifting events, a number of apatite and zircon grains, up to 40 grains per sample, were analyzed. In some grains, more than 2000 fission tracks were counted; however, the FT age determination, indicated in the inverse model, consider only those tracks which are parallel to the c-axis (Dpar).

The apatite fission-track (AFT) and zircon fission-track (ZFT) data yielded expected age trends, i.e. the older ages at higher elevations and the younger ages at lower elevations, except for the AFT age for Sample 4 (CH-9).

Table 4.3: Summary of Apatite and Zircon fission track data

Sample	Elev. (m)	Min.	Attempted spots	Accepted spots	N	Mean [U] (ppm)	Mean Dpar (μm)	Mean Dper (μm)	Pooled Age (Ma) $\pm 95\%$ CI	P(χ^2) (%)
CH-6	944	Apatite	40	40	2049	137.9	2.02	0.34	33.93 -2.11,+2.25	89.2
		Zircon	30	30	2525	387	-	-	97.47 -8.51,+9.32	57
CH-7	717	Apatite	40	40	1459	82.9	1.92	0.36	30.98 -2.08,+2.23	88
CH-8	577	Apatite	40	31	86	26.8	1.89	0.36	7.46 -1.67,+2.16	86.7
		Zircon	4	4	321	524.8	-	-	79.26 -15.9,+19.9	7.5
CH-9	340	Apatite	40	13	34	30.1	1.82	0.36	16.54 -4.94,+7.04	64
CH-10	178	Zircon	4	4	303	481.2	-	-	68.7 -15.5,+19.9	5.3

where, N= number of tracks; Dpar= mean etch pit figure diameter parallel to c-axis; Dper= mean etch pit figure diameter perpendicular to c-axis.

The fission track age data obtained from the apatite and zircon appear to have similar variation with elevation (Table 4.3 and Fig. 4.34). The zircon fission track ages closely follow the elevation variation. However, the apatite fission track age for Sample CH-9 is misleading as far as the FT age decrement with decreasing elevation is concerned. As Table 4.3 shows, the age of Sample CH-9 is based on 13 spots, from which a total of 34 tracks were counted. The biased older age in this sample is attributed to the existence of a single, slightly older grain which occurs in a sample full of tiny, and difficult to work with, apatite grains. Half of the counted tracks, out of the total 34 tracks, appeared in this single and slightly older grain. Nonetheless, when the older single grain age in question is not considered, a significant age decrement was observed in CH-9. Thus, the thermal modeling and the uplift rate estimation take into account only those data except CH-9.

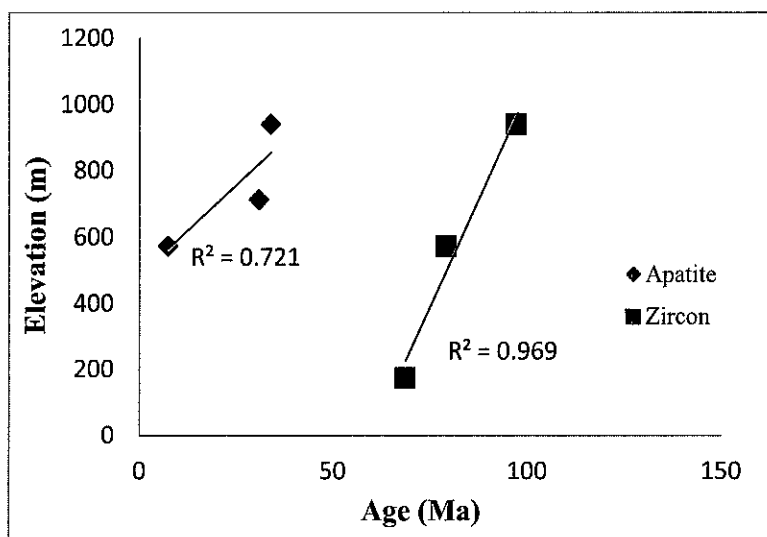


Figure 4.34: Illustrating similar variation of fission-track ages and elevation.

The statistical analysis indicates that all grain ages passed the chi-squared test ($P(\chi^2) > 5\%$), which exhibits the homogeneity of the ages of the grains population. Hence, all the samples have a high probability of coming from a single-age population. Both the apatite and zircon FT age appear younger than the age of the rock crystallization. The UPb age in zircon (Fig. 4.35) consistently suggests an intrusion age (rock crystallization) around the Late Triassic (210-220 Ma). This Late Triassic rock crystallization age is the same as the result obtained by previous workers including, Krähenbuhl (1991) and Sevastjanova et al. (2011).

Table 4.4: Apatite fission track length data

Sample	Mean (μm)	Std. dev. (μm)	N	Mean Dpar (μm)	Mean Dper (μm)
CH-6	13.37	1.55	204	2.06	0.35
CH-7	13.22	1.64	201	1.92	0.33
CH-8	12.52	1.95	28	1.91	0.32
CH-9	13.52	1.44	133	2	0.34

Table 4.5: Measured and modeled FT age and length in the inverse models

Sample	Age (Ma)				Length (μm)			Inverse Model		
	Measured	Model	GOF	Old	Measured	Model	GOF	Paths	Acceptable	Good
CH-6	33.9 +2.3/-2.1	33.9	0.96	36.8	14.51 ± 1.02	14.67 ± 1.06	0.94	20000	586	90
CH-7	31 +2.2/-2.1	31	0.99	33.8	14.45 ± 1.05	14.56 ± 1.08	0.99	20000	579	105
CH-8	7.65 +2.23/-1.7	7.65	0.99	9.42	13.96 ± 1.11	14.12 ± 1.43	0.93	20000	832	153

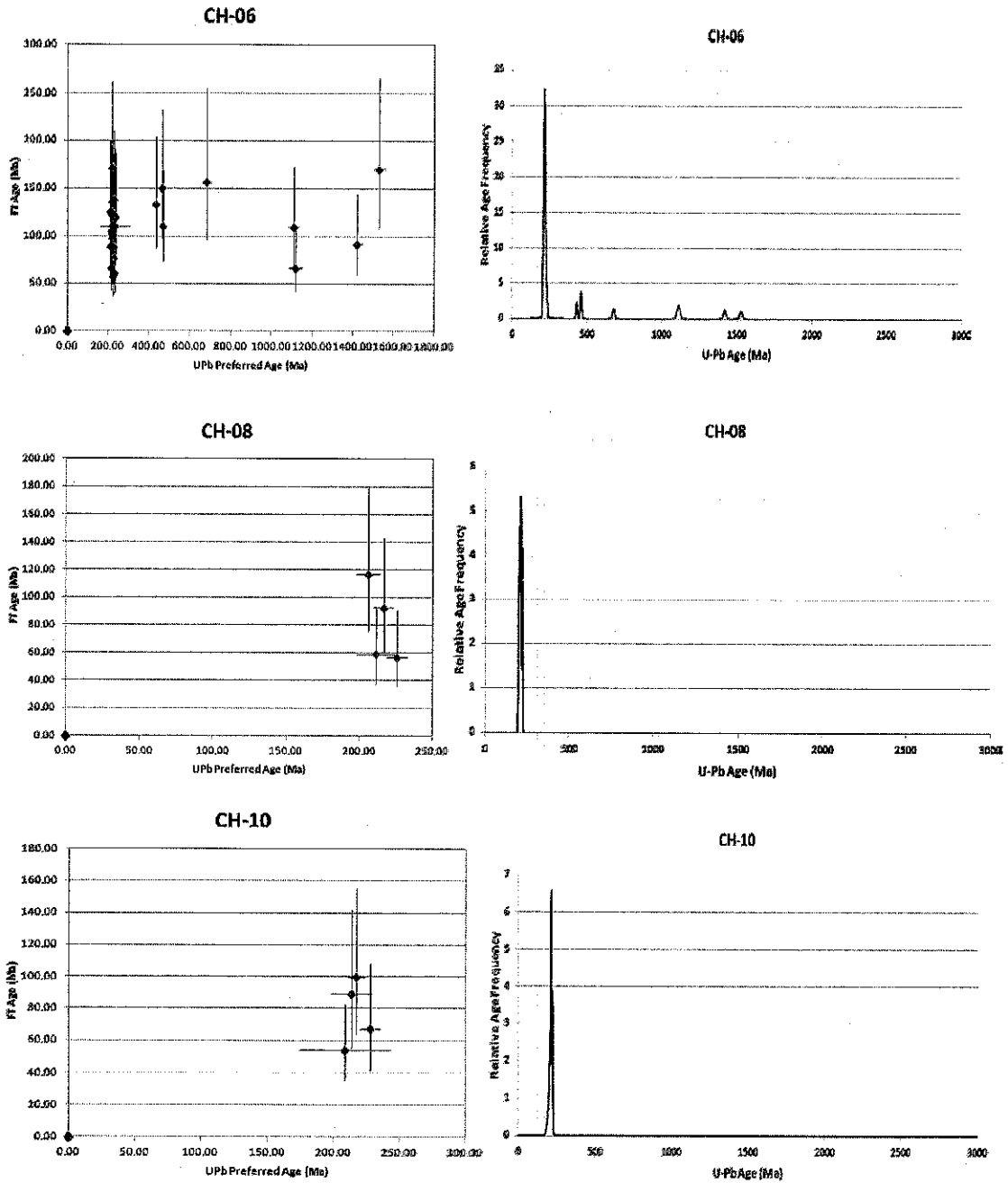


Figure 4.35: Graphs illustrating UPb age vs. FT age in zircon for the respective Samples. The UPb age indicates the time of granite emplacement around 215 Ma.

After undertaking a number of test runs, various possible time-Temperature paths, many statistical good and acceptable fits were obtained, and among them the best fits were chosen. Table 4.5 shows the results obtained in the inverse model, and the high goodness-of-fit (GOF) marks the most likely approximate value between the measured and the modelled age and fission-track length.

4.1.5.1 Cooling history

Figures 4.36-4.39 clearly illustrate the linear cooling episode experienced by the samples used in this study. The rate of cooling up to the Early Eocene is not constrained. However, the inverse model clearly displays the existence of two rapid cooling episodes, with relatively slower cooling in between, after the Mid Eocene (Fig. 4.36 and 4.37). Thus, the early episode of cooling brought the upper two Samples, i.e. CH-6 and CH-7, into the cooler zone and fixed them in older ages. However, a later episode occurred during the Late Miocene and resulted in bringing the base of the sampled section into cool temperatures as experienced by the top samples. The following section further describes this cooling history.

- Sample CH-6

The inverse model suggests the onset of fast cooling during Mid Eocene (~38Ma) up to late Upper Eocene (~33.4Ma). The second cooling event is marked by a relatively slower cooling which lasts up to Early Miocene (~18Ma). Then, the last episode of fast cooling continued.

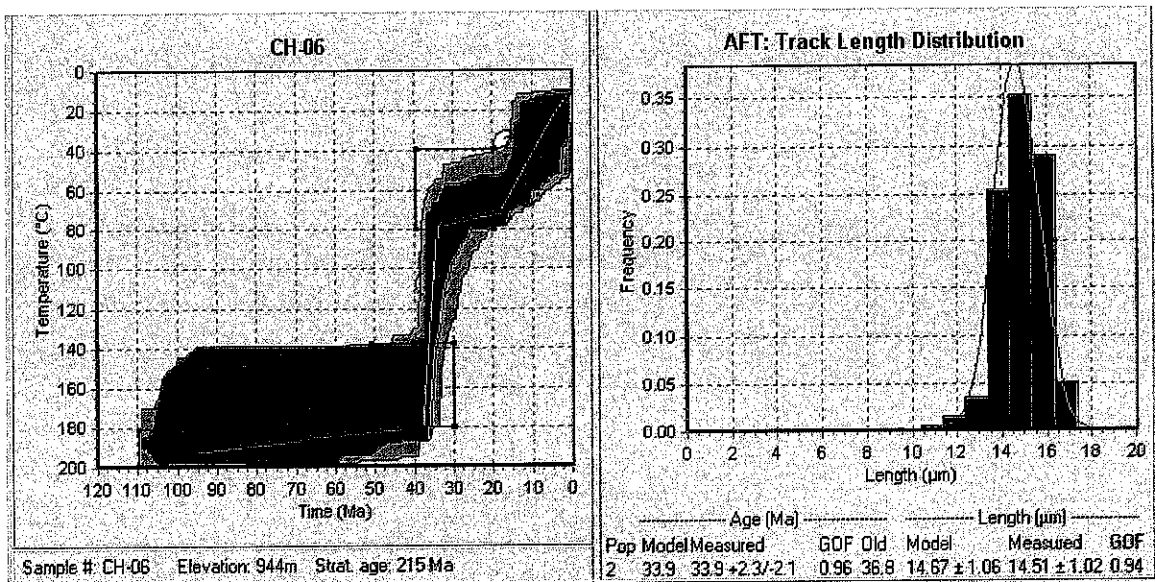


Figure 4.36: Inversion model of time-temperature history for Sample CH-6. It is based on 20, 000 time-temperature paths generated by a Montecarlo Method.

- Sample CH-7

Like Sample CH-6, Sample CH-7 has undergone a similar cooling history, where the first episode of cooling is characterized by a faster rate, which took place during Mid Eocene (~39 Ma) to Early Oligocene (~32.7Ma), and was followed by the later slower rate. Both samples have experienced faster cooling; however, the second younger episode in sample CH-7 is not as pronounced as CH-6; this can be expected to happen as the grains in the former sample (with MTL= $14.45 \pm 1.05 \mu\text{m}$, and Mean Dpar = $1.92 \mu\text{m}$) are more resistant to annealing than the latter sample (with MTL= $14.51 \pm 1.02 \mu\text{m}$, and Mean Dpar = $2.02 \mu\text{m}$) (see Fig. 4.36 & 4.37).

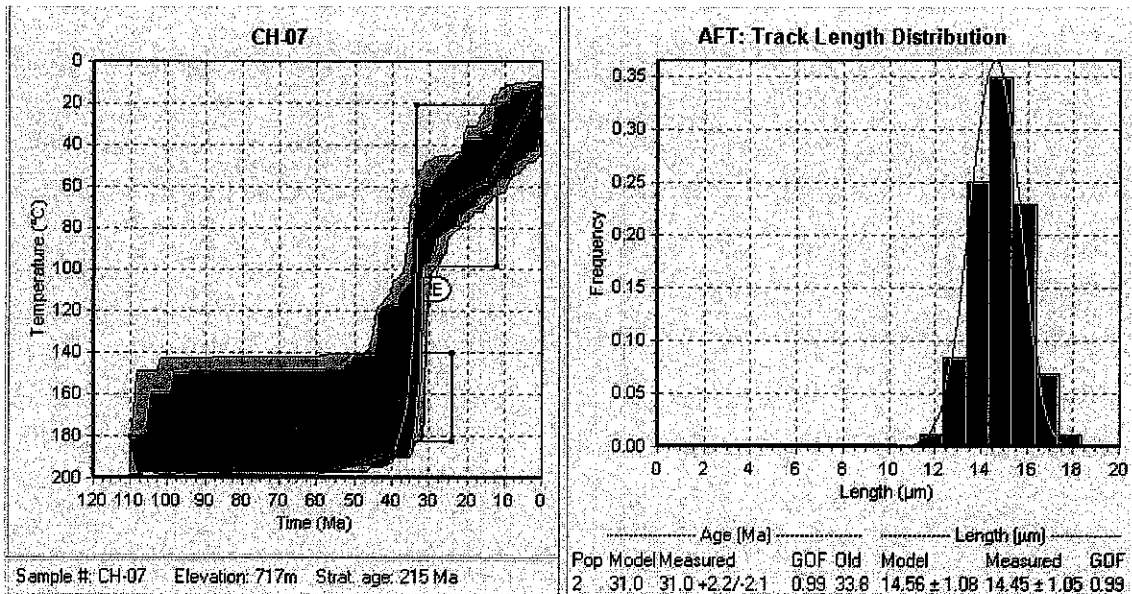


Figure 4.37: Inversion model of time-temperature paths depicting the cooling history of Sample CH-7. It is based on 20, 000 t-T paths generated by a Montecarlo Method.

- Sample CH-8

This sample indicates a hint of an early episode of cooling during the Late Eocene, but it clearly depicts a more recent cooling event. After the emplacement of the upper two samples in a cooler temperature zone, during the Late Eocene to Early Oligocene, the lower sample (CH-8) was emplaced into the lower temperature zone during the Late Miocene.

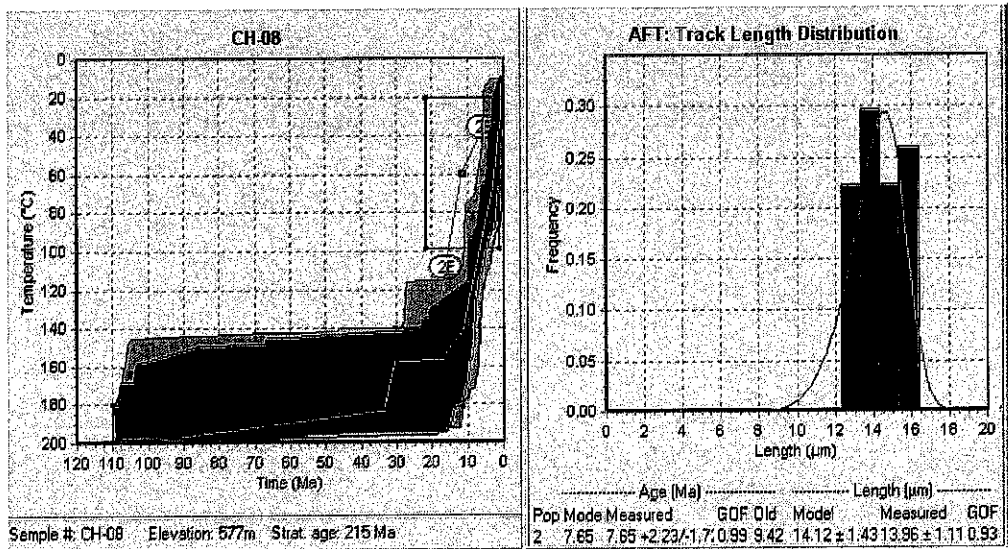


Figure 4.38: Inversion model of time-temperature history for Sample CH-8. It is based on 20,000 time-temperature paths generated by a Monte Carlo Method.

- Sample CH-9

Based on the fact that FT ages vary with elevation, this sample is expected to show the youngest age; however, it appeared to be older than CH-8. This is caused by the existence of more tracks in a single grain, which is slightly older than the other grains which appeared too small and thus too difficult to work with. In spite of that, modeling possibly suggests a more recent cooling event, further indicating that this part of the section was still exposed to elevated paleotemperatures after the first episode of cooling.

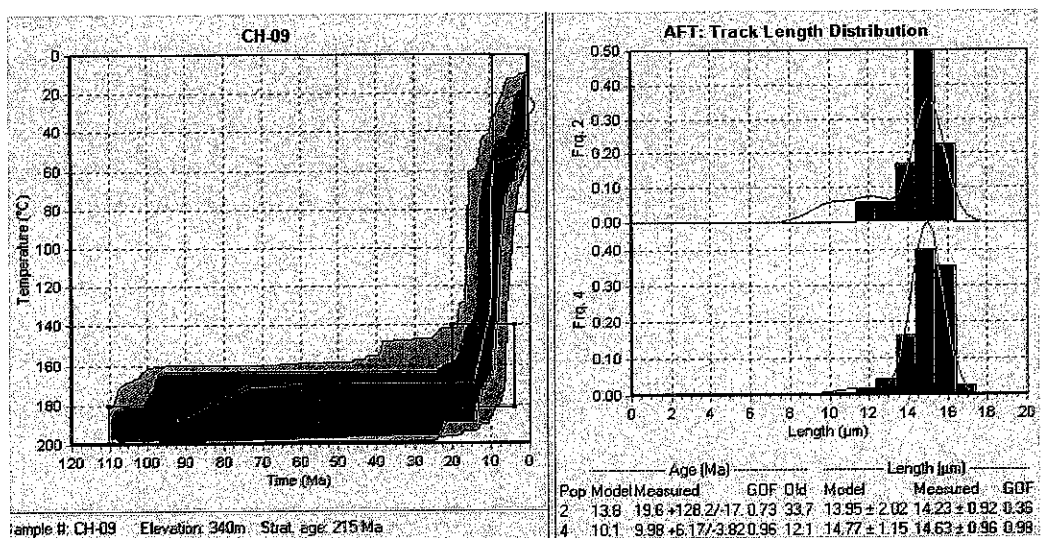


Figure 4.39: Inversion model of time-temperature history for Sample CH-9. It is based on 20,000 time-temperature paths generated by a Monte Carlo Method.

4.1.5.2 Uplift Rate

Using the mineral pair and relief approach, the following results of uplift rate were obtained.

a) Mineral pair

This approach uses the difference in cooling ages of two different minerals in a sample; their annealing temperatures and geothermal gradient are also considered. This approach is employed to Sample CH-6 and CH-8.

- Sample CH-6

The apatite and zircon fission track ages for this sample are 33.9 Ma and 97.47 Ma, respectively. Taking 110°C which is the commonly adapted effective annealing temperature for apatite and 240°C for zircon, the temperature offset between these minerals is 130°C. The 130°C offset in 63.57 Ma (97.47-33.9) implies that there was about 2.05°C/Ma cooling episode.

Taking the global geothermal gradient of 30°C/km into consideration, it is expected that there was about 68m/Ma rate of uplift; with this rate there was about 4323m of overlying material removed within 63.57 Ma, i.e. from the Early Upper Cretaceous to Upper Eocene.

b) Relief approach

This approach considers only the difference in cooling ages of a single mineral from two samples collected at different elevations.

If this approach is used, the possible uplift rate between Sample CH-6 and CH-7 will be 78m/Ma. It is obtained after taking the elevation difference between the two samples, which is 227m, and similarly taking into account the measured apatite fission-track age for CH-6, which is 33.9 Ma and 31Ma for CH-7. However, if Sample CH-7 (31Ma, 717m) and CH-8 (7.46Ma, 577m) are considered, the uplift rate will be 6m/Ma.

On the contrary, if the zircon fission-track age is taken into consideration for these samples, i.e. about 97.47Ma for CH-6 and 79.26Ma for CH-8, the expected rate of uplift will be 20m/Ma.

Similarly, considering the zircon fission-track age for CH-8 (79.26Ma, 577m) and CH-10 (68.69Ma, 178m) with an elevation difference between the two samples being 399m, then the uplift rate was about 40m/Ma.

In general, as the intrusion went into a temperature zone $>170^{\circ}\text{C}$, during the Upper Cretaceous period, the uplift rate was very slow, but increased slightly from 20m/Ma to 40m/Ma towards the end of the Upper Cretaceous. However, the average uplift rate from the Mid Cretaceous to the Upper Eocene was 68m/Ma. The uplifting episode from the Mid Cretaceous to the Late Miocene, can be represented by three different uplift rates, i.e. from 97.47 - 33.39 Ma, 33.39 – 31Ma, and 31 – 7.46 Ma to be 68m/Ma, 78m/Ma, and 6m/Ma, respectively (Fig. 4.40).

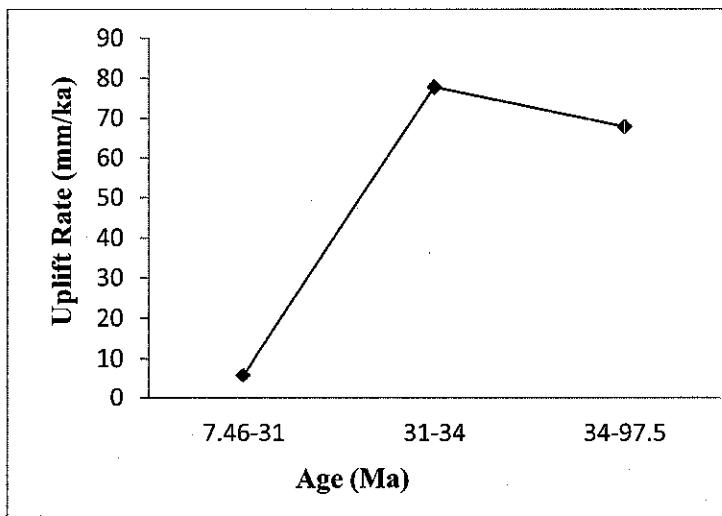


Figure 4.40: Graph displaying variation of uplift rate from the Upper Cretaceous to the Lower Miocene.

The apatite data clearly suggest a linear and rapid cooling event, with some degree of elongated period of cooling in between. From the data obtained in both apatite and zircon, it is possible to infer that about 4.7km of overlying material was removed within 90 Ma, i.e. from the Mid Cretaceous to the Late Miocene, if the onset of

karstification is 97.5 Ma and assuming that the gradual cooling attributed to the unroofing of overlying material.

4.2 Discussion

4.2.1 Karst development in the Kinta Valley

Relating the extant denudational processes and associated active karst system with the relict karst features enables unraveling the development of karst in the Kinta Valley. There are a number of clues in the remnant limestone hills that may attest to the processes or factors that are responsible for the commencement and gradual development of karst in the area. Such clues may include:

- (1) The distribution and alignment of the remnant hills in the valley,
- (2) The morphology and pattern of karstic caves,
- (3) The extant allogenic waters that arise from the bounding Main Range granite and flow via the limestone hills and within the caves, making their general trend to the southwest,
- (4) The paleoflow trend towards the current base level,
- (5) The presence of river sediments in relict caves which are situated at different elevations,
- (6) The absence of networked or dendritic passage caves,
- (7) The presence of dolines with evident conjugate fractures and uncollapsed linear conduits, and
- (8) The evidence of various dissolution features and associated characteristic patterns which appear different among the scattered remnant hills.

Furthermore, integrating these clues with the fission-track data interpretation enables to better characterize the development of karst in the area.

4.2.1.1 Factors influencing the development of karst in the Kinta Valley

The history of karst development in the Kinta Valley reflects the influence of various factors, mainly fractures, uplift, lithology, and climate. Although these factors are inextricably interlinked, the degree of their influence may vary in the development of karst. The detail of these factors, except climate which is indicated under section 2.1.1.2, is described as follows -

a) Fracture

The formation of karst features in the Kinta Valley appears to be controlled by both bedding planes and fractures, since evidence of karsts formed via the bedding plane (Fig. 4.41a) and fractures (Fig. 4.41b) are conspicuous. However, the influence of the latter appears to be greater than the former. The predominant impact of the fractures in facilitating the ease of solute attack, and the ultimate formation of karst in the Kinta Valley can easily be seen from the similarity of the overall main fractures trend and cave passage orientations (Fig. 4.42a and b). Although the isolated limestone hills occupy only a small proportion of the overall valley area and the fractures are extracted from these remnant hills, the similarity of the fractures orientation and the cave passages clearly shows the continuity of the fractures. This in turn may imply that the continuous fractures, which transected the carbonate rock, most likely have occurred before the removal of the major portion of the country rock, which once covered the whole valley. Similarly, it can also be inferred that most of the karst features may have a concomitant origin, as long as they were influenced by the same structure.

The influence of fractures in the development of karst in the Kinta Valley is better attested by the morphology of cave passages which mimic the trend of the fractures pattern. These general patterns can be linear trends (Fig. 4.1a and Fig. 4.16a), circular pattern (Fig. 4.8), and sinuous pattern (Fig. 4.4a and Fig. 4.14b). Where the general

patterns of the caves passages are not evident, particularly in the karstic caves characterised by collapsed passages and associated chambers formations, linearly aligned stalactites or pillars inside these caves (Fig. 4.11b) suggest the tremendous influence of fractures in controlling karst development.

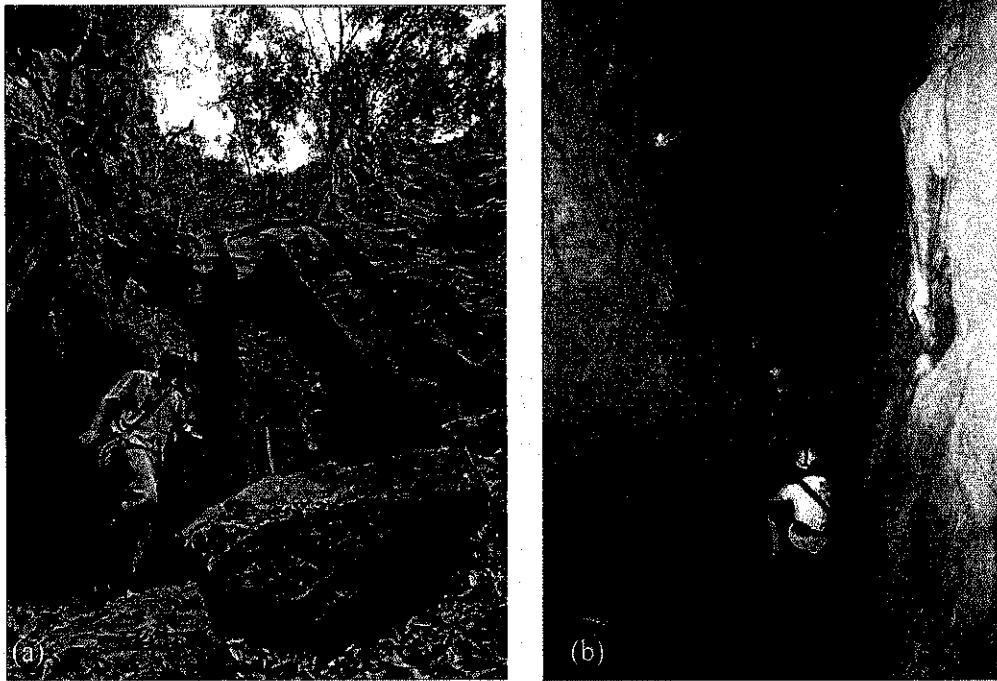


Figure 4.41: Formation of karst via an almost vertically dipping bed (a), and along a fracture (b).

Structures observed and extracted from the remnant hills of the Kinta Valley look utterly complex, and this may be attributed to the different phases of tectonics or various sets of stress system, although there may be a possibility that some minor faults might have feathered off at acute angles from the main fault as a result of wrenching of the rock. The Peninsula has a NNW-SSE elongated shape and the shape is controlled by the regional structures (Shuib, 2009). According to this work, the prominent NNW-SSE trending faults are common to the north and south of the Kinta Valley. Like the regional structures, the principal NNW-SSE lineament trend, observed in the Kinta Valley (Kassa et al., 2011), is superimposed by structures striking in five different trends. The similarity of these structural trends with the regional ones indicates that the geological elements in the Kinta Valley karst region might have been formed by the tectonic processes which gave rise to the regional structures, not the consequence of local processes. Hence, the NNW-SSE main

structural trend of the peninsula, most likely, controlled the karst landform of the study area.

The rose diagram in Figure 4.42b indicates the cave passage trends when all survey data, from different caves, are plotted together. These survey data are merged together after excluding short cave passages (lower than eight meters) which are thought to be non representative. Thus, the overall trend reveals the direction of the predominant passage trend which was formed, most likely, along the main fracture zone. Besides plotting all data together, to denote which fracture trend is prominently influencing the formation of karst features, observation of linear cave passages (for instance Fig. 4.1a and Fig. 4.16a) clearly indicate their development following similar fracture traces. In turn, this may further suggest the possible continuity of fractures and the influence of the same fracture in controlling the origin and development of various karst features, irrespective of their locations.

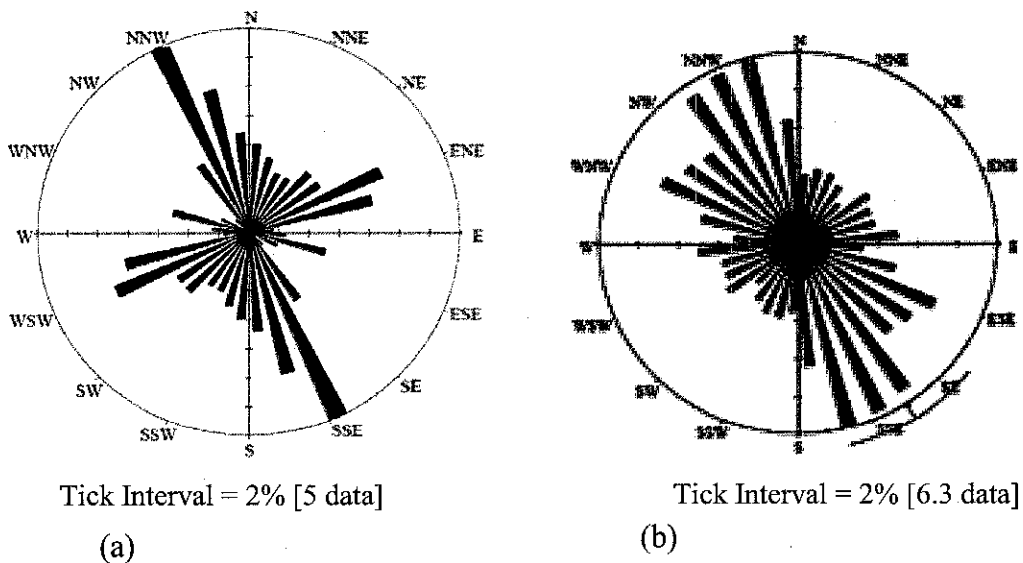


Figure 4.42: Rose diagrams showing (a) all fractures trends extracted from the remnant hills, and (b) the prominent caves passages trend obtained from different karstic caves formed in the vestige limestone hills.

Where the effect of fracturing is paramount, caves passage development is common via the failure zones, and the caves passage geometry in the study area illustrates their formation following the original fracture trace without subsequent fracturing effect related to their gradual development. Some karst caves morphology

appears to be a reflection of multi-fracturing phenomenon. For instance, the circular passage in Gua Kandu (Fig. 4.8) clearly suggests the influence of multi-fractures rather than being the consequence of fracturing related to the continuous dissolution process and associated collapse. Other evidence of caves morphology which appear to follow the fractures pattern is also evident in Gunung Tempurung. This hill is transected by fractures (Fig. 4.30), and is mainly characterized by convoluted cave passages which attest to the effect of multi-fracturing. Although the Gua Tempurung map (Fig. 4.14b) shows only the lower part of the cave marked by the river path, in some places, all the way from the first entrance to the outlet, there are relatively big chambers which may have formed at the point where various fractures intersect. During surveying it was noted that such chambers are located where the river path diverts. Thus, the effect of multi-fracturing which formed the complex structures could be responsible for the occurrence of the subsurface drainage systems, which are associated with the development of various karst features in the Kinta Valley.

In the remnant limestone hills, the fracture traces appear to be crossing each other, and it is common to see such fracture sets on the face or wall of the precipitous hills which bound a doline. The fractures, besides being quite notable on outcrops (Fig. 4.33a) and on the surface of a doline (Fig. 4.43a), are also very conspicuous inside the doline, as for instance Figures 4.43b and c indicate. The intersecting nature of the fracture traces could be a consequence of the multi-phase episodes of fracturing. If fractures are a prerequisite for the formation of karst, and if networks of fractures characterize the Kinta Valley karst system, it is expected that the development of karst to take place via all fractures. However, the prominent orientation in this karst features is NNW-SSE. The most likely reasons for this prominent trend are, (i) the fractures with the same trend may have formed first, and dissolution took place to sufficiently widen them, and collect the water that comes from other fractures which are superimposed later. This phenomenon might have made other fractures to be tributaries for the principal NNW-SSE trending ones, (ii) the impact of conjugate fractures on the development karst can be invaluable as the fractures extracted from the hills and those evident on the outcrops suggest.

The principal karst features, having a NNW-SSE trend, might have occurred

following the formation of open fractures along this trend. This is because, in a folded structure fractures cannot be associated with a single state of stress, but rather to several states of stress which may occur during the folding history, for instance as illustrated in Figure 4.44. The possible existence of the multi-stress system might have led the transformation of compressional joints to extensional joints. And this process might have made the NNW-SSE oriented structures to be extension fractures, so that they acted as a more favorable route to the flow of water, as extension fractures are more open and possess greater hydraulic conductivity.

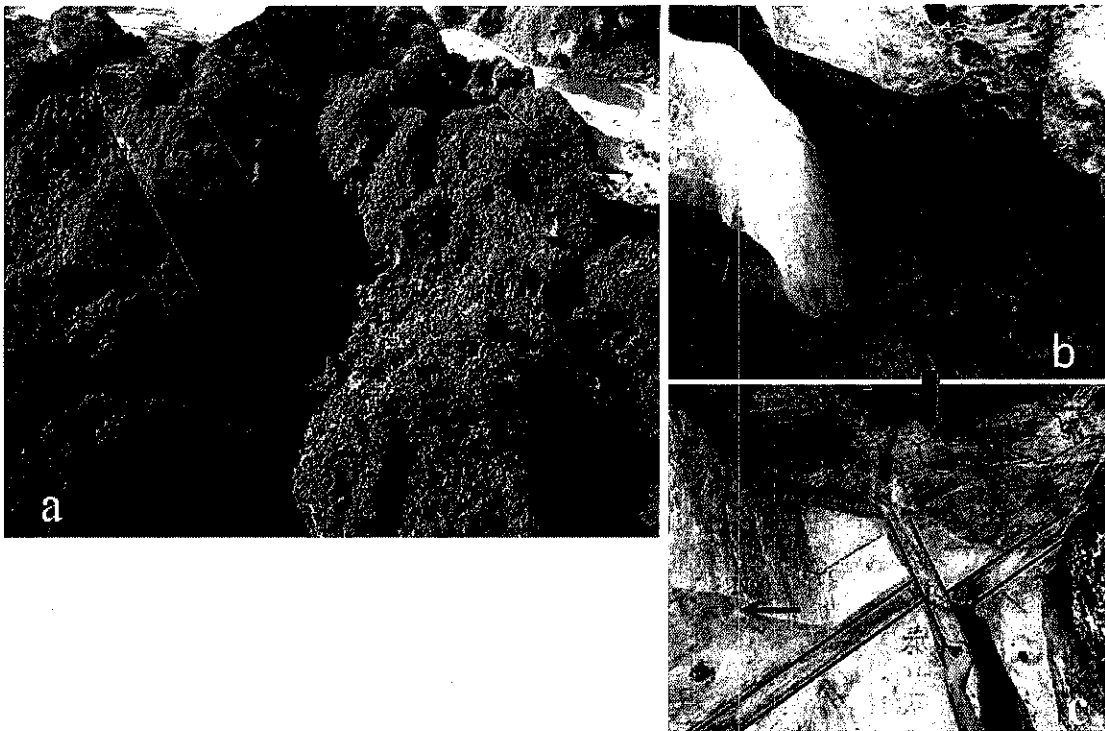


Figure 4.43: (a) Showing visible fractures (red line) on the surface of a doline, (b) Showing intersecting fractures further inside the doline, and (c) Illustrates after the intersection in (b) is zoomed out.

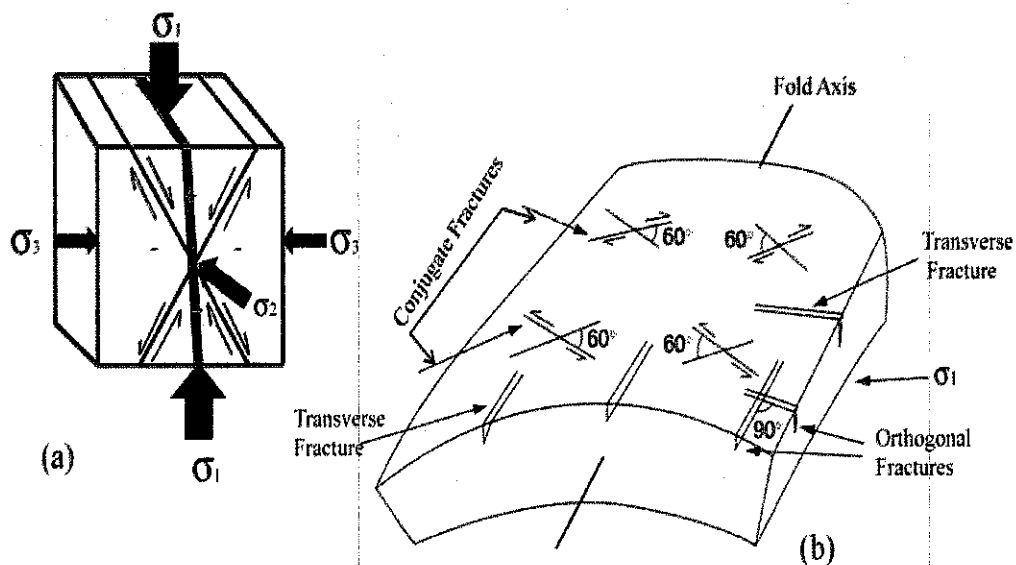


Figure 4.44: Schematic diagram showing (a) Extension and conjugate fractures, and (b) Ideal relationship between major joint sets in a folded bed (modified from Singhal and Gupta, 2010).

The matured karst in the Kinta Valley can be categorized as ‘Stripe Karst’, an extreme case of contact karst (for example limestone adjoining granite) (Lauritzen, 2001). According to Lauritzen (2001), originally flat lying strata may end up as an extremely elongated outcrop which could almost always be a product of tectonic and/or erosional modification. Hence, it is believed that orogenic tectonism is the most common and effective process to create stripe karst. The shape of present day Peninsular Malaysia and most of the regional structures are believed to be attributed to the Indosinian Orogeny. And the limestone in the Kinta Valley predates the adjoining granites (Ingham & Bradford, 1960; Hutchison, 2009). Thus, possibly the karstification process became so intense after the occurrence of the granite, as its gradual uplifting was accompanied by faulting (Madon, 1999). Similarly, the uplifted surface enhanced the mechanical denudational process, as the allogenic waters arise from it, and the associated faulting created conducive pathways that facilitated solute attack. Thus, the extant karst features in the area can be considered as a product of tectonic and denudational processes.

It is evident that the Kinta Valley karst features are controlled by fractures, mainly oriented in the NNW-SSE, which is also the prominent orientation of the regional

structures. The onset of karstification in this region may have taken place after the formation of these structures. According to Hutchison (2009), the emplacement of the Main Range Granite took place in the Late Triassic to Jurassic period. The development of NNW-SSE to N-S strike-slip faults followed at that time or at a late stage of this emplacement. Considering the geological structures in the Kinta Valley are related to the regional structures, and the NNW-SSE structures in the area are the principal lineaments, as evidenced by the cave passage orientations, lineament analyses, and ground truthing, the occurrence of the main faults which controlled the karst formation can be considered to date back to the Jurassic period. Taking the significant influence of the geological structures in the area into account, and considering that they are prerequisites for the occurrence of karst, it will be possible to infer that the Jurassic period marks the commencement of karst formation in the area, provided that the other factors substantiate this inference.

b) Lithology

The shape of dissolution features in carbonate rocks may appear as anastomosed, networked, branch work, and spongework (Palmer, 1991). The variation in dissolution rate and the occurrence of such pattern are attributed to the nature of the carbonate rock. In the study area, the limestone appears to have been slightly metamorphosed; however, it is possible to see sedimentary structures, such as interlayering of thin and thick beds. Many karstic caves in the study area are characterized by linear cave passage morphology, except where they are interrupted by the occurrence of small chambers. Although the remnant hills are intersected by fractures, the cave passage development did not mimic the fracture network. This could be due to, besides the prominent fractures occurrence, the relative hardness of the rock. If the carbonate rock was not subjected to any metamorphism, multi-passage conduits may have formed as a consequence of dissolution via primary pores and fractures. However, the crystalline nature of the carbonate rock in the study area, as a result of slight metamorphism, rendered the primary porosity not to have any significant influence on the karst development. Rather, the occurrence and evolution of karst in the Kinta Valley is constrained to the secondary porosity, i.e. fractures. Hence, the predominant occurrence of linear cave passage morphology in the area, and the absence of any

spongework or anastomose or branchwork pattern can be attributed to the crystalline nature of the carbonate rock, as the occurrence of spongework patterns of solutional caves attributes to poorly lithified carbonates.

Although the linear karstic caves are preferentially formed via the weak zones, which have a prominent trend of NNW-SSE, the crystalline nature of the carbonate rock also played a role in facilitating the formation of linear cave passage morphology. Furthermore, the crystalline nature has possibly reduced the effect of denudation, otherwise the extant 2.5% remnant carbonate rocks would not have survived. Because, if the karst features were characterized by the spongework or anastomose pattern, which is related to poorly lithified carbonates, their collapse and removal would not take as long as those karst features with single and linear passage morphologies.

c) Uplift

Since the limestone in the Kinta Valley is underlain by granite, the uplifting phenomenon that emplaced the granite has influenced the carbonate rock. Thus, the Kinta Valley karst system has also experienced a gradual but fluctuating uplift rate. Thermal modelling using apatite (Figs. 4.36-4.39) and zircon fission track data clearly documented this uplifting event at least from the Upper Cretaceous onward. The influence of this phenomenon is revealed in the morphology of the various karst features situated all over the valley. Hence, uplifting played a crucial role in the development of the Kinta Valley karst. For instance, some of the karst features that bear witness to the uplifting phenomenon include: –

- Gua Tempurung

This cave is characterized by two levels, where the upper level is marked by the formation of big chambers (Fig. 4.15), and the lower level, found underneath the chamber which is typified by a narrow conduit that is still being denuded by a stream coming from the adjoining granite. The cave morphology, the sediments embedded in the wall, and the extant stream flowing through the cave clearly suggest the gradual lowering of the water level through time as uplifting continues.

In addition to the fission track data, which indicate that the area has been influenced by uplifting, there is also other evidence that suggests the karst system was subjected to this phenomenon. For instance Figure 4.45, which is made in ‘Global Mapper’ by overlaying the Spot image on a slope map, shows stepping terrain marks (the inset graph) after the cross section is made at the bottom of Gunung Tempurung. If stepping terrain appears in the cross-section, it is a clear indicator that there has been gradual uplifting through time. Hence, it can be inferred that Gua Tempurung is a result of lowering of the stream, which was incising the hill through time, ensuing the uplifting phenomenon.

The formation of a big chamber in the upper level of Gua Tempurung can be attributed to the lowering of the water level whose continuous incision of the wall leaves the overlying rock unstable. As the uplifting process continued, the unstable rock collapsed to create small chambers, which through time merged to form the extant big chamber. Thus, the uplifting event enhanced the development of this karstic cave.

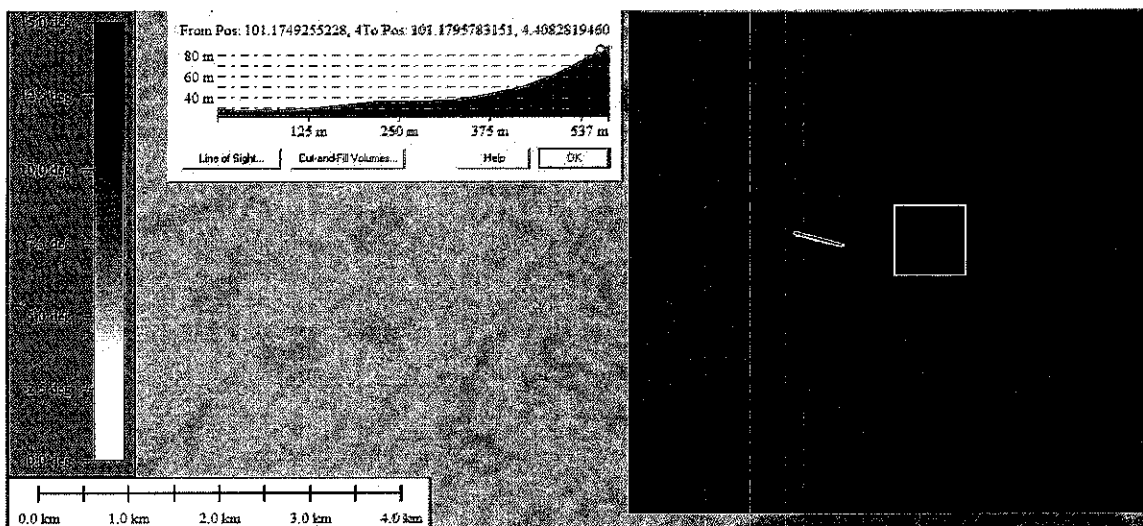


Figure 4.45: Displays a slope map of Gunung Tempurung after the Spot image is overlain on it. The inset cross-section, for the yellow line at the base of the hill, indicates stepping which marks gradual uplifting. Gua Tempurung, whose development through time is influenced by uplift is located within the box.

- Gua Kandu

This cave is also characterized by multi-level cave passages (Fig. 4.8). Although it has upper level passages that survived collapse, there are relatively big chambers formed by the merging of the different layers of the cave passages. The overall morphology of the cave passages clearly attests to the gradual lowering of the water level, and this lowering through time can be attributed to the uplifting event that has been influencing the area. This is because, if the water level was not lowering following the uplifting event, multi-level passages would not form. Instead, a single large chamber could be formed as there would be ample time for the water to incise the cave wall and form a deep groove. The deep groove may ultimately result in the collapse of the overhang rock which subsequently forms a chamber. Similarly, fine sediments embedded on the walls of the different cave passage levels are clear indicators of the uplifting phenomenon. Hence, the Kandu cave passage pattern is a reflection of its development as the karst system has been experiencing uplifting.

- Multiple notches

Commonly, notches appear horizontal, with shallow or deep indentation, probably marking paleowater level. If the level of stagnant or slowly flowing water remains stable for a long time, deeply incised notches develop. However, if the water level drops or retreats fast, shallow grooves or notches appear subsequently. These processes may be attributed to the uplifting events.

Simple and multiple notches are quite evident on the face of the precipitous hills and inside the karstic caves of the study area (Fig. 4.2, Fig. 4.20 a-c, and Fig. 4.21a-d). The scale of the notches varies from tens of centimeters to one and half meters. Such features are particularly conspicuous inside a doline where the multiple grooves appear shallower in the upper part and deeply incised in the lower part of a vertical wall bounding a doline (Fig. 4.46). Although the uplifting phenomenon was not reflected on all the multiple notches formed in different remnant hills of the study area, owing to the intervening influence of other factors, some of these features clearly illustrate the fluctuation of uplifting rate. For instance, in Figure 4.46, the shallow groove and highly frequent upper notches depict fast water level lowering,

whereas the lower deeply incised wall indicate relatively slower water level lowering. This is because, if the water stays stable for a long time, continuous incision will take place and the grooves of the notches appear deeper than where the water level resides only for a short time. Thus, it is possible to infer from Figure 4.46 that the upper level of those notches reflect fast water level lowering as a consequence of faster uplifting rate, and the lower level is characterized by slower uplift rate or relatively more stable conditions.

Notches height variation from place to place, and the different shape of notches existing in the same outcrop are clearly evident in the Kinta Valley. This observation suggests, (1) no similar genetic relation between the notches in the same hill, (2) no concomitant influence of the same factor in different hills, despite the notches exhibiting similar morphology. In turn, the most likely reason for this can be, (a) the occurrence of stagnant waters, ensuing collapse of a number of karst caves, and (b) the preferential flow of rivers through the different karst features (Fig. 1.2a), particularly via prominent fracture traces which are responsible for the formation of various karst features in the area, and (c) as the vestige limestone hills represent the pre-existing limestone deposit, which once covered the whole valley, most of the contemporary water level markers might have been removed during the persistent denudation processes in the area. Despite the absence of horizontally continuous similar elevation notches, based on the aforementioned justification, the influence of uplifting in the evolution of the Kinta Valley karst system cannot be ruled out.

Considering the fact that uplift is responsible for the gradual lowering of water level, it can be deduced that the pattern of multiple notches serves as a proxy or indirect evidence for the fluctuation of uplift rate. In general, it is possible to consider notches as a means of characterizing the nature of uplifting in a certain area.

It may seem difficult to exactly identify which factors are responsible for the formation of the notches in the Kinta Valley, but there is evidence that points to the origin of the notches. This evidence takes into account the morphology of modern notches and how they responded to the process which formed them. For instance, the river which is still denuding Gua Kanthan (Fig. 4.2) developed notches which resemble subaerial notches, and these features clearly suggest the gradual lowering of

the river level. Such gradual lowering is attested by the smooth and gently dipping part of the notch. However, if the drop of the water level was fast, the groove would probably be shallower. Thus, it has to be noted that the groove depth may increase following the impact of sediment-laden high discharge flow; this implies that a fast drop of water level may not necessarily be associated with shallow grooves. However, there is a possibility that shallow grooved notches with a high frequency of occurrence can be related to a fast drop of the water level, which is a consequence of the lowering of the base level as the karst denudation process continues or enhanced by the gradual uplifting.

In different parts of the Kinta Valley, the higher levels of the notches are not related to the pre-existence of stagnant water. Rather, in most places the notches appear to have formed inside a cave. There are evidence that indicate their formation before the collapse of caves, including the growth of stalactites (Fig. 1.3a) and cave



Figure 4.46: Picture of a doline and multiple notch patterns on the precipitous wall of the doline.

infilling sediments (Fig. 4.21b) partially covering the notches. One may argue that the formation of the stalactites took place after the collapse of the caves; however, the presence of hard, tough and compact stalactites attests to their formation in a closed

system. If their formation was in open system, the stalactites would not grow vertically downward and would become soft and fragile. In essence, they would appear as tufa, unlike those stalactites formed inside a cave. Thus, the higher level of notches formation took place before the cave collapsed, and has no genetic relation with the mechanism of river action after collapse or stagnant water or sea level rise. Since such kind of notches resembles those that are formed inside river caves (Fig. 4.1a), it is possible to relate the occurrence of the relict notches to the action of a river while it was denuding the caves. This inference leads us to point out: (1) if the higher level of notches formation is related to a river action, while it was flowing inside a cave, then it implies that the level of the river was in that position; that is, of course, if there was not vertical movement of the surface. (2) the notch formation might have occurred when the level of the caves was lower than the present position. Considering the influence of uplifting, it is possible to deduce that the second justification holds true.

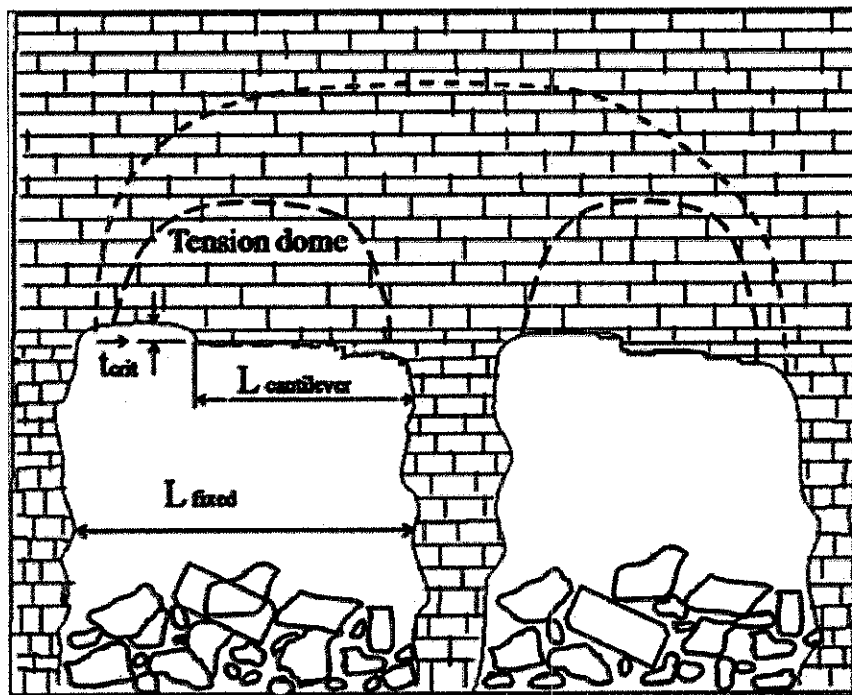


Figure 4.47: Schematic diagram showing the mechanism of rock breakdown and associated tension dome formation. As collapse of ceiling rock persists, individual chambers in a single cave passage coalesce to form a big chamber (red dot line) (modified from White, 2005).

In general, the uplifting phenomenon is undoubtedly imprinted on the Kinta Valley karst features, particularly, it is reflected on the extant dolines and multi-layered caves. Based on the fact that the uplift rate was varying through time, it is possible to infer that simultaneously karstic caves passage formation was taking place. This is because, as the uplifting was continuously occurring, it is inevitable that a denudation process was taking place with subsequent lowering of the base level. Since the uplifting was generally slow and with varying rates, there was most likely enough time for the formation of large conduits. As the cave breakdown mechanism in Figure 4.47 indicates, the continuous denudational process results in the collapse of ceiling rocks which ultimately leads to the formation of cave chambers. If neighboring chambers happen to intersect as a consequence of upward stopping, big cave chamber will be formed.

The big chamber in turn collapses to form a considerably large doline whose dimension may extend up to four times the size of the original chamber. However, it has to be noted that the collapse of caves and associated occurrence of dolines must be preceded by a very slow uplift rate which enables the formation of deep corrosion undercut. Such process will make the overlying rock unstable so that big caves collapse to form a doline. The various karst features in the study area attest to the occurrence of the same process, i.e. relatively the last stage of the karst development is characterized by a more stable condition which facilitated the formation of big chambers and collapsed caves. These features which show the stable condition includes, the large scallops in Figures 4.22a, 4.24a, 4.25b, 4.27a, 4.28b and the deep notch at the base of the doline (Fig. 4.46), deep corrosion grooves or undercut at the base of the tower karsts or foot caves, for e.g. Figures 4.48 a-c.

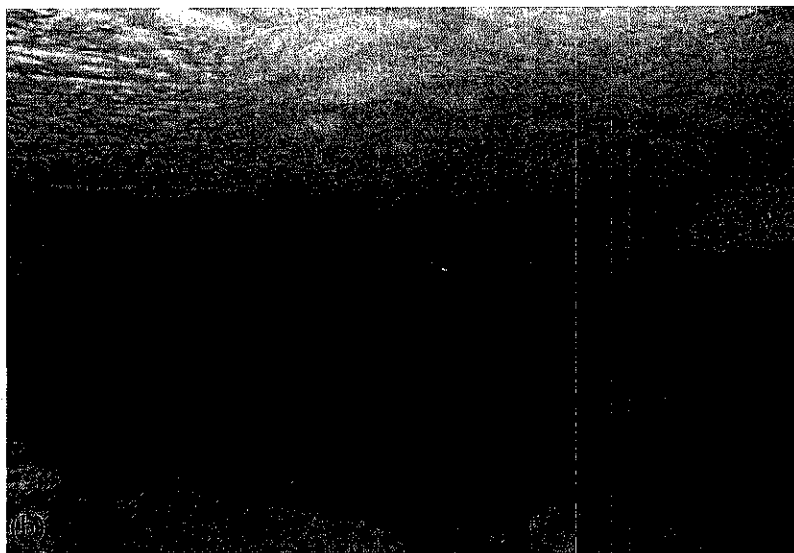
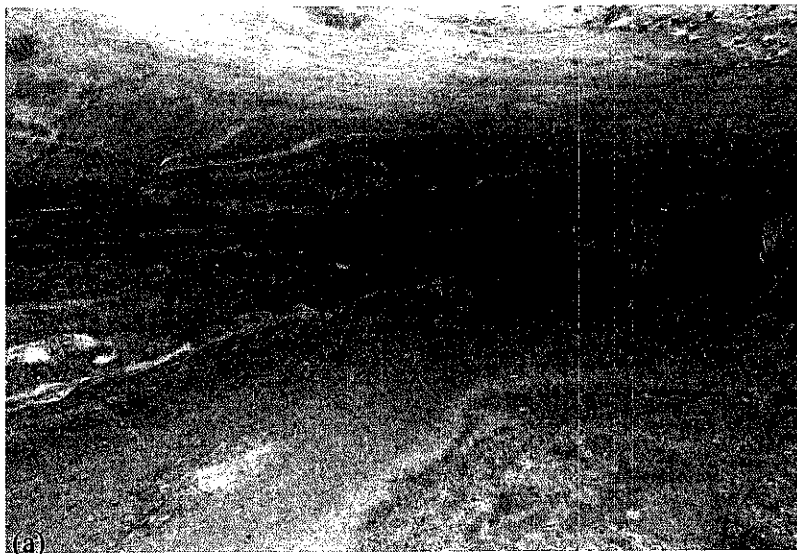


Figure 4.48: Picture (a) and (b) indicating deep corrosion grooves formed at the base of the hill in Gua Masoora; the undercut in picture 'b' is situated further deep inside this cave, and (c) indicates deep undercut in Gunung Kanthan.

d) Sea-level rise

Karst features can be formed and evolve through time as a consequence of sea-level rise and fall. The influence of sea-level rise can be manifested on coastal carbonate rocks as deeply incised notches (Bhatt and Bhone, 2006; Kershaw and Guo, 2001; Wziatek et al., 2011) or flank margin caves (Mylroie J.E. and Mylroie, 2009; Smart et al., 2006; Waterstrat et al., 2010). The formation of such karst features are the result of wave action or mixing corrosion.

It may be erroneous to utterly rule out the influence of sea-level variation on the development of karst in the Kinta Valley. Nonetheless, the sea-level fluctuations impact on the evolution of karst appears to be insignificant compared to the aforementioned factors. According to Haq et al. (1987), high sea-level was documented in the Cretaceous period, and a gradual decline of sea level began in the latest Cretaceous which continued through the Cenozoic, with the exception of relatively higher levels in the Danian, Ypresian, Rupelian, Langhian through early Serravallian, and Zancian, and the trend toward lower sea levels continues to the present time (Fig. 4.49).

Thus, considering those periods marked by high sea-level, one may relate the development of the Kinta Valley karst features with these periods. However, it is important to figure out how many meters of sea-level rise would possibly encroach the Kinta Valley before relating karst development in the area with periods of sea-level rise.

In order to show the possible infringing of sea-level rise, the following illustration (Fig. 4.50) is made in Global Mapper by varying the water level every 20m. As these figures indicate, the sea-level has to rise up to 60m to reach the Kinta Valley, and this is true only if the area of interest has not been influenced by any uplifting episodes or if it was stable. However, the karst features and fission-track data prove otherwise, i.e. the Kinta Valley karst region has been subjected to variable uplift events. Hence, in the area where there is continuous uplift, it is difficult to associate the development of karst with the impinging sea-level rise. Nevertheless, if the eustatic sea-level rise outpaced the uplift rate, the Kinta Valley could have been flooded by the infringing

water. Haq et al. (1987) indicated that there are periods in which the sea-level rose more than 100m, and it is possible that during these periods the sea-level reached the Kinta Valley. But the absence of any karst features in the study area, such as notches which are horizontally aligned and situated in similar elevation, attest to the significant influence of factors other than sea-level variation. Furthermore, Figure 4.19 strengthen the inference drawn about the absence of sea-level rise and its possible influence on the development of karst features.

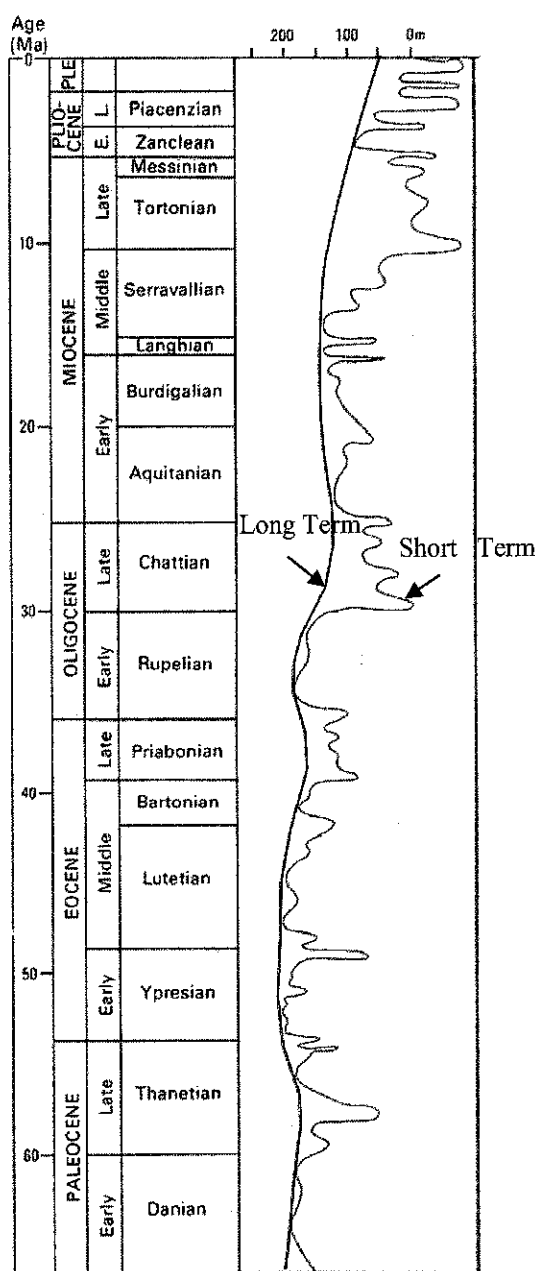
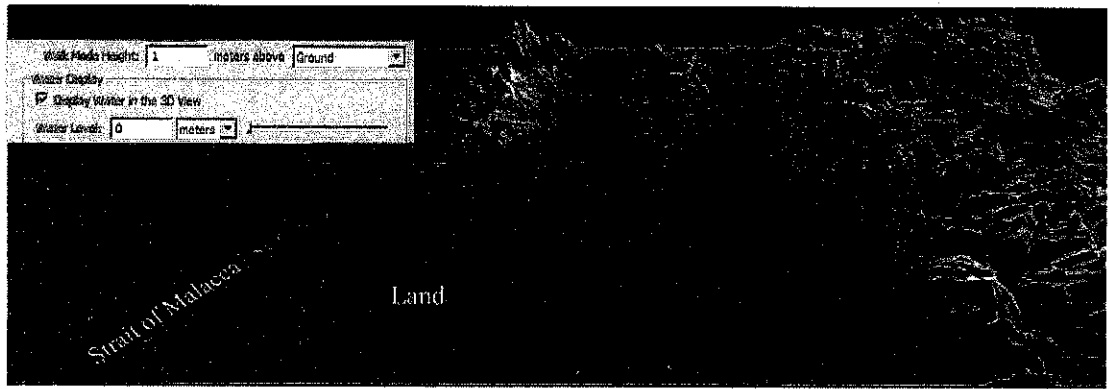


Figure 4.49: Global sea-level model for Cenozoic (after Haq et al., 1987).



(a)

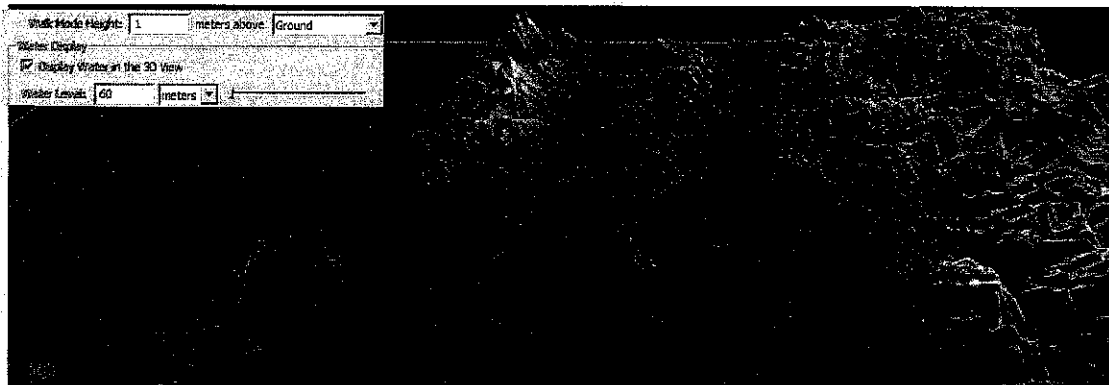
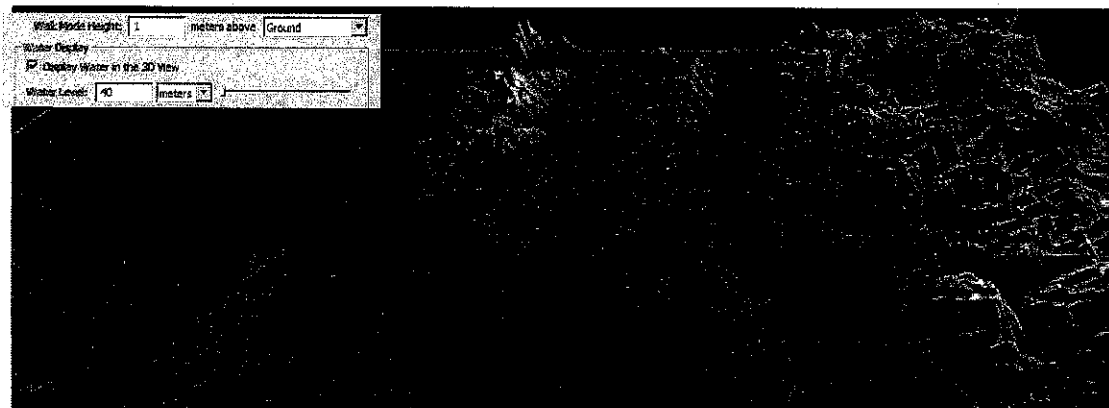
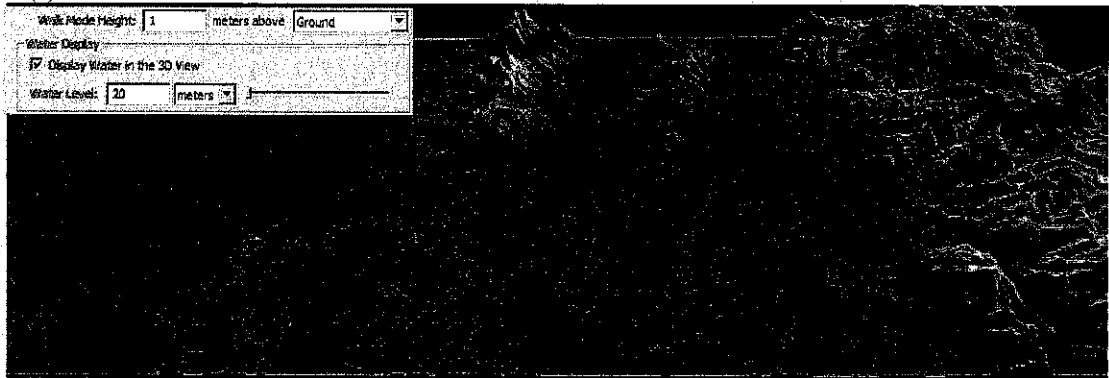


Figure 4.50: Displaying present day sea-level with respect to the Kinta Valley karst region, assuming an increase of the water level & its possible extent towards the valley after (a) sea-level (0 m), (b) 20m, (c) 40m, and (d) 60m. The inset box indicates the water level.

Batchelor (1979) indicated that the significant sea-level lowering during the Late Miocene exposed part of the Sundaland which includes Thailand, Sumatra, Java, Indochina (Cambodia, Laos, Vietnam), and Borneo. Such drastic lowering of the sea-level during the Early Tortonian (Fig. 4.49) may have an indirect impact on increasing the carbonate rock loss from the Kinta Valley. This is because, as indicated in the preceding discussion, the rate of carbonate rock loss after the Late Miocene is higher than the rate estimated in the preceding periods. Therefore, besides the increment in carbonate rock loss as a certain basin loses half of its deposit (Szunyogh, 2005; Ford and Williams, 2007 and reference therein), the drastic lowering of the sea-level during the Late Miocene (Early Tortonian) may have played a role in aggravating the unroofing of the carbonate rock from the Kinta Valley. Otherwise, those extant karst features at high elevation are not the consequence of any sea-level rise, rather they are the imprint of denudation via discontinuities as the continuous uplifting episodes have been taking place through time.

4.2.2 Estimation of long term denudation rate and onset of karstification

Unlike the short-term denudation rate estimation, the long-term one is more complex as various factors have to be taken into account. Despite its difficulty, the data or inputs considered in this study enabled to pinpoint the most likely long-term denudation rate of the area. These inputs include, estimated original thickness of the carbonate rock, measured denudation rates, the relation between the granite and the limestone, and fission-track age. The basic assumption here is that, if those inputs considered as supporting evidence for the calculation of long-term denudation rate are consistent with extant measured values in the Kinta Valley or similar karst region, then the output (the rate to be estimated) will reflect the authenticity of the data to be considered. The details are described as follows:-

4.2.2.1 Estimated original thickness of the limestone

The denudation process has left a small proportion of the original carbonate deposit in the area. Thus, the extant limestone hills distribution in the Kinta Valley

does not enable to infer the original thickness of the carbonate rock. However, considering contemporaneous carbonate deposits in South China and previous stratigraphic study of the area, it may not be erroneous to estimate the possible range of the original thickness of the carbonate rock in the area.

According to Woon (1991) and references therein, the carbonate rock in the Kinta Valley has been dated as Silurian to Devonian near Chemor, and Carboniferous and Permian near Kampar, i.e. it is getting young towards the southern part of the area. The thickness of the carbonate rock in the southern part of the Kinta Valley, near Kampar, is estimated to be more than 5500ft (>1676m) (Suntharalingam, 1968). According to Ingham and Bradford (1960), the thickness of the carbonate series in the Kinta Valley may be as much as 10,000ft (3048m) or more but since the beds are repeatedly folded, it may be much less. Similarly, South China had two periods of carbonate rocks deposition, including (a) from Upper Sinian to Upper Ordovician, mainly distributed in the southwestern part of China, (2) from Middle Devonian to Middle Triassic. The total thickness of this carbonate rock is estimated to be about 3,000 - 10,000 m (Daoxian, 1981; Guangzhong et al., 1985).

Considering concomitant carbonate deposit in Sibumasu terrain, where west Malaysia is located, and South China, it is possible to infer that more than 1.5 km of carbonate rocks may have been removed from the Kinta Valley. If this is so, there is a possibility that there was more than 3km thick carbonate deposit in the area, but it has to be further strengthened by other lines of evidence.

4.2.2.2 Measured denudation rates

Previous works, including Plan (2005) and Häuselmann (2008), indicated that measured short term denudation rate is not constant, as it differs with variations in karst morphology or elevation. According to these works, the short-term denudation rate may vary from 11-48mm/ka. Muhammad (2006) indicated different short-term denudation rate in the Kinta Valley, unlike the other workers who took morphology and elevation variations into account. Then, the average short-term denudation rate in the area is found to be 86-158 mm/ka (Muhammad, 2006), but Muhammad believes

that it is difficult to extrapolate this short-term denudation rate based on the data used in the estimation of this rate. Crowther (1989) also documented 56.6 to 70.9 mm/ka short-term (1 year period) chemical denudation rate in the Kinta Valley.

A long-term cave passage incision rate of 20-50mm/ka, has been documented in Ford and Williams (2007) and references therein. Ford and Williams (2007) summarized a number of works which documented denudation rates, and inferred that 50–1000 mm/ka is typical for tectonically active mountainous areas.

The karstification process in the Kinta Valley most likely occurred after the Indosinian orogeny, which marks the end of the collision of Sibumasu and Indochina/East Malay block, as described in detail in the aforementioned ‘tectonic setting’ section. Therefore, extreme denudation rate, which is typical of tectonically active areas, is not expected in the area of interest.

4.2.2.3 The relation between the granite and the limestone

The limestone in the Kinta Valley is older than the granite. According to the works of Suntharalingam (1968) and Woon (1991) and reference therein, the Silurian to Permian age of the limestone predates the Upper Triassic age of the granite (Krähenbuhl, 1991; Metcalfe, 2000; Sevastjanova et al., 2011). Similarly, the Upper Triassic (~215 Ma) intrusion age of the granite is obtained from zircon UPb age of the Samples (CH-6 to CH-10) used in this study. The slight metamorphism of the carbonate rock further indicates the post date of the granite emplacement. Hence, the uplifting of the granite has been influencing the carbonate rock through time, and in turn, the rate of karst denudation is constrained by this process. Since uplift rate is equivalent to base-level lowering or cave stream downcutting rate, the possible long-term denudation rate can be approximated from the estimation of uplift rate.

4.2.2.4 Fission-track age

The fission-track ages indicate that the first sample (CH-6) reached the effective closure temperature, ~240°C, about 97Ma. This sample later approached ~110°C

about 34Ma, as uplifting continued. Consequently, the uplifting episode emplaced the remaining samples into the lower temperature zone. Thus, the fission-track ages and associated uplift rates can easily be represented as: -

97.5Ma $\xrightarrow{68\text{mm/ka}}$ 33.93Ma $\xrightarrow{78\text{mm/ka}}$ 31Ma $\xrightarrow{6\text{mm/ka}}$ 7.46Ma

or see Figure 4.51. The approaches used to calculate these uplift rates are given in the aforementioned part under section 4.1.5.2. Based on these values, the average uplift rate is estimated to be 50.6 mm/ka. Since cave streams incise as a consequence of both chemical and mechanical processes, and their downcutting rate is equal to the rate of base-level lowering, which in turn is equivalent to the rate of tectonic uplift (Ford and Williams, 2007), it is possible to take the average rate (50.6 mm/ka) as an approximate value for the long-term denudation rate. Thus, in order to estimate the possible thickness of the carbonate rock and the time for the onset of karstification, the following evidence from fission-track ages are taken into account.

As explained in Section 4.2.2.1, the original carbonate rock thickness could be greater than 3km, but it is difficult to precisely pinpoint the maximum thickness. Nonetheless, the maximum thickness cannot be greater than 7.5km, as elaborated in the following discussion. The first sample (CH-6) reached $\sim 240^{\circ}\text{C}$, the effective closure temperature for fission-tracks in zircon, at 97.5Ma; this was at $\sim 8\text{km}$ depth, taking the $30^{\circ}\text{C}/\text{km}$ geothermal gradient into account. If this sample was 8km deep at 97.5Ma, this implies that karstification did not take place at this period unless the carbonate rock was 8km or more thick. In a nutshell, for Sample CH-6 to be exposed to the surface, there had to be unroofing of $\sim 8\text{km}$ thick rock. Then, with the estimated average denudation rate, i.e. 50.6mm/ka, it is impossible to get more than 8km thick original carbonate rock deposit; otherwise, the remaining carbonate rock in the Kinta Valley would have been much higher than what is found today. Thus, with this justification, it is possible to deduce that the carbonate deposit was less than 8km thick in the area, and this in turn means that the onset of karstification did not take place at 97.5Ma, by the time when sample CH-6 was emplaced $\sim 240^{\circ}\text{C}$.

The average denudation rate (DR), for the time range (t) of 97.5 to 7.46Ma, is estimated to be 50.6mm/ka. The thickness (T) of the overlying material which has been unroofed during this time range is-

$$\begin{aligned}
 T &= DR * t \\
 &= 50.6\text{m/Ma} * (97.5 - 7.46) \text{ Ma} \\
 &= 4556\text{m}
 \end{aligned}$$

If the thickness is calculated for each time range (Table 4.6), the sum is very close to the total thickness estimated using the average rate, which suggests the acceptable estimate of the average rate (50.6mm/ka).

Table 4.6: Approximate thickness of the carbonate rock for the respective time range and associated uplift rate

t (Ma)	RU (m/Ma)	ET (m)	TT (m)
97.5 – 33.93	68	4323	
33.93- 31	78	229	
31-7.46	6	141	
97.5 –7.46			4693

where, ET is the product of RU and t. ‘t’ is the difference in age, ‘RU’ is the uplift rate equivalent to base-level lowering, ‘ET’ is expected thickness that may have been removed in each time range, and ‘TT’ is for the total thickness.

When Sample CH-6 reaches the lower temperature zone around 7.46Ma, from 8km depth, about 97.5Ma, there was ~4.69km unroofing of overlying material. This estimate suggests that there may have been ~3.31km unroofing after the Late Miocene period (7.46Ma) (Fig. 4.52). However, some questions can be posed in order to show how the fission-track data supports this inference: (1) is the amount being removed after 7.46Ma not an overestimate compared to what has been unroofed from 97.5 to 7.46Ma? (2) is there any evidence that may substantiate whether there was more than 3km unroofing after 7.46Ma? (3) does this suggest what could be the possible original thickness of the carbonate rock?

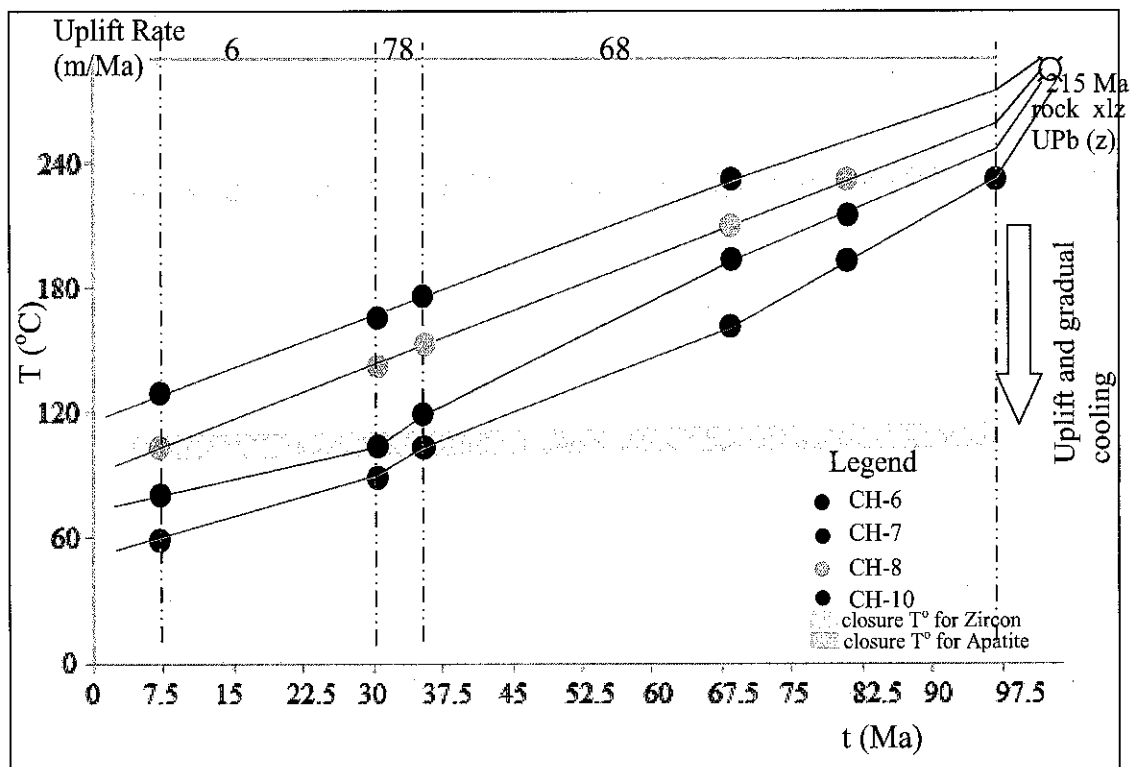


Figure 4.51: A cartoon illustrating the t-T relationship as the four samples (CH-6 to 10) are undergoing gradual cooling while they are uplifted from 97.5Ma onward, marked by zircon fission-track age.

The answers for these posed questions are given below after considering the fission track ages of Sample CH-6 and CH-8. The apatite fission-track age for Sample CH-8 indicates that this sample passed the 110-60oC closure temperature around 7.46Ma. Thus, the average depth of the sample would be ~3.7km, after taking 30oC/km for geothermal gradient. In turn, this suggests that at 7.46Ma Sample CH-6 was situated at a depth of ~3.3km (Fig. 4.53), after subtracting the elevation difference (Table 4.3) between the two samples. If we assume that the original thickness of the carbonate rock was 8km and the karstification started at 97.5Ma, there would be about 4323m unearthing of the overlying rock for 63.57Ma, i.e. from 97.5 to 34Ma. If the possible thickness from 34-7.46 Ma, i.e. 229m + 141m (Table 4.6), is added into the estimated thickness from 7.46 Ma onward, i.e. ~3.31km, there was ~3.67km thick rock being removed since 34Ma (Fig. 4.54a). However, with this estimated thickness, it is erroneous to infer that there was 8km thick carbonate deposit

in the Kinta Valley, and also it will be erroneous to deduce that the onset of karstification began at 97.5Ma. The evidence for this justification can be put forward if the nature of karst development and the late uplifting episode in the area of interest are taken into consideration. The summary of the following discussion is plainly indicated in Table 4.7.

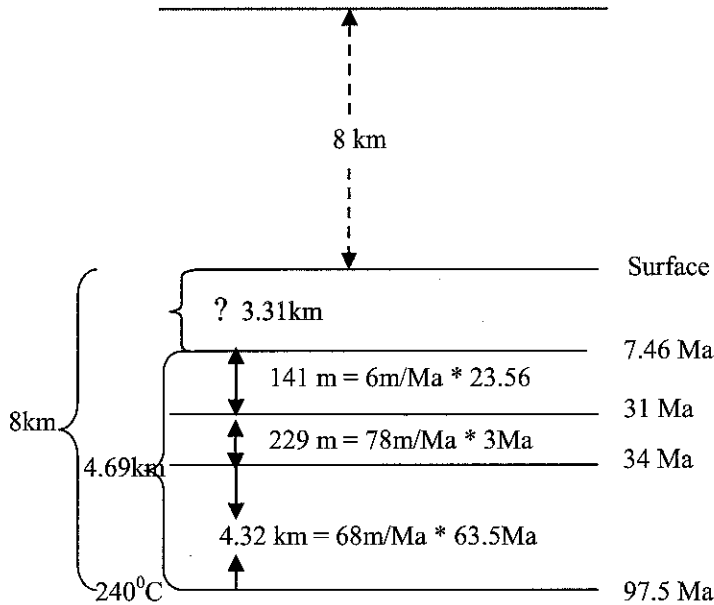


Figure 4.52: Simple sketch depicting the possible thickness of unroofed rock since 97.5 Ma, taking into account the estimated uplift rate is equivalent to the downcutting rate for the corresponding time range.

The degree of karst formation increases as the karstification process continues, since features that are formed subsequently facilitate the creation of more surface area for further karstification to take place. Considering the notion in Ford and Williams (2007) and reference cited therein, i.e. as a certain basin loses its limestone deposit from 100% to 50%, where the source of allogenic water is insoluble rock, there will be about 60% increment in dissolution rate. Similarly, (Gabrovšek, 2007) has shown using simple mathematical model that the denudation rate increases with the thickness of removed layer, after assuming uniformly infiltrating vertical flow on a limestone block dissected by vertical array of fractures.

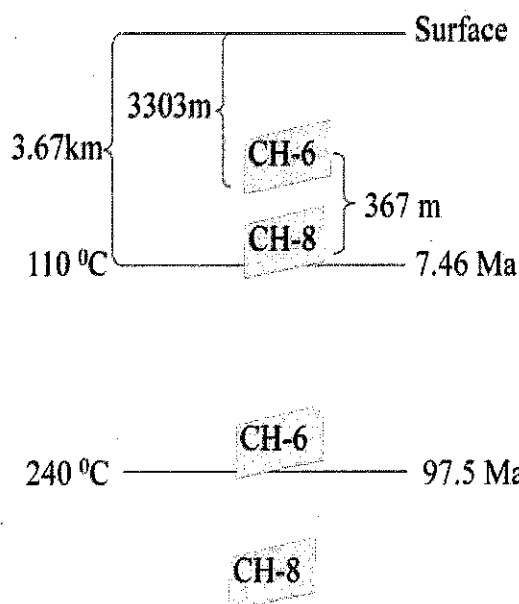
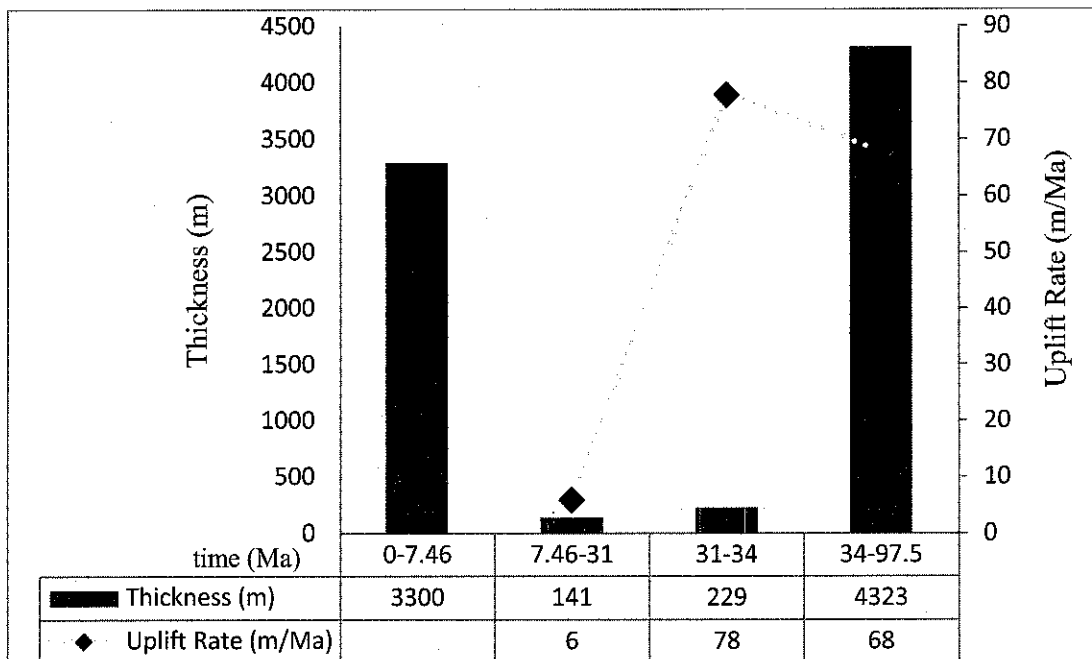


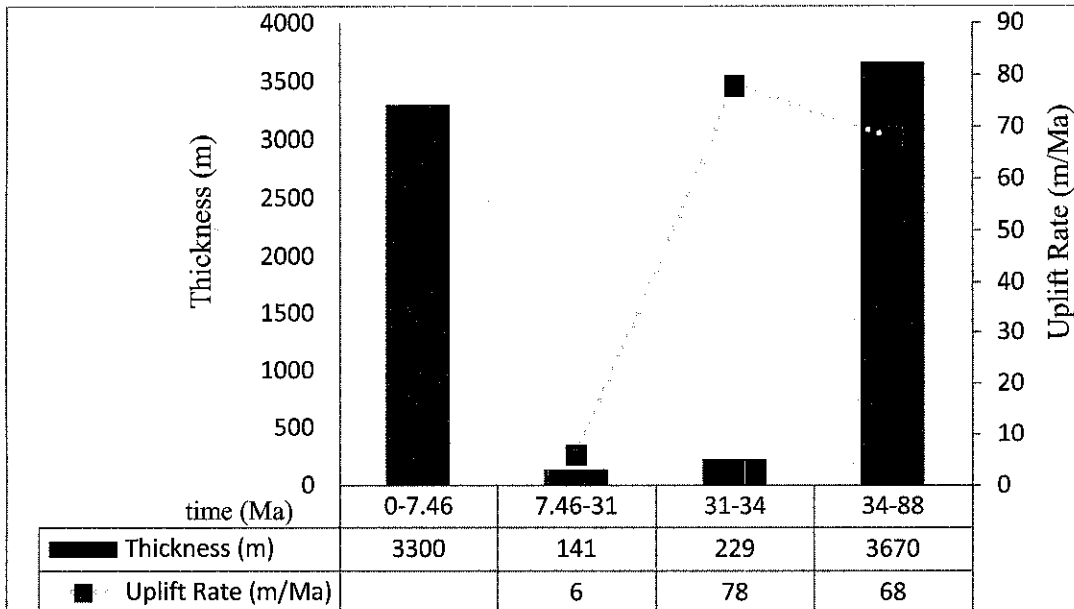
Figure 4.53: Simple sketch depicting the emplacement of Sample CH-6 and CH-8 at different time with corresponding closure temperatures.

In the Kinta Valley, there is evidence of a faster uplifting event after the Late Miocene. Although only 370m thick rock appears to be removed from 34 to 7.46 Ma, much of the rock may have been uncovered after 7.46Ma. As indicated above, rock approximately 3.67km thick was unroofed from 34Ma onward; then, by considering the aforementioned justification, there might have been uncovering of an almost similar thickness of overlying rock before 34Ma. When Sample CH-6 uplifted between 97.5-34Ma, from the depth of 8km, there was uncovering of about 4323m; thus, ~3.67km thick of rock to be removed up to 34Ma, the maximum original thickness should be ~7.34km. This is because, subtracting 653m thickness from 4.323km gives 3.67km which is equivalent to the thickness of rock estimated to have been removed since 34. In a nutshell, these estimated thicknesses give an answer for the aforementioned posed questions. Based on the fission-track ages, the estimated ~3.3km thick of rock being unroofed after the Late Miocene suggests that the carbonate rock was ~7.34km thick. Therefore, this possibly suggests when the karstification process commenced; i.e. Sample CH-6 was uplifted from 97.5Ma, ~8km depth, to 34Ma with a rate of 68m/Ma, and to arrive at a depth of 7.34km it had to move up ~9.6Ma (653m/68m/Ma). By the time this sample reached to a depth

7.34km, ~88Ma (Fig. 4.54b), most likely the overlying sediment cover had been removed so that the onset of karstification process could take place.



(a)



(b)

Figure 4.54: Graphs displaying uplift rate variation and estimated thickness of rock unroofed from the surface, for the corresponding time range, (a) since 97.5Ma, and (b) since 75.5Ma.

Table 4.7: Concise summary of the contemporaneous processes which have been taking place both under and on the surface, since the Triassic period.

Period	Series	Event
Present		The uplifting episode after the Upper Miocene is not quantified. Nonetheless, much of the carbonate rock possibly removed from the area after the Upper Miocene (7.46Ma). This is expected to happen since there is a high possibility of tremendous increment in karst denudation as the duration of the process increases.
Miocene	Upper	Generally this period is characterized by a minimum uplifting rate, i.e. 6m/Ma. However, it was typified by a relatively faster cooling episode or uplift after the late Upper Miocene. During this period carbonate rock of ~141m thick was unroofed. During the Upper Miocene period (7.46Ma), the first sample (CH-6) was probably emplaced ~3.3km depth.
	Lower	
Oligocene	Lower	The uplifting rate became faster, changed from 68m/Ma to 78m/Ma. During this time interval, i.e. Upper Eocene to Lower Oligocene, carbonate rock of about 229m thick was removed.
Eocene	Upper	The uplifting event continued with the same rate, i.e. about 68m/Ma, from the late Upper Cretaceous to the late Upper Eocene. Within this time range, the maximum thickness of rock being unroofed was about 3.67km.
Cretaceous	Upper	The rock was uplifted at a rate of 68m/Ma, and during this period it was emplaced at ~7.34 km depth. The onset of karstification in this period indicates that the maximum original thickness of the limestone was ~7.34km. About 88Ma, sediment unroofing was probably over, and the exposed limestone was subjected to karstification.
	Middle	The onset of karstification process did not occur in this period, as the original thickness of the carbonate rock was not 8km. At this age (97.5Ma), the granite (sample CH-6) was emplaced ~240°C, at about 8km depth.
	Lower	As uplifting of the granite continued, the simultaneous uncovering of overlying sediments was not deep enough to expose the limestone and the karstification process to commence.
Jurassic	Upper	A period characterized by dry conditions, and possibly with slower rate of granite uplifting which may have led to a similar rate of unearthing of sediments covering the limestone. Collision of Sibumasu with Indochina/East Malay block (Indosinian Orogeny).
	Middle	
	Lower	
Triassic	Upper	Granite intrusion, and possible sediment deposition on the limestone.
	Middle	
Permian	Upper	Marks the youngest age of the limestone deposition

4.2.3 Nature of subsurface karsts

Almost all subsurface karsts are originated in the surface except for hypogenic karsts (originated at depth without direct surface recharge), which constitute less than 5%. Thus, all subaerial conditions are considered responsible for the occurrence of paleokarst or subsurface karst, i.e. factors that characterise epigenic karsts (originated from direct surface recharge) can also be used to characterise subsurface karsts.

4.2.3.1 *Analogue from the Kinta Valley karst*

The mode of formation and development history of subaerial karst can be analogue to subsurface karst. Direct comparison may not always be possible; however, the Kinta Valley karst system is a good analogue to envisage the possible continuity of fracture traces in carbonate reservoirs, which might have undergone intensive subaerial karstification process. As a matter of fact, because of the intensive subaerial karstification process, positive paleokarst features may not appear in seismic section, and it can be difficult to infer the continuity of associated negative karst features and fracture traces. Nonetheless, such a problem can be addressed by comprehending the relation between structures and associated karst features in a matured karst system, such as the one in the Kinta Valley.

Despite the fact that a carbonate terrain is immensely intersected by fracturing, multiple channel development via the fractures may not occur, if one considers the Kinta Valley karst system as analogue. This is because, whenever fracture traces are interconnected, channels in the form of a loop (Fig. 4.8) or sinuous path (Fig. 4.14b) will take place, following the ease of solute attacks along the fractures. It has to be noted that, as the Kinta Valley karst features indicate, the convoluted and curvilinear passage morphologies may not always suggest the prime influence of fracturing. At times, similar conduit pattern can be controlled by bedding-plane partings or predominance of intergranular pores (Palmer, 1991) than being merely a consequence of the pre-existence of structures. Thus, it may be difficult to infer what controlled the development of similar patterns of subsurface karst features. However, according to Palmer (1991), solutionally enlarged joints and high-angle faults tend to produce

fissure-like passages with lenticular cross sections and angular intersections. But bedding-plane partings lead to the formation of branchwork or anastomotic pattern. Hence, it can be deduced that a good know-how of the origin and patterns of modern karst system may help to improve the interpretation of subsurface karst that may appear on seismic data.

The conduit diameter of karstic caves in the study area does not exceed 10 m and in many caves it is about 1.5-2.5 meters. Though most of the channels appear collapsed, forming various scales of chambers, there are also conduits that survived the collapse. The multi-layered Kandu cave (Fig. 4.8) is a prime example that illustrates collapsed and extant conduits. Coalesced collapsed paleocave reservoirs that may extend for hundreds of kilometres are believed to be formed from later burial and compaction process (Loucks, 1999); nonetheless, considering the fact that the average conduit diameter commonly is within the range of 2-3 meters and the distance between the channels is in the order of 10 m, the possibility of coalescence of channels after burial might be doubtful. At times, the possibility of occurrence of spongework patterns of solutional caves, and its resemblance with coalesced collapsed paleocave systems, needs to be taken into consideration in order to be able to alleviate the erroneous interpretation of these karst features.

Identifying the relation between karst channels and fractures is indispensable to understand the complexity of subsurface karst. In the Kinta Valley, the complex structures that characterize the carbonate rock are also visible at the micro fracture scale. This fracturing phenomenon will be more aggravated if the subaerial karst features are subjected to burial, further enhancing the interconnection between fracture traces, which may lead to the formation of good fracture reservoir. Therefore, understanding the complex fracturing phenomenon and the associated occurrence of karst features is an intrinsic part of acquiring information that can be crucial in the modeling of karst reservoirs. Considering the Kinta Valley karst system as an analogue, these information may include, (1) all fractures are not important in the ultimate fluid flow. The limestone hills in the study area are highly fractured but preferentially the karst development took place via the prominent fracture trend which, most likely, became open fracture, and this attests to the significance of such

fractures over others in the fracture network, (2) the karst features, for instance Figure 4.8 and Figure 4.14b, reflect the role of fractures connectivity in the ultimate development of the conduits. Thus, the morphology of the karstic caves, their distribution and alignment indicate a good intercommunication within the fracture network. In spite of that, the main cave passage morphology followed the prominent open fractures trend, making the other fractures tributaries to it, (3) the persistence of the fracture length is imprinted on the karst features, for instance Figure 4.1a and Figure 4.16a. These karsts clearly indicate the continuity of the fractures, and this in turn may imply that the karst features are not always the result of a high degree of fracturing. Therefore, it can be inferred that the persistence of open fractures characterised the Kinta Valley karst system, and this may suggest that open and persistent fractures are the ultimate pathways, despite the degree of fracturing.

The Kinta Valley karst system indicates that high degree of fracturing does not always result pervasive karstification, and this inference can be used to justify if previously interpreted subsurface karsts are authentic or not. For instance, Vahrenkamp (2004) interpreted the features observed in 3D seismic (Fig. 2.7a) as dendritic pattern karst network. This author elaborated that this karst network is closely related to faulting and associated fracturing of the rocks, and further indicated that it is best developed in tight and brittle unit. However, dendritic pattern karst network formation mainly marks the influence of primary porosity, not secondary porosity as Vahrenkamp (2004) indicated. Karstification in poorly lithified carbonate rocks results in dendritic pattern karst features, but in tight and brittle rock it is evident that linear or sinuous pattern karst channels are more prominent. The other doubt that one may pinpoint is the scale of the karst features shown in the 3D seismic and the chaotic reflection which was interpreted as collapsed cave (Fig. 2.7a); this cannot be analogues to modern or subaerial karst. Based on the knowledge of subaerial karst formation and development through time, it is ambiguous to classify those features in Figure 2.7a as karst networks. Thus, either these features are not karst network or their formation is not mainly controlled by secondary pores (fractures) unlike the inference drawn in Vahrenkamp (2004).

4.2.3.2 Analogue from tropical karst

Conduits which are formed by subaerial dissolutional processes may collapse after burial and form coalesced conduits. Because of the after-burial increase in area and volume of the pre-existing channels, isolated caves may end up forming longer and wider integrated cave systems. Nonetheless, there are exceptions that indicate coalesced karstic cave systems may not occur ensuing burial. Firstly, considering the fact that collapse of channels occurs when the width of the beam (passage width) is large enough and cannot support the weight on the ceiling, those conduits which have narrow width may survive breakdown after the karst system is subjected to burial. The presence of cave channels at a depth of -2191 m, Krubera (Voronja) cave (Fig. 4.55c), which is the deepest in the world (Klimchouk et al., 2009), is known and it is a clear indicator to the possible existence of uncollapsed cave systems at great depth. Hence, since most modern cave passages have narrow dimensions, it is possible to infer that the formation of coalesced channels, after burial, may not take place, and it can be difficult to take them as analogue for coalesced, collapsed paleocave systems.

Although the paleocave channels width and length may increase after the karst system has been subjected to burial, coalescence of the channels will not occur unless the initial distance (before burial) between the caverns is close enough to allow merging. In this case Gunung Lanno can be a good example to illustrate this condition. This hill (Fig. 4.29b), which is about 2.5 km long and hosts at least 32 caves as surveyed by Geyer et al. (2005), happens to be buried at great depth, the caves can collapse but because of the large distance among them, coalescence of all the caves may not happen. Similarly, the combined cave profile (Fig. 4.55c) clearly indicates the network of caves whose channel widths appear to be very small as compared to the distance between the different caves passages. Thus, as a result of the possible burial and compaction and associated dimensional increment, it cannot be expected that coalesced, collapsed cave systems will take place.

Secondly, merging of the various cave systems occurs during subaerial karstification process to form a single big chamber and large cave passage that can extend for hundreds of meter along and across the chamber. Such features are common in tropical karst, for instance in Malaysia, the Mulu and Deer caves

(Sarawak) and Tempurung cave (Ipoh), to mention a few, and in Vietnam, Son Doong cave (Hang Son Doong). Mulu cave is believed to have a dimension of 700 x 400 m and the Deer cave, which is the largest cave passage, can extend up to 100m width and 125m height in some place along the passage (Despain, 2005). For a kilometer of passage length, Deer cave has a general 100m width and height (Gunn, 2004). Although the Deer cave is still claimed to be the largest passage (Despain, 2005), the Son Doong cave is reported to have the largest cave passage whose dimensions reaches in some places up to 150m width and 200m height. Between the Deer cave and the Green cave there is a doline (Garden of Eden) (Fig. 4.55a) which is 800m wide, and the doline is believed to have grown as the stream sink has shifted its course (Gunn, 2004).

Furthermore, it is indicated in Gunn (2004) that although there is a debate over how much of the doline originated by the collapse of a cave passage or chamber, the concept of a single very large collapse becomes real when the doline's size is compared to the Sarawak Chamber. If the development of karst is controlled by fractures, for example Figure 4.30, wide channels may form as the diffuse flow ultimately drains via the prominent trend, where there will be less resistance to flow. This implies that there will be hardly any isolated cave passages development, as the fractures interconnect to form a principal passage (Fig. 4.14b). Thus, this can be the reason for the absence of another large passage caves in Tempurung Hill, despite the fact that it is shattered by fractures. The development of big chambers and large passage caves can be related to the intersection of a series of cave chambers, as a result of upward stopping, which takes place as denudation continues. This process can easily be illustrated if one considers the overall morphology of the Tempurung cave flow pattern of the river that moves underneath this cave. The Tempurung Hill which is highly affected by fracturing might have contributed to the formation of small chambers along the cave passage, which ultimately merged to form big chambers. Similarly, it is also documented in Gunn (2004) that there is evidence of wall scallops in the Green Cave which indicates stream flow through it at one stage, but the gradual lowering and shifting of flow path resulted in the ultimate formation of big chambers that might have led to later collapse and formation of a doline.

Attempts have been made by some workers to quantify the possible increment in the dimensions of subaerial karst features after they are subjected to burial. Thus, by considering the existing dimensions of the large cave passages found in tropical karst regions, one can easily draw an inference of what the dimensions would be for paleocaves. For example, for a presumed 8m diameter of an initial channel width, if the porosity, after burial, goes to 10%, according to Loucks (1999) simple mathematical approach, the diameter of the collapsed channel will be at least 300% higher, i.e. 25.3m. Based on the same simple mathematical approach used by Klimchouk and Andrejchuk (2005) and Ford and Williams (2007) and reference therein, considering that 8m as the initial height from the floor to the ceiling of the uncollapsed channel, the new height after collapse may reach up to 80m. Hence, based on these approaches, the width of the Mulu cave chamber, which is believed to have a diameter of 300-400m, may be able to reach up to 1000m, if subjected to burial. The Garden of Eden doline (Fig. 4.55a), which is presumed to be part of the large passage cave, appears to have a diameter of about 800 m, and it is likely to have resulted from the collapse of a big chamber that may be comparable to the Mulu cave chamber. Similarly, the width of Tempurung Cave and the largest passage caves can be presumed to have up to 400% dimension increment if they are subjected to burial. Such basic assumptions indicate that coalescence of collapsed paleocave systems may not necessarily take place during burial, rather the merging of the various cave chambers occur during subaerial karstification process.

Therefore, further emphasis has to be given to the importance of subaerial karst development and the scale of karst features in order to comprehend the complexity of subsurface karst which further helps to understand how such processes lead to the formation of heterogeneous karst reservoirs that may be thousands of meters long, and hundreds of meters across. Although the subsurface coalescence of narrow passage paleocave systems is not ruled out, it is stressed that more consideration needs to be given to the subaerial karstification process that produces large cave passages and to their evolution during deep burial.

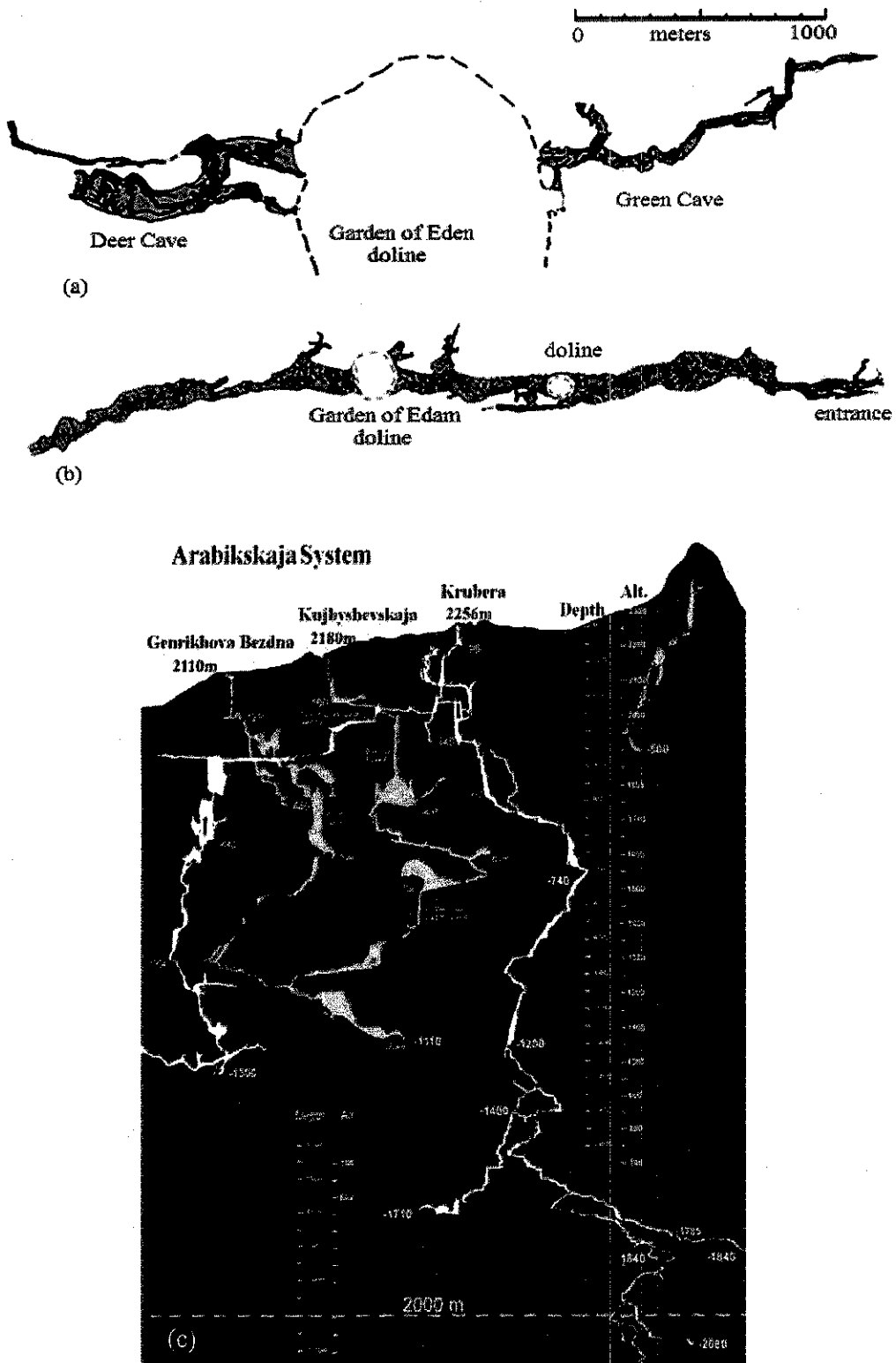


Figure 4.55: Profile of the largest sections of cave passage in the world (a) Caves of southern Mulu, Sarawak, (b) Hang Son Doong, Vietnam (both caves drawn at the same scale) (<http://www.mulucaves.org>), and (c) Combined caves system profile along the axis of the Ortobalagan valley (Klimchouk et al., 2009).

- Cave facies

It is documented in many works that the heterogeneity of karst reservoirs, which is characterised by the irregular distribution of porous zones and the complex nature of pore systems in karsted strata (Chilingarian et al., 1996), arises as a result of burial process. Such burial, compaction and diagenesis, which followed near-surface karst processes, is considered to be the reason for the complex histories of formation of paleocave hydrocarbon reservoirs (Loucks, 1999), since, according to Loucks, the pore network consists of karst-related cavernous porosity and/or of cave-collapse-related interclast and fracture porosity. Although it is believed that the pore network is not related to the collapse of single caverns, but rather to the coalescing of collapsed caverns within a cave system, the tropical karst regions give evidence that prove otherwise. Those typical large passage caves are good analogues for any paleokarst that can be considered as karst reservoirs.

The largest passage caves that are found in tropical areas are commonly typified by extensive development of speleothems. For instance in Gunung Tempurung, flowstones which are tens of meters long and high are common, and similar dimensions of speleothems are evident in different parts of the tropical karst regions. If the largest passage caves happen to be buried, it is inevitable that different cave facies will form. According to Loucks (1999), there are six types of cave facies in a paleocave system, i.e. undisturbed strata facies, disturbed strata facies, highly disturbed strata facies, fine-clast chaotic breccia facies, coarse-clast chaotic breccia facies, and sediment-fill facies (Fig. 4.56a); nonetheless, considering the immense speleothem deposits that characterize large tropical passage caves, for instance Figure 4.56b, this study suggests the incorporation of the seventh type of cave facies, i.e. massive to slightly fractured speleothems. Incorporating the possible existence of such facies may enable to comprehend the degree of karst reservoirs heterogeneity.

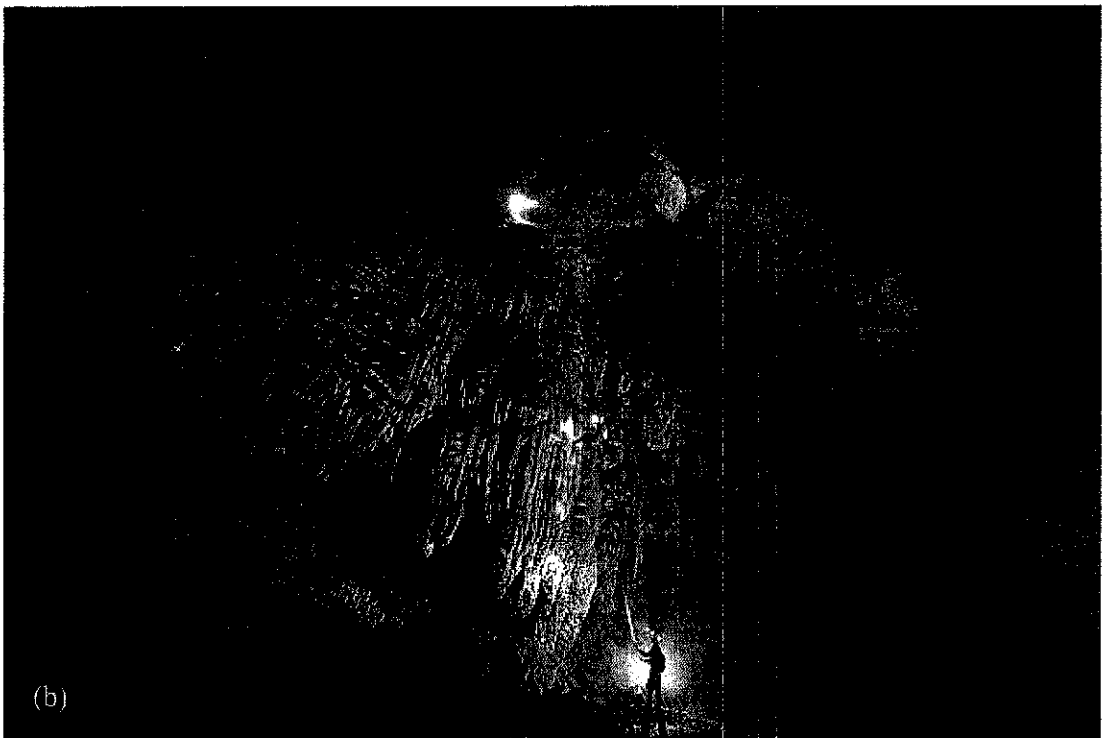
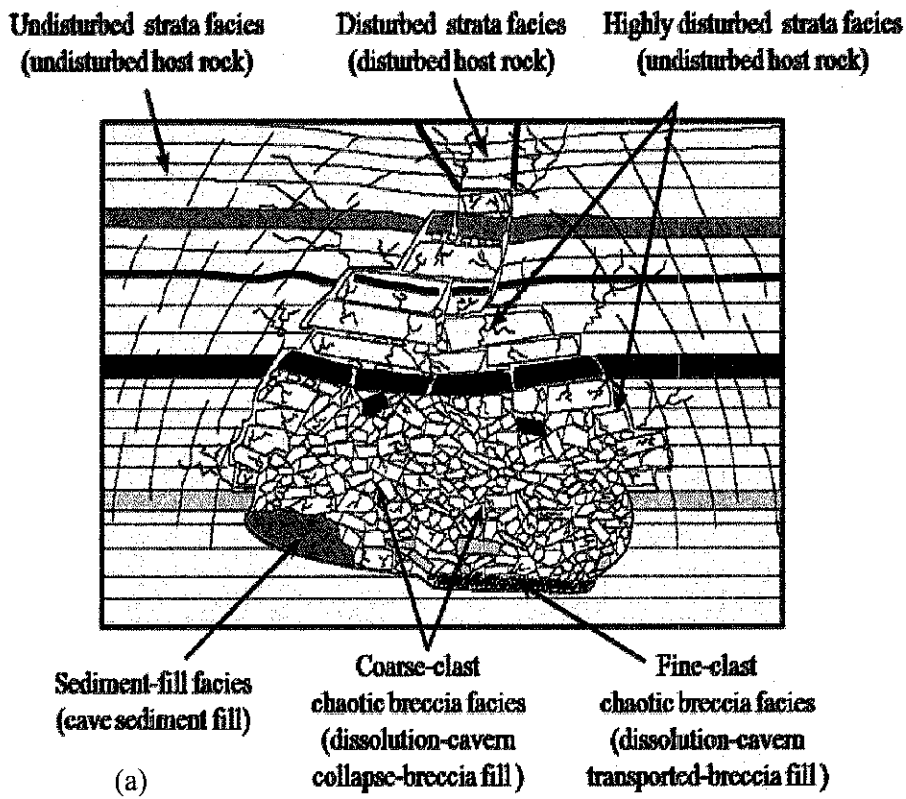


Figure 4.56: Shows (a) Paleocave facies classification (Loucks et al., 2004), and

(b) Extremely large speleothem deposit in Hang Son Cave

<http://www.messagetoeagle.com/worldslargestcave.php>

CHAPTER 5

CONCLUSIONS AND RECOMMENDATIONS

5.1 Conclusion

The Kinta Valley is characterized by remnant limestone hills which cover about 2.5% of the valley area. These limestone hills are typified by various karst features including, caves, sinkholes, dolines, and tower karsts. Although there is a lack of detailed study on the development of karst system in the area, a number of hypotheses have been suggested by previous workers for the possible occurrence of the limestone hills and associated karst features, which include, the influence of sea-level rise, block faulting, subaerial erosion, folding, and **local ponding behind mudflow deposits** (Ingham and Bradford, 1960 and references therein; Paton, 1964; Gillieson, 2005). Nonetheless, prominent factors including fractures, lithology, and uplift events which are responsible for the origin and development of karst system in the Kinta Valley have received little attention.

Once carbonate rocks are exposed to the surface, karstification process commences via weak zones, i.e. fractures or bedding planes. There are evidence of karst formation in the area along bedding planes; however, fracture appears to be the prominent factor that controlled the development of the karst features. In order to unravel the influence of fractures, lineament analyses have been undertaken from the remnant limestone hills using Spot image of 2.5 m resolution. Similarly, the karstic caves inside the vestige limestone hills were surveyed and mapped based on standard techniques.

Six trends of lineaments were extracted from the remnant hills and their prominent orientation appears to strike in a NNW-SSE trend. This orientation is also found to be the principal trend of the caves passage as obtained from the individual

caves situated all over the valley. It is inferred that such similarity clearly indicates the formation of the caves to be mainly controlled by the geological structures. The fault striking NNW-SSE is considered to be the first structure to affect the originally expansive limestone bedrock and karstification in the area is believed to have commenced and intensified after its formation, but was further influenced by the later structures that were superimposed on it. Besides the similarity of the main caves passage orientation and the prominent fractures trend, observed cross cutting relationship of fractures plainly illustrate the pre-existence of the NNW-SSE trending faults. This further substantiates the inference drawn for the main NNW-SSE faults to be the oldest and the most likely conduits for the onset of karstification. The effect of multi-fracturing made the Kinta Valley to be structurally complex, and this is evidenced by the karst features, such as circular caves passage morphology (for example in Gua Kandu) and sinuous cave passages (in the case of caves in Gunung Tempurung), which developed following fractures oriented in different directions.

The karst features morphology appears to be the imprint of the fractures trend; however, the nature of the carbonate rocks also played a significant role in the occurrence of the extant karst morphology. The crystalline nature of the carbonate rock in the Kinta Valley enabled the development of linear, circular, and convoluted karstic caves passages. If the crystalline rock was not hard enough, spongework and branchwork patterns of passages could have been formed, which in turn may allow a faster collapse and removal of the bed rock. Thus, the crystalline nature of the carbonate rock in the Kinta Valley played a role in lowering the denudation rate, otherwise the vestige carbonate rock may not have existed.

Since the amount of precipitation is an important factor for both allogenic and authogenic denudation processes, periods which were marked by dry and wet spells could have played a role in the karstification process. Hence, those periods indicated in previous works as prevalent dry conditions were associated with possibly lower denudation rate or karstification process. Although sea-level fluctuations can influence the development of karst, the geographic location of the Kinta Valley and the continuous uplifting episodes in the area made the Cenozoic sea-level variations less responsible for the origin and evolution of karst in the Kinta Valley.

The gradual development of the karst system in the area of interest is attributed, among other factors, to the uplifting phenomenon which has been taking place through time. In order to characterize this phenomenon, samples were collected from the granite adjoining the limestone at the foot of the Cameron Highlands. The apatite and zircon fission-track ages obtained from these samples allowed the cooling and uplifting episodes to be characterized. The fission-tracks appear to be archives for the variable uplifting rates in the area, from Middle Cretaceous to Late Miocene. From Mid Cretaceous to Late Eocene the uplift rate was 68m/Ma; this rate increased to 78m/Ma during the Late Eocene to Early Oligocene period, but the Early Oligocene to Late Miocene period is marked by the slowest uplift rate, which is 6m/Ma. After the Late Miocene the uplifting rate is not quantified by the apatite fission-tracks, but possibly a faster uplifting episode resumed after this period. It is quite evident that the uplifting history has not been constant, and this variable episode is marked by the karst features in the Kinta Valley. Since base-level lowering rate is equal to or less than uplift rate, the morphology of multiple notches reflected the variable uplift rate which is documented by the fission-tracks. Similarly, the extant multi-level cave passages also attest to the influence of uplifting in their gradual development. Hence, the uplift rate variation in the Kinta Valley likely had an immense impact on the evolution of karst system in the area.

Considering the variable uplift rate, the average long-term denudation rate is estimated to be 50.6m/Ma. This rate is within the acceptable range of modern measurements undertaken in various karst systems. Similarly, using the fission-track ages, the maximum thickness of the original carbonate rock is estimated to be 7.34km, which is also within the range of contemporaneous deposits and previous estimates. The Upper Cretaceous period marks the commencement of karstification in the Kinta Valley; nonetheless, the intensive karstification process most likely occurred after the Upper Eocene period. Most of the carbonate rock appears to have been removed after the Late Miocene, and this further substantiates the authenticity of the assumptions taken to estimate the long-term denudation rate and the thickness of the carbonate rock. This is owing to the fact that the rate of karst denudation increases as the duration of the karstification process increases.

When subaerial karsts are subjected to burial, commonly they form collapsed paleokarsts, which possibly produce paleokarst reservoirs. The only means of understanding the existence of subsurface karsts is via indirect evidence, such as high drilling speed, core and seismic data. However, these data do not provide detailed information about the nature of subsurface karsts. In order to comprehend and better interpret the nature of subsurface karsts or paleokarsts inferred from indirect data, it is immensely crucial to have a good understanding of how subaerial karsts develop over time, what factors control their evolution, and what morphology they display ensuing the prominent factor responsible for their formation. Thus, understanding the geometry of modern karst system is the base to unravel the origin, complexity, and burial evolution of subsurface paleokarst system. Similarly, it can also enable to visualize the possible geometry and scale of paleokarst features, which in turn may strengthen the interpretations to be made from indirect evidence. Although subsurface karst features consistent with the scale and dimensions of modern karst can be inferred, a direct correlation or comparison is not always possible. In spite of that, the matured karst system in the Kinta Valley is considered as a good analogue to envisage the continuity of fracture traces in carbonate reservoirs, which might have undergone intensive subaerial karstification process, as evidenced by the integrated approach of lineament analysis and cave surveying.

Karst is a distinctive landform that results from the dissolution of carbonate rocks, and the dissolutional process is considered to be an important geologic phenomenon that may lead to the formation of karst reservoirs. The process of burial, compaction and diagenesis is believed to transform subaerial multiple karst caves into coalesced collapsed paleocave systems, but it is suggested that large passage caves of tropical karst regions can be evidence for the existence of large scale collapsed single cavern. In order to comprehend the mechanism of formation and dimensional increment after burial, in addition to the surveyed and mapped caves in the Kinta Valley, the largest passage caves in the world were taken into consideration. Then, it is inferred that, it is not only the deep burial of paleocave systems that will result in the formation of interconnected fractures and coalesced breccias, such phenomenon can be manifested if large cave passages are subjected to burial. Moreover, because of the presence of immense speleothem deposits that typify tropical karst areas, it is suggested that

additional cave facies, i.e. massive to slightly fractured speleothems, be included in the pre-existing paleocave facies classification.

5.2 Recommendations

As far as karst denudation in the Kinta Valley is concerned, further work can be done, using other methods, to identify the long-term denudation rate, particularly after the Late Miocene period. One of the methods can be cosmogenic radio-nucleides, such as ^{10}Be and ^{26}Al , which serve as chronometer to date the exposure age of sediments. If sediments are deposited at various levels of karstic cave passages, by dating the sediments using cosmogenic radio-nucleides, it is possible to pinpoint the possible down cutting rate of the carbonate rock.

Further work can be carried out using (U-Th)/He thrmochronometer in apatite to reconstruct the thermal history of rock samples in the uppermost crust, probably less than three kilometers thick, which may allow the quantification of the uplifting rate after the Lower Miocene. This approach may help to double check the results obtained in this study using the apatite and zircon fission-track data. Moreover, it may help to indicate the pros and cons of different approaches in estimating the rate of long-term carbonate rock loss from the area. This may further strengthen the inference made about the original thickness of the carbonate rock in the Kinta Valley.

The apatite and zircon fission-track data clearly indicated the variation of the uplift rate in the Kinta valley. The increase of this rate until the Upper Eocene and its subsequent decrease can be related to the northward drifting of the Indian plate, which passed by the Peninsular Malaysia landmass around the Upper Eocene period, before making its ultimate collision with the Euroasian landmass. Further work, in other places, can be done using fission-tracks to compare the uplifting rate variation with the result documented in the Kinta Valley, and to identify the possible link with the northward drifting of the Indian plate.

5.3 Contributions

The outcome of this study and its contribution to knowledge include:

a) Integrated approach of satellite imagery and karstic cave survey data

This study has shown the link between lineaments extracted from satellite image and karstic cave mapping that unravels the prominent influence of secondary porosity (fractures) other than primary porosity for the development of karst features. This approach has also indicated the possible continuity of discrete entity fracture traces, further pinpointing the impact of regional structures to be responsible for the ultimate formation of karst in the area. This outcome suggests the possibility of inferring similar subsurface karst features, local or regional, where the subaerial karsts are characterized by such phenomenon.

b) Use of fission-track ages to estimate the long-term rate of carbonate rock loss

The contact type of the Kinta Valley karst system created a good opportunity to indicate the gradual development of karst. Furthermore, the application of fission-track ages provided an indirect means of estimating the original thickness of the carbonate rock and long-term denudation rate, which add up to the previously exercised approach, particularly for long-term denudation rate estimation. The method employed to estimate the original thickness of the carbonate rock opens the chance to promote the importance of this approach.

c) Karstic cave maps

The various karstic cave maps produced in this work have great importance in highlighting the relation between the carbonate rock and the continuity or network of fractures. This enables to advance the understanding of the diverse nature of the Malaysian karst, in particular, and the tropical karst system, in general. In turn, this provides further knowledge to other disciplines, which may study the subsurface karst hydrology or possible existence of channels in karst terrain.

REFERENCES

- Abdullah, N.T., 2009. Mesozoic Stratigraphy. In: Hutchison, C.S., Tan, D.N.K. (Eds.), *Geology of Peninsular Malaysia*. Geological Society of Malaysia, pp. 87-131.
- Auler, A.S., 1998. Base-Level Changes Inferred from Cave Paleoflow Analysis in the Lagoa Santa Karst, Brazil. *Journal of Caves and Karst Studies* 60, 58-62.
- Bakalowicz, M., 2006. Importance of regional study site conditions in elaborating concepts and approaches in karst science. *Special papers Geological Society of America* 404, 15.
- Batchelor, B., 1979. Discontinuously rising late Cainozoic eustatic sea-levels, with special reference to Sundaland. *Southeast Asia. Geologie en Mijnbouw* 58, 1-20.
- Benjamin, M.T., Johnson, N.M., Naeser, C.W., 1987. Recent rapid uplift in the Bolivian Andes: Evidence from fission-track dating. *Geology* 15, 680-683.
- Bhatt, N., Bhonde, U., 2006. Geomorphic expression of late Quaternary sea level changes along the southern Saurashtra coast, western India. *Journal of earth system science* 115, 395-402.
- Bosák, P., 2008. Karst processes and time. *Geologos* 14, 15-36.
- Bosák, P., Ford, D., Glazek, J., Horacek, I., 1989. *Paleokarst: a systematic and regional review*. Elsevier and Academia, Amsterdam, p. 725.
- Braun, J., Van Der Beek, P., Batt, G., 2006. *Quantitative thermochronology: numerical methods for the interpretation of thermochronological data*. Cambridge University Press, p. 258.
- Castillo, M.V., Mann, P., 2006. Cretaceous to Holocene structural and stratigraphic development in south Lake Maracaibo, Venezuela, inferred from well and three-dimensional seismic data. *AAPG bulletin* 90, 529-565.
- Chilingarian, G.V., Rieke, H.H., Mazzullo, S.J., 1996. Introduction. In: Chilingarian, G.V., Mazzullo, S.J., Rieke, H.H. (Eds.), *Carbonate reservoir characterisation: a geologic-engineering analysis, part II*. Elsevier Science B.V., pp. 1-57.
- Cobbing, E., 1992. The granites of the South-East Asian tin belt. *British Geological Survey Overseas Memoir London*, p. 369.

- Copeland, P., Mark Harrison, T., Kidd, W., Ronghua, X., Yuquan, Z., 1987. Rapid early Miocene acceleration of uplift in the Gangdese Belt, Xizang (southern Tibet), and its bearing on accommodation mechanisms of the India-Asia collision. *Earth and Planetary Science Letters* 86, 240-252.
- Coventry, R., Hopley, D., Campbell, J., Douglas, I., Harvey, N., Kershaw, A., Oliver, J., Phipps, C., Pye, K., 1980. The quaternary of northeastern Australia, *The Geology and Geophysics of North Eastern Australia*. Geological Society of Australia, Brisbane, pp. 365-417.
- Crowther, J., 1989. Groundwater Chemistry and Cation Budget of Tropical Karst Outcrops, Peninsular Malaysia, I. Calcium and Magnesium. *Journal of Hydrology* 107, 169-192.
- Curl, R.L., 1974. Deducing flow velocity in cave conduits from scallops. *National Speleological Society Bulletin* 36, 1-5.
- Daoxian, Y., 1981. A Brief Introduction to China's Research in Karst, Guilin, People's Republic of China, Inst. of Karst Geology, Ministry of Geol. and Min. Resources, p. 14.
- Deike, G., 1989. Fracture controls on conduit development. In: White, W.B., White, E.L. (Eds.), *Karst Hydrology: Concepts from the Mammoth Cave Area* Van Nostrand Reinhold, New York, pp. 259-291.
- Deike, R.G., 1969. Relations of jointing to orientation of solution cavities in limestones of central Pennsylvania. *American Journal of Science* 267, 1230-1248.
- Despain, J., 2005. Mulu Caves, Malaysia, in: Culver, D.C., White, W.B. (Eds.), *Encyclopedia of Caves*. Elsevier Academic Press, pp. 400-403.
- ERDAS, 1999. *Erdas Field Guide*. Erdas Inc., Atlanta, Georgia, p. 671.
- Evans, M.W., Snyder, S.W., Hine, A.C., 1994. High-resolution seismic expression of karst evolution within the upper Floridan aquifer system: Crooked Lake, Polk County, Florida. *Journal of Sedimentary Research* 64, 232-244.
- Faulkner, T., 2006. Tectonic inception in Caledonide marbles. *Acta Carsologica* 35, 7-21.
- Feazel, C.T., 2009. Using Modern Cave Systems as Analogs for Paleokarst Reservoirs. AAPG International Conference, Cancun, Mexico.

- Fleurant, C., Tucker, G., Viles, H., 2008. Modelling cockpit karst landforms. Geological Society, London, Special Publications 296, 47-62.
- Florea, L.J., 2002. Detection of Iapetan Rifting (Rome Trough Tectonism) by Quaternary Karstification: Pulaski County, Kentucky, in: Martin, J., Wicks, C., Sasowsky, I. (Eds.), *Karst frontiers. Karst Waters Institute* pp. 192-204.
- Ford, D.C., 2003. Perspectives in karst hydrogeology and cavern genesis. *Speleogenesis and Evolution of Karst Aquifers*, 1-12.
- Ford, D.C., Palmer, A.N., White, W.B., 1988. Landform development; karst. Geological Society of America, p. 401-412.
- Ford, D.C., Williams, P., 2007. *Karst hydrogeology and geomorphology*. Wiley, p. 562.
- Frakes, L., Francis, J., Syktus, J., 1992. *Climate Modes of the Phanerozoic* Cambridge Univ. Press, Cambridge, p. 274.
- Frumkin, A., Fischhendler, I., 2005. Morphometry and distribution of isolated caves as a guide for phreatic and confined paleohydrological conditions. *Geomorphology* 67, 457-471.
- Gabrovšek, F., 2007. On denudation rates in Karst. *Acta carsologica* 36, 7-13.
- Gabrovšek, F., Dreybrodt, W., 2010. Karstification in unconfined limestone aquifers by mixing of phreatic water with surface water from a local input: A model. *Journal of Hydrology* 386, 130-141.
- Galbraith, R.F., 2005. *Statistics for fission track analysis*. Chapman & Hall/CRC, p. 219.
- Gallagher, K., Brown, R., Johnson, C., 1998. Fission track analysis and its applications to geological problems. *Annual Review of Earth and Planetary Sciences* 26, 519-572.
- Gao, J., 2008. *Digital analysis of remotely sensed imagery*. McGraw-Hill Professional, p. 645.
- Gatinsky, Y.G., Hutchison, C.S., 1987. Cathaysia, Gondwanaland and the Paleotethys in the evolution of continental Southeast Asia. *Geological Society of Malaysia Bulletin* 20, 179-199.
- Geyer, E., Schmidt, F., Jeutter, P.W., 2005. *Speleological Expedition Gunung Lanno*. Verein für Höhlenkunde in Obersteier, p. 240.

- Ghani, A.A., 2009. Plutonism. In: Hutchison, C.S., Tan, D.N.K. (Eds.), *Geology of Peninsular Malaysia*. Geological Society of Malaysia, pp. 211-232.
- Gillieson, D., 2005. Karst in Southeast Asia. In: Gupta, A. (Ed.), *The Physical Geography of Southeast Asia*. Oxford University Press, pp. 157-176.
- Gillieson, D.S., 1996. *Caves: processes, development and management*. Blackwell Publishers Oxford, p. 324.
- Glazek, J., 1989. Tectonic conditions for karst origin and preservation. Paleokarst a systematic and regional review, *Academia*, 569-576.
- Gobbett, D., 1971. Joint pattern and faulting in Kinta, West Malaysia. *Bulletin of the Geological Society of Malaysia* 4, 39-47.
- Goodchild, M., Ford, D., 1971. Analysis of scallop patterns by simulation under controlled conditions. *The Journal of Geology*, 52-62.
- Guangzhong, G., Haoran, Y., Yuanfeng, Z., Xingrui, H., 1985. Rapid flow of karst groundwater system in China, *Karst Water Resources (Proceedings of the Ankara - Antalya Symposium)*. IAHS Publ., pp. 619-632.
- Gunn, J., 1981. Limestone solution rates and processes in the Waitomo district, New Zealand. *Earth Surface Processes and Landforms* 6, 427-445.
- Gunn, J., 2004. *Encyclopedia of karst and caves*. Fitzroy Dearborn, Chicago and London, PA.
- Hall, R., Morley, C.K., 2004. Sundaland basins. *Geophysical Monograph Series* 149, 55-85.
- Haq, B.U., Hardenbol, J., Vail, P.R., 1987. Chronology of fluctuating sea levels since the Triassic. *Science* 235, 1156-1167.
- Harrington, G.J., Kemp, S.J., Koch, P.L., 2004. Palaeocene–Eocene paratropical floral change in North America: responses to climate change and plant immigration. *Journal of the Geological Society* 161, 173-184.
- Häuselmann, P., 2008. Surface corrosion of an Alpine karren field: recent measures at Innerbergli (Siebenhengste, Switzerland). *International Journal of Speleology* 37, 107-111.
- Häuselmann, P., 2011. UIS Mapping Grades. *International Journal of Speleology*, IV-VI.

- Henderson, D.B., Ferrill, D.A., Clarke, K., 1996. Mapping geological faults using image processing techniques applied to hill-shaded digital elevation models, *Proceedings of the IEEE Southwest Symposium IEEE*, pp. 240-245.
- Hill, C.A., 2000. Overview of the geologic history of cave development in the Guadalupe Mountains, New Mexico. *Journal of Cave and Karst Studies* 62, 60-71.
- Hurford, A.J., 1986. Cooling and uplift patterns in the Lepontine Alps South Central Switzerland and an age of vertical movement on the Insubric fault line. *Contributions to mineralogy and petrology* 92, 413-427.
- Hutchison, C.S., 2005. The Geological Framework. In: Gupta, A. (Ed.), *The Physical Geography of Southeast Asia*. Oxford University Press, pp. 1-23.
- Hutchison, C.S., 2007. Geological Evolution of South-East Asia. *Geological Society of Malaysia*, p. 433.
- Hutchison, C.S., 2009. Tectonic Evolution. In: Hutchison, C.S., Tan, D.N.K. (Eds.), *Geology of Peninsular Malaysia*. Geological Society of Malaysia, pp. 309-330.
- Ingham, F.T., Bradford, E.F., 1960. The geology and mineral resources of the Kinta Valley, Perak. *Federation of Malaya, Geological Survey*, p. 347.
- Jameson, R.A., 2006. Identification and analysis of early flow paths in branchwork caves in West Virginia, USA. *Geological Society of America, Special Paper* 404, 23-30.
- Kassa, S., Pierson, B., Chow, W.S., Ab Talib, J., 2011. Identifying the link between lineament and cave passage trends to comprehend fractures continuity and influence on the Kinta Valley karst system, Peninsular Malaysia. *International Journal of Speleology* 41, 59-73.
- Kerans, C., 1988. Karst-controlled reservoir heterogeneity in Ellenburger Group carbonates of west Texa. *AAPG Bulletin* 72, 1160-1183.
- Kershaw, S., Guo, L., 2001. Marine notches in coastal cliffs: indicators of relative sea-level change, Perachora Peninsula, central Greece. *Marine Geology* 179, 213-228.

- Ketcham, R.A., 2005. Forward and inverse modeling of low-temperature thermochronometry data. *Reviews in Mineralogy and Geochemistry* 58, 275-314.
- Ketcham, R.A., Donelick, R.A., Balestrieri, M.L., Zattin, M., 2009. Reproducibility of apatite fission-track length data and thermal history reconstruction. *Earth and Planetary Science Letters* 284, 504-515.
- Klimchouk, A., 2009. Morphogenesis of hypogenic caves. *Geomorphology* 106, 100-117.
- Klimchouk, A., Andrejchuk, V., 2005. Karst breakdown mechanisms from observations in the gypsum caves of the Western Ukraine: implications for subsidence hazard assessment. *Environmental Geology* 48, 336-359.
- Klimchouk, A., Samokhin, G., Kasian, Y., 2009. The deepest cave in the world in the Arabika massif (Western Caucasus) and its hydrogeological and paleogeographic significance, 15th International Congress of Speleology, , Kerrville, TX, pp. 898-905.
- Koike, K., Nagano, S., Kawaba, K., 1998. Construction and analysis of interpreted fracture planes through combination of satellite-image derived lineaments and digital elevation model data. *Computers & Geosciences* 24, 573-583.
- Krähenbuhl, R., 1991. Magmatism, tin mineralization and tectonics of the Main Range, Malaysian Peninsula: consequences for the plate tectonic model of Southeast Asia based on Rb-Sr, K-Ar and Fission track data. *Geological Society of Malaysia Bulletin* 29, 1-100.
- Lauritzen, S.E., 2001. Marble stripe karst of the Scandinavian Caledonides: An end-member in the contact karst spectrum. *Acta Carsologica* 30, 47-79.
- Leech, D., Corresponding, P.J.T., Lucas, N., Grocott, J., 2003. Landsat TM analysis of fracture patterns: a case study from the Coastal Cordillera of northern Chile. *International Journal of Remote Sensing* 24, 3709-3726.
- Lillesand, T.M., Kiefer, R.W., Chipman, J.W., 2004. Remote sensing and image interpretation. John Wiley & Sons Ltd, p. 756.
- Lisker, F., Ventura, B., Glasmacher, U., 2009. Apatite thermochronology in modern geology. Geological Society, London, Special Publications 324, 1-23.

- Loucks, R.G., 1999. Paleocave carbonate reservoirs: origins, burial-depth modifications, spatial complexity, and reservoir implications. *AAPG Bulletin* 83, 1795-1834.
- Loucks, R.G., 2007. A review of coalesced, collapsed-paleocave systems and associated suprastratal deformation. *Acta Carsologica* 36, 121-132.
- Loucks, R.G., Mescher, P.K., McMechan, G.A., 2004. Three-dimensional architecture of a coalesced, collapsed-paleocave system in the Lower Ordovician Ellenburger Group, central Texas. *AAPG Bulletin* 88, 545-564.
- Lowe, D.J., 1999. Why and how are caves "organized": does the past offer a key to the present. *Acta Carsologica* 28, 121-144.
- Luo, C., Xue, F., Miao, Q., Yang, P., 2012. Seismic imaging and interpretation of paleo-cave systems in karstified carbonate reservoirs of Tarim Basin. *Warta Geologi* 38, 95-97.
- Madon, M.B.H., 1999. Plate Tectonic Elements and Evolution of Southeast Asia. In: PETRONAS (Ed.), *The Petroleum Geology and Resources of Malaysia*. The Petrolia Nasional Berhad (Petronas), Kuala Lumpur, pp. 59-76.
- Marco, F., Pierre-Yves, J., 2008. What makes a bedding plane favourable to karstification?—The role of the primary rock permeability, 4th European Speleological Congress, Vercors, pp. 32-37.
- Mazzullo, S., Chilingarian, G., 1996. Hydrocarbon reservoirs in karsted carbonate rocks. *Developments in Petroleum Science* 44, 797-865.
- McDonnell, A., Loucks, R.G., Dooley, T., 2007. Quantifying the origin and geometry of circular sag structures in northern Fort Worth Basin, Texas: Paleocave collapse, pull-apart fault systems, or hydrothermal alteration? *AAPG Bulletin* 91, 1295-1318.
- McInerney, F.A., Wing, S.L., 2011. The Paleocene-Eocene thermal maximum: A perturbation of carbon cycle, climate, and biosphere with implications for the future. *Annual Review of Earth and Planetary Sciences* 39, 489-516.
- McMechan, G.A., Loucks, R.G., Mescher, P., Zeng, X., 2002. Characterization of a coalesced, collapsed paleocave reservoir analog using GPR and well-core data. *Geophysics* 67, 1148-1158.

- Metcalf, I., 1996. Pre-Cretaceous evolution of SE Asian terranes. Geological Society, London, Special Publications 106, 97-122.
- Metcalf, I., 1998. Palaeozoic and Mesozoic geological evolution of the SE Asian region: multidisciplinary constraints and implications for biogeography. *Biogeography and geological evolution of SE Asia*, 25-41.
- Metcalf, I., 2000. The Bentong–Raub Suture Zone. *Journal of Asian Earth Sciences* 18, 691-712.
- Metcalf, I., 2002. Permian tectonic framework and palaeogeography of SE Asia. *Journal of Asian Earth Sciences* 20, 551-566.
- Morley, R.J., 1998. Palynological evidence for Tertiary plant dispersals in the SE Asia region in relation to plate tectonics and climate. In: Hall, R., Holloway, J.D. (Eds.), *Biogeography and Geological Evolution of SE Asia*. Backbuys Publishers, Leiden, The Netherlands, pp. 211-234.
- Morley, R.J., 2007. Cretaceous and Tertiary climate change and the past distribution of megathermal rainforest. In: Bush, M.B., Flenley, J.R. (Eds.), *Tropical Rainforest Responses to Climate Change*. Praxis Publishing Ltd, p. 396.
- Muhammad, R.F., 2006. Six-year Record of Rate of Limestone Dissolution at Three Sites in Gunung Rapat, Kinta Valley, Perak, Malaysia. *Geological Society of Malaysia Bulletin* 52, 103-107.
- Muhammad, R.F., Djin, T.H., 2003. The morphostructures of Kinta Valley karst, Annual Geological Conference. Geological Society of Malaysia, pp. 319-328.
- Myroie J.E. and Myroie, J.R., 2009. Caves as sea level and uplift indicators, Kangaroo Island, South Australia. *Journal of Cave and Karst studies* 71, 32-47.
- Myroie, J.E., Carew, J.L., 2003. Karst development on carbonate islands. *Speleogenesis and Evolution of Karst Aquifers* 1, 1-21.
- Nama, E.E., 2004. Lineament detection on Mount Cameroon during the 1999 volcanic eruptions using Landsat ETM. *International Journal of Remote Sensing*, 501-510.
- Odling, N., Gillespie, P., Bourguin, B., Castaing, C., Chiles, J., Christensen, N., Fillion, E., Genter, A., Olsen, C., Thrane, L., 1999. Variations in fracture

- system geometry and their implications for fluid flow in fractures hydrocarbon reservoirs. *Petroleum Geoscience* 5, 373-384.
- Osborne, R., 2002. Cave breakdown by vadose weathering. *Int. Jour. Spel* 31, 37-53.
- Palmer, A.N., 1975. The origin of maze caves. *National Speleological Society Bulletin* 37, 56-76.
- Palmer, A.N., 1991. Origin and morphology of limestone caves. *Geological Society of America Bulletin* 103, 1-21.
- Palmer, A.N., 2007. Variation in rates of karst processes. *Acta Carsologica* 36, 15-24.
- Paton, J., 1964. The origin of the limestone hills of Malaya. *Journal of Tropical Geography* 18, 134-147.
- Peng, L.C., 2009. Paleozoic Stratigraphy. In: Hutchison C.S. and Tan D.N.K. (Eds), *Geology of Peninsular Malaysia*. Geological Society of Malaysia. pp. 55-86.
- Pérez-Arlucea, M., Carter, A., Clemente, F., González, D., Nombela, M., 2005. Multi-approach, long and short term denudation rate calculations for the Galician Coast (Ría de Vigo, Spain): AFTD, DEM analysis, river loads and sediment budgets. *Journal of Coastal Research*, 9-14.
- Pierson, B.J., Askury, A.K., Chow, W.S., Zuhar, Z.T.H., 2009. The Limestone hills of the Kinta Valley: a part of Malaysian's geological heritage worth preserving. *EAGE*, 97-100.
- Plan, L., 2005. Factors controlling carbonate dissolution rates quantified in a field test in the Austrian alps. *Geomorphology* 68, 201-212.
- Rafferty, J.P., 2011. *Climate and Climate Change: the living earth*. Britannica Educational Publishing, p. 345.
- Raj, J.K., 2009. Geomorphology. In: Hutchison, C.S., Tan, D.N.K. (Eds.), *Geology of Peninsular Malaysia*. Geological Society of Malaysia, pp. 5-29.
- Reeder, P., Brinkmann, R., Alt, E., 1996. Karstification on the Northern Vaca Plateau, Belize. *Journal of Caves and Karst Studies* 58, 121-130.
- Rees, P.M., Ziegler, A.L., Valdes, 2000. Jurassic phytogeography and climates: new data and model comparison. In: Huber, B.T., Macleod, K.G., Wing, S.L. (Eds.), *Warm Climates in earth History*. Cambridge University Press, p. 462.
- Royer, D.L., 2006. CO₂-forced climate thresholds during the phanerozoic. *Geochimica et Cosmochimica Acta* 70, 5665-5675.

- Sevastjanova, I., Clements, B., Hall, R., Belousova, E.A., Griffin, W.L., Pearson, N., 2011. Granitic magmatism, basement ages, and provenance indicators in the Malay Peninsula: insights from detrital zircon U–Pb and Hf-isotope data. *Gondwana Research* 19, 1024-1039.
- Shen, F., Qi, L., Han, G., 2007. Characterization and preservation of karst networks in the carbonate reservoir modeling. 1-8.
- Shuib, M.K., 2009. Major Faults. In: Hutchison, C.S., Tan, D.N.K. (Eds.), *Geology of Peninsular Malaysia*. Geological Society of Malaysia, pp. 249-269.
- Simons, W., Socquet, A., Vigny, C., Ambrosius, B., Abu, S.H., Promthong, C., Subarya, C., Sarsito, D., Matheussen, S., Morgan, P., 2007. A decade of GPS in Southeast Asia: Resolving Sundaland motion and boundaries. *Journal of Geophysical Research* 112, 1-20.
- Singhal, B., Gupta, R.P., 2010. *Applied hydrogeology of fractured rocks*. Springer, p. 407.
- Smart, P.L., Beddows, P.A., Coke, J., Doerr, S., Smith, S., Whitaker, F.F., 2006. Cave development on the Caribbean coast of the Yucatan Peninsula, Quintana Roo, Mexico. *Geological Society of America Special Paper* 404, 105-128.
- Spatte, A., Jennings, J., Smith, D., Greenaway, M., 2006. The micro-erosion meter: Use and limitations. *Earth Surface Processes and Landforms* 10, 427-440.
- Spencer, E.W., 1969. *Introduction to the Structure of the Earth*. McGraw-Hill . New York, p. 597.
- Suntharalingam, T., 1968. Upper Palaeozoic stratigraphy of the area west of Kampar, Perak. *Geological Society of Malaysia*, 1-15.
- Sweeting, M.M., 1972. *Karst landforms*. Macmillan London, p. 362.
- Szunyogh, G., 2005. Theoretical investigation of the duration of karstic denudation on bare, sloping limestone surface. *Acta Carsologica* 34, 9-23.
- Tagami, T., Carter, A., Hurford, A.J., 1996. Natural long-term annealing of the zircon fission-track system in Vienna Basin deep borehole samples: constraints upon the partial annealing zone and closure temperature. *Chemical Geology* 130, 147-157.

- Tjia, H.D., 1999. Geological Setting of Peninsular Malaysia. In: PETRONAS (Ed.), The Petroleum Geology and Resources of Malaysia. The Petroliam Nasional Berhad (Petronas), Kuala Lumpur, pp. 141-169.
- Twidale, C.R., 2005. Granitic Terrains. In: Gupta, A. (Ed.), The Physical Geography of Southeast Asia. Oxford University Press, pp. 123-141.
- Vahrenkamp, V.C., David, F., Duijndam, P., Newal, M., Crevello, P., 2004. Growth Architecture, Faulting, and Karestification of a middle Miocene carbonate platform, Luconia Province, offshore Sarawak, Malaysia. In: Eberli, P., Masferro, J.I. and Sarg, J.F. (Ed.), Seismic imaging of carbonate reservoirs and systems. AAPG Memoir, pp. 329-350.
- van Golf-Racht, T.D., 1982a. Fundamentals of fractured reservoir engineering. Elsevier Scientific Publishing Company, Amsterdam, The Netherlands, p. 710.
- van Golf-Racht, T.D., 1982b. Fundamentals of fractured reservoir engineering. Elsevier Science, p. 710.
- Wang, B., Al-Aasm, I.S., 2002. Karst-controlled diagenesis and reservoir development: Example from the Ordovician main-reservoir carbonate rocks on the eastern margin of the Ordos basin, China. AAPG Bulletin 86, 1639-1658.
- Waterstrat, W.J., Mylroie, J.E., Owen, A.M., Mylroie, J.R., 2010. Coastal caves in Bahamian eolian calcarenites: differentiating between sea caves and flank margin caves using quantitative morphology. Journal of Cave and Karst Studies 72, 61-74.
- White, E., 2005. Breakdown, in: Culver, D.C., White, W.B. (Eds.), Encyclopedia of Caves. Elsevier Academic Press, pp. 56-60.
- White, W.B., Deike, G., 1989. Hydraulic geometry of cave passages. In: White, W.B., White, E.L. (Eds.), Karst Hydrology: Concepts from the Mammoth Cave Area Van Nostrand Reinhold, New York, pp. 223-256.
- White, W.B., White, E.L., 2003. Gypsum wedging and cavern breakdown: studies in the Mammoth Cave System, Kentucky. Journal of Cave and Karst Studies 65, 43-52.
- Woon, W.T., 1991. Geology and mineral resources of the Lumut-Teluk Intan area, Perak Darul Ridzuan. Geological Survey of Malaysia, p. 96.

- Wright, V., Smart, P., 1994. Paleokarst (dissolution diagenesis): its occurrence and hydrocarbon exploration significance. *Developments in Sedimentology* 51, 477-517.
- Wziatek, D., Voudoukas, M., Terefenko, P., 2011. Wave-cut notches along the Algarve coast, S. Portugal: Characteristics and formation mechanisms. *Journal of Coastal Research*, 855-859.
- Yan, Y., Hu, X., Lin, G., Liu, W., Song, Z., 2010. Detrital zircon and apatite fission track data in the Liaoxi basins: Implication to Meso-Cenozoic thermo-tectonic evolution of the northern margin of the North China Craton. *Journal of Earth System Science* 119, 541-551.
- Zachos, J., Pagani, M., Sloan, L., Thomas, E., Billups, K., 2001. Trends, rhythms, and aberrations in global climate 65 Ma to present. *Science* 292, 686-693.
- Zachos, J.C., Röhl, U., Schellenberg, S.A., Sluijs, A., Hodell, D.A., Kelly, D.C., Thomas, E., Nicolo, M., Raffi, I., Lourens, L.J., 2005. Rapid acidification of the ocean during the Paleocene-Eocene thermal maximum. *Science* 308, 1611-1615.
- Zambo, L., Ford, D.C., 1997. Limestone dissolution processes in Beke doline Aggtelek national park, Hungary. *Earth Surface Processes and Landforms* 22, 531-543.
- Zheng, D., Zhang, L., Shen, F., 2011. Characterization and Modeling Study of Karst Networks in the Ordovician Carbonate Reservoirs, Tarim Basin, AAPG Annual Convention and Exhibition, Texas, USA.

PUBLICATIONS

JOURNAL

Kassa, S., Pierson, B., Chow, W.S., Ab Talib, J., 2012. Identifying the link between lineament and cave passage trends to comprehend fractures continuity and influence on the Kinta Valley karst system, Peninsular Malaysia. *International Journal of Speleology* 41, 59-73.

** Characterizing Uplift Rate Variation Using Fission-Track Data: Implications for the Formation of Multi-Level Notches of the Kinta Valley Karst, Peninsular Malaysia . (In Preparation)

INDEXED CONFERENCES

Kassa, S., Pierson, B., Chow, W.S., Ab Talib, J., 2012. Mapping the Kinta Valley karst system, Peninsular Malaysia: Implications for Better Insight of subsurface paleokarst features. *Warta Geologi*, v.38, n.2, pp. 98-100.

Kassa, S., Pierson, B., Chow, W.S., Ab Talib, J., 2010. Indirect Way of Measuring the Denudation rate of the Kinta Valley Limestone, Peninsular Malaysia. *National Postgraduate Conference (NPC 2011)*, Malaysia.
DOI10.1109/NatPC.2011.6136460

Kassa, S., Pierson, B., Chow, W.S., Ab Talib, J., 2012. Understanding the Nature of Collapsed Subsurface karsts: Analogues from the Tropical Karst Regions. 2nd International Conference on Integrated Petroleum Engineering and Geosciences, Kuala Lumpur, Malaysia.

WORKSHOP

Kassa, S., Pierson, B., Chow, W.S., Ab Talib, J., 2011. History of Karst Development in the Kinta Valley: emphasis on the main controlling factors. *EAGE South-East Asia Regional Geology Workshop*, Ipoh, Malaysia. *Workshop programme & Proceedings*, p. 70-73.

Pierson, B.J., Kassa, S., Tsegab, H., Kadir, A.A., Chow, W.S., Hunter, A.W., 2011. Sedimentology of the Paleozoic Limestone of the Kinta Valley, Malaysia. *EAGE South-East Asia Regional Geology Workshop*, Ipoh, Malaysia. *Workshop Programme & Proceedings*, p. 16-20.

APPENDIX A
CAVE SURVEY MEASUREMENTS

1. Gua Kanthan

From	To	Length	Azimuth	Inclination	Left	Right	Up	Down
1	2	13.0m.	275	-33	14.0m.	1.7m.	3.8m.	1.8m.
2	3	18.0m.	270	-35	7.2m.	7.5m.	27.0	1.8m.
3	4	8.8m.	317	-16	10.0m.	14.0m	19.0	1.8m.
4	5	15.0m.	0	6	3.2m.	0.8m.	1.6m.	1.8m.
5	6	8.8m.	357	-1	3.5m.	1.3m.	29.0	1.8m.
6	7	12.0m.	295	11	12.0m.	5.7m.	32.0	1.8m.
7	8	11.8m.	23	0	8.5m.	12.0m	28.0	1.8m.
8	9	10.6m.	287	23	15.3m.	3.7m.	28.0	1.8m.
8	10	14.0m.	358	8	8.3m.	3.5m.	28.0	1.8m.
10	11	5.4m.	305	20	5.0m.	6.4m.	13.0	1.8m.
11	12	7.6m.	335	-5	0.7m.	9.8m.	7.8m.	1.8m.
12	13	7.0m.	342	-35	0.5m.	0.8m.	8.0m.	1.8m.
13	14	11.5m.	345	0	0.6m.	0.5m.	13.0	1.8m.
14	15	14.0m.	310	6	3.0m.	8.1m.	12.8	1.8m.
14	16	12.0m.	22	-13	3.0m.	8.1m.	12.8	1.8m.
16	17	12.0m.	307	7	6.5m.	5.3m.	17.0	1.8m.
17	18	11.0m.	339	12	1.6m.	12.0m	20.0	1.8m.
18	19	14.5m.	334	-5	2.5m.	0.8m.	15.6	1.8m.
19	20	10.0m.	316	-18	4.5m.	1.2m.	26.0	1.8m.
20	21	25.0m.	343	8	4.3m.	5.0m.	20.0	1.8m.
21	22	20.0m.	313	20	3.0m.	3.0m.	15.0	1.8m.

2. Gua Layang Layang

From	To	Length	Azimuth	Inclination	Left	Right	Up	Down
1	2	12.5m.	34	0	1.4	1.2m.	0.3m.	1.8m.
2	3	12.4m.	325	4	9.6	3.3m.	1.1m.	1.8m.
3	4	6.4m.	263	0	2.0	3.0m.	1.0m.	1.8m.
4	5	10.8m.	240	-1	1.2	1.0m.	0.5m.	0.5m.
5	6	10.8m.	141	0	8.6	1.2m.	1.4m.	0.5m.
5	7	8.5m.	305	-7	1.2	3.0m.	1.9m.	1.8m.
7	8	6.2m.	320	6	4.1	4.0m.	0.6m.	1.8m.
4	9	8.0m.	134	0	0.9	0.9m.	0.1m.	0.5m.
9	3	5.2m.	328	0	1.2	3.5m.	1.3m.	0.5m.
3	10	10.0m.	107	0	1.2	1.3m.	1.2m.	1.8m.
10	2	11.4m.	208	-1	10.0	14.5m	2.6m.	1.8m.
10	11	14.5m.	120	0	2.2	4.7m.	2.6m.	1.8m.
11	12	17.0m.	353	0	14.5	9.1m.	8.3m.	1.8m.
12	13	11.5m.	336	3	17.0	15.0m	8.0m.	1.8m.
12	14	17.0m.	269	3	5.8	5.8m.	8.0m.	1.8m.
14	15	11.0m.	15	4	2.7	17.0m	10.0m	1.8m.
15	16	4.0m.	30	3	0.9	1.2m.	1.6m.	0.5m.
16	17	7.3m.	357	0	0.7	0.7m.	0.7m.	0.5m.
17	18	7.4m.	295	1	2.3	0.9m.	1.4m.	1.8m.
12	19	15.0m.	106	1	5.4	16.0m	8.0m.	1.8m.
19	20	14.1m.	196	-1	10.7	8.2m.	7.8m.	1.8m.
20	21	14.0m.	131	5	5.3	8.0m.	2.6m.	1.8m.
20	11	9.1m.	270	0	6.4	8.3m.	2.6m.	1.8m.
19	22	10.7m.	62	16	9.5	8.2m.	7.8m.	1.8m.
22	23	15.0m.	163	33	10.8	2.0m.	7.0m.	1.8m.
22	24	9.7m.	118	20	4.4	2.0m.	7.0m.	1.8m.
24	25	16.0m.	120	0	2.0	2.1m.	3.0m.	1.8m.

25	26	6.8m.	130	15	2.8	2.2m.	2.8m.	1.8m.
26	27	2.7m.	115	15	1.5	2.0m.	2.3m.	1.8m.
26	28	10.4m.	235	45	4.1	3.1m.	2.3m.	1.8m.
28	29	5.0m.	265	30	1.7	2.3m.	15.9m	1.8m.
22	30	9.1m.	332	-1	1.7	7.3m.	7.0m.	1.8m.
30	31	8.7m.	350	0	5.4	8.2m.	4.7m.	1.8m.
31	32	8.3m.	246	0	10.0	6.6m.	3.0m.	1.8m.
32	33	13.8m.	308	3	4.3	10.6m	5.1m.	1.8m.
33	34	7.5m.	275	0	4.4	1.8m.	1.8m.	1.8m.
31	35	7.2m.	70	8	5.6	9.1m.	3.0m.	1.8m.
35	36	3.8m.	320	20	1.0	1.2m.	5.2m.	1.8m.
36	37	5.8m.	355	-30	1.2	3.1m.	4.5m.	1.8m.
36	38	4.7m.	40	63	2.0	3.0m.	4.5m.	1.8m.
38	39	7.1m.	355	16	2.3	0.3m.	2.4m.	1.8m.
39	40	3.2m.	165	25	3.4	1.3m.	2.0m.	1.8m.
40	41	3.9m.	95	13	1.5	0.1m.	0.5m.	1.4m.
41	42	6.2m.	125	50	1.0	0.7m.	0.2m.	0.5m.
39	43	4.2m.	356	50	4.0	1.8m.	2.0m.	1.8m.
43	44	4.7m.	252	13	1.9	0.8m	3.5m.	1.8m.
43	45	5.9m.	93	-3	0.8	1.8.	3.5m.	1.8m.

3. Gua Anak Tempurung

From	To	Length	Azimuth	Inclination	Left	Right	Up	Down
1	2	18.7m.	226	0	3.0m.	2.0m.	1.5m.	1.8m.
2	3	12.5m.	169	0	3.5m.	6.0m.	0.5m.	1.8m.
3	4	21.8m.	176	-2	3.0m.	7.0m.	12.0m.	1.8m.
4	5	12.2m.	170	-3	1.4m.	8.0m.	2.0m.	1.8m.
5	6	8.5m.	165	-1	3.5m.	6.0m.	0.5m.	0.5m.
6	7	14.2m.	135	-1	2.2m.	1.4m.	13.0m.	1.8m.
7	8	11.3m.	168	-3	2.8m.	4.0m.	0.3m.	0.5m.
8	9	13.5m.	167	-2	2.3m.	2.5m.	19.0m.	1.8m.
9	10	7.3m.	185	-4	2.0m.	1.2m.	14.0m.	1.8m.
10	11	6.7m.	200	-3	1.0m.	1.0m.	10.0m.	1.8m.
11	12	7.6m.	233	0	1.4m.	1.0m.	10.0m.	1.8m.
12	13	7.6m.	188	-7	1.2m.	2.0m.	12.0m.	1.8m.
13	14	9.7m.	147	0	1.3m.	1.4m.	10.0m.	1.8m.
14	15	9.8m.	166	-1	1.2m.	1.4m.	8.0m.	1.8m.
15	16	9.0m.	188	-5	2.5m.	1.7m.	16.0m.	1.8m.
16	17	9.3m.	218	-1	2.0m.	2.3m.	1.2m.	1.8m.
17	18	11.0m.	235	-1	2.2m.	3.0m.	3.0m.	0.5m.
18	19	16.6m.	188	-1	2.4m.	1.7m.	10.0m.	0.5m.
19	20	12.9m.	136	0	3.0m.	2.0m.	2.0m.	1.8m.
20	21	14.5m.	166	-1	1.0m.	1.5m.	20.0m.	1.8m.
21	22	4.2m.	138	-1	2.0m.	3.7m.	20.0m.	1.8m.
22	23	8.9m.	205	-2	2.0m.	2.3m.	13.0m.	1.8m.
23	24	5.1m.	155	0	1.3m.	3.0m.	15.0m.	1.8m.
24	25	11.2m.	191	-1	3.5m.	1.2m.	4.0m.	0.5m.
25	26	13.5m.	95	-1	4.0m.	4.0m.	0.7m.	0.5m.
26	27	27.5m.	128	0	3.0m.	2.0m.	1.9m.	0.5m.

27	28	12.0m.	70	-3	4.0m.	7.0m.	18.0m.	0.5m.
28	29	30.8m.	142	-1	2.5m.	3.2m.	8.0m.	0.5m.
29	30	20.3m.	160	-1	3.5m.	2.5m.	1.7m.	0.5m.
30	31	29.6m.	178	-1	2.3m.	3.2m.	10.0m.	0.5m.

4. Gua Datok

From	To	Length	Azimuth	Inclination	Left	Right	Up	Down
1	2	10.9m.	286	28	3.5m.	4.0m.	10.0m.	1.8m.
2	3	4.7m.	325	10	1.0m.	4.2m.	1.0m.	1.8m.
3	4	9.7m.	320	-23	0.6m.	0.4m.	7.0m.	1.8m.
4	5	4.7m.	280	-28	2.2m.	1.1m.	4.0m.	1.8m.
5	6	8.5m.	240	-15	0.5m.	0.3m.	7.0m.	1.8m.
6	7	17.0m.	297	0	9.0m.	4.0m.	13.0m.	1.8m.
7	8	15.2m.	267	20	2.3m.	3.8m.	10.0m.	1.8m.
8	9	16.0m.	264	3	10.0m.	15.0m.	6.0m.	1.8m.
9	10	15.7m.	270	-36	7.0m.	4.0m.	12.0m.	1.8m.
10	11	9.2m.	232	13	15.0m.	7.0m.	15.0m.	1.8m.
11	12	21.1m.	177	5	12.0m.	6.0m.	8.0m.	1.8m.
12	13	27.4m.	211	0	7.0m.	8.0m.	8.0m.	1.8m.
13	14	11.5m.	195	0	3.0m.	5.0m.	10.0m.	1.8m.
14	15	10.5m.	167	-23	2.5m.	1.7m.	20.0m.	1.8m.
15	16	15.9m.	160	-10	2.5m.	22.0m.	14.0m.	1.8m.
16	17	14.0m.	150	13	20.0m.	40.0m.	65.0m.	1.8m.
17	18	13.5m.	153	-12	4.5m.	1.8m.	7.0m.	1.8m.
16	19	25.0m.	240	-4	15.0m.	20.0m.	35.0m.	1.8m.
19	20	20.7m.	193	22	16.0m.	20.0m.	35.0m.	1.8m.
20	21	26.0m.	176	10	10.0m.	25.0m.	30.0m.	1.8m.

5. Gua Kandu

From	To	Length	Azimuth	Inclination	Left	Right	Up	Down
1	2	11.9m.	292	0	14.0m.	11.0m.	4.7m.	1.8m.
2	3	11.6m.	203	7	6.0m.	10.5m.	19.7m.	1.8m.
3	4	7.0m.	293	-1	2.4m.	2.3m.	18.0m.	1.8m.
4	5	4.4m.	265	0	0.7m.	0.3m.	2.7m.	1.8m.
5	6	4.8m.	260	15	0.3m.	0.3m.	2.0m.	1.8m.
6	7	11.2m.	122	10	3.6m.	1.4m.	0.9m.	1.8m.
7	4	4.7m.	355	-20	0.4m.	0.4m.	0.2m.	1.8m.
6	8	20.5m.	300	1	1.4m.	3.6m.	0.9m.	1.8m.
8	9	11.4m.	305	13	2.3m.	2.0m.	5.0m.	1.8m.
8	10	11.9m.	194	3	2.0m.	1.9m.	5.0m.	1.8m.
10	11	11.4m.	283	4	2.4m.	5.7m.	3.3m.	1.8m.
11	12	7.9m.	315	1	0.9m.	0.8m.	0.9m.	0.5m.
12	13	7.4m.	5	0	2.3m.	2.8m.	1.4m.	0.5m.
13	14	5.4m.	296	0	1.5m.	2.0m.	1.0m.	0.5m.
14	15	5.6m.	353	8	2.2m.	1.1m.	0.8m.	0.5m.
15	16	6.4m.	290	8	0.8m.	0.3m.	1.9m.	0.5m.
16	17	7.0m.	333	1	3.0m.	1.1m.	2.8m.	1.8m.
17	18	17.7m.	288	-3	2.9m.	1.2m.	2.0m.	1.8m.
18	19	14.2m.	253	1	6.3m.	2.4m.	2.6m.	0.5m.
19	20	9.6m.	138	6	10.5m.	1.4m.	0.5m.	0.5m.
20	21	7.5m.	186	12	2.1m.	2.4m.	2.2m.	1.8m.
21	22	6.6m.	144	-3	2.6m.	1.6m.	0.5m.	1.8m.
22	23	6.6m.	137	3	1.4m.	0.8m.	0.5m.	0.5m.
23	24	6.9m.	118	14	1.4m.	1.6m.	1.3m.	0.5m.
24	25	6.2m.	67	-13	2.7m.	3.4m.	0.8m.	0.5m.
25	26	4.4m.	10	2	2.3m.	2.8m.	1.6m.	1.8m.

26	27	4.3m.	335	-17	0.9m.	3.0m.	1.8m.	1.8m.
27	16	8.2m.	3	4	3.2m.	2.3m.	3.5m.	1.8m.
16	28	5.1m.	39	9	1.1m.	5.1m.	2.8m.	1.8m.
28	29	2.8m.	45	27	2.7m.	1.6m.	1.9m.	1.8m.
29	30	5.7m.	24	4	1.1m.	2.6m.	0.3m.	0.5m.
30	31	2.7m.	43	-12	1.5m.	2.9m.	0.5m.	0.5m.
31	32	4.4m.	227	-17	4.2m.	1.4m.	0.3m.	0.5m.
32	33	7.0m.	323	-12	7.0m.	1.2m.	1.0m.	1.8m.
33	34	10.9m.	330	6	5.0m.	1.3m.	4.0m.	1.8m.
34	35	5.3m.	215	-14	5.3m.	8.9m.	7.2m.	1.8m.
34	36a	12.0m.	355	28	6.0m.	10.0m.	7.2m.	1.8m.
34	36	6.6m.	123	13	4.9m.	8.9m.	7.2m.	1.8m.
36	37	7.8m.	132	42	1.8m.	1.0m.	8.7m.	1.8m.
37	38	7.6m.	163	39	0.9m.	2.1m.	9.0m.	1.8m.
38	39	5.9m.	175	2	2.4m.	1.5m.	5.7m.	1.8m.
39	40	4.8m.	226	20	1.6m.	1.1m.	4.3m.	1.8m.
40	41	4.7m.	215	8	3.7m.	0.6m.	6.0m.	1.8m.
38	42	7.1m.	85	26	5.6m.	2.2m.	5.7m.	1.8m.
42	43	8.4m.	151	20	13.8m.	0.8m.	9.3m.	1.8m.
43	44	8.8m.	348	-13	3.6m.	1.0m.	9.8m.	1.8m.
44	45	6.9m.	16	-17	1.8m.	4.0m.	7.6m.	1.8m.
45	46	12.5m.	15	-13	5.8m.	2.4m.	12.0m.	1.8m.
45	47	16.1m.	312	1	18.0m.	12.5m.	12.0m.	1.8m.
47	48	13.1m.	308	12	5.6m.	2.8m.	15.0m.	1.8m.
48	49	7.9m.	0	10	2.6m.	5.2m.	18.2m.	1.8m.
49	50	13.9m.	300	2	8.3m.	1.8m.	21.0m.	1.8m.
50	51	6.3m.	53	8	4.6m.	8.7m.	20.0m.	1.8m.
51	52	11.6m.	43	50	1.9m.	2.1m.	18.0m.	1.8m.

52	53	9.2m.	340	28	5.0m.	3.0m.	11.5m.	1.8m.
53	54	6.4m.	330	5	5.0m.	3.0m.	6.9m.	1.8m.
54	55	3.0m.	5	15	1.5m.	0.5m.	3.7m.	1.8m.
55	56	12.0m.	322	2	1.0m.	4.0m.	1.5m.	1.8m.
49	57	7.4m.	245	-38	10.9m.	2.8m.	21.0m.	1.8m.
57	58	11.6m.	267	0	3.9m.	5.6m.	20.0m.	1.8m.
58	59	10.2m.	235	23	1.5m.	2.6m.	21.0m.	1.8m.
59	60	5.0m.	245	28	5.6m.	3.1m.	20.0m.	1.8m.
60	61	6.1m.	170	28	72.0m.	0.3m.	14.8m.	1.8m.
61	62	10.4m.	190	14	2.7m.	3.7m.	12.4m.	1.8m.
62	63	10.3m.	293	14	14.5m.	9.5m.	24.3m.	1.8m.
63	64	9.1m.	290	6	9.2m.	7.8m.	9.5m.	1.8m.
64	65	6.3m.	335	50	7.9m.	4.8m.	28.0m.	1.8m.
65	66	12.5m.	313	11	8.1m.	12.3m.	3.0m.	1.8m.
66	67	5.5m.	242	-20	9.3m.	4.8m.	3.0m.	1.8m.
67	68	20.2m.	236	-40	8.1m.	9.2m.	9.7m.	1.8m.
68	69	10.0m.	210	-13	6.1m.	6.8m.	31.4m.	1.8m.
69	70	18.0m.	235	24	6.0m.	12.0m.	35.0m.	1.8m.
63	71	7.1m.	20	-2	9.1m.	17.0m.	9.5m.	1.8m.
71	72	2.9m.	60	-42	0.9m.	15.5m.	3.7m.	1.8m.
72	73	2.6m.	325	50	1.6m.	9.7m.	5.0m.	1.8m.
73	74	4.6m.	345	-8	0.6m.	0.3m.	0.9m.	1.8m.
74	75	6.2m.	0	0	1.1m.	0.9m.	2.3m.	1.8m.
75	76	4.5m.	72	-24	2.8m.	1.6m.	2.0m.	1.8m.
76	77	2.4m.	33	3	0.2m.	0.3m.	2.0m.	1.8m.
77	78	4.2m.	62	0	0.2m.	0.2m.	0.7m.	0.5m.
78	79	10.0m.	350	-17	2.0m.	0.5m.	2.0m.	1.8m.
78	80	8.0m.	120	0	1.7m.	1.5m.	2.0m.	1.8m.

62	81	21.3m.	153	19	13.0m.	7.4m.	24.3m.	1.8m.
81	82	14.7m.	60	1	18.0m.	4.0m.	10.0m.	1.8m.
82	83	17.2m.	107	7	4.7m.	1.5m.	10.2m.	1.8m.
83	84	13.1m.	140	-5	9.8m.	4.1m.	7.6m.	1.8m.
84	87	9.2m.	172	-55	3.2m.	2.0m.	4.1m.	1.8m.
83	85	7.7m.	186	-20	3.0m.	3.5m.	5.8m.	1.8m.
85	86	9.6m.	178	-20	1.5m.	0.6m.	5.0m.	1.8m.
86	87	12.4m.	93	-13	3.5m.	4.0m.	10.3m.	1.8m.
87	88	8.6m.	5	-23	3.9m.	2.4m.	14.0m.	1.8m.
88	89	30.0m.	20	-22	2.6m.	4.6m.	7.1m.	1.8m.
81	90	5.5m.	108	28	18.8m.	2.8m.	10.0m.	1.8m.
90	91	7.5m.	150	0	1.0m.	1.7m.	5.5m.	1.8m.
91	92	10.8m.	182	-11	3.1m.	2.3m.	5.0m.	1.8m.
92	93	5.7m.	141	20	11.7m.	1.9m.	10.0m.	1.8m.
93	94	10.4m.	125	15	2.2m.	2.2m.	5.0m.	1.8m.
94	95	13.2m.	136	29	6.8m.	1.3m.	6.0m.	1.8m.
94	87	28.4m.	230	30	13.2m.	6.0m.	6.0m.	1.8m.

6. Gua Kepayang

From	To	Length	Azimuth	Inclin.	Left	Right	Up	Down
1	2	14.4m.	350	-8	1.4m.	3.7m.	3.2m.	1.8m.
2	3	16.0m.	337	3	3.1m.	3.9m.	2.6m.	1.8m.
3	4	5.8m.	267	0	4.8m.	2.1m.	0.7m.	1.8m.
4	5	10.6m.	322	5	3.5m.	5.9m.	4.2m.	1.8m.
5	6	11.3m.	8	0	3.0m.	6.3m.	4.0m.	1.8m.
5	7	12.9m.	250	-1	7.2m.	2.6m.	17.0m.	1.8m.
7	8	6.5m.	142	-6	12.9m.	0.5m.	2.6m.	1.8m.
8	9	9.1m.	203	-7	2.0m.	2.5m.	2.6m.	0.5m.
9	10	14.0m.	145	0	6.1m.	10.0m.	7.0m.	1.8m.
10	11	11.0m.	140	1	12.5m.	11.8m.	7.8m.	1.8m.
11	12	11.6m.	151	6	3.2m.	7.1m.	5.6m.	1.8m.
10	13	11.4m.	62	4	11.0m.	22.0m.	7.8m.	1.8m.
13	4	8.2m.	0	7	2.1m.	1.2m.	4.3m.	1.8m.
10	14	12.3m.	246	-1	27.0m.	14.0m.	7.8m.	1.8m.
14	15	13.3m.	235	6	4.0m.	14.4m.	16.0m.	1.8m.
15	16	8.7m.	220	5	4.0m.	3.0m.	8.0m.	1.8m.
16	17	10.6m.	126	13	8.7m.	0.8m.	3.5m.	1.8m.
17	18	13.3m.	77	0	3.4m.	2.0m.	0.7m.	1.8m.
18	10	27.0m.	358	26	1.8m.	4.0m.	1.2m.	1.8m.
15	19	14.0m.	260	-4	8.7m.	18.0m.	4.7m.	1.8m.
19	20	9.5m.	245	0	4.7m.	1.8m.	0.8m.	1.8m.
20	21	15.0m.	342	1	0.0m.	2.3m.	1.3m.	1.8m.
21	22	14.0m.	309	-6	8.6m.	3.0m.	0.3m.	1.8m.
22	23	10.5m.	323	-3	8.8m.	2.8m.	1.9m.	1.8m.
23	24	10.3m.	225	4	13.3m.	2.3m.	0.7m.	1.8m.
24	25	15.3m.	215	0	3.3m.	4.1m.	0.7m.	1.8m.

7. Gua Masoora 1

From	To	Length	Azimuth	Incli.	Left	Right	Up	Down
1	2	11.9m.	50	0	7.4m.	10.4m.	5.9m.	1.8m.
2	3	10.0m.	110	4	3.5m.	7.6m.	2.5m.	1.8m.
3	4	10.0m.	173	-3	2.2m.	3.0m.	0.7m.	1.8m.
4	5	10.8m.	164	0	4.6m.	6.3m.	1.0m.	1.8m.
4	6	10.6m.	13	0	6.3m.	4.6m.	1.0m.	1.8m.
6	7	6.2m.	58	0	2.6m.	1.2m.	1.1m.	1.8m.
7	8	12.0m.	173	0	2.5m.	6.2m.	1.0m.	1.8m.
7	9	11.4m.	325	0	6.2m.	1.8m.	1.0m.	1.8m.
9	10	7.8m.	30	0	9.4m.	10.3m.	1.4m.	1.8m.
10	11	7.1m.	15	6	8.1m.	11.7m.	1.6m.	1.8m.
11	12	8.1m.	285	0	12.0m.	22.0m.	1.6m.	1.8m.
12	13	8.8m.	283	5	8.1m.	13.0m.	3.8m.	1.8m.
13	14	7.4m.	260	0	3.5m.	5.6m.	0.4m.	1.8m.
14	15	5.7m.	238	0	0.4m.	0.8m.	0.1m.	0.5m.
2	15	14.7m.	333	4	18.3m.	5.5m.	2.5m.	1.8m.
15	16	9.6m.	255	-5	14.7m.	1.6m.	3.4m.	1.8m.
16	17	2.7m.	338	3	2.2m.	3.8m.	7.3m.	1.8m.
17	18	9.1m.	296	3	1.7m.	2.0m.	6.0m.	1.8m.
18	19	14.0m.	340	-3	6.8m.	15.0m.	6.4m.	1.8m.
19	20	14.3m.	293	-3	4.9m.	5.2m.	5.3m.	1.8m.
20	21	12.9m.	290	0	14.0m.	14.5m.	1.7m.	1.8m.
21	22	13.5m.	255	3	9.7m.	3.9m.	1.6m.	1.8m.
22	23	11.0m.	343	0	0.0m.	1.5m.	0.8m.	1.8m.
23	24	5.9m.	327	-10	2.4m.	4.8m.	0.9m.	1.8m.
24	25	2.3m.	320	13	4.4m.	0.5m.	2.3m.	1.8m.

8. Gua Masoora 2

From	To	Length	Azimuth	Incli.	Left	Right	Up	Down
1	2	7.3m.	255	13	5.2m.	8.0m.	3.1m.	1.8m.
2	3	3.7m.	266	8	2.6m.	10.0m.	3.4m.	1.8m.
3	4	6.1m.	293	-10	2.8m.	3.7m.	2.7m.	1.8m.
4	5	6.2m.	215	4	3.7m.	1.0m.	2.2m.	1.8m.
5	6	6.9m.	188	-10	2.8m.	3.7m.	2.7m.	1.8m.
6	7	6.8m.	185	0	1.6m.	3.4m.	6.5m.	1.8m.
7	8	5.6m.	164	9	0.7m.	2.2m.	3.9m.	1.8m.
8	9	4.6m.	190	2	5.1m.	5.3m.	1.4m.	1.8m.
9	10	6.0m.	196	2	2.0m.	3.0m.	4.0m.	1.8m.
8	11	5.1m.	120	-8	5.6m.	4.6m.	4.0m.	1.8m.

9. Gua Tempurung

From	To	Length	Azimuth	Incli.	Left	Right	Up	Down
1	2	10.0m.	157	0	0.6m.	1.2m.	1.3m.	1.8m.
2	3	12.8m.	102	0	3.6m.	1.7m.	1.3m.	1.8m.
3	4	12.9m.	70	0	4.4m.	1.7m.	1.0m.	1.8m.
4	5	26.0m.	47	0	9.2m.	3.7m.	17.0m.	1.8m.
5	6	12.4m.	90	0	4.3m.	2.1m.	4.7m.	1.8m.
6	7	16.4m.	160	0	5.7m.	5.0m.	14.0m.	1.8m.
7	8	13.2m.	75	0	12.2m.	2.0m.	3.7m.	1.8m.
8	9	23.0m.	21	1	5.0m.	2.6m.	2.0m.	1.8m.
9	10	31.0m.	25	1	4.4m.	3.4m.	2.0m.	1.8m.
10	11	18.3m.	74	0	4.9m.	2.2m.	3.5m.	1.8m.
11	12	12.0m.	124	0	4.1m.	4.2m.	1.0m.	1.8m.
12	13	19.0m.	124	1	3.5m.	2.2m.	0.5m.	1.8m.
13	14	9.3m.	106	1	2.9m.	2.9m.	1.2m.	1.8m.
14	15	12.6m.	136	1	3.9m.	2.5m.	0.9m.	1.8m.
15	16	14.0m.	64	0	3.8m.	1.4m.	1.5m.	1.8m.
16	17	12.7m.	34	1	4.0m.	3.0m.	0.5m.	0.5m.
17	18	11.3m.	35	0	2.3m.	3.0m.	1.0m.	1.8m.
18	19	15.0m.	32	1	6.0m.	1.5m.	6.0m.	1.8m.
19	20	12.7m.	78	2	7.0m.	4.0m.	8.0m.	1.8m.
20	21	7.0m.	145	0	2.0m.	1.5m.	4.0m.	1.8m.
21	22	12.0m.	160	0	2.0m.	1.7m.	0.2m.	0.5m.
22	23	13.0m.	96	1	5.5m.	1.5m.	5.6m.	0.5m.
23	24	16.0m.	6	1	4.5m.	3.5m.	5.0m.	1.8m.
24	25	12.8m.	355	0	2.5m.	6.0m.	4.0m.	1.8m.
25	26	14.2m.	357	0	2.0m.	2.0m.	0.5m.	0.5m.
26	27	7.0m.	287	0	2.0m.	2.5m.	0.4m.	1.8m.

27	28	9.0m.	0	1	3.0m.	2.5m.	3.0m.	1.8m.
28	29	12.5m.	7	1	3.0m.	3.4m.	1.0m.	0.5m.
29	30	8.4m.	55	1	3.3m.	1.0m.	0.3m.	0.5m.
30	31	12.0m.	121	0	3.0m.	2.5m.	0.1m.	1.6m.
31	32	13.0m.	125	1	2.3m.	5.0m.	2.0m.	1.8m.
32	33	15.0m.	113	4	3.5m.	2.5m.	3.0m.	1.8m.
33	34	25.0m.	147	0	3.0m.	5.0m.	3.0m.	1.8m.
34	35	23.0m.	148	2	6.0m.	3.0m.	2.0m.	1.8m.
35	36	20.0m.	168	1	2.0m.	4.0m.	15.0m.	1.8m.
36	37	18.0m.	144	1	4.5m.	4.0m.	3.0m.	1.8m.
37	38	20.0m.	106	0	5.0m.	4.0m.	2.0m.	1.8m.
38	39	17.0m.	153	1	4.0m.	7.0m.	20.0m.	1.8m.
39	40	20.0m.	47	0	15.0m.	3.0m.	1.0m.	1.8m.
40	41	20.0m.	43	2	3.0m.	5.0m.	20.0m.	1.8m.
41	42	19.0m.	132	1	3.0m.	3.0m.	20.0m.	1.8m.
42	43	18.0m.	137	1	4.0m.	4.0m.	13.0m.	1.8m.
43	44	15.2m.	41	1	2.5m.	4.0m.	3.0m.	1.8m.
44	45	19.7m.	56	0	3.0m.	2.5m.	10.0m.	1.8m.
45	46	12.2m.	87	1	3.0m.	3.0m.	15.0m.	1.8m.
46	47	23.0m.	125	2	1.5m.	10.0m.	0.4m.	1.8m.
47	48	13.2m.	166	2	6.0m.	9.0m.	1.0m.	1.8m.
48	49	19.5m.	108	2	12.0m.	2.5m.	0.5m.	0.7m.
49	50	17.0m.	95	1	8.0m.	12.0m.	4.0m.	1.8m.
50	51	18.6m.	113	1	12.0m.	13.0m.	1.0m.	1.8m.
51	52	17.0m.	116	1	4.0m.	11.0m.	0.5m.	1.8m.
52	53	30.8m.	153	2	8.0m.	10.0m.	16.0m.	1.8m.
53	54	19.4m.	111	1	10.0m.	7.0m.	0.9m.	0.5m.
54	55	15.4m.	20	3	15.0m.	17.0m.	3.0m.	1.8m.

55	56	17.4m.	347	0	6.0m.	12.0m.	13.0m.	1.8m.
56	57	17.7m.	28	1	4.0m.	10.0m.	0.3m.	1.8m.
57	58	23.5m.	356	1	8.0m.	12.0m.	0.5m.	0.5m.
58	59	30.7m.	63	2	6.0m.	22.0m.	0.2m.	0.5m.
59	60	21.3m.	85	1	6.0m.	12.0m.	0.6m.	1.8m.
60	61	18.3m.	94	1	10.0m.	14.0m.	0.7m.	0.5m.
61	62	21.4m.	133	0	6.0m.	17.0m.	0.3m.	0.5m.
62	63	15.5m.	140	0	5.0m.	12.0m.	0.3m.	0.5m.
63	64	13.2m.	147	1	4.0m.	1.0m.	0.7m.	0.5m.
64	65	22.6m.	143	3	7.0m.	1.3m.	0.6m.	0.5m.
65	66	16.0m.	115	1	10.0m.	10.0m.	1.8m.	0.5m.
66	67	13.6m.	123	2	6.0m.	10.0m.	0.5m.	0.5m.
67	68	30.8m.	155	1	2.0m.	4.0m.	0.3m.	1.8m.
68	69	30.8m.	158	1	4.0m.	6.0m.	4.0m.	1.8m.
69	70	17.9m.	150	2	3.5m.	3.0m.	2.0m.	0.5m.
70	71	16.0m.	172	1	1.2m.	1.0m.	0.1m.	0.5m.
71	72	30.8m.	154	1	3.5m.	2.5m.	1.2m.	1.8m.
72	73	30.8m.	148	1	2.5m.	10.0m.	6.0m.	1.8m.
73	74	30.5m.	140	2	5.0m.	15.0m.	6.0m.	1.8m.
74	75	29.3m.	88	0	11.0m.	7.0m.	13.0m.	1.8m.
75	76	30.8m.	125	1	10.0m.	13.0m.	5.0m.	1.8m.
76	77	15.8m.	128	1	14.0m.	9.0m.	5.0m.	1.8m.
77	78	16.1m.	115	2	6.0m.	14.0m.	1.0m.	1.8m.
78	79	30.8m.	154	0	4.0m.	11.0m.	2.0m.	1.8m.
79	80	22.6m.	116	2	3.0m.	2.0m.	3.0m.	1.8m.
80	81	19.6m.	80	1	10.0m.	6.0m.	4.0m.	1.8m.
81	82	30.8m.	43	1	15.0m.	4.0m.	2.0m.	1.8m.
82	83	28.0m.	15	1	7.0m.	0.0m.	2.0m.	1.8m.

10. Gua Paradise Valley

From	To	Length	Azimuth	Inclin.	Left	Right	Up	Down
1	2	26.5m.	357	3	7.1m.	4.1m.	2.1m.	1.8m.
2	3	5.3m.	10	-10	1.0m.	2.1m.	0.5m.	1.8m.
3	4	6.8m.	330	10	0.9m.	2.5m.	1.6m.	1.8m.
4	5	2.2m.	252	30	0.6m.	1.7m.	0.9m.	0.3m.
5	6	5.5m.	295	0	0.6m.	1.2m.	0.3m.	0.2m.
6	7	6.6m.	315	0	0.5m.	2.2m.	0.5m.	0.2m.
7	8	7.4m.	356	1	0.9m.	2.6m.	0.5m.	1.8m.
8	9	3.8m.	23	6	0.2m.	6.4m.	0.2m.	1.8m.
9	10	10.3m.	10	3	0.8m.	5.1m.	6.6m.	1.8m.
10	11	16.0m.	335	15	3.7m.	0.7m.	12.5m.	1.8m.
11	12	10.6m.	300	10	9.2m.	1.3m.	8.8m.	1.8m.
12	13	20.3m.	345	-3	8.8m.	7.3m.	11.7m.	1.8m.
13	14	20.2m.	322	0	3.5m.	3.6m.	16.5m.	1.8m.
14	15	18.4m.	345	8	5.2m.	5.6m.	8.7m.	1.8m.
15	16	10.3m.	335	25	4.0m.	4.0m.	7.3m.	1.8m.
16	17	6.1m.	290	15	1.3m.	2.2m.	4.7m.	1.8m.
17	18	7.2m.	313	15	2.1m.	1.2m.	0.9m.	1.8m.
18	19	6.4m.	305	8	3.7m.	2.9m.	3.2m.	1.8m.
19	20	20.0m.	330	-15	6.9m.	5.5m.	13.6m.	1.8m.
20	21	16.0m.	190	20	5.4m.	6.8m.	13.6m.	1.8m.
21	22	11.1m.	300	0	2.6m.	6.1m.	5.1m.	1.8m.
22	23	10.4m.	310	0	1.3m.	0.5m.	1.0m.	1.8m.
23	24	13.4m.	293	15	2.6m.	1.3m.	5.2m.	1.8m.
9	9a	13.6m.	170	0	5.1m.	0.8m.	6.6m.	1.8m.
9a	9b	8.1m.	142	15	0.6m.	2.2m.	15.7m.	1.8m.
9b	9c	5.8m.	180	-5	1.1m.	1.5m.	10.2m.	1.8m.

11. Gua Naga Mas

From	To	Length	Comp.	Inc.	Left	Right	Up	Down
1	2	15.6m.	212	2	6.8m.	3.8m.	9.2m.	1.8m.
2	3	10.9m.	223	22	6.8m.	5.0m.	15.0m.	1.8m.
3	4	10.6m.	232	10	6.0m.	4.7m.	13.0m.	1.8m.
4	5	7.7m.	240	-30	7.4m.	0.6m.	2.4m.	1.8m.
4	6	9.3m.	194	25	7.4m.	0.6m.	2.4m.	1.8m.
6	7	4.7m.	173	-3	1.5m.	0.7m.	8.3m.	1.8m.
7	8	15.0m.	206	32	3.2m.	6.0m.	9.0m.	1.8m.
7	9	11.0m.	200	-40	2.0m.	1.5m.	9.0m.	1.8m.
3	10	8.5m.	192	15	6.0m.	4.7m.	13.0m.	1.8m.
10	11	5.3m.	235	7	1.6m.	0.9m.	3.1m.	1.8m.
11	12	5.6m.	210	-25	3.7m.	2.2m.	3.7m.	1.8m.
12	13	4.2m.	190	10	1.5m.	1.9m.	3.2m.	1.8m.
13	9	8.0m.	225	-40	1.1m.	1.6m.	0.9m.	1.8m.
1	14	7.9m.	293	10	0.0m.	0.0m.	9.2m.	1.8m.
14	15	5.3m.	7	1	1.3m.	0.6m.	3.5m.	1.8m.
15	16	4.7m.	290	13	3.5m.	9.8m.	4.0m.	1.8m.
16	17	7.2m.	283	-18	2.9m.	2.8m.	3.9m.	1.8m.

APPENDIX B

FRACTURES TREND MEASUREMENT

Hill Name	Fracture Trend (deg.)	Hill Name	Fracture Trend (deg.)	Hill Name	Fracture Trend (deg.)	Hill Name	Fracture Trend (deg.)	Hill Name	Fracture Trend (deg.)
	043		180		55		62		34
G	176	G	202	G	341	G	26	G	288
U	235	U	175	U	332	U	328	U	150
N	180	N	218	N	42	N	329	N	23
U	045	U	175	U	44	U	343	U	280
N	044	N	61	N	10	N	328	N	286
G	337	G	151	G	76	G	72	G	341
R	327	R	232	R	327	R	258	R	78
A	229	A	230	A	343	A	259	A	77
P	353	P	61	P	65	P	66	P	300
A	330	A	214	A	65	A	135	A	291
T	057	T	70	T	338	T		T	340
	053		155		344				357
	159		152		69				337
	331		59		328				24
	329		332		337				18
	022		218		350				3
	040		245		340				8
	075		153		331				10
	042		246		54				80
	067		80		328				347
	339		16		333				338
	014		212		298				0
	358		290		289				358
	022				311				354
	077				182				67
	085				185				339
	351				191				66
	164				83				253
	067				74				2
	072				178				80
	339				48				252

149			177			334
019			354			95
027			76			188
027			206			94
151			189			177
168			193			48
257			70			8
171			71			58
168			17			289
168			18			284
161			26			313
050			6			293
335			98			56
346			8			335
069			85			334
328			84			305
335			143			282
003			333			55
241			340			14
340			101			67
346			247			250
077			233			287
350			247			349
075			44			20
035			41			68
342			333			337
021			336			39
015			346			284
002			348			19
027			46			211
072			283			57
057			214			20
178			216			357
206			180			237

	000				68				279
	006				276				56
	339				173				350
	300				350				
	295				166				
	300				340				
	305								
	280								

APPENDIX C

URANIUM-LEAD AND FISSION-TRACK AGE

1. From Apatite

a) Sample CH-06

Analysis Name	UPb Age (Ma)	2 sigma (Ma)	FT Age (Ma)	95% - CI(Ma)	95% +CI(Ma)	[U] (ppm)
1283_001_Ap_a_1_1	224.96	18.27	47.69	12.22	16.40	189
1283_001_Ap_a_1_2	222.89	21.90	38.39	11.42	16.23	225
1283_001_Ap_a_1_3	240.51	35.19	23.77	8.67	13.63	108
1283_001_Ap_a_1_4	237.93	27.40	30.27	10.22	15.40	120
1283_001_Ap_a_1_5	230.87	35.47	34.49	10.11	14.30	91
1283_001_Ap_a_1_6	243.60	74.45	45.19	19.01	32.74	41
1283_001_Ap_a_1_7	224.62	24.67	45.20	13.43	19.08	189
1283_001_Ap_a_1_8	224.22	37.03	42.13	12.62	17.99	90
1283_001_Ap_a_1_9	214.06	21.69	17.90	4.42	5.87	329
1283_001_Ap_a_1_10	222.00	25.83	37.65	11.63	16.80	92
1283_001_Ap_a_1_11	231.70	34.65	22.53	6.49	9.10	114
1283_001_Ap_a_1_12	225.77	31.59	30.07	9.15	13.14	124
1283_001_Ap_a_1_13	230.39	37.76	23.38	8.40	13.11	88
1283_001_Ap_a_1_14	232.95	104.24	40.80	12.45	17.90	178
1283_001_Ap_a_1_15	225.56	27.02	38.46	10.66	14.73	110
1283_001_Ap_a_1_16	224.21	28.51	29.99	7.68	10.31	135
1283_001_Ap_a_1_17	237.66	31.69	52.54	14.02	19.10	92
1283_001_Ap_a_1_18	0.00	0.00	44.93	12.15	16.63	237
1283_001_Ap_a_1_19	223.66	35.19	26.99	6.31	8.23	109
1283_001_Ap_a_1_20	237.71	34.98	38.03	11.97	17.45	95
1283_001_Ap_a_1_21	230.32	37.75	35.20	12.31	18.91	112
1283_001_Ap_a_1_22	224.30	42.11	33.35	9.78	13.83	80
1283_001_Ap_a_1_23	223.77	43.51	38.17	11.72	16.89	78
1283_001_Ap_a_1_24	226.11	19.91	39.37	10.02	13.42	245
1283_001_Ap_a_1_25	239.53	55.09	21.33	5.91	8.16	297
1283_001_Ap_a_1_26	288.09	239.95	38.67	11.02	15.39	85
1283_001_Ap_a_1_27	234.74	47.55	39.05	13.52	20.64	80
1283_001_Ap_a_1_28	239.18	32.04	34.19	9.23	12.64	105
1283_001_Ap_a_1_29	237.77	34.36	49.76	12.14	16.04	113
1283_001_Ap_a_1_30	226.91	26.96	31.19	7.98	10.71	167
1283_001_Ap_a_1_31	244.34	17.64	35.91	9.85	13.55	188
1283_001_Ap_a_1_32	241.85	37.80	38.31	10.76	14.95	101
1283_001_Ap_a_1_33	236.51	48.02	39.99	12.83	18.86	62
1283_001_Ap_a_1_34	239.46	31.01	46.34	13.26	18.55	142
1283_001_Ap_a_1_35	239.86	30.47	33.56	10.39	15.03	112
1283_001_Ap_a_1_36	235.38	32.77	29.08	8.32	11.64	119
1283_001_Ap_a_1_37	208.60	39.63	39.80	10.71	14.63	122
1283_001_Ap_a_1_38	239.72	40.79	32.66	11.43	17.57	87
1283_001_Ap_a_1_39	238.48	46.00	46.43	13.02	18.07	90
1283_001_Ap_a_1_40	224.63	14.14	34.09	7.78	10.07	372

b) Sample CH-07

Analysis Name	UPb Age (Ma)	2 sigma (Ma)	FT Age (Ma)	95%-Cl(Ma)	95%+Cl(Ma)	[U] (ppm)
1283_002_Ap_a_1_1	239.47	40.01	37.53	10.87	15.28	75
1283_002_Ap_a_1_2	235.94	45.51	28.50	9.06	13.26	97
1283_002_Ap_a_1_3	233.17	38.40	41.23	13.61	20.28	86
1283_002_Ap_a_1_4	245.21	33.71	37.36	10.96	15.49	69
1283_002_Ap_a_1_5	254.17	55.72	50.03	18.23	28.62	45
1283_002_Ap_a_1_6	248.73	46.76	18.16	6.54	10.21	65
1283_002_Ap_a_1_7	226.22	33.74	21.41	6.93	10.25	107
1283_002_Ap_a_1_8	243.00	70.25	48.61	14.71	21.07	36
1283_002_Ap_a_1_9	225.24	32.19	33.46	8.93	12.16	94
1283_002_Ap_a_1_10	231.13	26.66	27.56	8.91	13.15	112
1283_002_Ap_a_1_11	223.94	20.23	12.58	4.98	8.23	152
1283_002_Ap_a_1_12	219.87	51.57	26.68	9.35	14.38	57
1283_002_Ap_a_1_13	232.64	25.58	27.76	10.11	15.89	101
1283_002_Ap_a_1_14	272.63	57.62	38.21	15.72	26.66	48
1283_002_Ap_a_1_15	230.86	37.83	31.65	10.68	16.10	95
1283_002_Ap_a_1_16	230.39	36.84	37.21	11.23	16.06	85
1283_002_Ap_a_1_17	250.12	70.45	55.88	18.83	28.33	36
1283_002_Ap_a_1_18	237.38	38.82	36.18	10.62	15.02	120
1283_002_Ap_a_1_19	232.96	38.75	20.53	7.28	11.27	91
1283_002_Ap_a_1_20	248.81	45.83	31.86	11.01	16.80	56
1283_002_Ap_a_1_21	218.70	37.08	20.43	5.60	7.70	122
1283_002_Ap_a_1_22	227.10	30.39	31.33	9.26	13.13	102
1283_002_Ap_a_1_23	235.03	26.00	26.23	6.50	8.64	158
1283_002_Ap_a_1_24	242.85	61.01	59.59	16.65	23.07	45
1283_002_Ap_a_1_25	214.73	49.67	27.52	7.35	10.02	106
1283_002_Ap_a_1_26	254.74	45.73	38.09	11.77	17.01	47
1283_002_Ap_a_1_27	216.81	45.32	29.19	8.77	12.52	86
1283_002_Ap_a_1_28	239.17	54.27	35.10	12.00	18.21	63
1283_002_Ap_a_1_29	225.87	43.91	32.93	10.27	14.90	72
1283_002_Ap_a_1_30	217.79	34.23	24.63	8.13	12.12	75
1283_002_Ap_a_1_31	229.61	46.57	40.68	12.83	18.72	69
1283_002_Ap_a_1_32	255.34	47.01	26.32	8.54	12.63	53
1283_002_Ap_a_1_33	227.81	28.06	35.02	11.22	16.50	143
1283_002_Ap_a_1_34	241.53	39.65	34.82	9.88	13.79	108
1283_002_Ap_a_1_35	234.79	27.76	28.64	8.71	12.50	113
1283_002_Ap_a_1_36	230.76	70.90	32.26	11.60	18.08	45
1283_002_Ap_a_1_37	205.18	33.48	32.50	10.73	16.01	103
1283_002_Ap_a_1_38	249.50	63.31	36.12	11.96	17.86	65
1283_002_Ap_a_1_39	243.99	62.20	32.24	13.57	23.38	48
1283_002_Ap_a_1_40	268.10	55.00	43.66	13.74	20.01	66

c) Sample CH-08

Analysis Name	UPb Age (Ma)	2 sigma (Ma)	FT Age (Ma)	95%-CI(Ma)	95%+CI(Ma)	[U] (ppm)
1283_003_Ap_a_1_1	284.55	121.98	6.97	6.03	44.78	29
1283_003_Ap_a_1_2	0.00	0.00	0.00	0.00	1.42	0
1283_003_Ap_a_1_3	83.65	425.02	0.00	0.00	10.92	31
1283_003_Ap_a_1_4	0.00	0.00	0.00	0.00	1031.35	2
1283_003_Ap_a_1_5	247.63	64.23	9.11	6.27	20.14	55
1283_003_Ap_a_1_6	0.00	0.00	0.00	0.00	0.00	0
1283_003_Ap_a_1_7	528.28	306.97	22.97	19.88	146.30	5
1283_003_Ap_a_1_8	321.42	119.97	37.48	19.39	40.04	31
1283_003_Ap_a_1_9	268.09	119.57	16.98	10.83	29.84	24
1283_003_Ap_a_1_10	333.49	227.64	0.00	0.00	0.00	11
1283_003_Ap_a_1_11	240.45	72.67	7.05	5.36	22.24	46
1283_003_Ap_a_1_12	241.75	81.52	22.55	14.38	39.55	37
1283_003_Ap_a_1_13	96.25	53.78	10.40	7.90	32.76	28
1283_003_Ap_a_1_14	440.92	576.62	3.04	2.17	7.61	49
1283_003_Ap_a_1_15	220.62	113.67	12.47	7.06	16.28	31
1283_003_Ap_a_1_16	296.69	137.62	35.26	24.30	77.70	35
1283_003_Ap_a_1_17	292.09	171.04	4.59	2.93	8.12	21
1283_003_Ap_a_1_18	1166.74	2280.00	0.00	0.00	0.00	52
1283_003_Ap_a_1_19	0.00	0.00	0.00	0.00	0.00	16027
1283_003_Ap_a_1_20	2932.99	2280.00	0.82	0.71	5.47	60
1283_003_Ap_a_1_21	0.00	0.00	0.00	0.00	0.00	256
1283_003_Ap_a_1_22	269.74	116.17	7.52	5.71	23.72	32
1283_003_Ap_a_1_23	228.75	60.92	6.64	4.58	14.70	61
1283_003_Ap_a_1_24	267.16	202.96	7.23	6.26	46.45	15
1283_003_Ap_a_1_25	337.11	233.62	24.87	21.53	158.25	8
1283_003_Ap_a_1_26	0.00	0.00	489.51	433.07	2960.43	0
1283_003_Ap_a_1_27	371.72	294.33	16.37	14.18	104.75	9
1283_003_Ap_a_1_28	0.00	0.00	0.00	0.00	4100.61	0
1283_003_Ap_b_1_1	334.92	158.56	13.91	7.88	18.16	20
1283_003_Ap_b_1_2	285.81	144.43	9.20	6.34	20.35	24
1283_003_Ap_b_1_3	274.61	136.18	6.81	4.69	15.09	28
1283_003_Ap_b_1_4	317.07	98.85	23.81	12.32	25.50	33
1283_003_Ap_b_1_5	315.41	198.94	23.32	11.63	23.14	27
1283_003_Ap_b_1_6	0.00	0.00	0.00	0.00	0.00	35
1283_003_Ap_b_1_7	0.00	0.00	0.00	0.00	0.00	19
1283_003_Ap_b_1_8	277.99	109.66	3.69	2.81	11.66	33
1283_003_Ap_b_1_9	275.90	123.35	11.47	7.93	25.62	26
1283_003_Ap_b_1_10	334.43	184.21	5.55	4.80	35.69	14

d) Sample CH-09

Analysis Name	UPb Age (Ma)	2 sigma (Ma)	FT Age (Ma)	95%-Cl(Ma)	95%+Cl(Ma)	[U] (ppm)
1283_004_Ap_a_1_1	961.37	352.50	13.95	9.62	30.90	28
1283_004_Ap_a_1_2	531.18	1116.27	19.60	17.02	128.18	8
1283_004_Ap_a_1_3	0.00	0.00	0.00	0.00	0.00	0
1283_004_Ap_a_1_4	1076.65	580.67	0.00	0.00	0.00	56
1283_004_Ap_a_1_5	0.00	0.00	0.00	0.00	0.00	0
1283_004_Ap_a_1_6	184.74	59.90	14.28	9.11	25.09	26
1283_004_Ap_a_1_7	0.00	0.00	74.70	31.41	53.96	29
1283_004_Ap_a_1_8	231.59	818.10	129.76	98.74	400.42	0
1283_004_Ap_a_1_9	147.11	33.52	14.04	10.72	45.17	240
1283_004_Ap_a_1_10	0.00	0.00	0.00	0.00	0.00	0
1283_004_Ap_a_1_11	0.00	0.00	0.00	0.00	0.00	0
1283_004_Ap_a_1_12	193.76	154.96	15.16	13.13	97.37	15
1283_004_Ap_a_1_13	0.00	0.00	0.00	0.00	0.00	0
1283_004_Ap_a_1_14	0.00	0.00	0.00	0.00	0.00	0
1283_004_Ap_a_1_15	0.00	0.00	5428.42	4946.29	14916.68	0
1283_004_Ap_a_1_16	0.00	0.00	0.00	0.00	0.00	0
1283_004_Ap_a_1_17	0.00	0.00	0.00	0.00	0.00	0
1283_004_Ap_a_1_18	0.00	0.00	0.00	0.00	5816.59	0
1283_004_Ap_a_1_19	0.00	0.00	0.00	0.00	0.00	0
1283_004_Ap_a_1_20	1471.43	2020.80	0.00	0.00	0.00	0
1283_004_Ap_a_1_21	0.00	0.00	0.00	0.00	0.00	0
1283_004_Ap_a_1_22	0.00	0.00	0.00	0.00	0.00	0
1283_004_Ap_a_1_23	0.00	0.00	0.00	0.00	0.00	0
1283_004_Ap_a_1_24	0.00	0.00	0.00	0.00	0.00	0
1283_004_Ap_a_1_25	0.00	0.00	0.00	0.00	0.00	0
1283_004_Ap_a_1_26	0.00	0.00	0.00	0.00	0.00	0
1283_004_Ap_a_1_27	0.00	0.00	0.00	0.00	0.00	0
1283_004_Ap_a_1_28	140.42	70.70	4.24	2.93	9.41	18
1283_004_Ap_a_1_29	0.00	0.00	0.00	0.00	0.00	0
1283_004_Ap_a_1_30	0.00	0.00	0.00	0.00	0.00	0
1283_004_Ap_a_1_31	3114.21	2280.00	0.00	0.00	3362.57	0
1283_004_Ap_a_1_32	0.00	0.00	0.00	0.00	0.00	0
1283_004_Ap_a_1_33	0.00	0.00	0.00	0.00	0.00	0
1283_004_Ap_a_1_34	0.00	0.00	0.00	0.00	0.00	0
1283_004_Ap_a_1_35	0.00	0.00	0.00	0.00	0.00	0
1283_004_Ap_a_1_36	0.00	0.00	0.00	0.00	0.00	0
1283_004_Ap_a_1_37	0.00	0.00	0.00	0.00	0.00	0
1283_004_Ap_a_1_38	970.42	2280.00	0.00	0.00	2130.07	0
1283_004_Ap_a_1_39	0.00	0.00	0.00	0.00	0.00	0
1283_004_Ap_a_1_40	151.55	88.68	5.33	4.06	16.95	27

2. From Zircon

a) Sample CH-06

Analysis Name	UPb age (Ma)	2 sigma (Ma)	FT age (Ma)	95%-CI(Ma)	95%+CI(Ma)	[U] (ppm)
1283 001 Zrn b 01 1	1116.64	31.16	66.07	24.82	39.63	614
1283 001 Zrn b 01 2	1420.12	23.28	91.76	33.27	51.97	467
1283 001 Zrn b 01 3	683.01	20.61	156.17	60.46	97.91	245
1283 001 Zrn b 01 4	215.92	8.96	170.76	59.27	90.14	219
1283 001 Zrn b 01 5	213.22	9.63	104.95	37.07	57.05	393
1283 001 Zrn b 01 6	461.40	10.91	150.20	52.77	80.84	305
1283 001 Zrn b 01 7	217.51	7.16	101.77	35.71	54.78	401
1283 001 Zrn b 01 8	217.50	7.47	87.20	31.74	49.72	290
1283 001 Zrn b 01 9	225.17	5.90	109.44	39.77	62.17	409
1283 001 Zrn b 01 10	207.08	7.21	125.04	46.91	74.64	246
1283 001 Zrn b 01 11	220.18	6.84	57.64	21.03	33.03	430
1283 001 Zrn b 01 12	223.09	5.39	105.08	39.44	62.84	316
1283 001 Zrn b 01 13	231.05	74.39	109.79	46.69	80.74	452
1283 001 Zrn b 01 14	434.27	11.99	132.78	46.31	70.73	348
1283 001 Zrn b 01 15	1527.77	27.31	170.16	61.55	95.73	164
1283 001 Zrn b 01 16	212.44	6.62	65.43	24.31	38.56	570
1283 001 Zrn b 01 17	219.08	7.82	135.93	48.90	75.92	238
1283 001 Zrn b 01 18	226.97	6.83	137.26	47.10	71.32	368
1283 001 Zrn b 01 19	1110.22	26.43	109.20	39.85	62.46	268
1283 001 Zrn b 01 20	236.77	7.92	119.86	42.67	65.91	252
1283 001 Zrn b 01 21	214.20	8.16	122.51	44.52	69.57	386
1283 001 Zrn b 01 22	209.70	6.12	88.29	31.51	48.80	375
1283 001 Zrn b 01 23	219.84	6.79	100.65	35.27	54.06	460
1283 001 Zrn b 01 24	224.36	8.35	87.13	30.47	46.68	654
1283 001 Zrn b 01 25	218.60	6.27	110.58	39.24	60.53	369
1283 001 Zrn b 01 26	217.58	9.44	98.23	34.07	51.96	249
1283 001 Zrn b 01 27	467.21	12.08	110.56	37.94	57.52	345
1283 001 Zrn b 01 28	226.65	6.75	76.30	26.86	41.31	646
1283 001 Zrn b 01 29	221.69	8.72	56.82	20.32	31.55	773
1283 001 Zrn b 01 30	231.20	10.31	59.75	20.45	31.01	355

b) Sample CH-08

Analysis Name	UPb age (Ma)	2 sigma (Ma)	FT age (Ma)	95%-CI(Ma)	95%+CI(Ma)	[U] (ppm)
1283 003 Zrn b 01 1	210.79	12.73	58.68	21.32	33.40	562
1283 003 Zrn b 01 2	205.47	8.15	116.33	40.72	62.36	328
1283 003 Zrn b 01 3	216.08	6.71	92.52	32.61	50.16	456
1283 003 Zrn b 01 4	225.40	6.72	56.51	21.39	34.32	754

c) Sample CH-10

Analysis Name	UPb age (Ma)	2 sigma (Ma)	FT Age (Ma)	95%-CI(Ma)	95%+CI(Ma)	[U] (ppm)
1283 005 Zrn b 01 1	213.00	15.17	88.72	33.25	52.97	631
1283 005 Zrn b 01 2	227.33	7.93	67.09	25.51	41.02	549
1283 005 Zrn b 01 3	217.15	6.21	99.54	35.94	55.99	348
1283 005 Zrn b 01 4	208.66	34.54	53.60	18.58	28.37	397

APPENDIX D

APATITE FISSION TRACK LENGTH DATA

a) Sample CH-06

Spot Name	Spot Index	Track	Length (μm)	Angle to c	UPb Age (Ma)	2 sigma (Ma)	Dpar (μm)	Dper (μm)
1283_001_Ap_a_2_1	1	1	12.35	43.47	238.15	30.69	1.84	0.35
1283_001_Ap_a_2_1	1	2	12.12	44.11	238.15	30.69	1.84	0.35
1283_001_Ap_a_2_1	1	3	15.00	49.90	238.15	30.69	1.84	0.35
1283_001_Ap_a_2_1	1	4	11.33	79.45	238.15	30.69	1.84	0.35
1283_001_Ap_a_2_1	1	5	11.27	63.40	238.15	30.69	1.84	0.35
1283_001_Ap_a_2_1	1	6	7.25	87.70	238.15	30.69	1.84	0.35
1283_001_Ap_a_2_1	1	7	13.13	30.69	238.15	30.69	1.84	0.35
1283_001_Ap_a_2_1	1	8	12.73	74.49	238.15	30.69	1.84	0.35
1283_001_Ap_a_2_1	1	9	12.35	39.50	238.15	30.69	1.84	0.35
1283_001_Ap_a_2_2	2	1	12.61	56.64	0.00	0.00	2.18	0.33
1283_001_Ap_a_2_2	2	2	13.72	49.32	0.00	0.00	2.18	0.33
1283_001_Ap_a_2_2	2	3	12.89	51.80	0.00	0.00	2.18	0.33
1283_001_Ap_a_2_2	2	4	14.65	36.93	0.00	0.00	2.18	0.33
1283_001_Ap_a_2_3	3	1	13.68	34.97	235.56	33.94	1.90	0.37
1283_001_Ap_a_2_3	3	2	12.87	55.83	235.56	33.94	1.90	0.37
1283_001_Ap_a_2_3	3	3	14.99	63.97	235.56	33.94	1.90	0.37
1283_001_Ap_a_2_3	3	4	12.92	75.12	235.56	33.94	1.90	0.37
1283_001_Ap_a_2_4	4	1	14.69	73.19	232.56	41.86	1.98	0.30
1283_001_Ap_a_2_4	4	2	16.60	28.68	232.56	41.86	1.98	0.30
1283_001_Ap_a_2_4	4	3	14.25	24.64	232.56	41.86	1.98	0.30
1283_001_Ap_a_2_4	4	4	12.11	64.36	232.56	41.86	1.98	0.30
1283_001_Ap_a_2_4	4	5	13.26	25.65	232.56	41.86	1.98	0.30
1283_001_Ap_a_2_5	5	1	12.34	80.48	238.39	28.92	2.12	0.35
1283_001_Ap_a_2_5	5	2	11.45	45.70	238.39	28.92	2.12	0.35
1283_001_Ap_a_2_5	5	3	13.19	48.90	238.39	28.92	2.12	0.35
1283_001_Ap_a_2_5	5	4	15.01	12.08	238.39	28.92	2.12	0.35
1283_001_Ap_a_2_6	6	1	12.33	49.35	236.81	37.46	2.21	0.31

1283_001_Ap_a_2_6	6	2	11.93	72.65	236.81	37.46	2.21	0.31
1283_001_Ap_a_2_6	6	3	14.22	69.87	236.81	37.46	2.21	0.31
1283_001_Ap_a_2_6	6	4	14.20	48.81	236.81	37.46	2.21	0.31
1283_001_Ap_a_2_6	6	5	12.85	32.92	236.81	37.46	2.21	0.31
1283_001_Ap_a_2_6	6	6	8.71	31.18	236.81	37.46	2.21	0.31
1283_001_Ap_a_2_6	6	7	11.34	53.12	236.81	37.46	2.21	0.31
1283_001_Ap_a_2_7	7	1	14.98	89.28	240.44	23.80	2.05	0.35
1283_001_Ap_a_2_7	7	2	13.78	60.18	240.44	23.80	2.05	0.35
1283_001_Ap_a_2_7	7	3	12.95	56.84	240.44	23.80	2.05	0.35
1283_001_Ap_a_2_7	7	4	12.13	66.14	240.44	23.80	2.05	0.35
1283_001_Ap_a_2_7	7	5	15.03	41.64	240.44	23.80	2.05	0.35
1283_001_Ap_a_2_7	7	6	16.24	67.98	240.44	23.80	2.05	0.35
1283_001_Ap_a_2_7	7	7	13.66	82.63	240.44	23.80	2.05	0.35
1283_001_Ap_a_2_8	8	1	13.57	35.53	282.26	70.32	1.95	0.42
1283_001_Ap_a_2_8	8	2	13.46	84.72	282.26	70.32	1.95	0.42
1283_001_Ap_a_2_8	8	3	10.16	59.47	282.26	70.32	1.95	0.42
1283_001_Ap_a_2_9	9	1	15.39	32.85	229.70	37.51	1.76	0.40
1283_001_Ap_a_2_9	9	2	10.37	31.64	229.70	37.51	1.76	0.40
1283_001_Ap_a_2_9	9	3	11.06	17.79	229.70	37.51	1.76	0.40
1283_001_Ap_a_2_9	9	4	11.04	84.96	229.70	37.51	1.76	0.40
1283_001_Ap_a_2_10	10	1	12.09	74.93	229.33	30.39	2.17	0.34
1283_001_Ap_a_2_10	10	2	13.48	51.41	229.33	30.39	2.17	0.34
1283_001_Ap_a_2_10	10	3	11.95	68.13	229.33	30.39	2.17	0.34
1283_001_Ap_a_2_10	10	4	11.65	80.19	229.33	30.39	2.17	0.34
1283_001_Ap_a_2_10	10	5	13.95	30.11	229.33	30.39	2.17	0.34
1283_001_Ap_a_2_10	10	6	13.68	51.64	229.33	30.39	2.17	0.34
1283_001_Ap_a_2_11	11	1	15.15	54.41	264.00	50.36	1.81	0.34
1283_001_Ap_a_2_11	11	2	14.38	56.98	264.00	50.36	1.81	0.34
1283_001_Ap_a_2_11	11	3	14.66	41.78	264.00	50.36	1.81	0.34
1283_001_Ap_a_2_12	12	1	12.30	73.93	244.36	31.68	2.07	0.36

1283_001_Ap_a_2_13	13	1	12.65	43.72	240.30	36.95	2.06	0.36
1283_001_Ap_a_2_14	14	1	11.36	77.27	233.59	37.45	2.15	0.35
1283_001_Ap_a_2_14	14	2	15.16	48.10	233.59	37.45	2.15	0.35
1283_001_Ap_a_2_14	14	3	11.36	49.76	233.59	37.45	2.15	0.35
1283_001_Ap_a_2_14	14	4	11.77	69.99	233.59	37.45	2.15	0.35
1283_001_Ap_a_2_14	14	5	12.25	51.24	233.59	37.45	2.15	0.35
1283_001_Ap_a_2_15	15	1	15.64	39.23	229.92	21.37	2.23	0.34
1283_001_Ap_a_2_15	15	2	12.86	42.65	229.92	21.37	2.23	0.34
1283_001_Ap_a_2_15	15	3	13.86	37.84	229.92	21.37	2.23	0.34
1283_001_Ap_a_2_15	15	4	12.90	37.47	229.92	21.37	2.23	0.34
1283_001_Ap_a_2_16	16	1	12.11	42.01	237.85	33.38	2.24	0.30
1283_001_Ap_a_2_16	16	2	8.68	71.56	237.85	33.38	2.24	0.30
1283_001_Ap_a_2_16	16	3	13.33	60.49	237.85	33.38	2.24	0.30
1283_001_Ap_a_2_17	17	1	12.29	60.69	228.38	28.01	2.37	0.47
1283_001_Ap_a_2_17	17	2	13.11	71.96	228.38	28.01	2.37	0.47
1283_001_Ap_a_2_17	17	3	14.94	33.24	228.38	28.01	2.37	0.47
1283_001_Ap_a_2_17	17	4	11.54	70.68	228.38	28.01	2.37	0.47
1283_001_Ap_a_2_17	17	5	12.60	57.83	228.38	28.01	2.37	0.47
1283_001_Ap_a_2_18	18	1	14.48	59.06	240.63	65.43	1.84	0.30
1283_001_Ap_a_2_18	18	2	12.29	49.83	240.63	65.43	1.84	0.30
1283_001_Ap_a_2_19	19	1	13.93	38.27	278.60	57.84	2.20	0.41
1283_001_Ap_a_2_19	19	2	14.58	32.43	278.60	57.84	2.20	0.41
1283_001_Ap_a_2_19	19	3	13.75	71.91	278.60	57.84	2.20	0.41
1283_001_Ap_a_2_19	19	4	14.13	32.08	278.60	57.84	2.20	0.41
1283_001_Ap_a_2_20	20	1	15.81	55.45	225.07	23.62	2.28	0.27
1283_001_Ap_a_2_20	20	2	12.19	71.66	225.07	23.62	2.28	0.27
1283_001_Ap_a_2_20	20	3	14.12	84.02	225.07	23.62	2.28	0.27
1283_001_Ap_a_2_21	21	1	10.88	46.01	231.48	30.14	2.35	0.46
1283_001_Ap_a_2_21	21	2	12.11	35.38	231.48	30.14	2.35	0.46
1283_001_Ap_a_2_21	21	3	12.07	45.66	231.48	30.14	2.35	0.46

1283_001_Ap_a_2_21	21	4	12.82	67.42	231.48	30.14	2.35	0.46
1283_001_Ap_a_2_21	21	5	10.35	34.68	231.48	30.14	2.35	0.46
1283_001_Ap_a_2_21	21	6	14.17	60.05	231.48	30.14	2.35	0.46
1283_001_Ap_a_2_21	21	7	12.12	71.15	231.48	30.14	2.35	0.46
1283_001_Ap_a_2_21	21	8	15.54	37.09	231.48	30.14	2.35	0.46
1283_001_Ap_a_2_22	22	1	15.78	69.27	256.62	50.60	2.10	0.29
1283_001_Ap_a_2_23	23	1	13.23	41.97	229.91	46.65	2.10	0.34
1283_001_Ap_a_2_23	23	2	13.51	43.98	229.91	46.65	2.10	0.34
1283_001_Ap_a_2_23	23	3	15.64	68.45	229.91	46.65	2.10	0.34
1283_001_Ap_a_2_23	23	4	11.60	38.86	229.91	46.65	2.10	0.34
1283_001_Ap_a_2_23	23	5	14.29	75.53	229.91	46.65	2.10	0.34
1283_001_Ap_a_2_23	23	6	14.21	34.86	229.91	46.65	2.10	0.34
1283_001_Ap_a_2_23	23	7	13.23	52.28	229.91	46.65	2.10	0.34
1283_001_Ap_a_2_23	23	8	11.83	67.64	229.91	46.65	2.10	0.34
1283_001_Ap_a_2_23	23	9	15.66	73.00	229.91	46.65	2.10	0.34
1283_001_Ap_a_2_23	23	10	13.60	55.60	229.91	46.65	2.10	0.34
1283_001_Ap_a_2_24	24	1	14.56	64.55	235.31	33.02	2.07	0.44
1283_001_Ap_a_2_24	24	2	15.31	57.73	235.31	33.02	2.07	0.44
1283_001_Ap_a_2_24	24	3	14.39	52.94	235.31	33.02	2.07	0.44
1283_001_Ap_a_2_25	25	1	13.28	45.74	251.22	61.84	1.93	0.36
1283_001_Ap_a_2_25	25	2	13.18	56.07	251.22	61.84	1.93	0.36
1283_001_Ap_a_2_25	25	3	14.16	58.85	251.22	61.84	1.93	0.36
1283_001_Ap_a_2_25	25	4	15.86	22.97	251.22	61.84	1.93	0.36
1283_001_Ap_a_2_25	25	5	12.26	41.06	251.22	61.84	1.93	0.36
1283_001_Ap_a_2_26	26	1	12.14	70.94	254.41	43.89	1.93	0.29
1283_001_Ap_a_2_26	26	2	14.91	35.72	254.41	43.89	1.93	0.29
1283_001_Ap_a_2_26	26	3	12.72	72.78	254.41	43.89	1.93	0.29
1283_001_Ap_a_2_27	27	1	11.71	77.79	225.83	33.74	2.08	0.35
1283_001_Ap_a_2_27	27	2	14.19	65.65	225.83	33.74	2.08	0.35
1283_001_Ap_a_2_28	28	1	15.38	54.79	249.16	31.77	2.06	0.35

1283_001_Ap_a_2_28	28	2	13.98	40.97	249.16	31.77	2.06	0.35
1283_001_Ap_a_2_28	28	3	13.04	56.26	249.16	31.77	2.06	0.35
1283_001_Ap_a_2_28	28	4	12.79	72.09	249.16	31.77	2.06	0.35
1283_001_Ap_a_2_29	29	1	13.06	55.41	225.08	24.17	1.93	0.40
1283_001_Ap_a_2_29	29	2	13.42	29.23	225.08	24.17	1.93	0.40
1283_001_Ap_a_2_29	29	3	15.08	65.78	225.08	24.17	1.93	0.40
1283_001_Ap_a_2_29	29	4	12.48	83.76	225.08	24.17	1.93	0.40
1283_001_Ap_a_2_29	29	5	13.85	32.52	225.08	24.17	1.93	0.40
1283_001_Ap_a_2_29	29	6	15.52	42.03	225.08	24.17	1.93	0.40
1283_001_Ap_a_2_30	30	1	14.45	76.53	245.02	40.88	2.18	0.42
1283_001_Ap_a_2_30	30	2	10.73	77.24	245.02	40.88	2.18	0.42
1283_001_Ap_a_2_30	30	3	13.40	47.04	245.02	40.88	2.18	0.42
1283_001_Ap_a_2_30	30	4	13.11	42.74	245.02	40.88	2.18	0.42
1283_001_Ap_a_2_30	30	5	15.51	41.27	245.02	40.88	2.18	0.42
1283_001_Ap_a_2_31	31	1	11.79	71.00	229.94	56.49	1.99	0.28
1283_001_Ap_a_2_31	31	2	10.56	71.09	229.94	56.49	1.99	0.28
1283_001_Ap_a_2_32	32	1	14.26	36.66	223.04	34.37	1.83	0.41
1283_001_Ap_a_2_32	32	2	14.84	34.43	223.04	34.37	1.83	0.41
1283_001_Ap_a_2_32	32	3	14.58	34.42	223.04	34.37	1.83	0.41
1283_001_Ap_a_2_32	32	4	14.69	76.80	223.04	34.37	1.83	0.41
1283_001_Ap_a_2_32	32	5	14.72	66.62	223.04	34.37	1.83	0.41
1283_001_Ap_a_2_33	33	1	11.20	46.14	249.78	28.93	1.90	0.33
1283_001_Ap_a_2_33	33	2	12.31	67.23	249.78	28.93	1.90	0.33
1283_001_Ap_a_2_33	33	3	16.05	41.25	249.78	28.93	1.90	0.33
1283_001_Ap_a_2_33	33	4	14.86	49.74	249.78	28.93	1.90	0.33
1283_001_Ap_a_2_33	33	5	13.16	44.90	249.78	28.93	1.90	0.33
1283_001_Ap_a_2_33	33	6	11.43	88.12	249.78	28.93	1.90	0.33
1283_001_Ap_a_2_33	33	7	14.45	39.23	249.78	28.93	1.90	0.33
1283_001_Ap_a_2_34	34	1	14.73	22.95	239.31	39.54	2.16	0.37
1283_001_Ap_a_2_34	34	2	14.25	42.12	239.31	39.54	2.16	0.37

1283 001 Ap a 2 34	34	3	13.53	68.99	239.31	39.54	2.16	0.37
1283 001 Ap a 2 34	34	4	13.48	60.12	239.31	39.54	2.16	0.37
1283 001 Ap a 2 35	35	1	15.68	35.54	250.70	36.77	2.19	0.37
1283 001 Ap a 2 35	35	2	13.26	70.44	250.70	36.77	2.19	0.37
1283 001 Ap a 2 35	35	3	13.65	43.03	250.70	36.77	2.19	0.37
1283 001 Ap a 2 35	35	4	15.39	32.94	250.70	36.77	2.19	0.37
1283 001 Ap a 2 35	35	5	13.82	73.65	250.70	36.77	2.19	0.37
1283 001 Ap a 2 35	35	6	14.97	41.93	250.70	36.77	2.19	0.37
1283 001 Ap a 2 35	35	7	13.17	37.93	250.70	36.77	2.19	0.37
1283 001 Ap a 2 35	35	8	12.18	75.04	250.70	36.77	2.19	0.37
1283 001 Ap a 2 36	36	1	14.58	45.58	239.19	34.22	1.95	0.30
1283 001 Ap a 2 36	36	2	11.99	55.27	239.19	34.22	1.95	0.30
1283 001 Ap a 2 36	36	3	12.48	63.87	239.19	34.22	1.95	0.30
1283 001 Ap a 2 36	36	4	14.28	81.08	239.19	34.22	1.95	0.30
1283 001 Ap a 2 36	36	5	12.55	30.33	239.19	34.22	1.95	0.30
1283 001 Ap a 2 37	37	1	15.21	67.13	241.76	35.31	2.05	0.36
1283 001 Ap a 2 37	37	2	15.54	7.24	241.76	35.31	2.05	0.36
1283 001 Ap a 2 37	37	3	13.35	73.08	241.76	35.31	2.05	0.36
1283 001 Ap a 2 38	38	1	13.93	46.87	240.71	44.42	1.95	0.36
1283 001 Ap a 2 38	38	2	13.40	53.53	240.71	44.42	1.95	0.36
1283 001 Ap a 2 38	38	3	15.19	34.27	240.71	44.42	1.95	0.36
1283 001 Ap a 2 38	38	4	13.07	30.28	240.71	44.42	1.95	0.36
1283 001 Ap a 2 38	38	5	13.43	68.04	240.71	44.42	1.95	0.36
1283 001 Ap a 2 38	38	6	13.27	42.63	240.71	44.42	1.95	0.36
1283 001 Ap a 2 39	39	1	10.70	74.32	227.14	30.75	2.24	0.34
1283 001 Ap a 2 39	39	2	12.47	20.24	227.14	30.75	2.24	0.34
1283 001 Ap a 2 39	39	3	13.05	46.41	227.14	30.75	2.24	0.34
1283 001 Ap a 2 39	39	4	12.70	65.68	227.14	30.75	2.24	0.34
1283 001 Ap a 2 39	39	5	12.79	56.34	227.14	30.75	2.24	0.34
1283 001 Ap a 2 39	39	6	13.97	33.91	227.14	30.75	2.24	0.34

1283_001_Ap_a_2_39	39	7	16.51	32.58	227.14	30.75	2.24	0.34
1283_001_Ap_a_2_39	39	8	14.90	54.42	227.14	30.75	2.24	0.34
1283_001_Ap_a_2_39	39	9	14.22	40.66	227.14	30.75	2.24	0.34
1283_001_Ap_a_2_39	39	10	14.50	50.25	227.14	30.75	2.24	0.34
1283_001_Ap_a_2_39	39	11	15.18	38.19	227.14	30.75	2.24	0.34
1283_001_Ap_a_2_40	40	1	14.29	53.11	253.50	23.12	2.11	0.28
1283_001_Ap_a_2_40	40	2	11.99	65.45	253.50	23.12	2.11	0.28
1283_001_Ap_a_2_40	40	3	15.13	41.38	253.50	23.12	2.11	0.28
1283_001_Ap_a_2_40	40	4	14.33	38.25	253.50	23.12	2.11	0.28
1283_001_Ap_a_2_40	40	5	11.39	59.77	253.50	23.12	2.11	0.28
1283_001_Ap_a_2_40	40	6	12.18	57.03	253.50	23.12	2.11	0.28
1283_001_Ap_a_2_40	40	7	14.55	22.57	253.50	23.12	2.11	0.28
1283_001_Ap_a_2_40	40	8	13.41	49.81	253.50	23.12	2.11	0.28
1283_001_Ap_a_2_41	41	1	16.40	24.79	242.26	45.60	1.90	0.33
1283_001_Ap_a_2_41	41	2	12.00	85.19	242.26	45.60	1.90	0.33
1283_001_Ap_a_2_41	41	3	11.55	48.73	242.26	45.60	1.90	0.33
1283_001_Ap_a_2_41	41	4	12.69	44.16	242.26	45.60	1.90	0.33
1283_001_Ap_a_2_41	41	5	13.62	53.99	242.26	45.60	1.90	0.33
1283_001_Ap_a_2_41	41	6	15.12	27.90	242.26	45.60	1.90	0.33
1283_001_Ap_a_2_41	41	7	13.78	81.96	242.26	45.60	1.90	0.33
1283_001_Ap_a_2_41	41	8	12.63	68.73	242.26	45.60	1.90	0.33
1283_001_Ap_a_2_42	42	1	12.69	85.05	245.39	43.97	1.83	0.33
1283_001_Ap_a_2_42	42	2	12.03	51.53	245.39	43.97	1.83	0.33
1283_001_Ap_a_2_42	42	3	10.80	89.21	245.39	43.97	1.83	0.33
1283_001_Ap_a_2_42	42	4	15.42	7.75	245.39	43.97	1.83	0.33
1283_001_Ap_a_2_42	42	5	12.54	44.71	245.39	43.97	1.83	0.33
1283_001_Ap_a_2_42	42	6	16.06	37.23	245.39	43.97	1.83	0.33

b) Sample CH-07

Spot Name	Spot Idex	Track	Length (µm)	Angle to c	UPb Age (Ma)	2 sigma (Ma)	Dpar (µm)	Dper (µm)
1283 002 Ap a 2 1	1	1	15.76	80.43	228.12	30.73	1.85	0.35
1283 002 Ap a 2 1	1	2	12.87	42.59	228.12	30.73	1.85	0.35
1283 002 Ap a 2 2	2	1	14.71	52.68	237.52	46.83	1.83	0.32
1283 002 Ap a 2 2	2	2	13.41	81.52	237.52	46.83	1.83	0.32
1283 002 Ap a 2 2	2	3	12.64	83.53	237.52	46.83	1.83	0.32
1283 002 Ap a 2 2	2	4	12.00	44.56	237.52	46.83	1.83	0.32
1283 002 Ap a 2 2	2	5	12.14	38.97	237.52	46.83	1.83	0.32
1283 002 Ap a 2 3	3	1	13.90	62.82	244.96	40.17	2.07	0.35
1283 002 Ap a 2 3	3	2	14.73	34.18	244.96	40.17	2.07	0.35
1283 002 Ap a 2 3	3	3	14.00	27.59	244.96	40.17	2.07	0.35
1283 002 Ap a 2 4	4	1	11.53	64.71	0.00	0.00	1.77	0.37
1283 002 Ap a 2 4	4	2	13.61	68.09	0.00	0.00	1.77	0.37
1283 002 Ap a 2 5	5	1	14.12	60.77	239.79	57.23	2.06	0.34
1283 002 Ap a 2 5	5	2	11.99	36.16	239.79	57.23	2.06	0.34
1283 002 Ap a 2 5	5	3	11.52	41.29	239.79	57.23	2.06	0.34
1283 002 Ap a 2 6	6	1	11.89	83.85	272.15	61.67	1.81	0.37
1283 002 Ap a 2 7	7	1	14.37	48.79	254.56	38.96	2.05	0.26
1283 002 Ap a 2 7	7	2	14.16	37.70	254.56	38.96	2.05	0.26
1283 002 Ap a 2 7	7	3	13.11	35.29	254.56	38.96	2.05	0.26
1283 002 Ap a 2 8	8	1	11.95	56.14	234.92	29.88	2.16	0.31
1283 002 Ap a 2 8	8	2	9.38	50.14	234.92	29.88	2.16	0.31
1283 002 Ap a 2 9	9	1	11.83	54.77	229.59	24.67	1.99	0.40
1283 002 Ap a 2 9	9	2	14.65	58.95	229.59	24.67	1.99	0.40
1283 002 Ap a 2 9	9	3	13.83	52.52	229.59	24.67	1.99	0.40
1283 002 Ap a 2 9	9	4	12.16	60.50	229.59	24.67	1.99	0.40
1283 002 Ap a 2 9	9	5	10.42	75.52	229.59	24.67	1.99	0.40
1283 002 Ap a 2 9	9	6	14.59	67.42	229.59	24.67	1.99	0.40
1283 002 Ap a 2 9	9	7	13.36	48.13	229.59	24.67	1.99	0.40
1283 002 Ap a 2 9	9	8	9.07	59.83	229.59	24.67	1.99	0.40
1283 002 Ap a 2 10	10	1	11.52	44.87	239.07	54.75	1.70	0.23
1283 002 Ap a 2 10	10	2	14.60	16.88	239.07	54.75	1.70	0.23
1283 002 Ap a 2 10	10	3	12.68	59.61	239.07	54.75	1.70	0.23
1283 002 Ap a 2 10	10	4	12.61	40.67	239.07	54.75	1.70	0.23
1283 002 Ap a 2 10	10	5	13.85	48.88	239.07	54.75	1.70	0.23
1283 002 Ap a 2 10	10	6	14.62	53.25	239.07	54.75	1.70	0.23

1283 002 Ap a 2 10	10	7	16.05	47.41	239.07	54.75	1.70	0.23
1283 002 Ap a 2 10	10	8	15.09	52.03	239.07	54.75	1.70	0.23
1283 002 Ap a 2 11	11	1	15.56	40.36	1736.52	#####	1.83	0.33
1283 002 Ap a 2 12	12	1	12.22	37.54	229.46	28.36	1.90	0.35
1283 002 Ap a 2 12	12	2	13.74	47.86	229.46	28.36	1.90	0.35
1283 002 Ap a 2 13	13	1	14.86	52.72	239.57	51.84	1.87	0.35
1283 002 Ap a 2 13	13	2	14.92	45.25	239.57	51.84	1.87	0.35
1283 002 Ap a 2 13	13	3	12.04	68.92	239.57	51.84	1.87	0.35
1283 002 Ap a 2 13	13	4	12.42	67.50	239.57	51.84	1.87	0.35
1283 002 Ap a 2 13	13	5	14.58	60.52	239.57	51.84	1.87	0.35
1283 002 Ap a 2 14	14	1	11.28	62.81	0.00	0.00	2.02	0.30
1283 002 Ap a 2 14	14	2	14.06	52.54	0.00	0.00	2.02	0.30
1283 002 Ap a 2 14	14	3	13.03	47.24	0.00	0.00	2.02	0.30
1283 002 Ap a 2 14	14	4	9.39	84.81	0.00	0.00	2.02	0.30
1283 002 Ap a 2 14	14	5	11.92	40.21	0.00	0.00	2.02	0.30
1283 002 Ap a 2 15	15	1	13.45	77.69	235.47	33.38	1.82	0.27
1283 002 Ap a 2 15	15	2	14.24	82.24	235.47	33.38	1.82	0.27
1283 002 Ap a 2 15	15	3	12.44	54.13	235.47	33.38	1.82	0.27
1283 002 Ap a 2 16	16	1	14.49	36.84	236.86	40.75	1.69	0.32
1283 002 Ap a 2 16	16	2	14.27	79.04	236.86	40.75	1.69	0.32
1283 002 Ap a 2 16	16	3	10.74	61.28	236.86	40.75	1.69	0.32
1283 002 Ap a 2 17	17	1	14.74	85.62	236.86	57.64	1.83	0.33
1283 002 Ap a 2 17	17	2	12.63	60.09	236.86	57.64	1.83	0.33
1283 002 Ap a 2 18	18	1	15.53	50.91	243.02	45.46	2.16	0.25
1283 002 Ap a 2 18	18	2	11.81	64.74	243.02	45.46	2.16	0.25
1283 002 Ap a 2 18	18	3	12.46	83.17	243.02	45.46	2.16	0.25
1283 002 Ap a 2 19	19	1	12.99	62.92	238.22	70.89	1.99	0.35
1283 002 Ap a 2 19	19	2	15.39	58.43	238.22	70.89	1.99	0.35
1283 002 Ap a 2 20	20	1	17.25	34.92	244.64	58.38	1.74	0.33
1283 002 Ap a 2 20	20	2	12.34	36.08	244.64	58.38	1.74	0.33
1283 002 Ap a 2 20	20	3	12.85	43.86	244.64	58.38	1.74	0.33
1283 002 Ap a 2 20	20	4	11.24	36.39	244.64	58.38	1.74	0.33
1283 002 Ap a 2 20	20	5	10.87	52.33	244.64	58.38	1.74	0.33
1283 002 Ap a 2 20	20	6	15.86	42.08	244.64	58.38	1.74	0.33
1283 002 Ap a 2 20	20	7	14.67	30.53	244.64	58.38	1.74	0.33
1283 002 Ap a 2 20	20	8	15.24	69.72	244.64	58.38	1.74	0.33
1283 002 Ap a 2 21	21	1	14.11	55.93	219.77	42.64	2.00	0.37
1283 002 Ap a 2 21	21	2	15.32	33.76	219.77	42.64	2.00	0.37

1283 002 Ap a 2 22	22	1	10.52	74.02	228.78	28.56	2.17	0.35
1283 002 Ap a 2 22	22	2	12.67	48.90	228.78	28.56	2.17	0.35
1283 002 Ap a 2 22	22	3	15.85	46.89	228.78	28.56	2.17	0.35
1283 002 Ap a 2 22	22	4	16.19	55.22	228.78	28.56	2.17	0.35
1283 002 Ap a 2 23	23	1	13.06	75.19	222.28	40.35	1.80	0.26
1283 002 Ap a 2 23	23	2	15.17	25.64	222.28	40.35	1.80	0.26
1283 002 Ap a 2 23	23	3	14.58	48.77	222.28	40.35	1.80	0.26
1283 002 Ap a 2 24	24	1	12.32	42.22	236.26	76.26	2.04	0.41
1283 002 Ap a 2 24	24	2	14.30	42.50	236.26	76.26	2.04	0.41
1283 002 Ap a 2 24	24	3	13.49	79.12	236.26	76.26	2.04	0.41
1283 002 Ap a 2 24	24	4	15.13	35.88	236.26	76.26	2.04	0.41
1283 002 Ap a 2 24	24	5	13.95	69.03	236.26	76.26	2.04	0.41
1283 002 Ap a 2 24	24	6	12.71	36.36	236.26	76.26	2.04	0.41
1283 002 Ap a 2 24	24	7	12.36	34.79	236.26	76.26	2.04	0.41
1283 002 Ap a 2 25	25	1	14.03	56.06	221.08	38.34	1.71	0.24
1283 002 Ap a 2 25	25	2	13.71	68.02	221.08	38.34	1.71	0.24
1283 002 Ap a 2 25	25	3	13.39	51.32	221.08	38.34	1.71	0.24
1283 002 Ap a 2 26	26	1	12.52	40.11	224.65	29.96	1.80	0.35
1283 002 Ap a 2 26	26	2	10.40	75.52	224.65	29.96	1.80	0.35
1283 002 Ap a 2 26	26	3	14.55	56.15	224.65	29.96	1.80	0.35
1283 002 Ap a 2 26	26	4	11.68	48.01	224.65	29.96	1.80	0.35
1283 002 Ap a 2 27	27	1	14.11	40.89	260.75	59.32	2.03	0.41
1283 002 Ap a 2 27	27	2	12.87	68.09	260.75	59.32	2.03	0.41
1283 002 Ap a 2 28	28	1	12.21	85.05	220.27	39.66	2.12	0.30
1283 002 Ap a 2 28	28	2	15.64	53.32	220.27	39.66	2.12	0.30
1283 002 Ap a 2 28	28	3	14.81	76.96	220.27	39.66	2.12	0.30
1283 002 Ap a 2 29	29	1	11.42	62.59	232.43	40.05	1.88	0.28
1283 002 Ap a 2 29	29	2	12.88	60.77	232.43	40.05	1.88	0.28
1283 002 Ap a 2 29	29	3	13.74	56.92	232.43	40.05	1.88	0.28
1283 002 Ap a 2 30	30	1	14.01	51.15	247.88	36.27	1.96	0.32
1283 002 Ap a 2 30	30	2	13.99	72.64	247.88	36.27	1.96	0.32
1283 002 Ap a 2 30	30	3	13.23	87.88	247.88	36.27	1.96	0.32
1283 002 Ap a 2 30	30	4	12.81	57.46	247.88	36.27	1.96	0.32
1283 002 Ap a 2 31	31	1	12.46	78.62	210.70	22.52	1.67	0.31
1283 002 Ap a 2 31	31	2	12.83	51.08	210.70	22.52	1.67	0.31
1283 002 Ap a 2 31	31	3	12.08	56.44	210.70	22.52	1.67	0.31
1283 002 Ap a 2 31	31	4	13.28	38.66	210.70	22.52	1.67	0.31
1283 002 Ap a 2 31	31	5	14.06	33.14	210.70	22.52	1.67	0.31

1283_002_Ap_a_2_31	31	6	12.92	61.08	210.70	22.52	1.67	0.31
1283_002_Ap_a_2_31	31	7	14.01	68.00	210.70	22.52	1.67	0.31
1283_002_Ap_a_2_31	31	8	12.67	46.07	210.70	22.52	1.67	0.31
1283_002_Ap_a_2_32	32	1	11.18	45.93	444.33	665.97	1.95	0.30
1283_002_Ap_a_2_33	33	1	12.01	48.58	252.59	45.26	1.92	0.32
1283_002_Ap_a_2_33	33	2	15.68	71.71	252.59	45.26	1.92	0.32
1283_002_Ap_a_2_33	33	3	13.59	61.45	252.59	45.26	1.92	0.32
1283_002_Ap_a_2_33	33	4	11.70	51.62	252.59	45.26	1.92	0.32
1283_002_Ap_a_2_33	33	5	13.46	43.49	252.59	45.26	1.92	0.32
1283_002_Ap_a_2_33	33	6	13.78	56.75	252.59	45.26	1.92	0.32
1283_002_Ap_a_2_33	33	7	14.36	19.51	252.59	45.26	1.92	0.32
1283_002_Ap_a_2_33	33	8	12.51	61.94	252.59	45.26	1.92	0.32
1283_002_Ap_a_2_34	34	1	14.27	43.26	232.49	74.22	2.05	0.31
1283_002_Ap_a_2_34	34	2	11.96	68.57	232.49	74.22	2.05	0.31
1283_002_Ap_a_2_34	34	3	12.15	51.14	232.49	74.22	2.05	0.31
1283_002_Ap_a_2_35	35	1	12.98	84.92	231.51	32.34	2.15	0.24
1283_002_Ap_a_2_36	36	1	8.51	76.96	214.50	38.79	1.87	0.31
1283_002_Ap_a_2_36	36	2	12.51	72.83	214.50	38.79	1.87	0.31
1283_002_Ap_a_2_37	37	1	12.63	80.93	215.22	19.48	2.14	0.36
1283_002_Ap_a_2_37	37	2	10.19	78.26	215.22	19.48	2.14	0.36
1283_002_Ap_a_2_37	37	3	13.36	33.72	215.22	19.48	2.14	0.36
1283_002_Ap_a_2_37	37	4	10.77	50.11	215.22	19.48	2.14	0.36
1283_002_Ap_a_2_37	37	5	14.00	38.25	215.22	19.48	2.14	0.36
1283_002_Ap_a_2_37	37	6	12.80	44.67	215.22	19.48	2.14	0.36
1283_002_Ap_a_2_38	38	1	12.73	39.72	212.33	26.71	2.05	0.35
1283_002_Ap_a_2_38	38	2	16.24	46.21	212.33	26.71	2.05	0.35
1283_002_Ap_a_2_38	38	3	16.59	41.75	212.33	26.71	2.05	0.35
1283_002_Ap_a_2_38	38	4	12.42	61.65	212.33	26.71	2.05	0.35
1283_002_Ap_a_2_38	38	5	13.51	47.57	212.33	26.71	2.05	0.35
1283_002_Ap_a_2_38	38	6	12.95	83.28	212.33	26.71	2.05	0.35
1283_002_Ap_a_2_38	38	7	16.52	36.38	212.33	26.71	2.05	0.35
1283_002_Ap_a_2_39	39	1	17.10	41.76	187.83	51.06	2.05	0.36
1283_002_Ap_a_2_39	39	2	12.62	33.80	187.83	51.06	2.05	0.36
1283_002_Ap_a_2_40	40	1	13.77	63.94	260.10	139.11	1.96	0.35
1283_002_Ap_a_2_40	40	2	12.01	61.13	260.10	139.11	1.96	0.35
1283_002_Ap_a_2_41	41	1	14.14	57.94	221.04	31.05	1.74	0.33
1283_002_Ap_a_2_41	41	2	13.60	44.36	221.04	31.05	1.74	0.33
1283_002_Ap_a_2_41	41	3	14.90	37.52	221.04	31.05	1.74	0.33

1283_002_Ap_a_2_41	41	4	13.95	61.63	221.04	31.05	1.74	0.33
1283_002_Ap_a_2_41	41	5	15.86	43.43	221.04	31.05	1.74	0.33
1283_002_Ap_a_2_42	42	1	15.37	74.91	226.65	53.32	2.12	0.46
1283_002_Ap_a_2_42	42	2	12.78	60.28	226.65	53.32	2.12	0.46
1283_002_Ap_a_2_42	42	3	13.82	61.72	226.65	53.32	2.12	0.46
1283_002_Ap_a_2_42	42	4	16.33	54.64	226.65	53.32	2.12	0.46
1283_002_Ap_a_2_43	43	1	15.14	39.21	211.55	22.39	1.79	0.33
1283_002_Ap_a_2_43	43	2	13.75	49.07	211.55	22.39	1.79	0.33
1283_002_Ap_a_2_43	43	3	9.74	51.65	211.55	22.39	1.79	0.33
1283_002_Ap_a_2_44	44	1	14.75	39.38	234.28	47.90	1.85	0.37
1283_002_Ap_a_2_45	45	1	12.51	43.73	0.00	0.00	2.07	0.37
1283_002_Ap_a_2_45	45	2	8.95	45.75	0.00	0.00	2.07	0.37
1283_002_Ap_a_2_46	46	1	14.13	78.29	236.64	50.58	1.97	0.30
1283_002_Ap_a_2_46	46	2	12.84	59.44	236.64	50.58	1.97	0.30
1283_002_Ap_a_2_46	46	3	9.29	81.32	236.64	50.58	1.97	0.30
1283_002_Ap_a_2_46	46	4	11.20	39.49	236.64	50.58	1.97	0.30
1283_002_Ap_a_2_46	46	5	11.14	54.69	236.64	50.58	1.97	0.30
1283_002_Ap_a_2_47	47	1	11.32	89.28	228.12	24.13	1.89	0.33
1283_002_Ap_a_2_47	47	2	12.69	44.47	228.12	24.13	1.89	0.33
1283_002_Ap_a_2_47	47	3	12.05	60.75	228.12	24.13	1.89	0.33
1283_002_Ap_a_2_48	48	1	15.30	53.13	234.01	46.55	1.84	0.31
1283_002_Ap_a_2_48	48	2	14.31	42.95	234.01	46.55	1.84	0.31
1283_002_Ap_a_2_49	49	1	13.04	56.87	240.79	81.86	1.94	0.35
1283_002_Ap_a_2_49	49	2	12.49	48.33	240.79	81.86	1.94	0.35
1283_002_Ap_a_2_49	49	3	14.52	44.48	240.79	81.86	1.94	0.35
1283_002_Ap_a_2_49	49	4	14.08	40.65	240.79	81.86	1.94	0.35
1283_002_Ap_a_2_49	49	5	9.78	50.97	240.79	81.86	1.94	0.35
1283_002_Ap_a_2_49	49	6	11.43	40.58	240.79	81.86	1.94	0.35
1283_002_Ap_a_2_50	50	1	13.51	39.96	246.13	56.84	2.08	0.36
1283_002_Ap_a_2_50	50	2	11.54	52.52	246.13	56.84	2.08	0.36
1283_002_Ap_a_2_50	50	3	10.91	66.41	246.13	56.84	2.08	0.36
1283_002_Ap_a_2_51	51	1	12.84	84.40	220.01	30.80	1.88	0.24
1283_002_Ap_a_2_51	51	2	12.30	65.11	220.01	30.80	1.88	0.24
1283_002_Ap_a_2_52	52	1	13.84	30.60	227.61	62.11	1.90	0.31
1283_002_Ap_a_2_52	52	2	14.07	44.29	227.61	62.11	1.90	0.31
1283_002_Ap_a_2_52	52	3	13.15	75.93	227.61	62.11	1.90	0.31
1283_002_Ap_a_2_52	52	4	11.59	68.01	227.61	62.11	1.90	0.31
1283_002_Ap_a_2_52	52	5	12.21	66.63	227.61	62.11	1.90	0.31

1283 002 Ap a 2 53	53	1	12.87	80.33	214.84	41.85	1.91	0.34
1283 002 Ap a 2 53	53	2	12.17	56.04	214.84	41.85	1.91	0.34
1283 002 Ap a 2 53	53	3	14.55	58.49	214.84	41.85	1.91	0.34
1283 002 Ap a 2 53	53	4	14.38	58.40	214.84	41.85	1.91	0.34
1283 002 Ap a 2 54	54	1	11.99	62.91	246.53	59.39	2.04	0.35
1283 002 Ap a 2 54	54	2	14.94	57.17	246.53	59.39	2.04	0.35
1283 002 Ap a 2 54	54	3	14.19	37.74	246.53	59.39	2.04	0.35
1283 002 Ap a 2 54	54	4	12.89	51.50	246.53	59.39	2.04	0.35
1283 002 Ap a 2 54	54	5	16.11	29.48	246.53	59.39	2.04	0.35
1283 002 Ap a 2 55	55	1	12.39	64.62	222.07	38.21	1.70	0.36
1283 002 Ap a 2 55	55	2	14.02	84.03	222.07	38.21	1.70	0.36
1283 002 Ap a 2 55	55	3	10.90	61.83	222.07	38.21	1.70	0.36
1283 002 Ap a 2 55	55	4	14.39	55.42	222.07	38.21	1.70	0.36
1283 002 Ap a 2 55	55	5	11.89	47.03	222.07	38.21	1.70	0.36

c) Sample CH-08

Spot Name	Spot Index	Track	Length (μm)	Angle to c	UPb Age (Ma)	2 sigma (Ma)	Dpar (um)	Dper (um)
1283 003 Ap a 2 1	1	1	13.97	39.07	263.78	136.16	1.87	0.41
1283 003 Ap a 2 2	2	1	14.84	62.84	741.75	2056.33	1.99	0.39
1283 003 Ap a 2 3	3	1	14.35	6.99	0.00	0.00	1.93	0.33
1283 003 Ap a 2 4	4	1	14.62	60.03	0.00	0.00	1.67	0.33
1283 003 Ap a 2 5	5	1	9.08	86.15	439.22	219.70	2.00	0.29
1283 003 Ap a 2 5	5	2	14.16	52.25	439.22	219.70	2.00	0.29
1283 003 Ap a 2 6	6	1	10.76	71.41	309.62	162.08	2.10	0.30
1283 003 Ap a 2 7	7	1	14.73	53.36	220.25	92.32	2.12	0.32
1283 003 Ap a 2 7	7	2	12.76	42.14	220.25	92.32	2.12	0.32
1283 003 Ap a 2 7	7	3	13.24	68.31	220.25	92.32	2.12	0.32
1283 003 Ap a 2 7	7	4	8.10	65.93	220.25	92.32	2.12	0.32
1283 003 Ap a 2 7	7	5	12.90	44.66	220.25	92.32	2.12	0.32
1283 003 Ap a 2 8	8	1	11.67	46.12	272.50	105.18	1.73	0.30
1283 003 Ap a 2 9	9	1	10.56	60.70	264.71	74.72	1.89	0.27
1283 003 Ap b 2 1	1	1	10.91	48.96	263.09	114.64	1.97	0.41
1283 003 Ap b 2 2	2	1	11.30	53.98	267.93	98.90	1.86	0.28
1283 003 Ap b 2 2	2	2	13.53	28.91	267.93	98.90	1.86	0.28
1283 003 Ap b 2 2	2	3	14.26	39.59	267.93	98.90	1.86	0.28
1283 003 Ap b 2 3	3	1	12.79	26.88	235.06	74.69	1.81	0.25
1283 003 Ap b 2 4	4	1	13.84	58.69	0.00	0.00	1.64	0.29
1283 003 Ap b 2 5	5	1	11.57	54.19	226.16	91.31	2.04	0.32
1283 003 Ap b 2 6	6	1	14.00	67.94	0.00	0.00	1.72	0.30
1283 003 Ap b 2 7	7	1	14.11	55.04	906.02	1021.91	1.89	0.33
1283 003 Ap b 2 8	8	1	12.76	42.01	247.63	102.93	1.75	0.29
1283 003 Ap b 2 9	9	1	10.62	38.35	273.91	109.04	1.87	0.28
1283 003 Ap b 2 10	10	1	15.15	28.13	0.00	0.00	1.85	0.37
1283 003 Ap b 2 10	10	2	9.15	77.20	0.00	0.00	1.85	0.37
1283 003 Ap b 2 10	10	3	10.76	70.97	0.00	0.00	1.85	0.37

d) Sample CH-09

Spot Name	Spot Index	Track	Length (µm)	Angle to c	UPb Age (Ma)	2 sigma (Ma)	Dpar (µm)	Dper (µm)
1283_004_Ap_a_2_1	1	1	14.94	46.84	161.29	58.65	1.98	0.35
1283_004_Ap_a_2_1	1	2	13.68	56.14	161.29	58.65	1.98	0.35
1283_004_Ap_a_2_1	1	3	11.68	42.65	161.29	58.65	1.98	0.35
1283_004_Ap_a_2_2	2	1	14.05	66.87	147.44	94.14	1.69	0.32
1283_004_Ap_a_2_3	3	1	11.69	32.64	174.26	54.65	1.85	0.32
1283_004_Ap_a_2_4	4	1	15.07	36.31	114.74	58.26	2.02	0.29
1283_004_Ap_a_2_4	4	2	14.79	14.36	114.74	58.26	2.02	0.29
1283_004_Ap_a_2_4	4	3	13.22	55.28	114.74	58.26	2.02	0.29
1283_004_Ap_a_2_4	4	4	14.05	48.26	114.74	58.26	2.02	0.29
1283_004_Ap_a_2_4	4	5	15.62	9.11	114.74	58.26	2.02	0.29
1283_004_Ap_a_2_4	4	6	15.88	51.25	114.74	58.26	2.02	0.29
1283_004_Ap_a_2_5	5	1	12.43	46.49	181.57	62.25	1.99	0.38
1283_004_Ap_a_2_5	5	2	14.54	39.01	181.57	62.25	1.99	0.38
1283_004_Ap_a_2_5	5	3	11.49	75.46	181.57	62.25	1.99	0.38
1283_004_Ap_a_2_5	5	4	12.02	68.30	181.57	62.25	1.99	0.38
1283_004_Ap_a_2_6	6	1	11.62	71.37	135.94	45.82	2.37	0.41
1283_004_Ap_a_2_6	6	2	15.50	14.22	135.94	45.82	2.37	0.41
1283_004_Ap_a_2_7	7	1	10.89	70.85	805.99	2280.00	1.62	0.41
1283_004_Ap_a_2_8	8	1	15.23	66.66	204.22	80.10	1.78	0.36
1283_004_Ap_a_2_9	9	1	14.15	60.04	0.00	0.00	1.92	0.28
1283_004_Ap_a_2_9	9	2	15.00	79.49	0.00	0.00	1.92	0.28
1283_004_Ap_a_2_10	10	1	12.63	73.70	218.62	67.74	2.12	0.35
1283_004_Ap_a_2_11	11	1	13.52	26.16	203.62	210.46	1.94	0.32
1283_004_Ap_a_2_11	11	2	10.77	49.79	203.62	210.46	1.94	0.32
1283_004_Ap_a_2_11	11	3	11.02	75.10	203.62	210.46	1.94	0.32
1283_004_Ap_a_2_12	12	1	13.56	65.23	178.72	54.85	1.92	0.30
1283_004_Ap_a_2_12	12	2	13.56	43.71	178.72	54.85	1.92	0.30
1283_004_Ap_a_2_12	12	3	13.13	65.31	178.72	54.85	1.92	0.30
1283_004_Ap_a_2_13	13	1	12.51	25.92	139.88	79.08	1.93	0.33
1283_004_Ap_a_2_14	14	1	13.61	41.53	106.60	66.69	1.74	0.46
1283_004_Ap_a_2_15	15	1	14.85	82.70	164.39	93.99	1.78	0.37
1283_004_Ap_a_2_16	16	1	15.47	56.04	208.22	35.71	2.03	0.39
1283_004_Ap_a_2_16	16	2	12.99	58.73	208.22	35.71	2.03	0.39
1283_004_Ap_a_2_17	17	1	14.01	89.75	172.31	73.57	1.98	0.35
1283_004_Ap_a_2_18	18	1	8.99	49.88	0.00	0.00	1.96	0.34
1283_004_Ap_a_2_18	18	2	9.16	41.75	0.00	0.00	1.96	0.34
1283_004_Ap_a_2_19	19	1	11.88	80.96	157.19	127.89	1.77	0.25

1283 004 Ap a 2 19	19	2	14.68	15.05	157.19	127.89	1.77	0.25
1283 004 Ap a 2 19	19	3	14.96	9.35	157.19	127.89	1.77	0.25
1283 004 Ap a 2 20	20	1	10.06	43.12	230.66	127.43	2.36	0.38
1283 004 Ap a 2 20	20	2	14.03	31.84	230.66	127.43	2.36	0.38
1283 004 Ap a 2 20	20	3	14.05	33.19	230.66	127.43	2.36	0.38
1283 004 Ap a 2 20	20	4	13.46	39.26	230.66	127.43	2.36	0.38
1283 004 Ap a 2 20	20	5	14.44	58.57	230.66	127.43	2.36	0.38
1283 004 Ap a 2 21	21	1	15.02	60.60	198.78	109.27	2.09	0.35
1283 004 Ap a 2 21	21	2	13.72	63.60	198.78	109.27	2.09	0.35
1283 004 Ap a 2 22	22	1	14.16	78.83	179.50	59.32	1.78	0.29
1283 004 Ap a 2 23	23	1	13.43	54.49	180.57	48.97	1.60	0.35
1283 004 Ap a 2 23	23	2	14.33	50.33	180.57	48.97	1.60	0.35
1283 004 Ap a 2 23	23	3	14.84	63.54	180.57	48.97	1.60	0.35
1283 004 Ap a 2 23	23	4	13.51	33.50	180.57	48.97	1.60	0.35
1283 004 Ap a 2 23	23	5	13.43	55.28	180.57	48.97	1.60	0.35
1283 004 Ap a 2 24	24	1	11.97	71.39	176.38	82.11	2.02	0.41
1283 004 Ap a 2 24	24	2	14.22	62.81	176.38	82.11	2.02	0.41
1283 004 Ap a 2 25	25	1	10.23	53.85	180.04	156.97	1.88	0.35
1283 004 Ap a 2 26	26	1	14.41	77.19	481.70	321.51	2.00	0.36
1283 004 Ap a 2 26	26	2	12.48	60.08	481.70	321.51	2.00	0.36
1283 004 Ap a 2 27	27	1	14.88	52.91	223.11	69.93	1.87	0.33
1283 004 Ap a 2 28	28	1	14.17	32.96	101.61	91.71	1.84	0.29
1283 004 Ap a 2 28	28	2	14.67	29.59	101.61	91.71	1.84	0.29
1283 004 Ap a 2 29	29	1	15.19	52.69	155.96	67.58	2.26	0.31
1283 004 Ap a 2 30	30	1	15.21	74.15	147.76	64.02	2.36	0.30
1283 004 Ap a 2 30	30	2	14.27	27.89	147.76	64.02	2.36	0.30
1283 004 Ap a 2 30	30	3	14.06	42.11	147.76	64.02	2.36	0.30
1283 004 Ap a 2 30	30	4	14.00	81.97	147.76	64.02	2.36	0.30
1283 004 Ap a 2 30	30	5	14.30	63.56	147.76	64.02	2.36	0.30
1283 004 Ap a 2 30	30	6	14.10	37.31	147.76	64.02	2.36	0.30
1283 004 Ap a 2 30	30	7	13.97	72.95	147.76	64.02	2.36	0.30
1283 004 Ap a 2 30	30	8	12.26	41.20	147.76	64.02	2.36	0.30
1283 004 Ap a 2 31	31	1	14.06	35.36	0.00	0.00	2.01	0.35
1283 004 Ap a 2 32	32	1	15.03	70.02	195.40	170.60	1.59	0.29
1283 004 Ap a 2 33	33	1	14.50	43.24	183.05	83.84	2.04	0.36
1283 004 Ap a 2 33	33	2	14.12	42.64	183.05	83.84	2.04	0.36
1283 004 Ap a 2 34	34	1	14.14	61.74	205.71	100.30	2.09	0.36
1283 004 Ap a 2 34	34	2	12.39	51.76	205.71	100.30	2.09	0.36
1283 004 Ap a 2 34	34	3	12.66	48.03	205.71	100.30	2.09	0.36
1283 004 Ap a 2 34	34	4	11.62	64.31	205.71	100.30	2.09	0.36

1283_004_Ap_b_2_1	1	1	14.82	60.74	0.00	0.00	1.75	0.31
1283_004_Ap_b_2_2	2	1	13.45	72.08	134.36	50.59	2.00	0.36
1283_004_Ap_b_2_2	2	2	13.40	73.07	134.36	50.59	2.00	0.36
1283_004_Ap_b_2_3	3	1	14.12	27.22	202.59	68.21	2.16	0.29
1283_004_Ap_b_2_4	4	1	13.16	59.24	243.80	104.66	2.12	0.43
1283_004_Ap_b_2_5	5	1	12.38	71.80	333.22	311.42	2.01	0.37
1283_004_Ap_b_2_6	6	1	13.63	61.76	143.69	53.08	1.92	0.45
1283_004_Ap_b_2_6	6	2	14.39	23.25	143.69	53.08	1.92	0.45
1283_004_Ap_b_2_6	6	3	14.19	51.86	143.69	53.08	1.92	0.45
1283_004_Ap_b_2_7	7	1	13.75	50.03	0.00	0.00	2.22	0.45
1283_004_Ap_b_2_8	8	1	13.61	32.43	210.16	135.86	2.07	0.30
1283_004_Ap_b_2_8	8	2	13.80	34.82	210.16	135.86	2.07	0.30
1283_004_Ap_b_2_9	9	1	14.97	47.78	223.04	106.23	2.14	0.34
1283_004_Ap_b_2_9	9	2	14.08	52.95	223.04	106.23	2.14	0.34
1283_004_Ap_b_2_10	10	1	13.23	61.64	151.55	95.81	1.64	0.38
1283_004_Ap_b_2_10	10	2	14.93	28.22	151.55	95.81	1.64	0.38
1283_004_Ap_b_2_11	11	1	13.87	30.13	197.56	61.59	1.89	0.32
1283_004_Ap_b_2_11	11	2	14.03	11.82	197.56	61.59	1.89	0.32
1283_004_Ap_b_2_11	11	3	11.47	41.67	197.56	61.59	1.89	0.32
1283_004_Ap_b_2_11	11	4	11.71	54.50	197.56	61.59	1.89	0.32
1283_004_Ap_b_2_11	11	5	13.66	29.72	197.56	61.59	1.89	0.32
1283_004_Ap_b_2_12	12	1	13.37	72.87	156.21	64.95	1.97	0.32
1283_004_Ap_b_2_12	12	2	13.51	24.11	156.21	64.95	1.97	0.32
1283_004_Ap_b_2_12	12	3	9.11	71.61	156.21	64.95	1.97	0.32
1283_004_Ap_b_2_13	13	1	14.69	62.87	145.85	73.06	1.97	0.30
1283_004_Ap_b_2_14	14	1	11.51	55.30	157.03	159.61	1.57	0.26
1283_004_Ap_b_2_14	14	2	14.37	24.64	157.03	159.61	1.57	0.26
1283_004_Ap_b_2_15	15	1	14.72	35.51	291.08	161.71	1.86	0.31
1283_004_Ap_b_2_16	16	1	13.38	41.82	251.50	240.57	2.19	0.30
1283_004_Ap_b_2_16	16	2	12.58	58.59	251.50	240.57	2.19	0.30
1283_004_Ap_b_2_16	16	3	14.52	26.51	251.50	240.57	2.19	0.30
1283_004_Ap_b_2_17	17	1	13.71	71.41	158.45	126.09	2.02	0.29
1283_004_Ap_b_2_18	18	1	12.62	74.70	247.88	135.76	2.07	0.47
1283_004_Ap_b_2_18	18	2	14.09	30.47	247.88	135.76	2.07	0.47
1283_004_Ap_b_2_18	18	3	11.83	41.68	247.88	135.76	2.07	0.47
1283_004_Ap_b_2_19	19	1	15.80	20.56	172.69	305.63	1.64	0.25
1283_004_Ap_b_2_19	19	2	10.54	81.30	172.69	305.63	1.64	0.25
1283_004_Ap_b_2_20	20	1	13.64	47.08	182.91	68.53	1.99	0.30
1283_004_Ap_b_2_21	21	1	14.11	64.48	238.16	96.88	2.14	0.37
1283_004_Ap_b_2_22	22	1	12.10	47.58	170.41	84.39	1.93	0.30

1283 004 Ap b 2 23	23	1	14.94	73.07	229.87	102.81	1.96	0.30
1283 004 Ap b 2 23	23	2	16.08	52.85	229.87	102.81	1.96	0.30
1283 004 Ap b 2 23	23	3	13.20	86.33	229.87	102.81	1.96	0.30
1283 004 Ap b 2 23	23	4	14.22	48.90	229.87	102.81	1.96	0.30
1283 004 Ap b 2 23	23	5	13.61	69.09	229.87	102.81	1.96	0.30
1283 004 Ap b 2 24	24	1	14.16	37.15	194.53	98.29	2.33	0.40
1283 004 Ap b 2 24	24	2	14.66	58.04	194.53	98.29	2.33	0.40
1283 004 Ap b 2 24	24	3	13.63	83.15	194.53	98.29	2.33	0.40
1283 004 Ap b 2 24	24	4	13.05	47.98	194.53	98.29	2.33	0.40
1283 004 Ap b 2 25	25	1	14.91	64.77	248.97	109.95	1.92	0.28
1283 004 Ap b 2 26	26	1	13.31	46.94	206.16	143.39	2.05	0.35
1283 004 Ap b 2 27	27	1	10.75	74.34	235.40	107.74	1.98	0.32
1283 004 Ap b 2 27	27	2	15.09	53.87	235.40	107.74	1.98	0.32
1283 004 Ap b 2 28	28	1	11.66	29.39	134.05	65.34	2.21	0.30
1283 004 Ap b 2 28	28	2	12.77	67.93	134.05	65.34	2.21	0.30
1283 004 Ap b 2 29	29	1	14.79	54.12	0.00	0.00	1.91	0.33